PETROLOGY AND GEOCHEMISTRY OF THE TJAKASTAD (BARBERTON) ICDP CORES

By:
Grace Coetzee

Supervisors :
Prof. Allan Wilson (University of the Witwatersrand)
Prof. Nicholas Arndt (University of Grenoble-France)

Dissertation submitted to the Faculty of Science,
University of Witwatersrand
in the fulfilment of the requirements for the degree of
Master of Science

February 2014

DECLARATION

I declare that this Dissertation is my own, unaided work. It is being submitted for the Degree of Master of Science at the University of Witwatersrand, Johannesburg. It has not been submitted before for any degree or examination at any other University.

.....Coetzee.....

Grace Coetzee

20th day of May 2014 in Johannesburg

ABSTRACT

The Komati Formation of the Barberton Greenstone Belt is the type locality of the rock type known as *Komatiites*. Komatiites are ultramafic lavas that were generated and erupted mainly during the Archaean. They give insight into volcanism on the early Earth as well as the nature of the mantle and melting processes. During 2010-2011 the International Continental Drilling Programme (ICDP) Barberton Project drilled two cores (BARB 1 and BARB 2) into the Komati Formation to obtain continuous sections of the komatiite strata. These cores were drilled to gain knowledge about the structure, textures, compositions, processes and contact relationships of komatiite flows, which could not be obtained from surface outcrop because of lack of continuity and relatively poor exposure. The drill holes also intersected a volcanic tumulus unit, the first of its type recognized in komatiite lava flows, allowing insight into the processes that created the tumulus and the processes responsible for creating the differentiated komatiite flows.

The core was logged in detail, revealing a variety of rock-types and styles of volcanism. The rock-types encountered range from massive and differentiated ultramafic komatiites, through komatiitic basalts to mafic basalts. Some minor later intrusions of gabbros and dolerite are also present. The komatiites and komatiitic basalts are extrusive lavas and represent continuous eruptive sequences. The gabbros are typically intrusive, but can represent late stage crystallization. Contact relationships are evident in the core, where they have not been eroded by overlying flows, and are used to distinguish 85 individual flows in BARB 1 and 65 in BARB 2. Chill margins are typically between 5 and 50 cm thick and brecciated contacts are usually 5- 15 cm thick where present. Only rare examples of original mineralogy (olivine and pyroxene) are preserved because of pervasive alteration of the rocks. Alteration minerals are serpentine, chlorite, tremolite and magnetite. Early serpentine veining was followed by later stage magnesite veining. The opaque minerals – chromite with secondary magnetite overgrowth – are mostly located at olivine grain boundaries.

The tumulus unit in the BARB 1 core was created by upward doming of the upper skin of a lava tube. The unit is 90 m thick and consists of five textural sections: basal cumulates, harrisite, pyroxene spinifex, gabbro-pyroxenite and a hyaloclastite unit that caps the sequence. The

cumulates contain macrocrystic olivine grains that reach 15 mm in length; they are elongated and rounded, aligned in certain horizons and are tightly packed, with a maximum of 20 % matrix. The harrisite is a form of skeletal olivine (with crystals up to 5 cm in length) that grew upwards from the underlying cumulate layer. Between the skeletal olivine crystals are small (< 2 mm) crescent-shaped pyroxenes contained within the melt residue. Pyroxene grains in the spinifex lava reach 20 cm in length and are surrounded by a fine-grained matrix. The gabbro and pyroxenite layers contained within the spinifex layer are interpreted to represent the last stage of crystallization within the structure since they are chemically related to the tumulus and no chill margins are present between the gabbro and surrounding pyroxene spinifex. Both the spinifex and gabbro contain unaltered pyroxene crystals and the gabbro also contains relatively fresh plagioclase. The hyaloclastite breccia consists of fragmented fine-grained chill margin blocks derived from the upper crust of the lava tube. The fragments are surrounded and supported by a glassy shard-like matrix. Inflation processes are evident in the tumulus and gave rise to multiple layers of large elongated olivine cumulates together with the upward and outward bulging of the upper crust to form a hyaloclastite breccia. Chemically the tumulus exhibits a Fo_{93} olivine control. Fractionation processes are clear in MgO vs. depth, binary diagrams and REE plots. Element concentrations are between 1 and 11 times chondrite with a very small LREE enrichment.

Differentiated komatiite flows are composed of three lithologies: basal cumulates, olivine spinifex and chill margin zones. The cumulus olivines have a crystal size of 0.5-1 mm, are euhedral and enclosed by a 30 to 60 % melt component. The spinifex olivine forms random or parallel sheets on a centimetre scale and is completely altered to serpentine. Between the olivine spinifex are chemically more evolved pyroxene spinifex blades, which are smaller (millimetre to centimetre scale) and altered to a combination of serpentine-chlorite-tremolite. The fine-grained chill margins of the flows are typically 1-10 cm wide and in some cases contain contact breccias or hyaloclastites.

Three packages of differentiated komatiite flows occurring at several stratigraphic intervals where sampled in detail. The lowest package BARB 1 (89-118 m) exhibits chemical trends that are interpreted to indicate a combined crystallization control by olivine and pyroxene. This is evident in the rock compositions and by petrographic studies that reveal the presence of two

cumulus phases. The chemical compositions of the other two differentiated packages, BARB1 (378-420 m) and BARB 2 (252-274 m) are controlled by crystallization or accumulation of Fo_{93} and $Fo_{94,}$ respectively. These packages have olivine cumulates which are surrounded in some cases by pyroxene oikocrysts. In some samples the pyroxenes have unaltered cores. The REE plots are well constrained between 2 and 9 times chondrite values, and have slight LREE enrichment.

The tumulus structure and differentiated flow packages BARB 1 (378-420 m) and BARB 2 (252-274 m) have similar mineralogies and compositions but contain different textures. This is attributed to the size of the tumulus in comparison to the differentiated flows and implies similar magma processes and origins for all three units. The BARB 1 (89-118 m) interval appears to have undergone slightly different processes, as indicated by the presence of the two cumulus phases. This package is also altered to a greater extent than the others and no unaltered pyroxene is present.

ACKNOWLEDGMENTS

This project came about through a large scale interest in the Barberton Greenstone Belt. Many people were involved in the ICDP (International Continental Drilling Program) Barberton project. I would like to acknowledge and thank those people and institutions that have contributed to this thesis with special thanks to:

My primary supervisor, Prof. Allan Wilson and my second supervisor, Prof. Nick Arndt for their input and guidance through the thesis.

I would further like to thank Prof. Allan Wilson for the financial support provided during the course of the study.

The ICDP Barberton drilling project for creating the opportunity to study core from the Komati Formation and for financial support in terms of analytical costs.

The NRF for financial support.

Geospectral Imaging for the access to the scanned images of the BARB core.

The staff at Wits for their help with academic, analytical and administrative tasks.

Special mention to Gordon Chunnett for his assistance with the core, Marlin Patchappa, Musa Cebekhulu and Jaquie Pienaar for sample preparation and analysis.

My friends for their assistance and all the great times that made the experience unforgettable.

TABLE OF CONTENTS

LIST OF FIGURES AND CAPTIONS

Figure 6.10:
Hyaloclastite breccia indicating a contact.
Figure 6.11:
A) Example of the white varioles found within the spinifex layer. **B**) Vesicles found within the cumulate layer, show distinct boundaries and a reaction rim.

CHAPTER 7
Figure 7.1
Olivine cumulate samples from the tumulus unit. Evident are the elongated aligned olivines that have rounded edges. Complete serpentine alteration is distinct. **(A,B)** are sample GC-2. (**C,D)** are sample GC-19.
Figure 7.2
Harrisite texture formed by skeletal olivine blades surrounded by melt residue. The skeletal shape is evident in **(A,B)** from sample GC-20. Surrounding the olivines is melt containing crescent shaped pyroxene blades in sample GC-21 **(C,D)**. The olivine is altered to serpentine and the pyroxenes and melt residue are a combination of chlorite, tremolite and actinolite.
Figure 7.3
Unaltered pyroxene (augite) present in the harrisite. Surrounding the pyroxene is matrix altered to fine grained actinolite and chlorite from sample GC-24.
Figure 7.4
Pyroxenite layer consist of unaltered pyroxene grains, surrounded by a fine grained matrix in sample GC-27 **(A,B)**, altered to actinolite and chlorite. Present also is plagioclase grains, which are relatively unaltered in sample GC-27 **(C).**
Figure 7.5
Gabbro samples from the tumulus unit. There is more chlorite alteration present in the gabbro layer with has blades of unaltered pyroxene in sample GC-29 **(A,B)**. Plagioclase and pyroxene are relatively unaltered, however they have become overgrown by chlorite, actinolite and tremolite in sample GC-8 **(C,D)**.
Figure 7.6
The pyroxene crystals found in the spinifex zone of the tumulus unit are randomly oriented and almost completely altered in sample GC-7 **(A,B)**. Chlorite alteration occurs on the rims of the blades and actinolite- tremolite alteration occurs in the centre of the blades, plagioclase is present and the matrix is altered to a fibrous serpentine chlorite combination in sample GC-4 **(C,D)**. In a single sample unaltered pyroxene (augite) is present within a fine grained altered matrix in sample GC-26 **(E,F)**.
Figure 7.7
Magnesite overgrowth occurs in the pyroxene spinifex layer of the tumulus unit. They form euhedral grains which overprint the original igneous features and the serpentine alteration in sample GC-7.
Figure 7.8
Subtype (1) the fragment in contact with subtype (2) the glass shard matrix. Both components create the hyaloclastite texture found in the tumulus unit. A clear sharp contact is evident, with magnesite overprinting the magmatic and metamorphic features from GC-25.
Figure 7.9
The chilled and fragmented blocks of the upper carapace of the tumulus unit, from sample GC-20, are fine grained and contain elements such as vesicles **(C)** and olivine grains **(D)** in the fine grained chill fragment **(A,B)**.

Figure 7.10
The glass shard matrix consists of zoned glass fragments that are rounded and irregular in shape in sample GC-32 **(A,B)**. These shards can amalgamate to form a single round shard made up of smaller irregular shards seen in sample GC-10 **(C,D)**. Microcrystalline magnesite occurs in zones around these shards causing the zoning of the shards evident in sample GC-34 **(E,F)**. Alteration to serpentine and chlorite is present, but the predominant alteration is to magnesite, as it forms as euhedral grains and as a microcrystalline replacement.

Figure 7.11
Olivines from the differentiated komatiite flows directly above the tumulus unit, between 89-118 m, are completely surrounded by melt residue as is evident in AHW/DM 9 **(A,B,C,D)**. Chlorite rims the olivines and magnetite (Mgt) is concentrated in specific grains (Mgt-rich vs. mgt-poor). The samples are altered to serpentine and chlorite.

Figure 7.12
Olivine cumulates from the (378-420 m) differentiated komatiites have a dark matrix between the cumulates **(A,B)**. Unaltered pyroxene (CPX) grains are found in the matrix **(C,D)** and form oikocrysts around the olivine cumulates as evident in sample AHW/TM 42.

Figure 7.13
Olivine cumulates from sample BARB 2-22 in the BARB 2 (252-274 m) differentiated komatiite set. The olivines are surrounded by melt residue. The cumulates are altered to serpentine and the matrix to a tremolite-chlorite mixture.

Figure 7.14
Sample BARB 2-2 showing pseudo cumulates, where the melt residue has formed pockets and is surrounded by olivine crystals. It appears that the cumulate and melt residue reversed textural roles in this sample. Alteration of the olivines to serpentine, while the matrix alters to a chlorite-actinolite combination.

Figure 7.15
Evidence of unaltered pyroxene is present between the altered olivine crystals of the cumulate in sample BARB 2-19 from the differentiated komatiite package BARB 2 (252-274 m). The pyroxene is clearly formed after the olivine as it grows in the interstitial spaces and forms the beginning of an oikocryst.

Figure 7.16
Olivine spinifex from sample GC-41 forms a dendritic or feather like structure **(A,B).** Between the olivine blades are smaller pyroxene blades and fibrous acicular pyroxene **(C,D)**. Magnetite is concentrated along the olivine blades.

Figure 7.17
Pyroxene spinifex forms both large and small scale blades in sample AHW/TM 26 **(A,B)**. The blades are blocky and have sharp geometric shapes. Present in the pyroxene spinifex is kernels of fresh pyroxene **(C,D)** which is surrounded by needles of tremolite and chlorite.

Figure 7.18
Sample BARB 2-10 shows evidence of partially unaltered pyroxene surrounded by a matrix of actinolite-tremolite blades and chlorite alteration in the BARB 2 (252-274 m) package **(A,B)**. Unaltered clinopyroxene is evident in **(C,D)** with a higher relief and minimal green colouring which is associated with alteration. The opaque minerals are irregular in shape and have no association to the pyroxenes.

Figure 7.19
(A) Sample BARB 2-28 shows the small melt bubble inclusions that remain in the spinifex between the pyroxene blades and the elongated opaque minerals. The host minerals are unstrained (**B**).

Figure 7.20
(A,B) Sample BARB 2-16 illustrate the large olivine blades which create a structure that is filled in by the smaller pyroxene blades. **(C)** Sample AHW/DM 24 shows the blocky nature of the pyroxene blades. Between the pyroxene blades are radiating fibrous pyroxene growths **(C,D)**. **(D)** Sample AHW/TM 18 shows the large olivine blades with only fibrous pyroxene between them, lacking the pyroxene spinifex.

Figure 7.21
Chill zone with sharp contact from sample BARB 2-8 **(A,B)**. On the left hand side is the cumulate of the overlying flow **(C)** and on the right hand side is the spinifex from the underlying flow **(D).**
Figure 7.22
Sample BARB1 REF 21 shows a massive komatiite containing small (<0.5 mm) olivine grains which are altered to serpentine while the matrix is altered to chlorite and tremolite. The sample has a homogeneous texture.
Figure 7.23
Sample BARB 1 REF 17 is a komatiitic basalt. Fine grained poorly formed olivines are altered to serpentine and the matrix is altered to chlorite, tremolite and actinolite. **(A,B)** show the mineralogy whilst **(C)** shows the large scale texture and structure of the homogeneous komatiitic basalt.
Figure 7.24
Sample BARB 2 REF 28 is an intrusive basalt sample. Fine grained matrix material containing plagioclase phenocrysts **(A,B,C)**. The matrix is altered to chlorite with tremolite fibres overgrowing the igneous features **(C,D)**.
Figure 7.25
Sample BARB 1 REF 30 shows a gabbro containing plagioclase and fresh pyroxene. **(A,B)** illustrate the homogeneity of the texture. Plagioclase is evident in (**D).**
Figure 7.26
Surface cumulate sample GC-C-2. **(A,B)** indicate the presence of fresh pyroxene which creates a poikilitic texture with the olivine cumulates. **(C,D)** indicate the presence of kernels of fresh olivine which are <0.1 mm in size.
Figure 7.27
Surface map of tumulus zone, from Dann 2001.
Figure 7.28
Schematic diagram comparing surface geology to geology found in the BARB 1 core, tumulus unit.
Figure 7.29
Vesicle rich olivine cumulate (sample GC-V2) taken from the surface outcrop above BARB 1, within the vesicular komatiite zone identified by Dann (2001). The distinct boundary between the vesicle and the cumulate is evident. Vesicles may have irregular shapes **(C)**.
Figure 7.30
Illustrates the magnesite alteration present in the BARB 1 and BARB 2 cores. It forms as euhedral grains and as a microcrystalline infill observed in sample GC-35 **(C,D)** as well as forming veins. In the glass shard matrix of the tumulus unit in sample GC-34 **(A,B)** there is almost total magnesite alteration.

CHAPTER 8
Figure 8.1 (A)
Jensen cation plot showing the sample positions of the BARB 1 samples. The majority plot near the komatiite-komatiitic basalt boundary. The samples plot in a curve, indicating a systematic change in olivine composition during fractional crystallization. A single tholeiite basalt is present and identified as an intrusion in Chapter 4.
Figure 8.1 (B)
Jensen cation plot showing the chemistry of all the BARB 2 samples. The majority plot near the komatiite-komatiitic basalt boundary. The samples plot in a line, indicating a chemical relationship.
Figure 8.2 (A)
Portion of a Jensen cation plot for the samples taken from the tumlus section. A chemical trend is evident between the cumulates and the spinifex, with the hyaloclastite (which represents the chill zone and hence original liquid composition) plotting midway between them.

Figure 8.2 (B)
Portion of a Jensen cation plot for the samples taken from the BARB 1 section between 89-118 m. A chemical trend is evident between the cumulates and the spinifex, with the chill plotting midway between them. A single basalt sample from an intrusive layer plots in the high Fe- tholeiite basalt field, however, it is unrelated to the chemical process of the komatiites.

Figure 8.2 (C)
Portion of a Jensen cation plot for the samples taken from the BARB 1 (378-420 m) section. A chemical trend is evident between the cumulates and the spinifex, with the chill plotting throughout the cumulate and spinifex composition. A single komatiitic basalt sample is present and indicates a chemical relationship between the differentiated komatiite flows and the more evolved komatiitic basalt.

Figure 8.3
Al_2O_3 vs. TiO_2 graph shows the samples from BARB 1 and BARB 2 plot within the Al-depleted ratio line of the graph. Some samples plot in the Al-undepleted area, but they plot close to the boundary line, indicating that they most likely belong to the depleted population.

Figure 8.4
Depth vs. major element oxide plot of the entire BARB 1 core showing detailed and overall variations. The top of the core represents the lowest stratigraphic point, thus the graphs show changes in element abundance with stratigraphic height. Base section and top section are sampled in more detail and represent differentiated komatiites, whilst the middle section (150-350 m) is a combination of komatiitic basalt, basalt/gabbro and massive komatiites. A) is MgO, B)SiO_2, C)FeO, D)Ni

Figure 8.4 cont.
Depth vs. major element oxide plot of the entire BARB 1 core showing detailed and overall variations. E) plots Al_2O_3, F) plots TiO_2, G) plots Zr, H) plots Sc

Figure 8.5
Depth vs. element plot of the entire BARB 2 core. The mafic rock types are distinguishable by low or high element anomalies. A detailed sample section is present in the middle of the core (252-274 m). Alternating rock types are responsible for the zig-zag pattern present in the depth graphs.

Figure 8.5 cont.
Depth vs. major element oxide plot of the entire BARB 2 core.

Figure 8.6
Stratigraphic change in element concentrations through the 90 m thick tumulus unit. **A,D** illustrate the high concentration of MgO and Ni in the cumulates, decrease in the pyroxene rich layers and slight increase in the hyaloclastite. **B,E** show the mirror image of the MgO and Ni plots. **C,F** show a consistent increase with stratigraphy in FeO and Cr.

Figure 8.7
Stratigraphic changes in element concentrations through the differentiated komatiite package BARB 1 (89-118 m). All the figures illustrate the element variation with stratigraphic height. **A,B,D** illustrate the basalt layer (113.03 m) via an extremely low or high value with respect to the surrounding komatiites. **C** illustrates the irregular change in FeO concentration throughout the different rock-types. The red plots indicate samples of olivine cumulates.

Figure 8.8
Stratigraphic change in element concentrations through the differentiated komatiite package in BARB 1 (378-420 m). The figures illustrate the slight concentration change with depth. **A** illustrates the increase in MgO with stratigraphic height. **B,C,D** illustrate the predominant decreasing trend (opposite to MgO and Ni) with stratigraphic height. The vesicle rich sample and komatiitic basalt sample are plotted in **A,B** to illustrate the effect they possess over the trend. Clearly they do not alter the trends greatly.

Figure 8.9
Stratigraphic change in element concentrations through the differentiated komatiite package in BARB 2 at (252-274 m). The graphs illustrate a slight sinusoidal trend on a small scale, while no overall pattern is present. **A,C,D** illustrate the sinusoidal trend. **A,C** are mirror images of one another. **B** indicates that SiO_2 has no trend with depth or association between cumulate and SiO_2 content. The two MgO rich samples marked with arrows are chill zones which contain phenocrysts which increase the MgO content.

Figure 8.10
Variation diagrams of MgO and various elements for the tumulus section in BARB 1. **A,F** show positive linear/kinked correlations of LOI and Ni with MgO respectively. In **F** the trend flattens out at 20% MgO. **C,D,E,G** illustrate a negative correlation with MgO and indicate a MgO intercept of 50-52%. **B** shows no trend with MgO. **H** illustrates the typical chromite parabola trend associated with komatiites, where Cr is concentrated in the melt until a critical level (occurring at MgO <25 %) is reached and chromite is able to crystalize.

Figure 8.10 cont.
Harker diagrams of Al2O3 vs. various elements. **J,L** show good positive linear correlations with Al2O3. **I** shows an inverse exponential trend whilst **K,M** show no correlation between Al2O3 and Ni, CaO, respectively which is most likely due to mobilization of CaO.

Figure 8.11
Plot of MgO vs. FeO, TiO_2, Al_2O_3 (**A,C,D**) of the tumulus unit in BARB 1 shows a Fo_{92-93} control. A trend is evident, beginning with the olivine cumulates moving to the harrisite and then into the pyroxene spinifex and lastly into the pyroxenite and gabbro layer, found at the centre of the tumulus unit. The hyaloclastite represents the chill, since it plots between the MgO enriched cumulates and the MgO depleted spinifex. The hyaloclastite (blue) is the closest composition to the original liquid composition. The olivine cumulates create their own individual trend (**B**) that is parallel to the olivine control line and has an MgO intercept of 48 %.

Figure 8.12
Variation diagrams of MgO and various elements in the BARB 1 (89-118 m) differentiated package. **F** shows a positive linear correlations with MgO. **C,D,E,H** illustrate a negative correlation with MgO and indicate a MgO intercept of 40-42 % **A,G** show no trend with MgO indicting mobilization of SiO_2 and CaO. Regression lines calculated in SigmaPlot.

Figure 8.12 cont.
Variation diagrams of Al_2O_3 and various elements. **K,L** show good positive linear correlations with Al_2O_3. **J** shows a negative linear trend with an 8 % intercept whilst **L** shows no correlation between Al_2O_3 and CaO, which is most likely due to mobilization of CaO.

Figure 8.13 a
Diagram of MgO vs. FeO in the BARB 1 (89-118 m) differentiated package. The olivine (Forsterite) composition line is plotted to determine whether olivine controls the crystallization processes in these flows. Clearly the trend line does not intercept the olivine control line, which indicates that olivine does not solely control the crystal processes of these flows.

Figure 8.13 b
Diagram of MgO vs. FeO in the BARB 1 (89-118 m) differentiated package. The olivine (Forsterite) and orthopyroxene (Enstatite) control lines are plotted, with tie lines. Extrapolating the MgO intercept of 40-42 % from Figure 8.12 , it intersects the data trend line along the Fo_{91}-En_{92} tie line. Indicating an olivine pyroxene dual control on the crystallization processes in a proportion of 1(ol):2(px).

Figure 8.14 a
BARB 1 (378-420 m) differentiated package shows a large scatter in values with no trends emerging from any binary diagrams.

Figure 8.14 b
BARB 1 (378-420 m) data set of samples separated into individual flow units within the package. This sample set does not show individual flows creating distinct trends which would indicate different sources.

Figure 8.14 c
BARB 1 (378-420 m) data set of samples classified by texture. This sample set has been filtered using certain realistic criteria, to remove samples that are unrepresentative of typical komatiites. The data now shows a Fo_{93} control on crystallization.
Figure 8.15
BARB 1 (378-420 m) filtered data set. **B,C,D,E** show negative linear trends with an MgO intercept at 48-52 %. **F** shows a positive linear trend with the most magnesian rocks containing the highest Ni content. **G** shows no trend. **H** shows two trends, the negative linear trend, and within the cumulates a dome shaped trend. Regression lines calculated in SigmaPlot.
Figure 8.15 cont.
BARB 1 (378-420 m) filtered data set. **I,K** show positive linear trends and the process of fractionation. **J** shows a rather scattered negative trend and **L** shows no trend in CaO, again indicating the likelihood of CaO mobility.
Figure 8.16
BARB 2 (252-274 m) differentiated komatiite package. The data were filtered using the given criteria and 6 out of 29 samples were removed. They yield a trend line with an intercept of Fo_{93} on the olivine control line.
Figure 8.17
BARB 2 (252-274 m) filtered data set. **A,C,D,E** show negative linear trends with an MgO intercept between 52-55 %. **F** shows a positive linear trend with the most magnesian rocks containing the highest Ni content. **G** shows no trend. **H** shows two trends, the negative linear trend, and within the cumulates a dome shaped chromite trend. The lines drawn are regression lines.
Figure 8.17 cont.
BARB 2 (252-274 m) filtered data set. **I,K** show positive linear trends whilst **J** shows a negative scattered trend and **L** shows no trend.
Figure 8.18
MgO vs. FeO binary diagram illustrating the range in compositions for the chill margins of each differentiated komatiite package together with the chilled hyaloclastite block and the hyaloclastite matrix.
Figure 8.19
REE diagram from Furnes et al. (2013) illustrates the flat pattern found in the Komati Formation. Values for komatiites are 1-10 times chondrite values, while komatiitic basalts are between 8 and 11 times chondrite. Basalts are up to 100 times chondrite value.
Figure 8.20
Multi element diagram from (Robin-Popieul *et al.*, 2012) for Al-depleted komatiites from the Komati Formation. The pattern is relatively flat and only the slightest LREE concentration is present. Nb and Ti anomalies are identified. The plots are >10 times primitive mantle values and plot in a well constrained shape.
Figure 8.21
MgO vs. $(Gd/Yb)_N$ and $(La/Sm)_N$ give details about slopes and trends in the immobile multi-element diagrams.
Figure 8.22
REE diagram of representative samples from each textural section of the tumulus unit. The cumulates are depleted, while the other rock-types are enriched with the pyroxenite - gabbro layer being the most enriched (11x chondrite). The LREE are slightly enriched compared to the HREE. There is a minor negative Eu anomaly for most samples which is consistent in all rock types which is attributed to alteration.
Figure 8.23
Multi element diagram of representative samples from each section of the tumulus unit. The cumulates are depleted, while the other rock types are enriched with the pyroxenite - gabbro layer being the most enriched (10x primitive mantle). There is a well-defined decreasing trend from the more mobile element

(left) to the more immobile elements (right). Anomalies are present for Eu and Ti being both positive and negative.

Figure 8.24
Multi element diagram of representative samples from BARB 1 (89-118 m) package. Slight LREE enrichment, with a relatively flat pattern and a distinct Eu anomaly. Samples plot in a parallel fashion with the cumulates in the lower portion whilst the spinifex defines the maximum and minimum values of 5 to 9 times chondrite. The chill samples plot toward the top of the data range.

Figure 8.25
Multi element diagram of representative samples from BARB 1 (89-118 m) package. Samples range from 1 to 3 times primitive mantle values, with a dome shape in the LREE. The samples create a tight trend except for Eu which shows both positive and negative anomalies, creating a scatter, a negative Ti and slight positive Y anomaly.

Figure 8.26
REE diagram of representative samples from BARB (378-420 m) package. The data create a flat trend, with a slight upwards bulge from La to Dy (MREE), which decreases again in the HREE. The data are well constrained and a single Eu anomaly shows scatter. The samples have concentrations from 3 to 8 times chondrite

Figure 8.27
Multi element diagram of representative samples from BARB 1 (378-420 m) package. The data create an increasing trend from Th to Sm which dips at Zr and flattens out at the HREEs. There is a single positive anomaly at Nb in a cumulate sample. Eu has both positive and negative anomalies. The rest of the elements plot with precision and the data forms parallel trends with concentrations from 0.5 to 4 times primitive mantle values.

Figure 8.28
REE diagram of representative samples from BARB 2 (252-274 m) package. The data create a flat trend, with a slight increase from La to Sm and a decrease from Sm to Lu with an overall increase from LREE to HREE. The data are 2 to 7 times chondrite values and form parallel, well constrained trends. A positive and negative anomaly at Eu cause scatter.

Figure 8.29
Multi element diagram of representative samples from BARB 2 (252-274 m) package. The data increase from Th to Sm, dip slightly at Zr and the gently decrease from Hf to Lu. The concentrations are from 0.5 to 2 times primitive mantle and the data is evenly spaced over this range. Eu and Nb anomalies are present with a small spike at Ti.

CHAPTER 9

Figure 9.1
Schematic cross section of the tumulus unit perpendicular to flow direction. The textural sections of the surface map correspond to the textural zones of the core.

List of tables

CHAPTER 1

INTRODUCTION

1.1 Rationale

The Barberton Greenstone Belt, located within the Kaapvaal Craton of South Africa, has remnants of some of the oldest and best preserved komatiites on Earth. Despite the age, extensive deformation and metamorphic history of the greenstone belt, magmatic textures remain well preserved in these rocks. The Komati Formation is stratigraphically the lowest and therefore the earliest occurrence of these well preserved, though chemically altered, komatiites in the Barberton Greenstone Belt. The preservation and compositions of these rocks gives insight into the nature of the early Archaean.

Textural relationships and chemical analyses of komatiites allow investigations into the structure, source and flow dynamics of early eruptions. Such investigations are greatly aided by complete sections of rock units and stratigraphic continuity, which can only be obtained by studying drill core. This drill core was made available for study through the International Continental Drilling Program in the Barberton greenstone belt which commenced in July 2011 (see section 1.4: The ICDP Barberton drilling project).

One of the principal aims of the Barberton International Continental Drilling Program (ICDP) was to attain the first ever extensive core sample coverage of the Komati Formation. All previous work was done exclusively on surface outcrops. Limitations of studies on surface outcrops include a lack of continuity of textural features, lack of stratigraphic continuity and possible additional chemical alteration due to surface weathering. The goals of the ICDP drilling were to obtain two 400 m-long core sections, which sampled continuous and consecutive komatiite flows and a unique tumulus unit previously identified on the surface. These cores reveal detail of the flow contacts that were previously unseen in the field due to discontinuous outcrop and surface weathering.

The object of this study is to log the BARB 1 and BARB 2 core, both of which were drilled in the lower Komati Formation, and describe these newly available contact relations. Furthermore, flow features, textures and chemistry between adjacent flows and to flows at different stratigraphic positions, are compared. This will give insight into flow processes over

the period represented by the rock sections and possible changes in the composition of the flow units, which would reflect the magmatic processes and the sources of the komatiites.

1.2 What do Komatiites Reveal about Earth's History?

Komatiites are an extinct type of rock representing the most primitive type of volcanic rock in Earth's history. They were discovered by Morris and Richard Viljoen (Viljoen & Viljoen, 1969), who recognised that they are a new class of high magnesium volcanic rock. Komatiites were named after the Komati River, which flows through the type locality. These rocks formed almost exclusively in the Archaean (4.0 to 2.5 Ga.) and remnants are found in Archaean greenstone belts worldwide (Arndt *et al.*, 2008, Jahn *et al.*, 1982). The abundance of komatiite lavas in the Archaean and near absence of komatiite lavas in the rest of geological time, implies that there were certain conditions present during the Archaean which allowed the formation of komatiites (Chavagnac, 2004, Robin-Popieul *et al.*, 2012). The lack of komatiites from the end of the Archaean until present day indicates that the komatiite forming conditions are no longer present in the Earth's mantle.

By studying komatiite flow dynamics, petrography and geochemistry, it becomes possible to interpret some of the conditions of the early Earth (Nisbet *et al.*, 1987). Chavagnac (2004) used geochemistry and isotope signatures to obtain information about the 'mantle source, melting conditions and post crystallization processes' (Chavagnac, 2004, p 254). Komatiites are divided into three different types depending on their Al_2O_3 and TiO_2 contents, and their REE patterns. The variability of komatiite chemistry is thought to indicate a heterogeneity of the mantle in the early Archaean. Specific focus is given to garnet fractionation within the melt source (Chavagnac, 2004, Jahn *et al.*, 1982), or to variation in the conditions and processes of partial melting.

One of the defining features of komatiites is their high MgO content (between 18 and 28 wt. %). It has been hypothesised by many scientists that this high MgO content can form due to a large percentage of partial melting at great depths (high pressure), from an undepleted mantle source (Arndt *et al.*, 2008, Furnes *et al.*, 2013, Nesbitt & Sun, 1976, Wilson *et al.*, 2003). These conditions are considered to occur in mantle plumes that are exceptionally hot. This indicates higher mantle temperatures for the early Earth compared to later geological periods. The alternative hypothesis revolves around the presence of hydrous phases in the komatiites (known as the wet hypothesis), which allows the same abundance of MgO to form under

mantle conditions that are more similar to present day (Grove & Parman, 2004, Parman *et al.*, 1997, Parman *et al.*, 2001, Parman *et al.*, 2003). This debate is on-going, but most scientists prefer the mantle plume-related, hotter Earth explanation.

Textures associated with komatiites, such as the renowned spinifex, cumulates, pillow structures and chill margins/ hyaloclastite breccias, all give information about the environment in which the komatiite magma was emplaced.

1.3 The Importance of the Barberton Greenstone Belt

There are many greenstone fragments preserved around the world (Arndt *et al.*, 2008, Arndt & Nisbet, 1982). Most of them have undergone extensive chemical alteration and often physical deformation to the extent that the original textures and minerals are no longer preserved. The Barberton Greenstone Belt (BGB) is one of the oldest and one of the least structurally deformed greenstone belts (Arndt *et al.*, 2008, Chavagnac, 2004, Dann & Grove, 2007).

The belt consists of an estimated 12 km sequence of metamorphosed sediments and volcanic rocks. This unique preservation of the sedimentary features, igneous textures and in a few places; the igneous mineralogy, creates an ideal situation to study the sedimentary and volcanic processes, crustal evolution and mantle conditions of the early to mid- Archaean. Due to preservation, the volcanic rocks of the Onverwacht Group were recognized early on as an area of high interest during the International Upper Mantle Project in the 1960's.

The belt once again became the focus of a large scale academic study in 2007, when metavolcanic and metasedimentary rocks were targeted in a project of the International Continental Drilling Program (ICDP). The sedimentary sequences are being studied for evidence of the first bacterial life in the Fig Tree Group (Figure 1.1). This group contains spherule layers derived from meteorite impacts which yield information on the composition of both the meteorite and the impact rock (Stiegler *et al.* 2010).

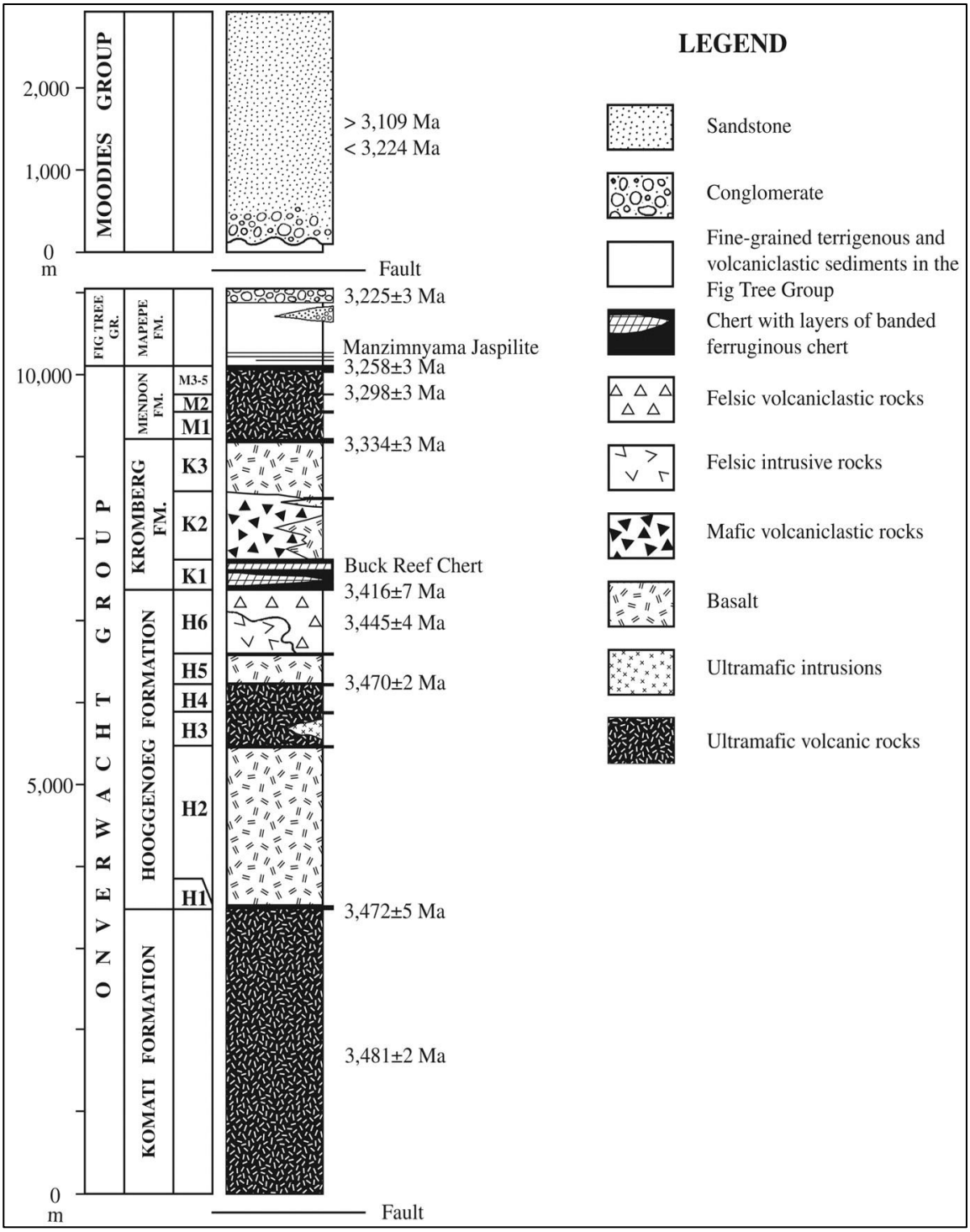

Figure 1.1:
Stratigraphy of the Barberton Greenstone Belt, missing the Sandspruit and Theespruit formations (Lowe and Byerly, 2007).

The focus of this study is volcanic rocks and in particular komatiites of the Komati Formation. These rocks have well preserved textures, and in some places, intact mineralogy. Furthermore, they are the most magnesium rich ultramafic volcanic rocks, indicating some of the highest mantle temperatures. Since the BGB is one of the oldest greenstone belts on Earth, and contains the most magnesium rich ultramafic volcanic rocks, it has been proposed that the hottest mantle corresponded with the oldest time (Parman *et al.*, 1997) and progressively younger ultramafic rocks originated from an ever cooling mantle source. The origin of plate tectonics is another unresolved scientific topic, whose resolution might be found by studying the rocks of the BGB.

1.4 The ICDP Barberton Drilling Project

On a regional scale, the Komati Formation has in the past been well mapped, documented and sampled, notably by Viljoen and Viljoen (1969) and (Lowe & Byerly, 2007). However, due to sparse outcrop and the easily erodible nature of some of the rock types, detailed mapping of small scale features such as flow textures and boundaries between adjacent flows had not been possible. Since the initial discovery of the komatiites, only surface sampling and surface mapping have been performed. To obtain a more complete and more detailed understanding of komatiite flow relationships and interactions, it has become necessary to study drill cores.

The ICDP (International Continental Drilling Program) was officially created during a scientific meeting held in Potsdam, Germany in 1993. It is an organization aimed at drilling continental boreholes to improve the knowledge and understanding of the Earth and its processes. The ICDP goals are focused on scientific issues and topics relating to human sustainability with respect to Earth and its processes. Examples include the study of volcanoes and earthquakes to reduce their impact on human populations and the sustainability of energy, mineral and water resources.

Since the Barberton Greenstone Belt holds such unique information of Archaean processes, a proposal was developed to drill various sites in the belt to obtain cores that reveal information on the magmatic and geodynamic processes in the Archaean and early life on Earth. A full list of scientific objectives is found on the following website:

http://www.icdp-online.org/sites/tpl/tpl_proposal_co.htm?label=ICDP-2008/07

Two main aspects of research were defined for the ICDP Barberton drilling project.

1. Sedimentary sequences from the BGB: These would provide information about sedimentary processes, composition of Archaean seawater along with Earth-Moon system dynamics. Spherule layers provide insights into meteorite composition and magnitudes of impact. A further objective is the search for evidence for the possible emergence of bacterial life.
2. Ultramafic and felsic volcanic successions: These offer new information regarding Archaean volcanic processes and dynamics of the mantle, such as mantle heterogeneity and mantle temperature in the Archaean.

In order to achieve these goals it was decided that 6 diamond drilled boreholes would sample a variety of strata throughout the belt: three from the Onverwacht Group and three from the Fig Tree Group (Figure 1.1). The drill sites were identified with specific goals in mind. A summary of the drill sites is as follows:

BARB 1 (420 m) and BARB 2 (431 m) –Cores were drilled into the ultramafic lavas of the Komati Formation of the Tjakastad Subgroup (Figure 1.1 and 1.2). These drill sites are in close proximity to each other, and sampled a variety of ultramafic volcanic rock types in order to obtain continuous sections through the Komati Formation. The continuous sections give insight into the poorly exposed volcanic units, their contacts and their compositions compared with adjacent flows and with flows at different stratigraphic height. The BARB 1 core was drilled with the aim of obtaining more textural and chemical details of a unique tumulus unit, identified by Dann (2000). The BARB 2 core was drilled with the objective of obtaining samples containing fresh igneous minerals, since surface outcrop had previously yielded samples of unaltered olivine and pyroxene.

BARB 3 (899 m) – Drilled into the Buck Reef Cherts of the upper Onverwacht Group. This core, samples mainly sedimentary cherts and iron formations, but also contains ultramafic to felsic volcanic units. The main focus of this borehole was to study the evidence of early life.

BARB 4 (520 m) – This borehole was drilled into the middle of the Fig Tree Group. It samples sedimentary sequences of turbiditic greywackes, mudstone, banded iron rich cherts and true banded iron formation.

BARB 5 (800 m) – This borehole sampled sedimentary units of the lower Fig Tree Formation in the "Barite Valley Syncline". The core also sampled a spherule layer along with a series of cherts, iron formation and shales.

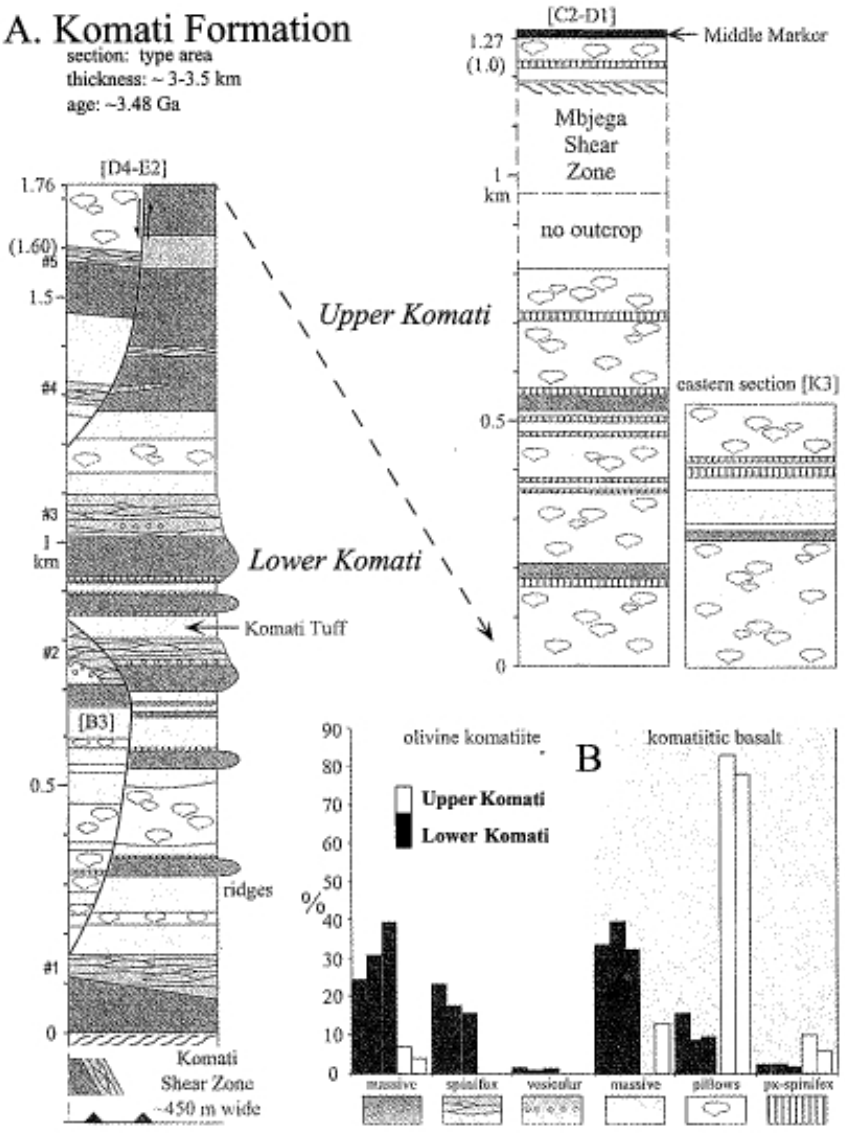

Figure 1.2:
Stratigraphy of the Komati Formation illustrating the division between lower and upper Komati Formation, together with the lower bounding Komati Shear Zone and the upper Middle Marker chert (Dann 2000).

1.5 Aims of this Study

BARB 1 and BARB 2 are the first continuous borehole cores drilled through the ultramafic volcanic units of the Komati Formation. This has created the opportunity to obtain geochemical, petrological, textural and structural information that was previously inaccessible, due to lack of surface exposure. The specific aims of this project are to obtain:

- Detailed logs of the BARB 1 and BARB 2 cores
- Detailed descriptions of the rock types encountered
- Geochemical analyses of BARB 1 and BARB 2
- Identification of different styles of volcanism
- Detailed chemical and petrological study of four selected sections from both BARB 1 and BARB 2
- Delineation of individual komatiite flows, and the internal structure of each flow from the tumulus unit and from selected sections
- Textural, petrological and chemical comparison between the tumulus and komatiite flows

CHAPTER 2

THE BARBERTON GREENSTONE BELT

2.1 Introduction to the Barberton Greenstone Belt

The Barberton Greenstone Belt is located on the eastern edge of the Kaapvaal Craton in the Mpumalanga Province of South Africa. It is a north-east trending belt approximately 100 km in length by 50 km wide and has a triangular- tricuspate shape (Figure 2.1). The first interest shown in understanding and mapping the geology of the belt was initiated in the 1950's by the discovery of commercial gold deposits, but the belt had been mined on a minor scale from the 1800's (Brandl *et al.*, 2006). The economic interest led to further academic investigation of the stratigraphy, age, structure and environment of deposition. Only 10 years later, in 1969, the rock-type known as komatiite was discovered by the Viljoen brothers and named after the type locality in the Komati River (Viljoen & Viljoen, 1969). The belt was identified as one of the oldest, most well preserved Archaean greenstone belts with the rocks dating between 3.1 and 3.6 Ga (Brandl *et al.*, 2006, de Wit *et al.*, 2011) . It has subsequently become a world-renowned area for studying Archaean rocks.

2.2 Major Geological Features of the Barberton Greenstone Belt

The Barberton Greenstone Belt, previously known as the Swaziland Supergroup, is divided into three main lithostratigraphic groups: (1) the Onverwacht Group (3.55-3.26 Ga), composed mainly of mafic-ultramafic and felsic volcanic suite of rocks, (2) the Fig Tree Group (3.26-3.225 Ga), consisting of dacitic volcaniclastic and sedimentary shales and greywackes with some cherts, and (3) the Moodies Group (3.225-3.1 Ga), which consists of coarser sediments such as conglomerates, feldspathic sandstone, siltstone and shales (Brandl *et al.*, 2006, Dirks *et al.*, 2009) (Figure 1.1).

The focus of this study is the Onverwacht Group (3.55- 3.26 Ga), which is further divided into six formations; (1) Sandspruit, (2) Theespruit, (3) Komati, (4) Hooggenoeg, (5) Kromberg, and (6) Mendon (Figure 1.1) (Brandl *et al.*, 2006, Chavagnac, 2004, Lowe & Byerly, 2007).

These formations consist predominantly of ultramafic–mafic volcanic rocks with minor sedimentary horizons. Each formation is cut by a variety of tectonic faults and shear zones,

making the stratigraphic relationship between the formations difficult to determine. Armstrong *et al.* (1990) in their paper on zircon age dating concluded that the Komati Formation is older than the underlying Theespruit Formation, as a consequence of tectonic thrusting. This result was later called into question on the basis of geological information, but clearly illustrates the complexity and inter-relationship of these formations. It has been previously suggested by various authors such as Lowe, de Wit and Cloete and recently championed in a paper by de Wit *et al.* (2011), that the formations of the Onverwacht Group be renamed and reclassified as complexes, which combined make up the Onverwacht Suite.

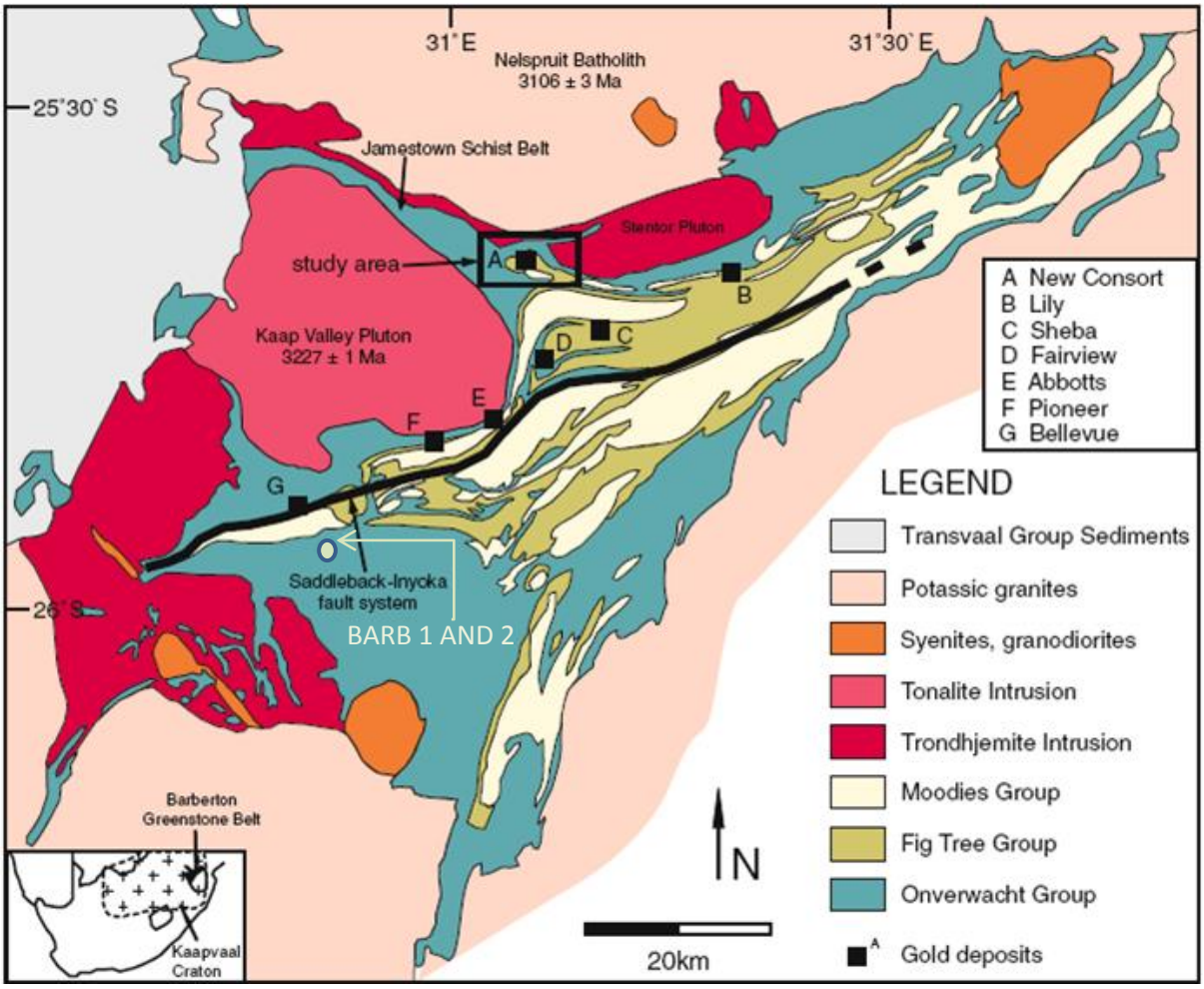

Figure 2.1
Geographic and geological map of the Barberton Greenstone belt with the position of BARB 1 and BARB 2 drill sites. (Otto et al. 2007)

The Fig Tree Group (3.26- 3.225 Ga), overlies the Onverwacht Group conformably, and is divided into four formations (1) Loenen Formation, consisting of carbonaceous shales and sandstones, (2) Ngwenya Formation, composed of shales, sandstone and jaspilite banded ironstone, (3) Mapepe Formation, consisting of dacite ash, mudstone and chert (ferruginous chert and brecciated chert) together with spherule layers and thin layers of barite, and (4) Auber Villiers Formation, which contains dacitic volcaniclastics and terrigenous sediments (Brandl *et al.*, 2006).

The Moodies Group is the youngest in the BGB sequence being 3.225-3.1 Ga. The base is defined by a conglomerate layer, overlain by a quartz rich sandstone unit. Upward fining cycles define the rocks of the Moodies Group, which is widely recognized as a foreland basin depositional environment. However, it is also understood that the Moodies Group sediments were deposited syn-tectonically in structurally isolated basins created by folding and thrusting (Brandl *et al.*, 2006, Dann & Grove, 2007).

During the deposition of the BGB two events of pluton emplacement took place. These are: (1) Tonalite-Tronjhemite-Granodiorite plutons that were emplaced during the formation of the Onverwacht Group, and (2) Granite-Monzonite-Syenite plutons that were emplaced post Moodies Group deposition at about 3.1 Ga (Lowe & Byerly, 2007).

2.3 Metamorphism and Deformation of the Barberton Greenstone Belt

Three major metamorphic processes have been identified (Brandl *et al.*, 2006): (1) sea-floor metamorphism, during which the igneous textures were well preserved, but the igneous mineralogy was changed, (2) burial metamorphism, which occurred as the strata became buried and is identified using mineral geochemistry and geothermometry on fluid inclusions, and (3) dynamic metamorphism characterised by the presence of pervasive fabrics in some rocks of the belt. The Onverwacht Group is pervasively metamorphosed to greenschist facies, with some amphibolite contact metamorphism near the granite plutons.

The Onverwacht, Fig Tree and Moodies Groups have undergone intense structural deformation and regional metamorphism. Lowe and Byerly (2007), identify five separate regional deformation events. The early events are attributed to horizontal thrusting, and the last event was responsible for large scale tilting and folding, causing horizontal bedding to become near vertical. These events range from compression and thrusting (D1 at 3.44 Ga,

D2at 3.25-3.24 Ga and D5 at 3.216 Ga) to extension (D1.5 at 3.3 Ga to form the Mendon Formation, and D3 during the emplacement of the Moodies Group). Deposition and deformation were commonly synchronous. The Fig Tree is a basin-filled sedimentary sequence whilst the Moodies Group comprises 'molasse deposits associated with fold and thrust (nappe) deformation' (Dann & Grove, 2007, p 528). This indicates that deposition was occurring during tectonically active times, making the geological history much more complex.

A summary of the deformation events is:

D0: 3550 Ma, deposition of the lower Onverwacht Group with associated island arc type subduction deformation (Dirks *et al.,* 2009).

D1: 3445±4 to 3416±7 Ma, shortening event, creating thrust sheets, 3330 Ma extension deformation and emplacement of volcanic rocks of the Mendon Formation (Byerly, 1999).

D2: 3230 to 3225 Ma, deposition and deformation of Fig Tree Group. Isoclinal folds with E-W trending axes and thrust complexes in conjunction with a metamorphic peak and pluton emplacement (Brandl *et al.,* 2006).

D3: Deposition and deformation of Moodies Group. This was probably continuous with the D2 event, since the Moodies Group appears to have been deposited in separate basins that form during thrusting or extensional events. (Dirks *et al.,* 2009) separated this event into early and late stages due to the lack of exact dates.

D4: D4 is a thrusting of conformable Moodies and Fig Tree Groups sequences over one another from a NW to SE direction, possibly due to pluton emplacement (Lowe, 1994).

D5: Post Moodies deformation. 3216±2 to 3084±54 Ma. (Is also called D4- by (de Ronde *et al.*, 1994) . NE-SW trending thrust faults, folding and rotation of strata to a vertical plane (Lowe, 1994, Viljoen *et al.,* 1983) and structural deformation during pluton emplacement.

2.4 Geological Sequence of the Onverwacht Group

The Onverwacht Group is divided into the underlying Tjakastad Subgroup and the overlying Geluk Subgroup, separated by the Middle Marker cherts (Viljoen *et al.*, 1983). The Tjakastad Subgroup consists of the Sandspruit, Theespruit and Komati Formations which have been dated between 3.55 Ga and 3.47 Ga (Lowe & Byerly, 2007, Viljoen *et al.*, 1982).

The Sandspruit Formation (approximately 2 km thick), is identified as the stratigraphically lowest and thus oldest unit. It is found only as xenoliths and stringers of mafic and ultramafic rocks within the surrounding Theespruit and Stolzburg plutons. This formation is associated with peak metamorphic conditions of 650-700 °C and 8-11 kbar pressure (Brandl *et al.*, 2006). The overlying Theespruit Formation (1.8 km thick), consists of metamorphosed tuffs and lavas, with rare occurrences of pillowed or ocelli-rich high-magnesium basalts. Very few komatiites are associated with this formation and it is identified by the presence of pyroclastic and volcaniclastic units. The Komati Formation (3.5 km thick), is the type locality for komatiites, and it consists of komatiites and komatiitic basalts, with minor mafic intrusions. This formation will be discussed in detail in section 2.5.

The Geluk Subgroup is made up of the Hooggenoeg, Kromberg and Mendon Formations. The base of the subgroup is the easily identifiable Middle Marker chert that occurs above the Komati Formation. The Hooggenoeg Formation (4.8 km thick), contains the Middle Marker chert layer, overlain by 3 km of mafic pillowed and massive basalts and is capped by a section of felsic rocks, and finally by the 1 km thick Buck Reef Cherts. It is commonly accepted that the felsic rocks are a result of silica rich metamorphic fluids associated with the intrusion of the Theespruit and Stolzburg plutons. The Kromberg Formation (1.7 km thick), consists of massive and pillowed mafic and ultramafic rocks, mafic lapilli tuffs and chert (solid black and banded- black and white) (Lowe & Byerly, 1999). The Mendon Formation (1 km thick), is the uppermost formation of the Onverwacht Group. This formation consists mainly of alternating massive komatiite/komatiitic basalts with chert layers. Present in this formation are spherule layers, barite layers and jasper units.

2.5 Rock-Types of the Komati Formation

The Komati Formation is between 3.1 and 3.5 km thick (Brandl *et al.*, 2006, Stiegler *et al.*, 2010) and consists of komatiite at the base with an increase in komatiitic basalt toward the

top. The depositional environment of this formation has been proposed as an oceanic spreading centre (de Wit *et al.*, 1987), a back arc environment (Dann & Grove, 2007) or an oceanic plateau formed via plume activity (de Wit *et al.*, 1992, Nisbet *et al.*, 1993, Robin-Popieul *et al.*, 2012). The Komati Formation (Tjakastad Subgroup) is separated from the overlying Hooggenoeg Formation (Geluk Subgroup) by the Middle Marker chert horizon (Brandl *et al.*, 2006, Chavagnac, 2004, Viljoen & Viljoen, 1969). The age of the Komati Formation ranges from 3481± 2 Ma to 3467 ± 5 Ma (Armstrong *et al.*, 1990, Dann & Grove, 2007, de Wit *et al.*, 2011, Kröner *et al.*, 1996, Lopez-Martinez *et al.*, 1992). Viljoen *et al.* (1983) separated the Komati Formation into six alternating layers of komatiite and komatiitic basalt. The lower Komati Formation consists mainly of komatiites whilst the upper Komati Formation contains nearly 65% komatiitic basalt. A single 20 cm thick volcaniclastic horizon is present in the lower Komati Formation, which indicates a single break in the almost continuous volcanic eruption (de Wit *et al.*, 2011, Puchtel *et al.*, 2013). Stiegler *et al.* (2010) suggest that the entire Komati Formation may have taken only 10^5-10^6 years to form. Metamorphic conditions reached between 300 and 500 °C and pressures of 2-5 kbar, which are associated with sea-floor alteration and moderate burial metamorphism. Structural deformation is confined to discreet, thin layer parallel zones, which separate packages of strata with minimal deformation in which igneous textures are preserved (de Wit *et al.*, 2011).

The pre-metamorphism Komati Formation mineralogy is predominantly olivine, pyroxene and chromite (Chavagnac, 2004, Viljoen *et al.*, 1982). However, due to the hydrothermal alteration and metamorphism (Cloete, 1991, Parman *et al.*, 1997), these minerals have been almost completely altered to a greenschist mineral assemblage. Since the original igneous textures are well preserved, it is usually possible to determine the original igneous mineralogy (Viljoen & Viljoen, 1969, Viljoen *et al.*, 1982, Viljoen *et al.*, 1983). Chavagnac (2004), Viljoen *et al.* (1982) indicate that olivine has altered to serpentine, chlorite, magnetite and tremolite, while chromite has magnetite overgrowths and clinopyroxene (augite) is chemically zoned and has associations of tremolite and minor replacement of serpentine and chlorite. In certain places in the Komati Formation, unaltered cores of igneous minerals are still present. Most often pyroxene and chromite are preserved, but rare olivine kernels are also present. This exceptional occurrence of fresh igneous chemistry allows for a more accurate understanding of the Archaean environment and the origin of the lavas.

Viljoen *et al.* (1983) and Viljoen *et al.* (1982) divided the Komati Formation into six major zones of komatiite, alternating with less resistant komatiitic basalt layers. At the base of the formation the thicker layers are mostly komatiite, whereas towards the top of the formation the rock-type becomes predominantly massive or pillowed komatiitic basalt.

Dann and Grove (2007) divided the Komati Formation into lower and upper portions using geochemistry and petrology.

Lower Komati Formation:

The Lower Komati Formation unit consists mainly of alternating thin, differentiated, spinifex-textured flows and thicker massive units. The latter are more resistant and crop out as prominent ridges. In many cases it is not clear if these units are extrusive or intrusive. Dann and Grove (2007) divided the lower Komati Formation into five geochemically distinct flow fields and identified a unique tumulus structure at the base of the Komati Formation.

According to published reports (Chavagnac, 2004, Nesbitt & Sun, 1976, Robin-Popieul *et al.*, 2012) the komatiites are Al-depleted (Al_2O_3/TiO_2=8-12), with high CaO/Al_2O_3 ratios up to 2.5. Their rare earth element (REE) patterns are slightly depleted in the heavy REE.

A tumulus is a dome-shaped feature that forms along the top of lava flows. The cooled outer crust becomes flexed outwards and upwards, creating a dome or ridge shape (Anderson, 2012, Rossi & Gudmundsson, 1996, Walker, 1991). This feature often forms due to the inflation of a lava flow, when more lava enters the flow than the amount that leaves it. This inflation causes the upward flexure of the top crust, which creates space to accommodate the influx of lava (Anderson, 2012, Dann & Grove, 2007). Anderson (2012) states that a tumulus can form due to a velocity increase across the flow, when the lava at the centre of the flow moves at a higher velocity than the cooled lava at the edges of the flow (Walker, 1991, Kauahikaua *et al.*, 1998) .

The tumulus structure, which occurs near the base of the formation, consists of three textural sections: a lower olivine cumulate zone, a central olivine spinifex zone and an upper vesicular zone (Dann, 2000, Dann, 2001, Dann & Grove, 2007). The tumulus in the study section has a 20 m-thick vesicular crust, which was fractured and rotated due to inflation of the lava tube. The investigation of the tumulus was one of the objectives of the ICDP drilling.

The upper portion of the lower Komati Formation is predominantly komatiitic basalt, which formed sheet flows and pillow structures (Figure 2.2)

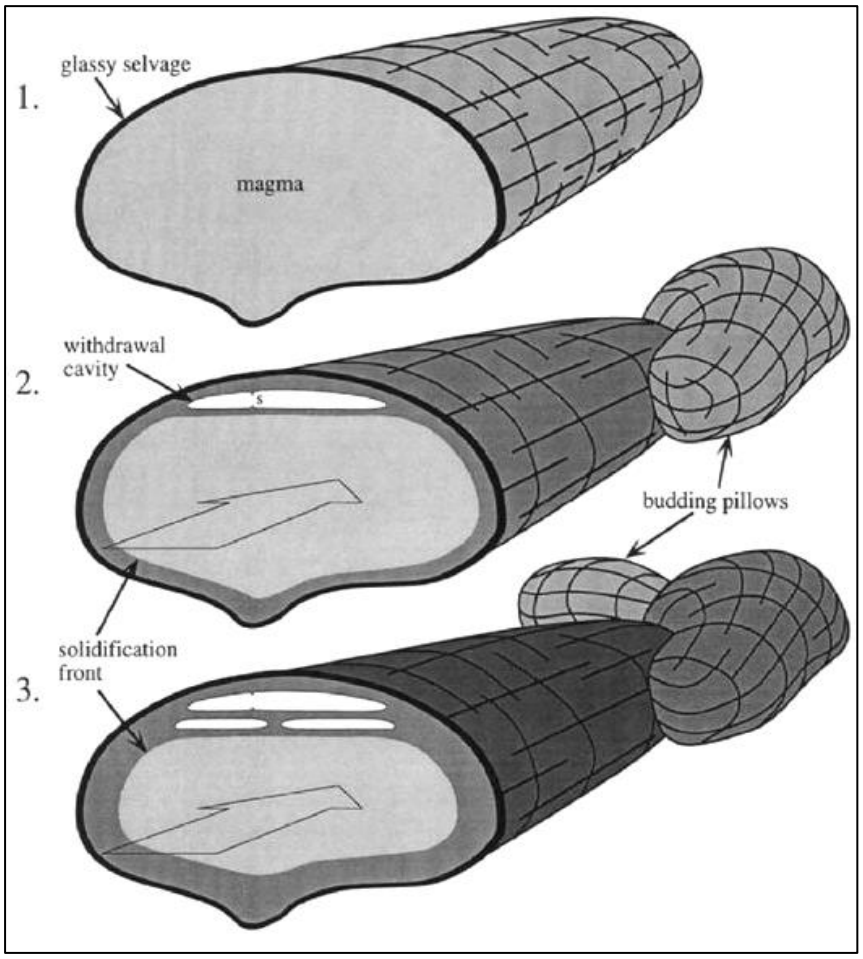

Figure 2.2:
Illustration of the formation of a pillow structure and the creation of withdrawal cavities. (Dann & Grove, 2007, pp547)

Upper Komati Formation:

The upper section of the Komati Formation is composed of massive and pillowed komatiitic basalts that are Al-undepleted with Al_2O_3/TiO_2= 18, CaO/Al_2O_3 = 1.1 to 1.5; and flat REE patterns (Chavagnac, 2004). It is hard to distinguish sheet flows from subsequent intruded sills. This part of the formation contains more pyroxene spinifex, which is associated with komatiitic basalts (Brandl *et al.*, 2006, de Wit *et al.*, 2011). The upper Komati Formation has not been analysed and studied in enough detail to divide the komatiitic basalts into distinct flow fields (Dann & Grove, 2007).

2.6 Summary and Conclusions

Due to its well preserved nature and age, the Barberton Greenstone Belt gives unique insight into processes occurring during the Archaean Period. The Onverwacht, Fig Tree and Moodies Groups, which make up the BGB, span a range of ages from 3.55 to 3.1 Ga. The Onverwacht consists mostly of volcanic lavas with minor sedimentary (sandstone, shale and chert) horizons, which indicate periods of quiescence. The Fig Tree Group consists of fine sandstone, shale and cherts with minor volcaniclastic deposits and is thought to have formed in a fan-delta and shallow to intermediate subaqueous environments. The Moodies Group is associated with terrestrial deposition of sands, shales and conglomerates in fold-and-thrust basins. Surrounding the Barberton Greenstone Belt (BGB) are plutons from two emplacement events: Tonalite-Tronjhemite-Granodiorite during the Onverwacht deposition and the Granite-Monzonite-Syenite during and post Moodies Group deposition. The BGB has undergone five distinct deformation events, most of which involve folding and thrust faulting. The alteration of the BGB is mostly to greenschist facies, with amphibolite facies occurring in the contact aureole of the plutons.

The aim of the study is the Komati Formation of the Onverwacht Group. The Lower Komati Formation consists of a unique tumulus unit and five differentiated komatiite flow packages, with massive komatiites and komatiitic basalts present between the differentiated packages. The komatiites in this section are Al-depleted (Al_2O_3/TiO_2 =8-12) and have slight HREE depletion. The Upper Komati Formation consists mainly of komatiitic basalts and contains more pyroxene spinifex than the Lower Komati Formation. The komatiites are Al-undepleted (Al_2O_3/TiO_2= 18) and have flat REE patterns. The primary minerals (olivine, pyroxene, chromite and glass) have been largely, but not completely, replaced by secondary hydrous minerals.

CHAPTER 3

KOMATIITES – OCCURRENCE AND ORIGIN

3.1 Introduction to Komatiites

Komatiites have been identified around the world from as early as the 1920's but were not recognised as a distinct extrusive ultramafic rock type until 1969 (Arndt *et al.*, 2008, Hill, 2001, Viljoen & Viljoen, 1969). The Viljoen brothers, Morris and Richard, during their field mapping of the Barberton Greenstone Belt, discovered high-magnesian volcanic rocks and concluded that these were not merely magnesium-rich basalts, but rather the extrusive or volcanic equivalents of ultramafic peridotitic rocks. These ultramafic lavas were termed *komatiite*, after the type location near the Komati River which flows through the Barberton Greenstone Belt. Since the recognition of komatiites as a unique magma type, many occurrences of these rocks have been identified and studied world-wide.

Komatiites are found predominantly in Archaean greenstone belts, with a few examples in the Proterozoic and a single example in the Phanerozoic (the Gorgona Island komatiites, Colombia) (Arndt *et al.*, 2008). This skewed distribution through geological time indicates that the main komatiite-forming conditions were in the Archaean, and that these conditions became effectively absent in the Proterozoic.

Komatiitic basalts are high-magnesium basalts that have a clear link to komatiites via texture, petrology and geochemistry. Komatiites and komatiitic basalts are found associated in certain localities.

3.2 Mode of Occurrence - Lava Channel/ Flow Field Processes

Since there are no komatiite flows currently forming on the Earth, it is not possible to directly evaluate the flow process of komatiite lavas. Flow-field processes in modern basalts have been studied in detail (Anderson, 2012, Hon *et al.*, 1994) and can be used as a proxy for komatiite-flow processes. Using the known basalt flow processes together with the results of komatiite field mapping, a good understanding of the processes of komatiite emplacement is obtained.

Komatiites are low-viscosity lavas because of their high MgO contents and high temperatures that therefore created extensive networks of lava tubes and flow fields (Arndt et al., 2008).

Dann and Grove (2007) define flow fields (or flow units) as layers of lava that erupted within a short time period, which have similar geochemical compositions. Sediment horizons (when they occur) indicate a break in volcanism and hence the limits of a flow field. Alternating komatiites and komatiitic basalts are further indicators of different flow fields. Individual komatiite flows are typically between 0.5 and 5 m thick, but they usually occur as a series of compound flow units, which often reach tens of meters in thickness and up to 60 km in length (Arndt et al., 2008). Komatiites were emplaced both as surface flows and near-surface sills (Dann, 2001). Viljoen et al. (1983) cite evidence such as basal and upper chill margins, hyaloclastite breccias and palagontic alteration (quench alteration associated with intrusion into sea water (McPhie, 1993)), for their extrusive nature.

An important process identified during the extrusion of basalts, and thus also applicable to komatiites, is the concept of flow inflation (Barnes, 1985, Hill, 2001, Kauahikaua *et al.* 1998) (Figure 3.1). As lava erupts, it forms a quenched skin on its outermost surface and at the front of the flow lobe. During continuous extrusion and advancement of the flow lobe, this quenched skin insulates the inner part of the flow, allowing the magma to remain liquid for longer. The lava directly beneath the chilled skin becomes visco-elastic due to its slower cooling rate. This visco-elastic rheology can inhibit forward movement of the flow and when this occurs, the volume of lava within the flow channel begins to build up, causing the outermost skin to bulge and expand. This is the process of lava inflation. In some instances the influx of lava is too great and the pressure causes a fracture in the skin of the flow lobe, known as a *breakout*. This creates a new flow lobe and the entire process of flow propagation, advancement and inflation is repeated until a new breakout occurs. The repeated and continuous break-outs and formation of new flow lobes from older ones creates a network of lava channels (Arndt *et al.*, 2008). These are adjacent to or overlie one another, making it difficult to correlate flows at a distance (Figure 3.2). A single flow or channel can also coalesce with adjacent channels to form a sheet flow. Huppert *et al.* (1984) indicate that komatiite lavas would have been turbulent flows, which explain the transport of olivine crystals. The thermal gradient between the surface and interior of the flow accounts for the crystallization of spinifex crystals (Faure *et al.*, 2006).

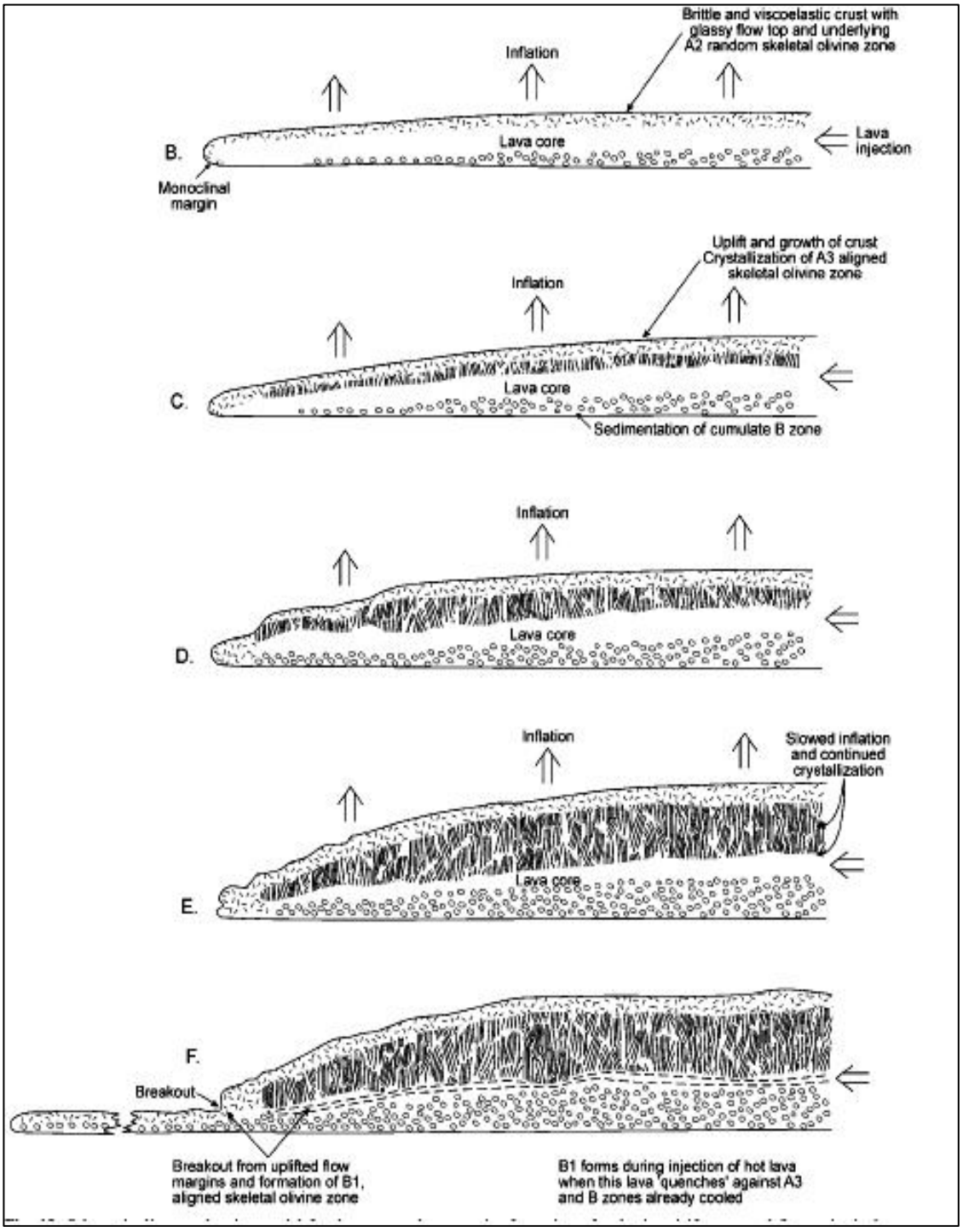

Figure 3.1:
Step by step process of inflation of a lava channel by Hill (2001)

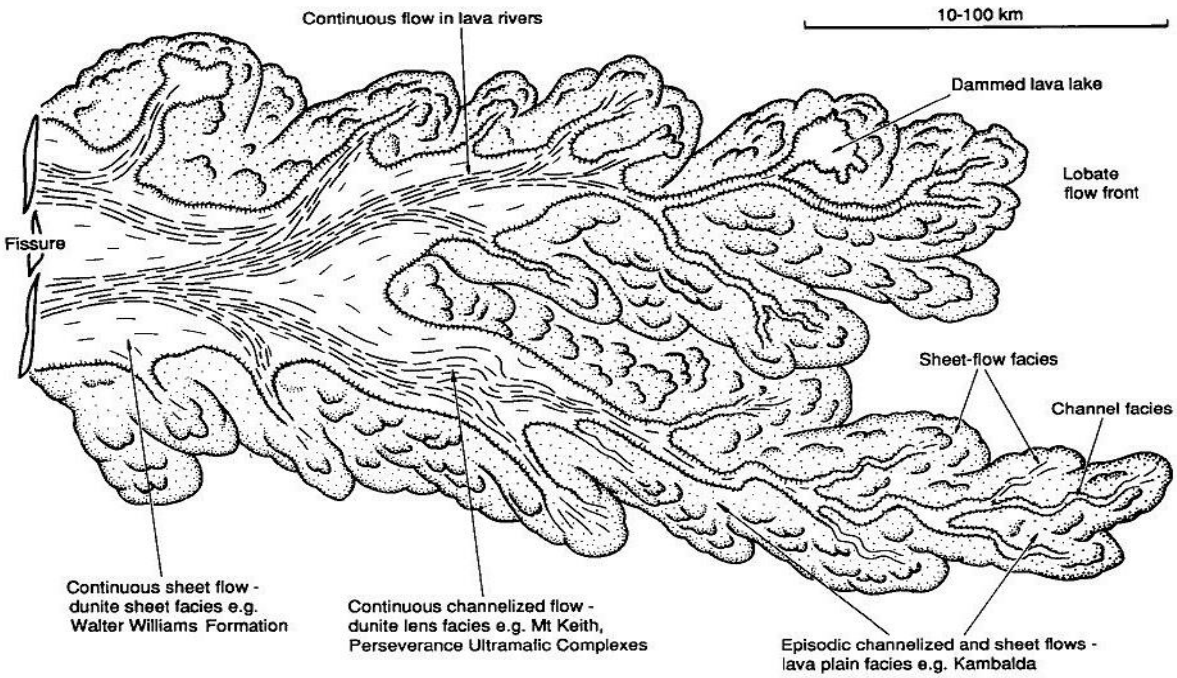

Figure 3.2
Flow lobe generation and growth of komatiite lava channels to create an extensive network of flows. (Hill *et al.*, 1995)

3.3 Textures

Komatiite rocks have become famous for their unique and interesting textures. Most notable is spinifex texture, named after the spinifex grass (*Triodia spinifex*) of Australia, with which it shares a similar shape. Other common textures in komatiite flows are olivine cumulates, chill margins, radiating and aligned spinifex blades, pillow structures and hyaloclastite breccias (Arndt *et al.*, 2008, Faure *et al.*, 2006). The best documented textures form in the differentiated komatiite flows which are divided into various sections depending on their textures, as illustrated by Pyke *et al.* (1973) and later by (Faure *et al.*, 2006) These are (Figure 3.3):

A1: Chilled fractured flow top

A2: Spinifex zone: random and platy, oriented large grains

B1: Foliated olivine (not always present)

B2: Peridotite zone, phenocryst olivine

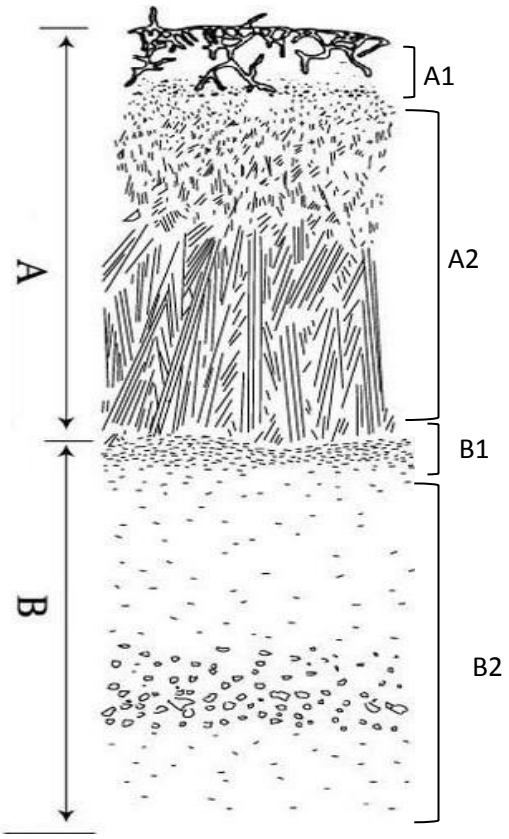

Figure 3.3
Textural sections through a typical komatiite flow. A) Indicates the spinifex and B) indicates the cumulate. (Pyke *et al.*, 1973)

The base of the flow consists of olivine cumulates (layers B1 and B2), which grade into platy olivine spinifex (A2), random spinifex and fine grained spinifex with height. The flow is capped by a chill zone (A1) (Pyke *et al.*, 1973, Viljoen *et al.*, 1982). This volcanic layering is attributed to the high temperature and low viscosity of komatiite liquids. The low viscosity allowed rapid eruption, formation of extensive flow networks and rapid settling of olivine crystals. The magmas erupted at temperatures of 1600°C and contained olivine phenocrysts in suspension, which were able to settle out of the liquid as the magma flow slowed down. This resulted in an accumulation of olivine crystals on the floor of the flow, which grew larger *in situ* during lava cooling. The second crystal phase that formed was pyroxene at 1200 °C, indicating a large temperature difference between the first and second forming phases. This large temperature difference allowed the basal zone of the flows to accumulate abundant olivine crystals before pyroxene could crystalize (Arndt *et al.*, 2008).

Spinifex was formed by the crystallization of olivine grains within a temperature gradient between the roof and the centre of the flow. Olivine crystals forming in the temperature gradient preferentially grew downwards into the hotter interior of the flow unit, because

growth occurred more effectively in the hotter interior. Various types of spinifex have been identified and are summarized by Donaldson (1982):

1-Radiating (or random) spinifex: randomly arranged blades up to 2cm long
2-Porphyritic spinifex: skeletal, hollow, euhedral olivine phenocryst containing spinifex
3-Plate spinifex: parallel, platy olivine/pyroxene crystals with a glass groundmass
4-Bladed olivines: euhedral outlines but dendritic internal features
5-Close packed equant olivines surrounded by bladed pyroxene

Due to the variability in nature of the flows, the cumulate and spinifex textures may be continuous up to tens of meters along strike, but are known to diminish or pinch-out over short lateral distances. This makes lateral correlation between komatiite flow units difficult.

3.4 Petrography and Alteration

Komatiite flows originally contained three main minerals that are found in different textural forms, now pseudomorphed to varying degrees by secondary hydrous phases. The dominant mineral found is olivine, which occurs as euhedral cumulates and as blades of spinifex. Pyroxenes are present as both cumulate and spinifex in certain types of komatiite. Three types of pyroxene are found in komatiite flows – pigeonite, augite and orthopyroxene. They occur as elongated skeletal spinifex crystals; as euhedral cumulates within the cumulate zone, and as small needles and feathery/frond growths (Arndt *et al.*, 2008). Small, irregular pyroxene grains form fan like/feathery needles or occur as curved, stubby prisms within the matrix of spinifex textures. Chromite is the predominant oxide mineral formed in komatiite lavas, but only makes up 3% of the mineral assemblage. It is observed as euhedral and skeletal or dendritic grains in spinifex zones (Arndt *et al.*, 2008, Godel *et al.*, 2013). Plagioclase is a rare mineral in komatiites although Arndt *et al.* (2008) indicate its presence in the interior of thick flows and more commonly in komatiitic basalts. Glass is identified in a devitrified but still anhydrous form in the Cretaceous Gorgona komatiites. However, in komatiites of Archaean age, the glass phase has been completely altered and recrystallized into metamorphic minerals and is only preserved as melt inclusions in olivine and chromite grains.

Archaean terrains have undergone multiple episodes of chemical and physical alteration, therefore the petrology and geochemistry of komatiites should always be interpreted with

care. The alteration is both temperature and pressure dependant, but also depends strongly on the bulk composition and mineralogy of the rocks that have undergone alteration. Komatiites that have undergone greenschist metamorphism contain minerals such as serpentine, chlorite, magnetite, talc, actinolite and tremolite (Arndt & Nisbet, 1982, Dann & Grove, 2007, Viljoen *et al.*, 1983). Olivine most commonly alters to serpentine. Pyroxenes are predominantly altered to a combination of tremolite and chlorite, whilst the groundmass is often converted to an indistinguishable combination of tremolite, chlorite and serpentine. The chromite grains are usually surrounded by a secondary rim of magnetite (Barnes, 2000, Parman *et al.* 1997, Robin-Popieul *et al.*, 2012). Arndt *et al.* (2008) note that carbonatisation in komatiite rocks results from post depositional alteration and often post-dates the greenschist-facies metamorphism.

3.5 Geochemistry

Komatiites are ultramafic lavas characterized by a variety of geochemical and textural features. They are defined geochemically, as rocks containing MgO>18%, SiO_2<54%, K_2O and TiO_2<0.9%, and CaO/Al_2O_3 > 1. These parameters exclude komatiitic basalts but include some non-komatiitic cumulate rocks. Hence textural features such as spinifex, which is closely associated with komatiite rocks, can be used as a means of distinguishing komatiite from other high magnesium volcanic rocks. A further feature of most komatiites (but not certain types of Barberton komatiites) is that they have slightly depleted LREE and low Ti, Nb, Y and Zr values, which can be used as a further diagnostic tool together with Al_2O_3/TiO_2<25 (Arndt *et al.*, 2008, Chavagnac, 2004, Nesbitt *et al.*, 1982).

Komatiites can be divided into three major groups depending on their aluminium (Al_2O_3) content: (1) Al-undepleted, (2) Al-depleted and (3) Al-enriched. This characteristic is quantified by the Al_2O_3/TiO_2 ratio, which commonly correlates with the $\left(\frac{Gd}{Yb}\right)_n$ ratio (Arndt *et al.*, 2008, Arndt & Nisbet, 1982, Chavagnac, 2004). The two most common types of komatiite found in Barberton are Al-undepleted (type 1) with Al_2O_3/TiO_2 =20, CaO/Al_2O_3< 1.1, $\left(\frac{Gd}{Yb}\right)_n \cong 1$, and Al-depleted (type 2) with Al_2O_3/TiO_2 =10, CaO/Al_2O_3< 1.33, $\left(\frac{Gd}{Yb}\right)_n \cong 1.4$ (Chavagnac, 2004, Jahn *et al.*, 1982). The origin of the two types of komatiite is discussed by Arndt and Nisbet (1982), Parman *et al.* (2004), Parman *et al.* (2003), Robin-Popieul *et al.* (2012), Smith and Erlank (1982).

Komatiitic basalts have lower MgO content of 12-19 wt.% (Viljoen *et al.*, 1983). They are spatially and chemically linked to komatiites and are thought to represent interim compositions between komatiites and basalts (Arndt & Nisbet, 1982, Cameron & Nisbet, 1982).

3.6 Implication and Role of Komatiites to Determine Archaean Mantle Conditions

The high MgO content (19-30 weight %) means that komatiites have high melting temperatures (1380-1600°C) which are up to 400^0 C higher than the eruption temperature of present-day mid ocean ridge basalts. This implies that the Earth had a hotter mantle in the past, specifically during the Archaean. Barberton komatiite liquid compositions have some of the highest MgO content and hence define the highest melt temperature in the history of the earth (Nisbet *et al.*, 1993) They can also provide an estimate of the composition of the Archaean upper mantle and give insight into tectonic processes occurring at that time (Donaldson, 1982, Nisbet, 1982).

3.7 Summary and Discussion

From the time of their discovery as a new volcanic rock type, komatiites have been studied in detail because they formed via conditions in the mantle of the Archaean, which are no longer present on Earth. The petrography and chemistry of these rocks provide information about the Archaean mantle and crustal conditions, as well as lava source compositions. Textures and flow conditions give insights into processes which occurred within each flow. This can be compared to modern day flow processes occurring in basalts.

The Barberton Greenstone Belt is one of the oldest and best preserved belts in the world, making it an exceptional study area. Outcrops containing textural and contact relationships are not always well preserved and this inspired the ICDP (International Continental Drilling Program) to initiate a Barberton Drilling project to obtain core samples of continuous sections from the Komati Formation. These cores now allow a clearer understanding of the textural relationships in individual komatiite flows and between adjacent flows. Their better preserved chemistry and petrography will contribute to a clearer and more detailed understanding of the Archaean mantle processes and komatiite flow field processes.

CHAPTER 4

METHODOLOGY AND SAMPLING

4.1 Introduction

The International Continental Drilling Program (IDCP) diamond drilled holes in the Komati Formation to produce information about rock types, contacts and structures that are not exposed in surface outcrops. The BARB 1 and BARB 2 cores, which are located in the Tjakastad area of the lower Komati Formation, in the southern part of the Barberton Greenstone Belt (Figure 2.1), yielded a continuous section through part of the Komati Formation, allowing individual flow units to be identified and geochemically compared to one another. The cores consist predominately of komatiite and komatiitic basalt and the BARB 1 core contains a unique tumulus structure.

This master's project consists of two major sections; 1) detailed geochemical and petrological analysis of the BARB 1 and BARB 2 cores and 2) petrographic analysis of outcrop samples that contain some unaltered olivine and pyroxene. The samples used for this project are taken from the BARB 1 and BARB 2 cores.

4.2 BARB 1 and BARB 2 Cores

The BARB 1 and BARB 2 cores were drilled in close proximity within the base of the Komati Formation. The location was near the Komati River, a few hundred meters west of the Spinifex Stream locality; the type locality of the Komati Formation. The BARB 1 core was drilled to sample the tumulus unit and was initially planned to be only 150 m in length. The BARB 2 core was planned to be 800 m in length and aimed to obtain samples of the rock-types and contact relations of the lava flows through the Komati Formation. Due to an apparent lack of fresh minerals, the BARB 2 drilling was terminated at 431 m, and the drill rig was returned to BARB 1 where a further 250 m was drilled.

The core was logged in the field during July 2011 before being transported to the University of the Witwatersrand for further logging, analysis and storage. This study began with a second round of core logging of BARB 1 and BARB 2 cores, once they were at the University of the Witwatersrand.

4.3 Core Log

The core was washed, and centre lines were drawn. Wherever possible, the core was oriented using the down-hole mark where it was visible. The initial objective of this project was to log the tumulus unit of the BARB 1 core, but subsequently all of the BARB 1 and BARB 2 cores were logged. The core was logged on a detailed scale, and features such as changes in spinifex length/ orientation and cumulate grain sizes were noted and incorporated into the logs. Rare but important features such as vesicles were also noted, even though they usually occur confined to thin 10 to 50 cm horizons. The focus of the logging was the mineralogy, textures and contact relationship between adjacent flows. Veining and shear zones were noted, and in many cases it was difficult to distinguish the brecciated chill margins from networks of veins.

The logs for BARB 1 and BARB 2 were prepared using a free core logging program called Core-view, developed by Visidata (Pty) Ltd. This program allows for storage of all data related to the core, such as assays, sample positions, photographs and provides the opportunity to produce summary core logs of important features. It also allows comparison of specific aspects of the core, such as stratigraphic position, assay results and alteration to establish possible relationships. The full core logs for both BARB 1 and BARB 2 can be found in Appendix A. It should be noted that the core lengths given in the log do not represent true stratigraphic thicknesses, but rather apparent thickness created by the 45° angle between the core and the sub-vertically dipping flows.

4.4 Field Sampling

An ICDP-sponsored drilling workshop was held in Johannesburg during February 2013 in order to establish procedures of sampling for the five BARB cores. A three-day field trip to the drill sites followed the workshop. During this field excursion, an afternoon was spent at the BARB 1 and BARB 2 drill sites to observe the surface outcrop of the corresponding drill cores. Previous petrographic studies had revealed the presence of unaltered pyroxene and olivine kernels in the cumulate zones of komatiite flows collected on the surface directly above the BARB 2 drill site. Three additional samples were taken of the cumulate zone, spanning an along-strike distance of 25 m from sample 1 to sample 3. These samples were taken to reinvestigate fresh igneous minerals, in the hope of identifying their unaltered equivalent in the BARB 2 core. Similarly, on the surface corresponding to the BARB 1 core,

three samples were taken to compare the surface exposure of the tumulus unit with corresponding units in the core.

4.5 Sample Selection

Though surface samples were taken, the focus of this study is the core, and most sampling was of the BARB 1 and BARB 2 cores. The methods used were geochemical, petrographic and textural analysis and therefore samples were chosen that contained minimal veining, brecciation and conspicuous alteration, such as bleaching of the rock within contact aureoles of intrusions.

A further objective of this study is the comparison between packages of differentiated komatiites at different stratigraphic heights in the Komati Formation. Three of these differentiated komatiite packages were identified in the BARB 1 and BARB 2 cores and were sampled in detail. The tumulus section was sampled on a metre-scale, whilst the differentiated komatiite packages were sampled on a 10-20 cm scale. All rock-types present were characterised and each textural section of the differentiated flows were sampled. The detailed sample suites consist of 31 samples from the BARB 1 (89-118 m) differentiated package, 44 from the BARB 1 (378-420 m) differentiated package and 29 from the BARB 2 (252-274 m) differentiated package. To gain insight into the changes that occur between individual flows, samples were taken close together. An attempt was made to sample each section of each flow, but in some instances the core was highly altered or not structurally intact, and samples were not taken in these zones.

4.6 Sample Preparation

Once the samples were selected, the sample position within the core (top-bottom), together with the rock-type, was noted on the core tray and in a notebook. The information was later transferred to electronic format Samples were cut in half down the orientated centre line. One half was retained in the core tray as a record of the core, whilst the other half was cut again to yield quarter-core samples. One quarter sample was allocated for geochemical analysis and the other for the preparation of a thin section.

The geochemical quarter core was scrubbed and left to dry for 24 hours. Each sample was then collected and placed in a clean, clearly labelled sample bag. These samples were crushed using a Mo-hardened jaw crusher and milled, in a pure C-steel pot, to a fine powder. The jaw

crusher and miller are manufactured by Dickie & Stockler (Pty) Ltd. Care was taken to clean the equipment by milling pure quartz between each sample, so as to minimize the possibility of contamination. To prepare samples for X-ray fluorescence (XRF) analysis, the powders were put into small aluminium containers which were pressed into pellets by a 10 ton press. A portion of the left over powder was used for ICP-MS analysis. For details about the XRF and ICP-MS sample preparation and analysis procedure, the reader is referred to Appendix D.

4.7 Petrographic Analysis

100 samples were taken for petrographic analyses. These samples were cut and mounted on glass slides to prepare standard 0.3 mm thick thin sections. These thin sections were analysed and photographed under a petrographic microscope, with the aim of gaining insight into the textural and mineralogical features of the tumulus and the differentiated komatiite flows. Thin sections were not made for fine grained material because this chilled material is highly altered and does not yield useful information on mineralogy or textures. In addition, many of the fine-grained chills were highly veined and turned to rubble, making it difficult to create a thin section. Photomicrographs of the thin sections were taken on an ALTRA 20 Soft Imaging System, attached to an Olympus U-TV0.5XC-3 microscope. The summarized petrographic results and photomicrographs can be found in Appendix B and Appendix C respectively.

4.8 Geochemical Analysis

A set of 152 samples was taken from the BARB 1 core, whilst 73 samples were selected from the BARB 2 core for geochemical analysis, creating a total of 225 samples for the thesis. The sample set includes samples of all rock types encountered in the cores. The aim was to sample the core at consistent intervals. In four selected sections of the core (three differentiated komatiite packages and the tumulus unit), detailed sampling has been done.

The three differentiated komatiite flow packages contain between 8 and 12 differentiated flows, hence sampling in these packages was on a centimetre scale so that each texture of each flow could be sampled, to allow for a more detailed comparison. Thus 30-40 samples are taken over 30-50 m intervals from each of these differentiated packages.

The tumulus sampling consists of 38 samples taken over 100 m. Due to the relatively homogeneous nature of individual units in the tumulus structure, more detailed or closer sampling was not considered necessary.

All 225 samples were analysed using XRF to determine major and minor element compositions. 75 of these samples were also analysed using ICP-MS methods, to determine their trace element compositions. The aim of the project is to study the igneous history of the lavas and since these lavas are normally assumed to be anhydrous, a simple calculation must be done to recast the data from hydrous to anhydrous. The major element analyses are anhydrous because Loss of Ignition (LOI) is analysed for, but the trace elements need to be converted to anhydrous values. To convert trace elements to anhydrous values, the value of the element must be multiplied by a conversion factor *K*, to account for the hydration.

$$K_{Sample\ x} = \frac{Total_{Sample\ x} + LOI_{Sample\ x}}{Total_{Sample\ x}}$$

Major elements (weight %) analysed are: SiO_2, Al_2O_3, Fe_2O_3, FeO, MnO, MgO, CaO, Na_2O, K_2O, TiO_2, P_2O_5, Cr_2O_3, NiO and LOI.

Trace elements (ppm) analysed are: Sc, V, Cr, Co, Ni, Cu, Zn, Ga, Rb, Sr, Y, Zr, Nb, Mo, Ba, Pb, Th, U, Li, P, Ti, As, Sn, Cs, Hf, Ta, W including the REE: La, Ce, Pr, Nd, Sm, Eu, Gd, Tb, Dy, Ho, Er, Tm, Yb and Lu.

The reader is directed to Appendix D for details concerning the sample preparation for the XRF and ICP-MS analyses. Appendix E contains the full geochemical analyses.

4.9 Infra-Red Analysis (Geospectral Imaging)

A final method of core analysis was used by a spectral imaging company, Geospectral Imaging. The company scanned all 3.5 km of the ICDP Barberton cores and allowed free access to the results in return for the use of the scanned imaging information, to create and refine the imaging processes and techniques.

The core was scanned in February 2013 and has since been processed and uploaded to the internet. Access is available through Geospectral Imaging http://www.geospectral.co.za/ upon request.

The company scanned each tray using a high resolution RGB (Red-Green-Blue) camera and an infra-red camera. This creates extremely high-resolution images, whilst the infra-red camera records spectral signatures of the minerals in the rock. The end result is a good quality scan of each tray, with the associated metamorphic mineralogy.

This study focuses on the scanned RGB images, which provide insight into the alteration present in the core, variations in the chemistry of the specific alteration minerals and can show down-hole data in a succinct manner. This online system makes the core available to scientists around the world for inspection, without the need to see the physical core.

CHAPTER 5

GEOLOGY AND STRATIGRAPHY OF THE TJAKASTAD SITE KOMATIITES

5.1 Introduction

The BARB 1 and BARB 2 cores contain a continuous section through a portion of the Komati Formation. Previously, only selected flows had been sampled from surface outcrops. These drill cores give a total of 700 m of continuous core, allowing rock units and contacts to be analysed and recorded. The core can therefore give a much more detailed insight into the structure of the flows, variation between adjacent flows and systematic variation with depth.

5.2 BARB 1 and BARB 2 Drill Sites and Stratigraphy Overlap

The strata of the Komati Formation have been deformed by a minimum of five recognised events (Dirks *et al.*, 2009, Lowe & Byerly, 2007), which have caused the layers to be tilted sub vertically, with an east-west strike. The deformation began with early horizontal thrusting and ended with several stages of folding.

5.2.1 Drill Site Location

The BARB 1 and BARB 2 drill sites are located in the komatiites of the Komati Formation in the lower Onverwacht Group. They are drilled from the Komati River valley into the side of a hill, in a northerly direction (Figure 5.1). In order to allow optimum stratigraphic intersection of the strata, the holes were drilled at the minimal possible angle of 45°, in a northerly direction perpendicular to the east-west strike of the flows. The BARB 1 hole consists of 420 m of core and the BARB 2 hole consists of 430 m of core, which would indicate that BARB 1 overlaps the stratigraphy of BARB 2. Due to the overturned/ sub vertical nature of the strata, the top of the BARB 1 core sampled the lowest stratigraphic horizons. As the core got deeper, it progressively intersected higher stratigraphic levels. Like BARB 2, the top part of the core sampled the lowest part of the strata.

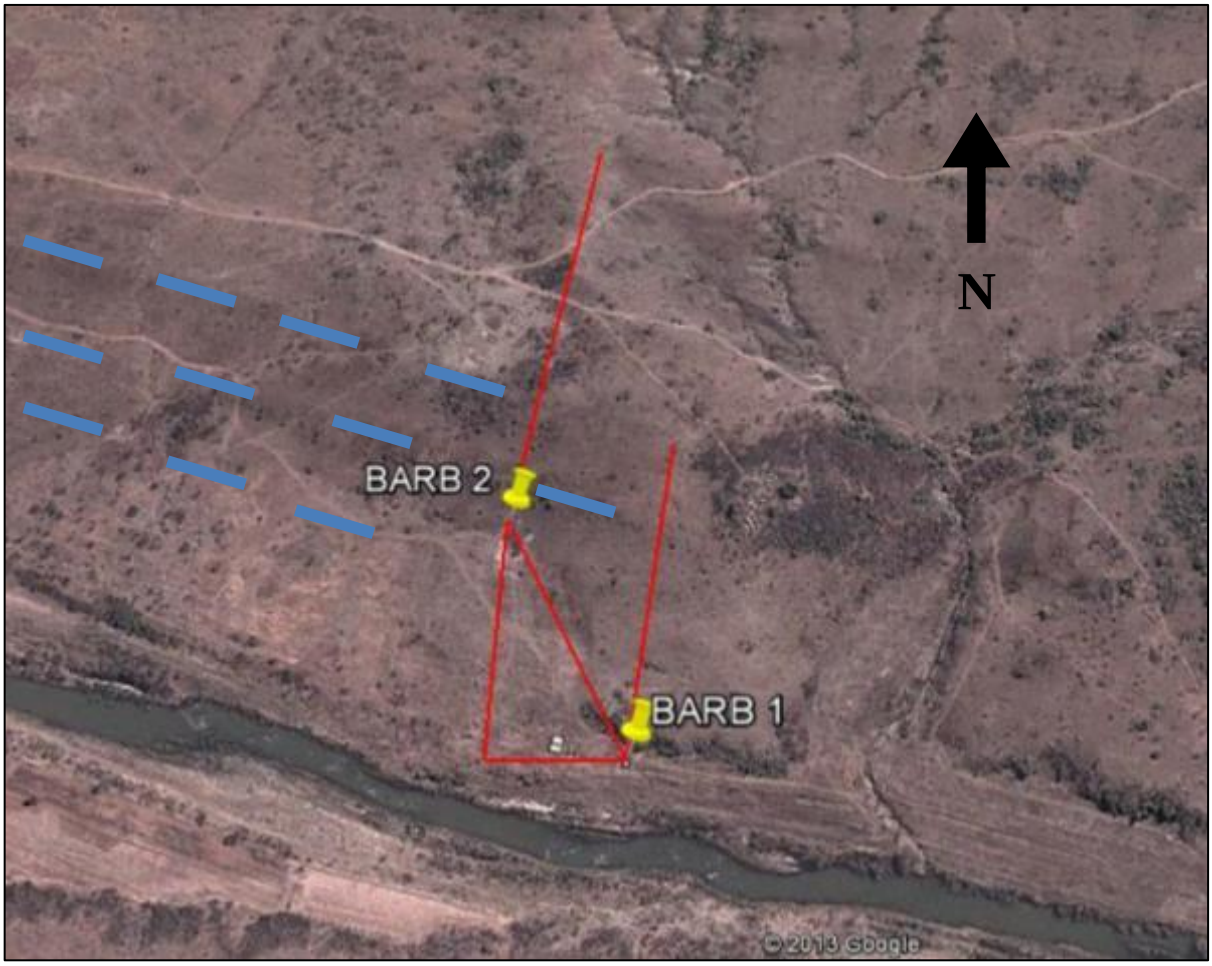

Figure 5.1:
Google Earth image of BARB 1 and BARB 2 positions, with approximated surface length of drill hole and approximate delineation of strata.

5.2.2 Theoretical Overlap

Since the BARB 1 hole was drilled to a greater depth than planned, there should theoretically be an overlap of the stratigraphic units sampled by the two cores (Figure 5.1). Confirmation of the overlap should be possible on the basis of physical and chemical comparisons of the cores.

Taking the co-ordinates of each hole, their distance apart, the difference in elevation, the depth and angle (inclination and azimuth) of each hole, the dip and strike of the strata and other necessary factors (Table 5.1), is it possible to determine the extent of the potential overlap in the intersected strata.

	BARB 1	BARB 2
Southing	25°58.926'S	25°58.840'S
Easting	30°50.678'E	30°50.626'E
Elevation	846	854
Bearing	005	008
Inclination	-48	-45
Length of core	419.9 m	431.47 m

Table 5.1: Summary of BARB 1 and BARB 2 core collar position and length

Using this information, it is possible to calculate the overlap in surface or plan view and in vertical cross section (Figure 5.2). Combining the two, the theoretical overlap can be evaluated. It is assumed that the strata have consistent strike and dip, that the layers are continuous over the distance between the two holes, and that faulting did not occur between the two sections (no evidence is found in surface outcrops).

5.2.3 Structural Integrity of the Core

The core is relatively intact and recovery was over 90%. Unfractured lengths are between 10 cm and 1 m in length, but in some sections the core is highly fractured. The breaks in the core have mostly occurred along serpentinized veins or in sections of less homogeneous material, such as at chill margins between flow units and in veins. Veins of serpentine and magnesite occur together. The extensive veining in small sections of the core causes the core to turn to rubble when it is split using a diamond cutter. Shear zones may also contribute to the fractured and fragmented nature of the core.

5.2.4 Visible Overlap

Using both geochemistry and the textural and petrographic features of the core logs, it is possible to ascertain whether the stratigraphy of the cores overlapped.

Simplified core logs of the overlapping section do not show any distinct layers that could be used to correlate the stratigraphy between the two holes (Figure 5.3). With this limitation in mind, there is no absolute evidence that a single layer or a suite of layers is continuous and can be uniquely correlated between BARB 1 and BARB 2. On a large scale, by grouping flows together and by allocating the groups as komatiite or komatiitic basalt, some patterns emerge that may be considered as an overlap. Additional possible evidence of correlation is

provided by several gabbroic layers, which exist in the expected positions within each core, but these may have occurred later and possibly be discordant intrusions. A complication arose because certain rock types may have been incorrectly identified and logged. There are instances where the rock type had been visually logged as one type, but the chemistry revealed it to be a different rock type. This came about because of the different degrees of alteration in various parts of the cores. Alternatively, the assumption that layers are continuous may be invalid and this may account for the fact that there is no evident overlap in the strata. However, the drill holes are only a small distance apart (150 m) and the flows appear to be continuous along strike in surface outcrops (Dann, 2001, Robin-Popieul *et al.*, 2012). Further mapping and more detailed analysis of the geochemical data may help to resolve this issue.

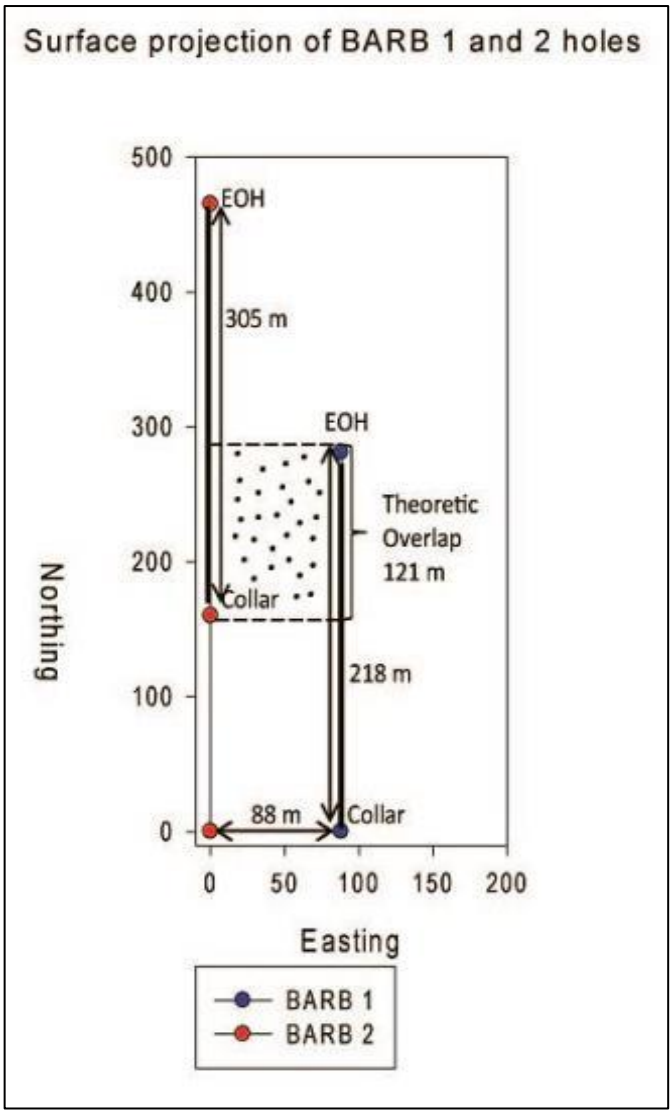

Figure 5.2 :
Theoretical surface representation of the BARB 1 and BARB 2 holes, including the length of overlap.

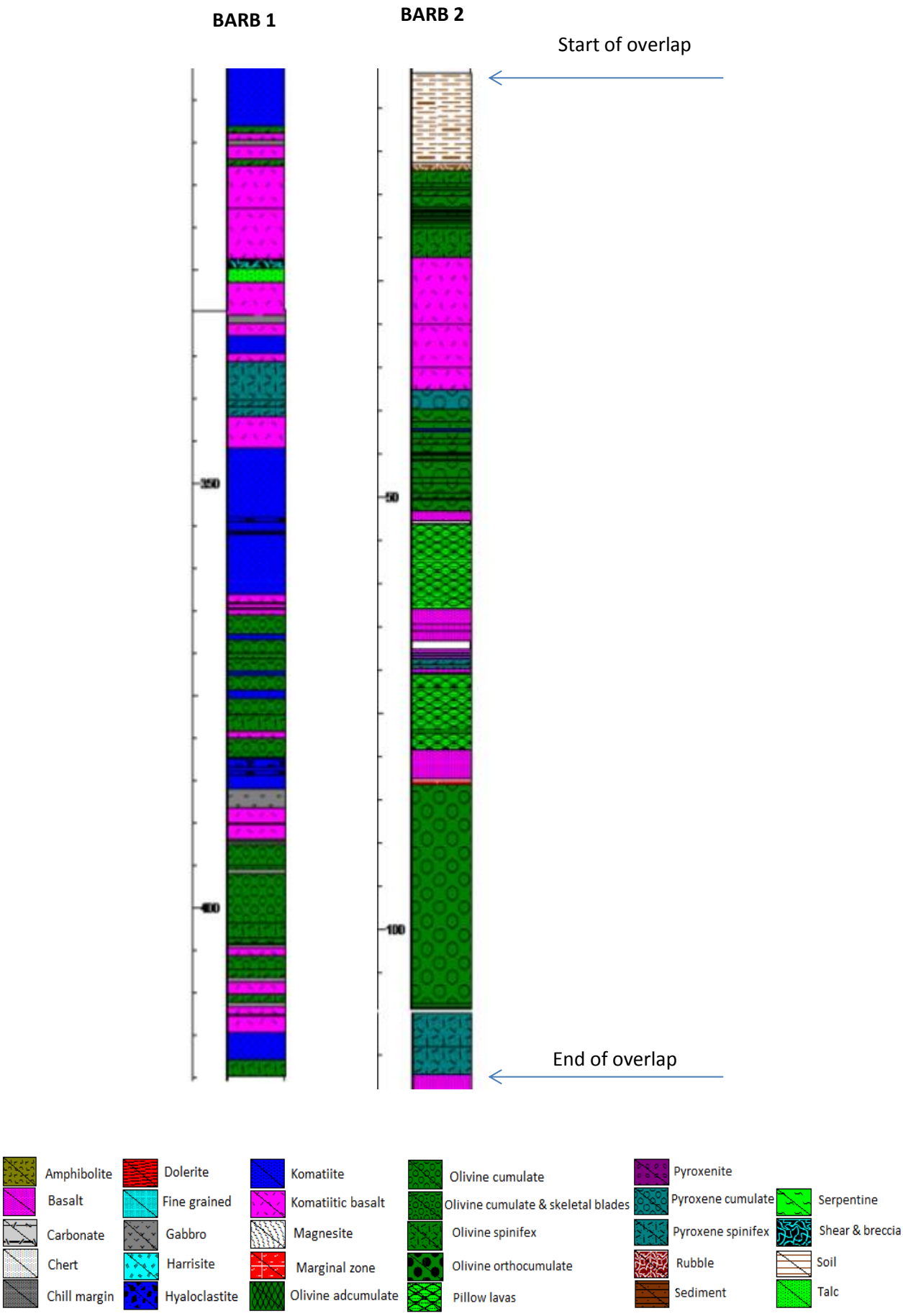

Figure 5.3:
Large scale illustration of theoretical BARB 1 and BARB 2 overlap in the core

5.3 BARB 1 and BARB 2 Core Description

The BARB 1 and BARB 2 cores contain essentially the same rock types, which can be grouped into ultramafic and mafic rocks. The basalts are commonly intrusive; however some of the gabbros and all the pyroxenites form as the final stage of crystallization within a differentiated flow. The BARB 2 hole intersected a higher level of the stratigraphy and in some places shows textures that are not evident in BARB 1.

5.3.1 Komatiites and Komatiitic Basalts

The ultramafic rocks are generally dark grey to black in colour, but some have a green tinge caused by the presence of altered olivine crystals (Figure 5.4). These are extrusive ultramafic rocks, hence are labelled *komatiites* and have the associated chemistry of komatiites, MgO >18%, SiO_2<50 %, with a low alkali content. These rocks are separated into different types depending on their textures (e.g. cumulate, spinifex), as discussed in Chapter 6.

The komatiitic basalts are a medium-grey colour with a green-brown tinge, which can vary to a lighter and greener shade (Figure 5.5). Komatiitic basalts have a 'veld-like' or speckled texture, which has been used to characterize them in the field and in the core (Figure 5.6). Pillows were mapped in surface outcrops (Dann, 2000) but because the core does not sample laterally, no unambiguous pillows are evident. However, white, tricuspate shapes are common in the komatiitic basalts (Figure 5.7) and these are considered to represent pillow selvages (the material found between pillows) (Figure 5.8). These basalts contain cream-white, 1-5 mm sized varioles in certain horizons.

Figure 5.4:
Komatiite in half core. Dark grey in colour with minimal textures evident.

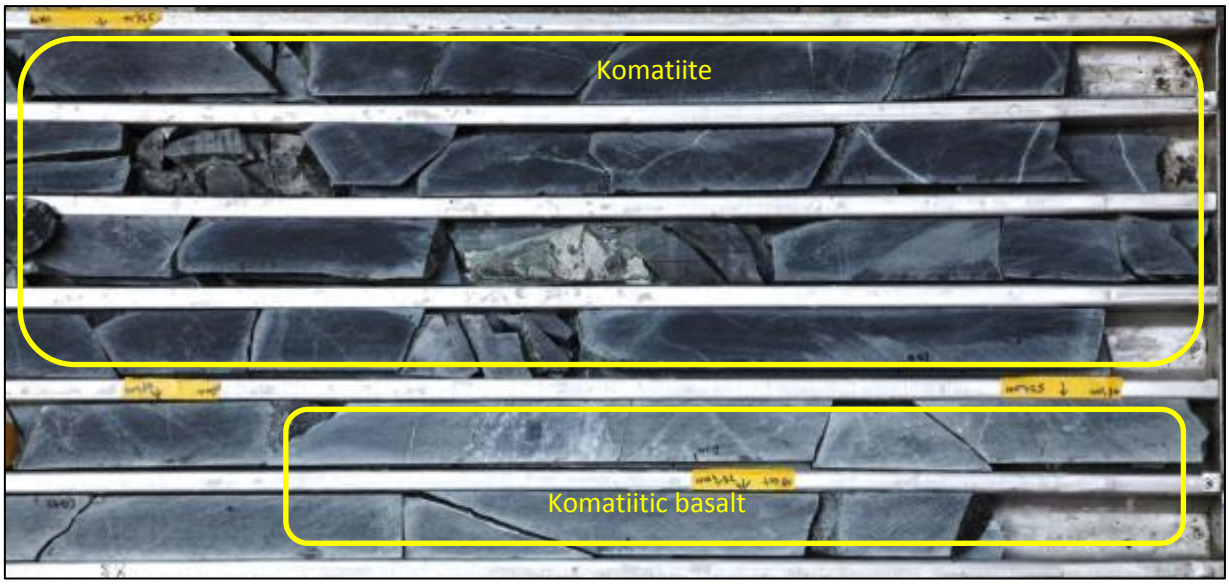

Figure 5.5:
Komatiitic basalt, showing the green-grey colour with a brown tinge and speckled 'velt like' texture on the core.

Figure 5.6:
Veld-like or speckled texture of the komatiitic basalt.

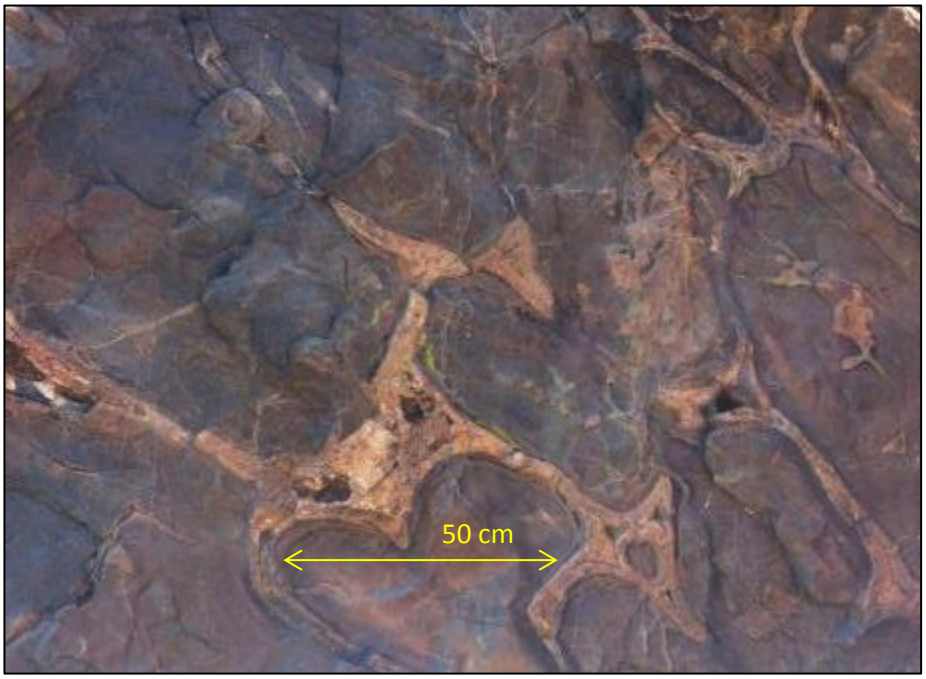

Figure 5.7:
Outcrop of pillow basalts, showing white tricuspate shapes between pillows. Image taken from the pillow basalts in the Hooggenoeg Formation to illustrate the tricuspate inter pillow material.

Figure 5.8:
Pillow selvage as seen in the BARB 1 and BARB 2 core.

5.3.2 Basalts

The basalts are fine-grained, and quite often contain pale, 1-3 mm wide, evenly dispersed variole-like features (Figure 5.9). These basalts are relatively easy to recognise as the majority have a unique blue sheen to their dark grey colour. They are also harder and less fragmented than the other rock types with a much smoother core surface than the komatiitic basalts and they generally have less late-stage veining. They are present as both extrusive and intrusive layers within the ultramafic volcanic pile. Figure 5.9 illustrates the chill margins of the intrusive basalt layer.

Figure 5.9:
Example of basalt from the half core. This specific image does not illustrate the common blue tinge to the basalts.

5.3.3 Dolerite, Gabbros and Pyroxenites

A single 17 m thick, dolerite dyke is present in BARB 1 between 120 and 137 m. This intrusion has a green-brown colour and a characteristic medium-grained homogeneous texture. The basal contact of the dolerite is sharp with the underlying differentiated komatiite flow. A 6 cm chill zone grades into the green-grey-colour of the dolerite. The dolerite has visible mineral grains and also contains a white variolitic texture similar to that of the basalts (Figure 5.10). The upper contact is not clearly discernible, but the dolerite becomes extremely fine grained and therefore a contact can be positioned reasonably accurately. There appears to be less veining in the dolerite than in the komatiites and basalts.

The gabbros are found as either intrusive units or as late-stage crystallization of thick ultramafic flows. They are dark green in colour and contain medium to coarse grained pyroxene crystals interspersed with lighter-coloured feldspar grains and have a homogeneous phaneritic texture (Figure 5.11). The gabbro layers range in thickness from 0.5 m to 7 m. Intrusive gabbros are typically found dividing a thick layer of komatiitic basalt. In these instances, the gabbro has a chill margin (but no brecciated contact) that clearly divides the

medium to fine grained komatiitic basalt from the coarse grained gabbro. These chill margins are evident in the gabbros in BARB 1 at 264 m and at 330 m. Typically, chill zones are only present at one end of the gabbro layer, the other end is commonly brecciated and highly veined, which destroys any evidence of chills or contacts.

The gabbros that formed via late stage crystallization typically grade from the surrounding rock type into the coarse grained gabbro. A distinctive gabbro layer is found in the tumulus unit of BARB 1. There are no chill zones at the margins of this unit; instead the rock grades over 30 cm into the surrounding pyroxene spinifex layers.

Like the gabbros, there is evidence that several pyroxenite layers formed as the final stage of crystallization of thick ultramafic flows. They are dark grey-green in colour and consist mainly of euhedral, medium to coarse (1-3 mm) crystals. Some contain elongated blades of clinopyroxene and minor feldspar is evident in the hand samples (Figure 5.12).

Figure 5.10:
Dolerite dyke contact with underlying differentiated flow, clearly showing variole like features similar to the basalts.

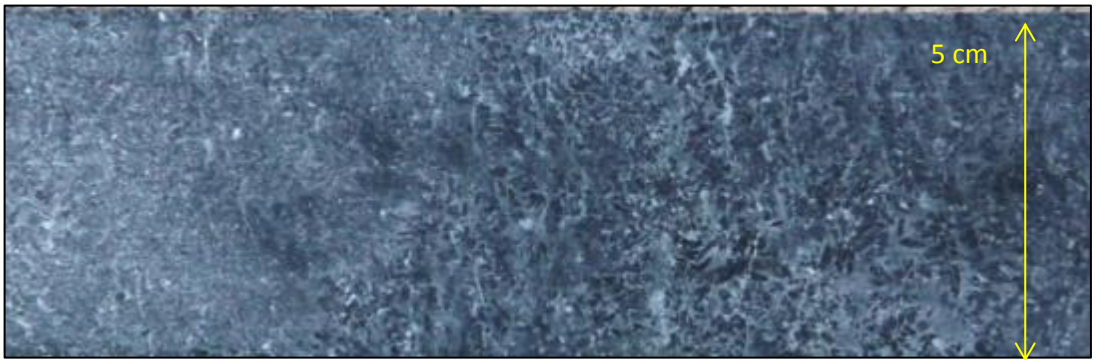

Figure 5.11:
Gabbro, showing coarse-grained pyroxene and feldspar grains.

Figure 5.12:
Pyroxenite associated with gabbro and late stage crystallization

5.4 Contacts between Flows

The ultramafic flows consist of differentiated or massive units. Using chill margins as indicators of individual flow margins, it is possible to accurately quantify the number of flows represented in the drill cores. However, it must be considered that due to the density of komatiite magma, the magma may not have always extruded onto the surface. Rather it may have intruded into the interior of previously erupted flows. In such cases there would be no distinct chill margins associated with the intrusive portion and the resultant composite flows may appear as a single flow unit.

The differentiated komatiite flows consist of an olivine cumulate base, overlain by either olivine or pyroxene spinifex and capped by a chill margin, occasionally with a distinct hyaloclastite breccia (Figure 5.13). Basal chill margins overlie the upper chill margins of underlying flows. This can lead to confusion as to the precise separation of the flows, unless a distinct contact is present (Figure 5.14). If a distinct contact is absent, but a chill margin is evident, it is possible to infer a contact. Textural features of differentiated flows can also be used to infer contacts. In cases where cumulate and spinifex layers are visible, but the spinifex is directly overlain by another cumulate layer (and no chill is visible), the following can be inferred: the overlying flow had eroded and destroyed the chill (Williams *et al.*, 1999) or it had intruded into the earlier flow before it had time to solidify. Using these inferred contacts and a basic understanding of the structure of a differentiated komatiite flow, the number of flows through the BARB 1 and BARB 2 sections can be determined with a reasonable degree of certainty.

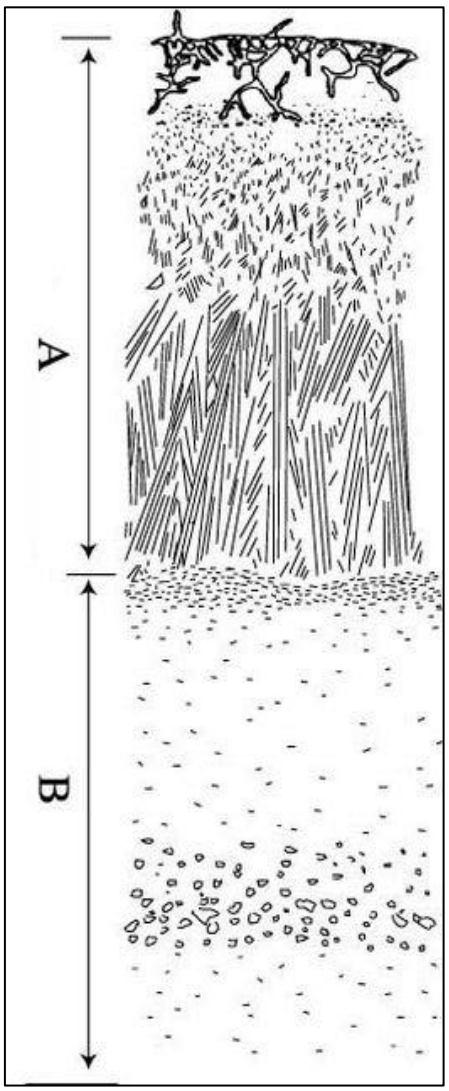

Figure 5.13:
Typical textural structure of a differentiated komatiite flow. (Pyke et al. 1973)

Massive komatiite flows contain few textural features that can distinguish them from each other. Distinct contact zones are very rare and chill margins are extremely important in order to define the top of a flow. Veining and alteration are problematic in massive komatiites because the alteration around a vein causes the rock to appear fine-grained and therefore resemble a chill margin. In some cases such 'pseudo-chills' can be confused with an actual chill, causing an incorrect definition of the flow boundary.

Komatiitic basalt flows, share some of the characteristics used to define the flow boundaries of komatiites. The lack of a lateral dimension in the core makes it difficult to determine the

extent of certain chill features. Hence a tricuspate feature (Figure 5.7) could indicate a pillow boundary or it may just be an alteration feature associated with a vein. Lack of lateral continuity of the core restricts the identification of pillow basalts. However, Arndt in 2012 identified unambiguous pillow features in the BARB 1 core at 284 m.

The extrusive basalts have distinct fine-grained chill margins on the border of the flows. In most cases the grains coarsen towards the centre of the flow. Notably, these basalts have a high concentration of vesicles adjacent to the chill margin, confirming the extrusive nature of the units (Figure 5.9).

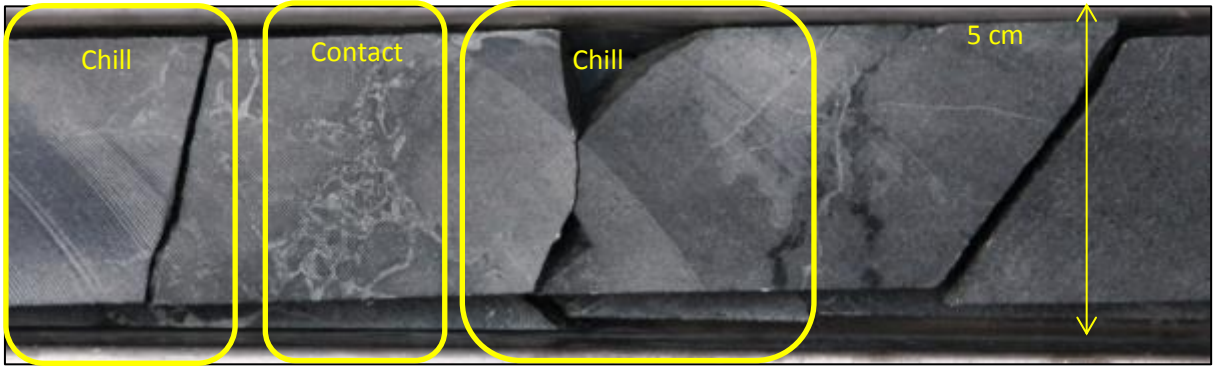

Figure 5.14:
Example of a distinct contact between differentiated komatiite flows

Some chills are distinct with clear hyaloclastite textures that imply extrusion into a wet environment, either sea water or wet sediment. Other chills do not have distinct contacts and rather consist of zones of finer grained material. These chills may not indicate surface extrusion but could represent the margins of shallow sub-volcanic sills (Dann & Grove, 2007). Alternatively the contact zone may have been eroded by the overlying flow.

These contact relationships are important to define the boundaries between flows. However it is assumed that each overlying flow-unit is distinct and younger than the underlying flow-unit. When dealing with komatiites and komatiitic basalts it needs to be appreciated that the low viscosity of the material allows for extensive flow fields. Hence, if a pillow forms above a flow and then develops into a new flow, two flows would exist that originate from a single entity. Geochemical signatures would determine whether the flows are genetically related, or if they are actually different flows.

5.5 General Stratigraphy of the BARB 1 Core

The BARB 1 core is from the lowest and therefore the oldest part of the Komati Formation. It samples an important volcanic feature identified by Dann (2000), Dann (2001) as a tumulus structure. This feature was intersected at the top of the BARB 1 core, implying that the tumulus is the lowest feature sampled by the drilling (due to the overturned nature of the strata). The remainder of the core consists of massive, differentiated komatiite flows and komatiitic basalts. A possible 2 cm thick, grey, fine grained, sedimentary layer was identified in the middle of BARB 1 at 251.5 m (BARB 1 Preliminary core log- Arndt, Chunnett 2011).

5.5.1 Number, Thickness and Flow Statistics

The number of flows was established by using the flow boundary and contact criteria described above. Approximately 85 flows were identified in the BARB 1 core. Due to the lack of chill margins in some sills and the possible elimination by erosion or alteration of certain chill margins, the number of flows may change upon further detailed evaluation of the core. The tumulus is dealt with separately, as it can be considered as a single major flow feature, or as a continuously fed, sub-volcanic magma channel.

The 85 flows consist of both differentiated and massive komatiites, komatiitic basalts and basalts. In cases where a flow may have intruded into another flow, the unit is counted as a single composite flow rather than two separate flows. Flow thicknesses are summarized in Table 5.2

Flow type	Number of flows	Thickness range (m)	Average thickness (m)	Standard deviation (σ)
Differentiated komatiites	25	1-3	2.97	2.24
Massive komatiites	37	0.5-10	3.46	3.34
Komatiitic basalts	18	1-9	4.40	4.96
Basalts	3	10	4.61	5.66

Table 5.2: Summary of flow types and thicknesses present in the BARB 1 core

Gabbro and pyroxenite layers are also present in the core, but these form as final stage crystallization of flows (pyroxenite) and as intrusions (gabbro). Hence, the gabbros and pyroxenites are not counted as individual flows, but rather as part of the flows in which they are contained, or as later intrusions.

5.5.2 Associations of Flow Packages in BARB 1

The tumulus at the top of the core sequence is considered in a later section. In BARB 1, differentiated komatiite flows occur in packages of 5 or more flows. Basalt and gabbroic layers are more commonly associated with the massive komatiite flows and the komatiitic basalt flows. The massive komatiites and the komatiitic basalts usually form thicker flows than the differentiated komatiite flows. The core shows an increase in the abundance of massive komatiites and komatiitic basalt towards the middle of the core length (from 225 to 345 m). As discussed later, some units that were logged as komatiitic basalts have been reclassified as komatiites on a basis of geochemical analyses.

5.6 General Stratigraphy of the BARB 2 Core

The 430 m BARB 2 core samples 225 m of stratigraphy with a probable 120 m overlap with the lower part of BARB 1: the BARB 1 interval from 300 to 420 m overlaps with the interval from 0-120 m in BARB 2. The rock types encountered are similar to those of BARB 1. The core in the deepest (stratigraphically highest) portion of BARB 2 contains thicker flows of differentiated komatiite. It has less massive komatiites and contains more komatiitic basalts than was encountered in BARB 1. Similarly, this core contains more evidence of pillow structures in the komatiitic basalts. BARB 2 does not contain a dolerite dyke, which is present in BARB 1.

5.6.1 Number, Thickness and Flow Statistics

The BARB 2 core intersected 65 distinct flows. However, the komatiitic basalts are commonly pillowed and therefore add a degree of uncertainty as they could represent a single compound flow consisting of many pillowed units instead of individual pillowed flows. Hence, for simplicity, the komatiitic basalt contacts have been counted as representing a single compound flow. Intrusive mafic sills are more common in BARB 2. For example: the cumulate layer of a komatiite flow appears to have been intruded by two basaltic layers: one layer occurs adjacent to a very fragmental and highly altered section of rocks, which may be a shear zone, whereas the second layer shows distinct contact zones. Furthermore, the cumulate bounded by the two basaltic intrusions is light green in colour and has a bleached characteristic, which decreases away from the contact (Figure 5.15) indicating the intrusive nature of the mafic layers.

The flow types and thicknesses are summarized in Table 5.3

Flow type	Number of flows	Thickness range (m)	Average thickness (m)	Standard deviation (σ)
Differentiated komatiites	41	0.5-10	3.50	3.64
Komatiitic basalts	18	2-23	9.82	11.72
Basalts	6	0.3-4	6.39	7.47

Table 5.3: Summary of flow types and thicknesses of the flows present in BARB 2

5.6.2 Associations of Flow Packages in the BARB 2 Core

As is expected, the BARB 2 core contains very similar rock groupings to the BARB 1 core, due to the close proximity of the drill holes. The BARB 2 drill hole is higher in the stratigraphy than BARB 1. The proportion of komatiitic basalts, increase with stratigraphic height (towards the base of the BARB 2 drill hole). Pillows are more abundant in the komatiitic basalt in this core. The differentiated flows are on average, thicker and, on the basis of visual estimates, have a larger cumulate-spinifex ratios (Table 5.2 and Table 5.3).

5.7 General Similarities between BARB 1 and BARB 2

Due to the general close proximity of the drill holes, and the fact that they sample a continuous section through the Komati Formation, it is expected that these two cores have very similar rock types and features. Both contain packages of differentiated komatiite flows, komatiitic basalts, basalts, gabbros and pyroxenites. Both cores are highly altered in places and veining is extensive in localized zones and pervasive throughout the cores. In parts of both BARB 1 and BARB 2 the concentration of veining produces very rubbly rock that might be related to early sea-floor alteration or to later deformation. Both drill holes are inclined at a similar angle and on a similar azimuth, which makes comparison between layer thicknesses easier as there is no need to adjust for the apparent thickness due to different angles. Texturally, aside from the tumulus, the cores contain cumulates, spinifex, chill margins, pillow basalts, and massive flows. The gabbros are commonly associated with massive komatiites and komatiitic basalts. The differentiated komatiite flows are typically thinner than the massive komatiites and komatiitic basalts. These textures give insight into the environment of deposition.

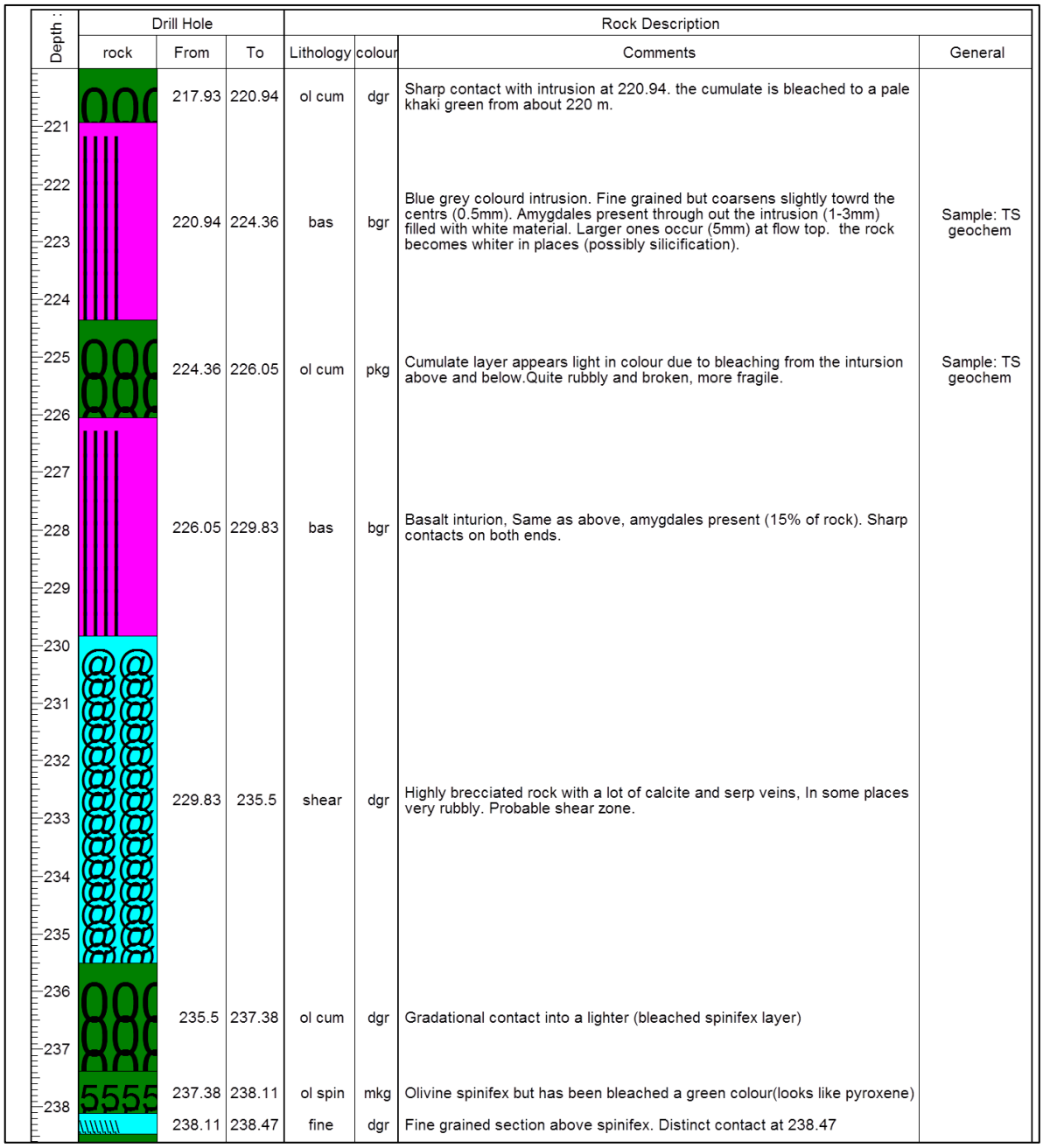

Depth :	Drill Hole			Rock Description			
	rock	From	To	Lithology	colour	Comments	General
221		217.93	220.94	ol cum	dgr	Sharp contact with intrusion at 220.94. the cumulate is bleached to a pale khaki green from about 220 m.	
222		220.94	224.36	bas	bgr	Blue grey colourd intrusion. Fine grained but coarsens slightly towrd the centrs (0.5mm). Amygdales present through out the intrusion (1-3mm) filled with white material. Larger ones occur (5mm) at flow top. the rock becomes whiter in places (possibly silicification).	Sample: TS geochem
223							
224							
225		224.36	226.05	ol cum	pkg	Cumulate layer appears light in colour due to bleaching from the intursion above and below.Quite rubbly and broken, more fragile.	Sample: TS geochem
226							
227		226.05	229.83	bas	bgr	Basalt inturion, Same as above, amygdales present (15% of rock). Sharp contacts on both ends.	
228							
229							
230							
231							
232							
233		229.83	235.5	shear	dgr	Highly brecciated rock with a lot of calcite and serp veins, In some places very rubbly. Probable shear zone.	
234							
235							
236		235.5	237.38	ol cum	dgr	Gradational contact into a lighter (bleached spinifex layer)	
237							
238		237.38	238.11	ol spin	mkg	Olivine spinifex but has been bleached a green colour(looks like pyroxene)	
		238.11	238.47	fine	dgr	Fine grained section above spinifex. Distinct contact at 238.47	

Figure 5.15:
Evidence for intrusive basalt sills. The green 0 symbol represents olivine cumulate. The green 5 symbol represents spinifex, the light blue layer at the base is the chill margin. Clearly the pink layers have intruded into the regular differentiated flow.

5.8 Summary and Discussion

The BARB 1 hole samples from the deepest part of the Komati Formation and includes a tumulus feature, as identified by Dann (2000). The remainder of the BARB 1 core and the entire BARB 2 core is composed of differentiated and massive komatiite flows, komatiitic basalt and basalts. It contains gabbros and pyroxenite layers that formed as later stage crystallization of thick flows or as later intrusions. Vesicles are very rare in the ultramafic lavas, but both vesicles and varioles are present throughout most of the mafic lavas. The flow types in BARB 1 are in general, thinner than in BARB 2, reaching a maximum of 10 m thick. BARB 2 samples are from a higher level in the stratigraphy than BARB 1 and contain an increase in komatiitic basalts with depth, or from higher in the stratigraphy.

There is a theoretical stratigraphic overlap between the base of BARB 1 and the top of BARB 2. This overlap is not evident in the core logs or visible in the core. The lack of a discernible overlap indicates that the flows were probably not laterally equivalent between the two drill holes. Alternatively the flows may be extensive but each core sampled a different textural section of the flow. The contact relationships between the different flows have been used to determine the number of flows in each core (85 in BARB 1 and 65 in BARB 2). The contacts are seen as fine- grained chills, which sometimes show extrusion of the lava into water. This is seen by the hyaloclastite breccia fragments, which occur when the lava enters the water and freezes. The other type of chill has less defined contacts and can be associated with intrusive sill contacts.

5.9 Conclusions

The drill cores from the lower Komati Formation reveal a sequence of rocks consisting solely of extrusive and near surface intrusive mafic and ultramafic units. The lavas make up a minimum of 367 m in true stratigraphy. The cores indicate previously unknown contact relationships. There is a theoretical overlap between BARB 1 and BARB 2, but correlation between the two sections cannot be made because of a lack of distinctive volcanic units. The two drill cores contain the same rock types and the flows have similar and comparable features. Komatiitic basalts become more prevalent towards the base of BARB 2, or height in the stratigraphy. BARB 1 samples approximately 85 different flows, while BARB 2 only samples 65 different flow units.

CHAPTER 6

DETAILED LITHOLOGICAL SECTIONS OF THE BARB 1 AND BARB 2 CORE

6.1 Introduction

Samples (petrological and geochemical) were taken at evenly spaced intervals throughout both cores to gain a broad appreciation of how the lithology and chemistry changes with depth. Each rock type was sampled to create a general reference suite that describes the BARB 1 and BARB 2 cores.

Four sections of interest were selected to obtain a more detailed study of chemistry and petrography. These sections include the unique tumulus feature from the top of the BARB 1 hole (referred to subsequently as "tumulus"), a 30 m section of differentiated komatiites immediately overlying the tumulus at 89 m ("BARB 1 (89-118 m) differentiated package"), a 40 m section of differentiated komatiites and komatiitic basalts at the end of BARB 1 ("BARB 1 (378-420 m) differentiated package") and finally a 20 m section of differentiated komatiites from BARB 2 between 252 and 274 m ("BARB 2 (252-274 m) differentiated package").

Each set comprise 30-40 geochemical samples and each sample was taken in close proximity to the previous one. The close sampling gives information on smaller scale processes that occurred within a single flow. Sampling adjacent flows in detail allows for a realistic comparison between flows and allows similarities in lava flow processes to be deduced.

The tumulus section is 90 m long, and has slightly wider sampling intervals. The larger sample spacing is appropriate, since the length of the different lithological zones in the tumulus extend over 10 meters and are internally homogenous, making sampling on a centimetre scale excessive.

The lengths given in this chapter are length in the core and do not represent true layer thickness. When describing the core, terms like "above" or "overlying" refer to the original stratigraphy, not to structural depth in the core as it was drilled.

6.2 Selected Sections from the BARB 1 Core

Three sections were selected for a detailed study in BARB 1. The tumulus feature identified by Dann (2000), Dann (2001) was sampled to obtain a better understanding of the volcanic processes that formed this unusual feature. The section directly overlying the tumulus contains some exquisite spinifex textures in the package of differentiated komatiites BARB 1 (89-118 m). The samples at the end of the hole BARB 1 (378-420 m) also sample a package of differentiated komatiites. Both differentiated sets were chosen as a means of comparing the chemistry and textural features between adjacent flows and flows at different stratigraphic heights. Similarly, the set from BARB 2 (252-274 m) is a means of comparing differentiated flows over depth and lateral distance.

6.2.1 Tumulus

A tumulus is defined as "a 1-10 m high dome shaped feature that forms due to lava under localised hydrostatic pressure beneath a solid upper crust of the lava flow" (Walker, 1991, Anderson *et al.* 2012, p 931). Excess influx of magma causes the upward flexure of the top crust, which creates space to accommodate the increase in lava volume. Dann (2001) proposed that upward flexure formed the ridge and domelike features characteristic of the tumulus structure that was intersected by the drilling.

The tumulus structure in BARB 1 is located at the top of the hole (Figure 6.1), which corresponds to the lowest section in the stratigraphy. It is 90 m long in the core (50 m true thickness) and consists of 5 major rock components; namely: olivine adcumulate, harrisite, pyroxene spinifex, gabbro and pyroxenite, and is capped by hyaloclastite. These sections are somewhat comparable to the structures seen in differentiated komatiites but on a larger scale. In addition, the degree of differentiation is far greater.

The cumulate layer of the tumulus is 15 m thick (Figure 6.1). The olivine crystals that make up the cumulate layer are between 0.5 and15 mm in size and range in shape from euhedral crystals to rounded and ellipsoid (almost pebble like) shape. The larger elongated olivines occur in zones within the cumulate layer and within these zones they are strongly aligned. The olivine becomes more finely grained and euhedral with stratigraphic height from these horizons of aligned ellipsoidal olivines, creating a series of upward-fining cycles. Minimal matrix or melt residue is present in the cumulates (range of 3% to 20%) and hence the

description adcumulate - mesocumulate is appropriate. Apart from the ellipsoidal grains, the cumulate layer is homogeneous and does not change in texture or mineral composition with height. In a thin contact zone, cumulate and harrisite formed together and became inter-grown.

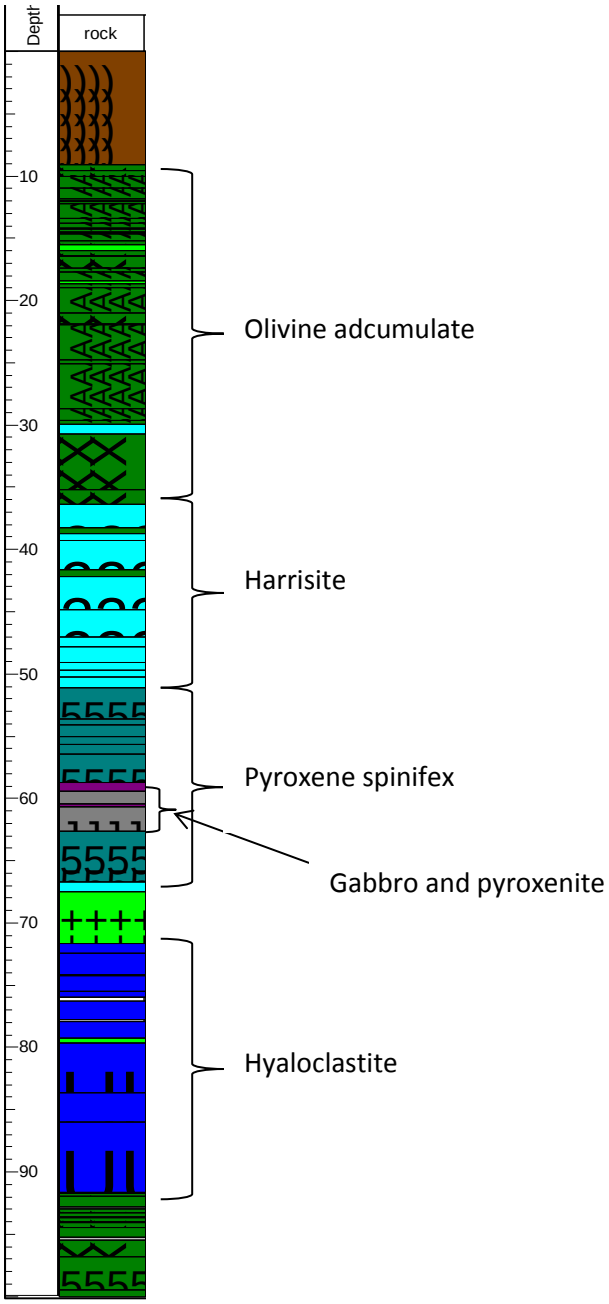

Figure 6.1:
Top section of the BARB 1 core illustrating the textural sections of the tumulus (adcumulate, harrisite, pyroxene spinifex, gabbro and pyroxenite and hyaloclastite)

Harrisite is defined by Donaldson (1974) and Donaldson (1982), p 201, as "dendritic or skeletal olivines that grow at a high angle to the igneous layering plane". These skeletal olivines commonly grew upwards from a cumulate mush layer into a super-cooled or super-saturated magma. Donaldson (1982) illustrates that not all harrisite needs to have formed at the cumulate-magma interface. "Pods, lenses and tongues" of harrisite are found in the Rum intrusion Donaldson (1982), p 201. The crystallization mechanism for these structures is thought to be upward percolation of melt from cumulus crystallization, which ponds and forms a super-cooled, super saturated liquid with few olivine nuclei.
This melt became trapped and ponded beneath an impermeable layer, causing a supercooling effect and hence crystallization of skeletal olivines. Further, Donaldson (1982) shows that the base of the harrisite layer grades from cumulate into skeletal olivines, whereas the top of the layer has a very distinct and abrupt contact with the overlying layers.

In the BARB 1 tumulus, a 15.8 m thick harrisite layer overlies the cumulate zone. The first appearance of harrisite occurs 30 m from the top of BARB 1. This layer is only 0.8 m thick and is overlain by a 5.5 m thick layer of megacrystic olivine (Figure 6.1). The final cumulate layer grades over 50 cm, into the harrisite layer at 36 m depth in the core. Contained within the 15 m-thick harrisite layer, are two thin (20 cm) olivine spinifex layers, which can be intrusive sills similar to those discussed by Houle *et al.* (2009) . In both the harrisite and the spinifex, the relict olivine blades are white in colour and are surrounded by a dark grey to black melt residue (Figure 6.2). Pockets of melt are sectioned off by these olivine blades, and within these pockets (polygons) grew randomly oriented needles, probably of pyroxene (Figure 6.3). Amygdales of 1-3 mm in diameter that are filled with dark green serpentine occur near the top of the harrisite layer. At 51 m the harrisite grades upwards into finely-grained and aligned pyroxene spinifex.

Figure 6.2:
Harrisite in the core. The white patches are olivine blades, which are inter-grown with the black melt residue. The yellow outline indicates a euhedral skeletal olivine, which contains melt residue.

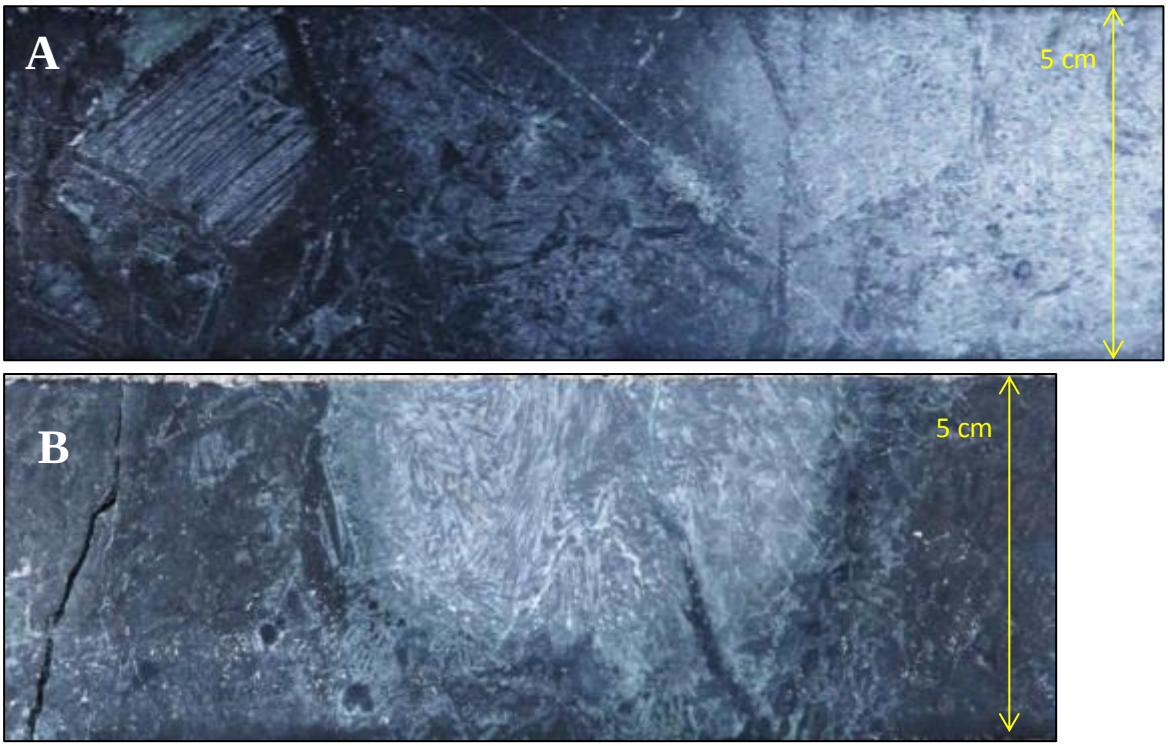

Figure 6.3 (A,B):
Pockets of melt that have crystalized spinifex-like blades inside polygon shapes formed by the skeletal olivine.

The pyroxene spinifex layer has a total thickness of 11.8 m. It is divided into two sections (8 m thick and 3 m thick) by a gabbro and pyroxenite layer (Figure 6.1). The pyroxene spinifex needles have a distinct dark green colour, and are surrounded by a lighter green – brown matrix (Figure 6.4). The needles are randomly orientated and found near the lower contact only reach 3 cm in length. The needle length increases to a maximum of 20 cm at 56 m in the core. The needles decrease in size toward the pyroxenite contact at 58.7 m. The pyroxene spinifex has a gradational contact into the overlying pyroxenite layer. Some elongated (up to 1 cm) pyroxene grains are present within the pyroxenite layer. The second and thinner pyroxene spinifex layer is similar to its counterpart, found lower in the stratigraphy, but in this layer the needles reach only 5 cm in length. These spinifex needles formed in sub-parallel packages which created an overall alignment in the spinifex.

The 3.8 m thick intervening layer consists of alternating gabbro and pyroxenite. A 0.7 m thick, dark grey green, pyroxenite (Figure 5.12) layer is in gradational contact with the underlying spinifex layer. The pyroxenite is dark green to black in colour and has pyroxene grains (up to 2 mm) that are visible on a hand sample scale. The pyroxenite is homogeneous

and coarse grained. A 1 m-thick gabbro layer (Figure 5.11) follows the pyroxenite (down hole and up-stratigraphy). The gabbro is coarse grained (up to 2 mm), homogeneous and is dark green with small speckles of white minerals (feldspar). The contacts between the pyroxenite and gabbro layers are gradational and indistinct. A second 0.3 m-thick pyroxenite layer is followed by a second 1.8 m-thick gabbro layer. This gabbro is in contact with the overlying (down hole) spinifex layer. The contact is gradational over a few centimetres and only minimal skeletal grains are found within the gabbro.

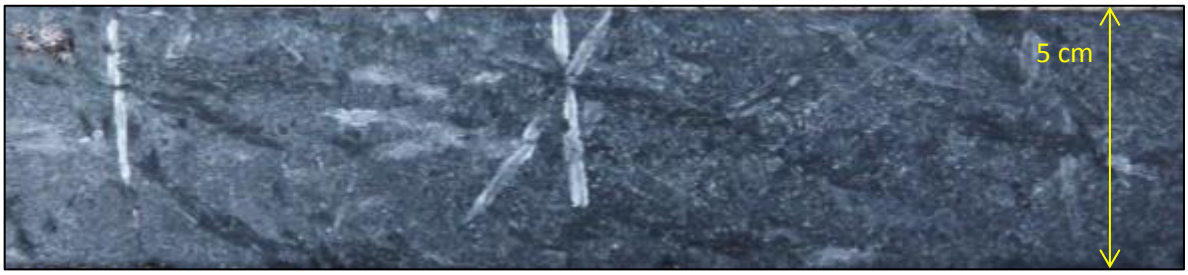

Figure 6.4:
Pyroxene spinifex, showing randomly oriented needles. The shining X like needles is due to the reflection of the cleavage and the light.

Hyaloclastite is defined by McPhie (1993), p 54 as brecciated "clastic aggregates formed by non-explosive fracturing and disintegration of quenched lavas" during extrusion into water. As the lava erupted into a cold, wet substrate, the uppermost skin became instantly quenched and brecciated via thermal shock to form a hyaloclastite. With continuous pressure build up and movement of magma within the flow, the hyaloclastite could fracture further and become reworked. The spaces between the blocks became filled with sedimentary or volcanic material depending on the depositional environment.

The hyaloclastite formed the upper carapace and is the domed feature that defines the tumulus in the BARB 1 core. It is 20 m thick and consists of fine-grained, grey, irregular – sub-angular to amoeboid - shaped blocks, surrounded by paler grey to green glassy spherical to angular shards, which in turn lie in a pale green to white matrix. The blocks represent the quenched and fractured lava crust, whilst the glassy material originated from the chilled fragments of the hyaloclastite but was more heavily altered by sea water interaction. The glass shards are 1 – 5 mm in size. They are commonly zoned, and each zone is either dark grey, light grey or brown in colour (Figure 6.5). The contact between the blocks and the matrix is distinct, and minimal alteration has occurred at these boundaries (Figure 6.5).

Vesicles are present within the hyaloclastite between 73 and 75 m. This is the deepest part of the hyaloclastite i.e. furthest away from the sea-water. These vesicles are rounded to ellipsoidal, 1- 10 mm in size and are filled with a dark serpentine material (Figure 6.6). The boundary between the vesicles and the surrounding rock is distinct, but each sphere has an inward zonation, seen by a change in colour of concentric layers. The zoning in the vesicles is attributed to the serpentine infill in a concentric fashion.

The hyaloclastite layer grades from a blocky and vesicular rich section at the base, into the large (30 cm) blocks/fragments, which are supported by the glass-shard matrix at 77 m. The glassy shards then become smaller (1 mm) and acquire a yellow green tinge. At 83 m the clast/ fragment size begins to decrease and the clasts/ fragments are less common. Some blocks have a white reaction rim, whilst others are in direct contact with the matrix shards. The top of the hyaloclastite ends abruptly at 91 m where it is directly overlain by the chill zone of a differentiated komatiite flow. A large (5 cm wide) magnesite vein is present adjacent to the contact which obscures the finer details.

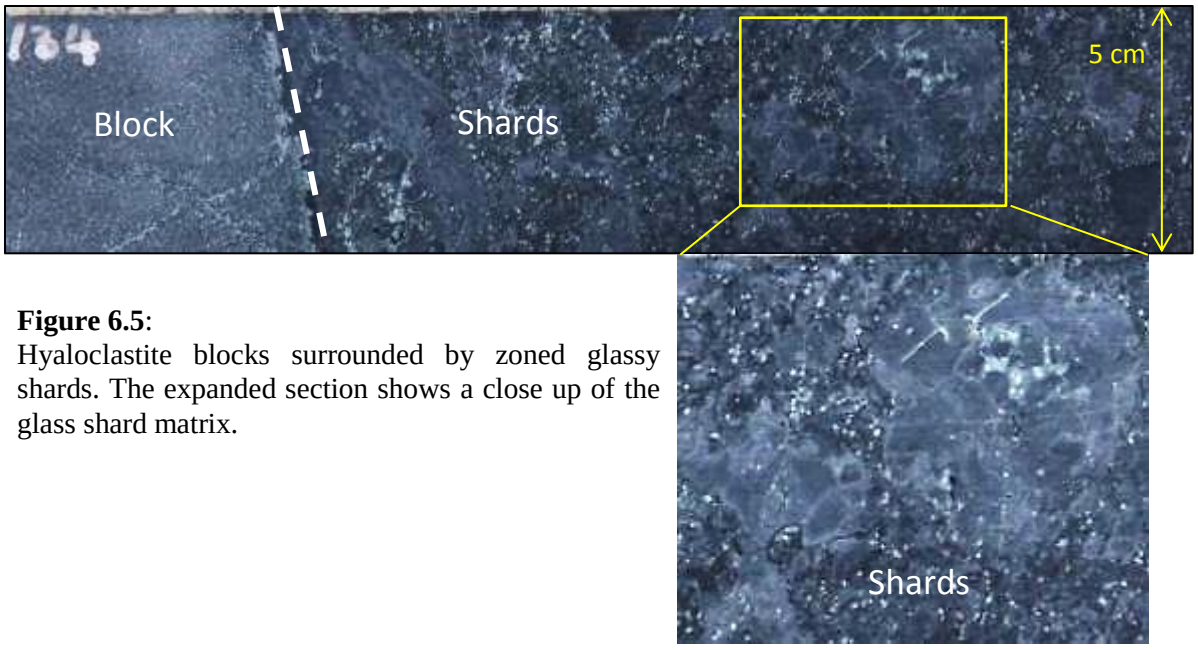

Figure 6.5:
Hyaloclastite blocks surrounded by zoned glassy shards. The expanded section shows a close up of the glass shard matrix.

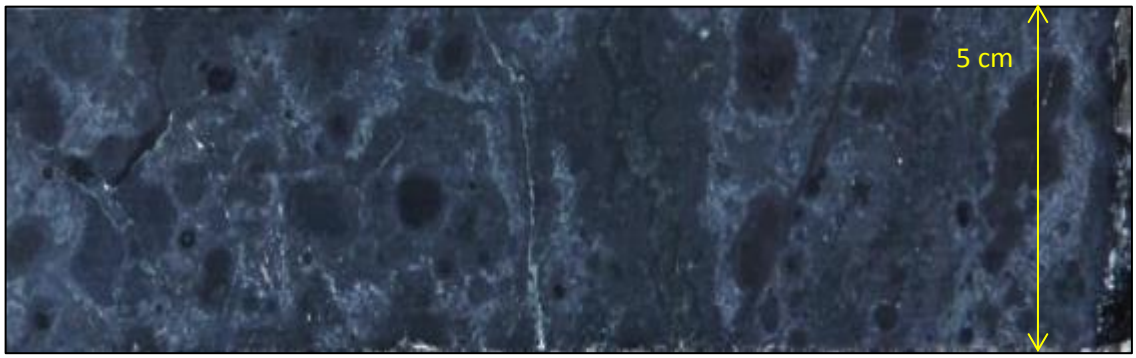

Figure 6.6:
Vesicles present in the hyaloclastite. Colour changes show inward zonation or alteration.

6.2.2 BARB 1 (89-118 m) Differentiated Komatiite Package

The sample set immediately overlying the tumulus section is composed of a package of differentiated komatiite flows. The sampled interval is 29 m thick and contains nine differentiated komatiite flows and an intrusive basalt flow at 103 m. These flows consist of the typical cumulate, spinifex and chill units. In some cases the chill is missing, but a contact can usually be inferred using textural information.

The cumulate, spinifex and chill zones range in size and the maximum, minimum and average values are recorded in Table 6.1

Rock texture	Minimum (m)	Maximum (m)	Average (m)
Cumulate	0.17	1.35	0.59
Spinifex	0.3	3.3	1.29
Chill	0	0.49	0.15

Table 6.1: Summary of flow thickness of the 12 differentiated komatiite flows

The proportions of cumulate to spinifex to chill are given in Figure 6.7 B. Spinifex is the major component in the flows (56 %), cumulate makes up a smaller portion (30%) and chill margins are a minor component (14%).

The cumulates in these differentiated flows consist of pseudomorphed euhedral olivine crystals 0.5-1 mm in size. The cumulate zones are homogeneous, except in a few sections where a pseudo-fabric is evident (Figure 6.8). The cumulus crystals are small and sometimes

not evident on the hand-sample scale. More detailed descriptions will be given in the petrography chapter.

Olivine spinifex makes up the largest proportion of most of the differentiated flows in this package. Each flow in the package contains olivine spinifex, but most spinifex units have different dimensions and textures. The most common form of spinifex consists of feathery blades that grow in a radiating fashion from a single point, or blades aligned sub-parallel in a vertical direction (perpendicular to the flow contacts). This type of spinifex consists of blades of olivine that are short (3 mm) to long (20 mm) but invariably very thin (<1 mm). This spinifex grew downwards from the chill margin initially as small, randomly oriented blades that developed into long, aligned blades, which then became shorter again towards the underlying cumulate zone.

A less common type of spinifex is present in flows 8 (106-109 m) and 9 (111- 113 m). The spinifex in these flows has variable blade lengths, but the blades are exceptionally thick (5-20 mm) (Figure 6.9). The thick blades grade from thin olivine laths to thick blades over 15 cm. Only one case is present where the thin blades are juxtaposed next to the thick blades, but even in this case, no contact boundary is evident. These thicker spinifex blades are uncommon and are noted in literature by Gole *et al.* (1987) who refer to the texture as "Jackstraw". Munyai (2012) noted these thick spinifex blades in this sample suite, which was the focus of his honours thesis. Munyai suggested that the thick blades are the result of metamorphic recrystallization. The entire BARB 1 and BARB 2 cores are metamorphosed and in most cases the metamorphic minerals form pseudomorphs of the original igneous mineralogy. Thus the recrystallization and crystal growth of these thicker spinifex blades is unique in the BARB 1 and BARB 2 cores.

The chill margins and contacts of these flows are typically between 3 and 15 cm wide. The chill is a fine grained dark grey rock. The contact itself is commonly a brecciated 3-5 cm wide zone, which contains a fracture network filled in by a white material, most likely magnesite. In some cases the contact is not evident. However, as discussed in Chapter 5 on the Tjakastad Komatiites, changes in textures can be used to infer their locations.

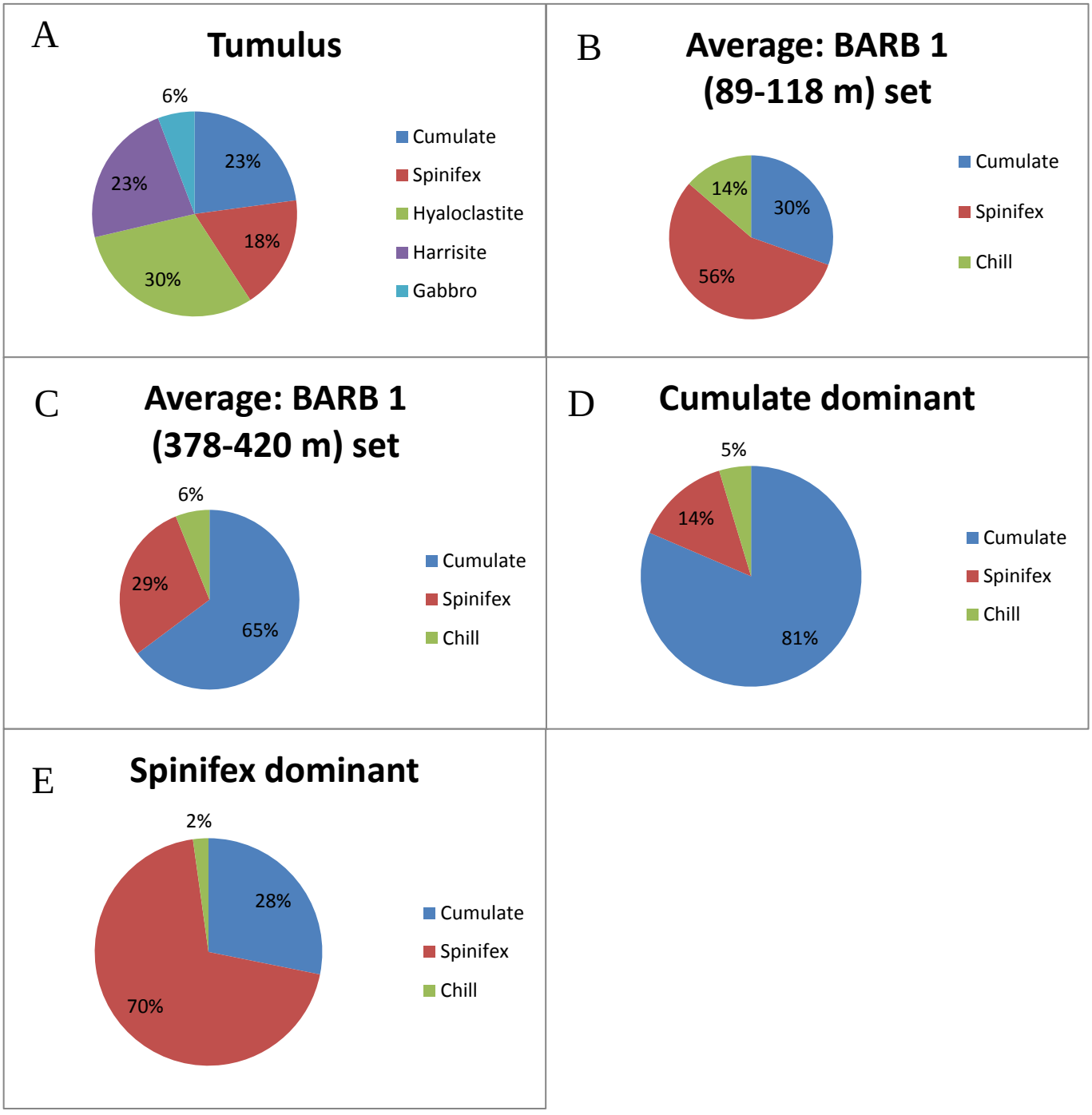

Figure 6.7:
A) Pie chart representing the components of the tumulus zone. **B**) Pie chart representing the average proportions of the constituents of the differentiated komatiite flows in the BARB 1 (89-118 m) sample set. **C**) Represents the average proportions of the textures found in the 8 differentiated flows in the BARB 1 (378-420 m) sample set. **D**) Represents the average proportions of the cumulate dominant flows found in the BARB 2 (252-274 m) sample set. **E**) Represents the average proportions of the spinifex dominant flows found in BARB 2 (252-274 m) sample set.

Figure 6.8:
Pseudo fabric present in the olivine cumulate layer of the BARB 1 (89-118 m) set.

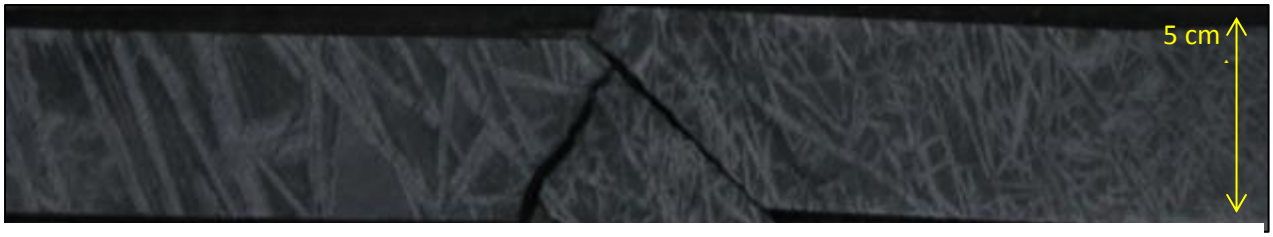

Figure 6.9:
Both thin (right) and very thick (left) spinifex blades that grade from one to the other.

6.2.3 Flows at BARB 1 (378-420 m) Differentiated Komatiite Package

A package of differentiated komatiites occurs near the end of the bore hole of BARB 1. This section is 42 m thick, from 378 m to 420 m, and was sampled comprehensively. It consists of ten differentiated flows and contains an intrusive gabbro (2.2 m) between a massive komatiite and a komatiitic basalt. The texture and structure of these flows are slightly different from the typical differentiated flows described elsewhere. Their bases are komatiitic basalt (as recorded in the core logs), followed by an olivine cumulate layer, which in turn is overlain by olivine spinifex and capped by a chill zone. This unusual structure is clearly evident in four flows of this interval. A further anomaly observed in two flows is that instead of the cumulate layer, the basal layer was logged as komatiitic basalt. It is important to note at this point that the core log is based on visual characteristics, which in some cases are not borne out by the chemistry. The komatiitic basalt is identified by its medium khaki- green colour, its speckled, veld-like surface appearance and its homogeneous fine- grained texture. However, these visual characteristics are not in accord with the geochemical classification which indicates that the rock type is true komatiite.

The cumulate, spinifex and chill zone sizes are recorded in table 6.2

Rock texture	Minimum (m)	Maximum (m)	Average (m)
Cumulates	0.46	5.8	2.46
Spinifex	0.24	1.97	1.1
Chill	0	0.42	0.23

Table 6.2: Summary of flow texture thicknesses for eight differentiated flows in the BARB 1 (378-420 m) sample set.

The proportions of these components are given in Figure 6.7 C. On average, the cumulate zone (composed of the mis-identified komatiitic basalt) is the dominant proportion of the flow (65 %) and grades into the spinifex zone, which makes up (29 %). The chills make up (6%) of the flows. In some cases the chill margin is not evident and the core changes from fine grained spinifex texture back into cumulate. The problem of missing chill margins and flows intruding other flows has been discussed previously.

The cumulates consist of very small (<0.5 mm) and quite sparse (35-45%) olivine crystals, surrounded by melt residue. The layers are relatively homogeneous, and are visually distinct from the komatiitic basalts. Further details on these cumulates are given in the petrography section. In general, the cumulate layers grade over several centimetres into spinifex-textured rock.

The spinifex blades are not as prominent, in terms of colour or size, as in other sections of the core. The blades are randomly oriented and usually on a scale of a centimetre in length or smaller; and only 1 mm in width.

The chill margins of these differentiated flows are commonly 20-40 cm thick, but in some cases the fine grained chill is absent. A thin (up to 8 cm) contact zone in these chill margins is commonly brecciated and blocky, which allows distinction between overlying and underlying layers. Two hyaloclastite units are evident within a massive komatiite layer at 383 m. Since hyaloclastite is associated with flow contacts and chill margins (McPhie, 1993), it is evident that these hyaloclastites represent flow-tops. These hyaloclastite breccias comprise 1- 5 mm-sized jigsaw-type pieces, which fit together with a small amount of white (magnesite) material that fills the gaps (Figure 6.10).

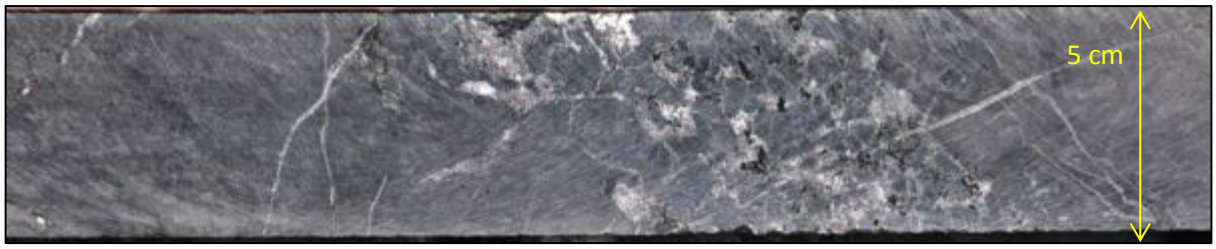

Figure 6.10:
Hyaloclastite breccia indicating a contact.

Vesicles and varioles are present in two localities in this sample interval, occurring in adjacent flows. The varioles are found at 402.46 m within a spinifex layer. They are ellipsoidal, 2-10 mm long and are filled with a white mineral, most likely magnesite. The variole boundaries are not distinct and are similar to the varioles seen in the basalt layers (Figure 6.11 A). The set of vesicles is found within a cumulate layer (Figure 6.11 B) at 403.68 m, which directly overlies the spinifex variole layer. These vesicles are perfect spheres, up to 3 mm in diameter and filled with a dark green serpentine and rimmed by white magnesite. They are numerous and make up approximately 15 % of the rock. This vesicle layer is overlain by a thin (20 cm) spinifex layer, which does not contain any vesicles and is capped by a chill margin with a distinct contact.

In this interval there are also isolated komatiitic basalt flows, <1 m thick which are not associated with any differentiated flows. These flows contain the white tricuspate features interpreted as pillow selvages.

Figure 6.11:
A) Example of the white varioles found within the spinifex layer. **B**) Vesicles found within the cumulate layer, show distinct boundaries and a reaction rim.

6.3 Selected Section BARB 2

A single detailed section was sampled in BARB 2. This section consists of differentiated komatiites, which, on a correlative basis, occur further up the stratigraphy (deeper in the bore-hole) than the differentiated komatiites sampled in BARB 1.

6.3.1 Differentiated Flows in BARB 2 (252-274 m)

This interval is 22 m thick and comprises seven differentiated komatiite flows. These flows have the typical structure of differentiated komatiites; but most lack distinct chill margins. A single flow at 262- 266 m is entirely massive and contains no spinifex. The cumulate, spinifex and chill zones are summarized and recorded in Table 6.3a

Rocky texture	Minimum (m)	Maximum (m)	Average (m)
Cumulates	0.11	4.67	1.75
Spinifex	0	3.01	1.06
Chill	0	0.57	0.11

Table 6.3a: Summary of flow details averaged for seven flows.

There appears to be two types of differentiated flows: cumulate dominant flows and spinifex dominant flows. Details of these flows are recorded in Tables 6.3 b and c.

Rocky texture	Minimum (m)	Maximum (m)	Average (m)
Cumulates	0.88	4.67	3.31
Spinifex	0	1.16	0.56
Chill	0	0.57	0.19

Table 6.3b: Summary of flow details, for the three cumulate dominant flows.

Rocky texture	Minimum (m)	Maximum (m)	Average (m)
Cumulates	0.11	1.16	0.58
Spinifex	0.57	3.01	1.43
Chill	0	0.18	0.05

Table 6.3c: Summary of flow details, for the four spinifex dominant flows.

These features are documented in Figures 6.7 D and E.

The crystals in the olivine cumulate are small, < 1 mm, euhedral and completely surrounded by melt residue. The cumulate layer is dominant in three of the seven flows making up 81 % as an average of the three flows, with a minimum of 14 %.

The olivine spinifex typically grades from small, randomly oriented or radiating sheets into longer (12 cm maximum) aligned sheets, towards the centre of the flows. The larger sheets contain smaller interstitial sheets, which grew perpendicular to the larger sheets. The spinifex dominated flows have an average spinifex component of 70 %

Chill zones in these flows are commonly absent. Only two of the seven flows have chill margins and one of these chills is found within the massive komatiite flow. These chills do not make up a significant part of any of the flows (2-5%).

6.4 Similarities and Differences between Selected Sections

The reason for the selection and sampling of the tumulus, and three additional packages of differentiated komatiites, is to compare the different textural component of flows at different stratigraphic positions within the sequence.

The differentiated komatiite flows consist of cumulates, spinifex and chill zones. The sample set BARB 1 (89-118 m) directly overlies the tumulus and is a spinifex dominant flow package. The BARB 1 (378-420 m) sample set is higher up stratigraphy and the flows are dominated by the cumulate zones. The BARB 2 (252-274 m) sample set is the stratigraphically the highest and has a combination of cumulate-dominant and spinifex-dominant flows in an alternating arrangement. The packages of differentiated flows consist of cumulates, spinifex and in most cases chill margins. These are similar for adjacent flows and for flows at various depths. Within the differentiated komatiite flows, the olivine crystals in the cumulates are similar in size, shape and abundance. The spinifex found in these flows is solely platy olivine spinifex. The size of the spinifex crystals ranges from very small (1 mm) up to tens of centimetres (15 cm). The variation in size depends on position within the flow. Commonly the thicker flows have longer sheet crystals at the centre of the spinifex layer. The chill margins are fine grained, and some contain clearly defined contacts.

The tumulus can be contrasted with the differentiated flows on a qualitative basis. The cumulates of the tumulus contain significantly larger crystals (0.5 to 15 mm) than in the flows (<0.5 mm). The spinifex is pyroxene dominant rather than olivine dominant and hyaloclastite

makes up a much larger proportion of the tumulus unit (30%), whilst the chills range from 2 % to 14% of the flows composition. The tumulus unit also contains harrisite and gabbro, which are absent from the differentiated flows. The layers in the tumulus are much thicker (on a meter scale), whilst those in the differentiated flows are on a smaller scale (centimetres – meters).

6.5 Summary and Discussion

The four selected sections comprise of a tumulus feature and 3 packages of differentiated komatiite flows.

The cumulate zone of the tumulus consists of olivine grains that are ellipsoidal and much larger (up to 15 mm) in size than the common 0.5 mm olivine cumulate grains of the differentiated komatiite flows. The large scale nature of the grains probably implies further growth after settling, which is consistent with the relatively low proportion of trapped melt present between the cumulates. Tait *et al.* (1984) indicate that adcumulates grow larger without showing zonation, which is the case with the cumulates of the tumulus. The lack of matrix can be attributed to close packing and possible annealing of the enlarged olivine grains. The additional crystals that settled would cause the mass of the overlying layers to increase, which would have created a higher degree of compaction in the lower cumulate zone, forcing the melt to squeeze out and percolate upwards (Wager *et al.*, 1960). The cumulate layer behaves as a typical mesocumulate - adcumulate.

The lens of harrisite observed between the cumulate layers can be explained by a process similar to that put forward by Donaldson (1982). The 0.8 m thick harrisite layer is located between two adcumulate layers, which presumably are relatively impermeable. This supports Donaldson's (1982) concept of upward percolation of melt, from the underlying cumulates, that became trapped by the overlying impermeable cumulate layer. This trapped melt become supersaturated and crystalizes dendritic olivines. This idea of melt migration upward from the cumulates is supported by the lack of matrix (trapped melt) in the underlying mesocumulates.

Due to compaction by both the overlying strata and the ocean water, the more buoyant melt percolated upwards causing the cumulates to become more closely packed and therefore to contain less interstitial material.

Pyroxene spinifex needles are present from 51 to 66 m and reach the maximum length of 15 cm towards the centre of the spinifex zone in the interval (55-56 m). However, the pyroxene spinifex zone is separated into two sections by the pyroxenite-gabbro layer at 58-62 m. The pyroxene-gabbro layer shows no distinct contact with the pyroxene spinifex. This implies that it was not an intrusion but rather the product of the final stage crystallization of the last remaining melt in the lava channel. This is consistent with what is known about the dynamics of lava channels and crystallization processes (Hill, 2001, Hill *et al.*, 1995, Papunen *et al.*, 1998). As the outer layers of the channel lost heat, the magma began to crystalize, leaving the centre of the flow as the hottest zone, and hence the most likely area for the last portion of melt to remain and to later crystalize. This late stage crystallization would explain the placement of the pyroxenite-gabbro layer in the centre of the tumulus unit. The late stage crystallization in the centre of the flows would also explain the coarse grain- size caused by slow crystallization in a well-insulated lava channel.

The hyaloclastite unit consists of large irregular-shaped blocks of fine-grained grey quenched lava. Between these blocks is a glass shard like matrix. The outer skin of the lava channel erupted underwater, which resulted in a freeze fragmenting of the upper carapace of lava. These fragments were further fractured and rotated during the bulging to form the tumulus. The tumulus is noted for its thick hyaloclastite layer, compared to the differential komatiite flows chill zones. The thickness of the hyaloclastite may be attributed to the formation of the tumulus. The upward doming of the tumulus widened the already formed fractures in the hyaloclastite, and with further bulging the cracks expanded, exposing the insulated magma to the water. This resulted in further hyaloclastite brecciation.

The BARB 1 differentiated package (89-118 m) consists of 12 typical differentiated komatiite flows and an intrusive basalt layer. The flows are spinifex dominated. The spinifex crystals are typically thin and long, but in flows 8 and 9, a zone comprising very thick crystals (3 mm – 1 cm) of spinifex is evident. These thick spinifex blades have a gradational contact (5-15 cm) with the smaller and thinner blades. This very coarse-grained spinifex may represent a recrystallization of the olivine spinifex under metamorphic conditions (Munyai 2012).

In the BARB 1 differentiated package (378 – 420 m), the sample set consists of eight cumulate dominant differentiated flows, a gabbroic layer and several true komatiitic basalt layers. Some komatiitic basalts were found in association with the olivine cumulate layer in six of the eight differentiated komatiite flows. Geochemistry indicates that the komatiitic

basalts were misidentified in the logging, and actually represent massive or cumulate komatiites.

The BARB 2 (252-274 m) package consists of seven differentiated komatiite flows, which are either cumulate or spinifex dominant in equal proportions. The cumulus crystals range in size from 0.5-2 mm and are euhedral.

6.6 Conclusions

Four sections of the BARB 1 and BARB 2 cores were selected to be sampled in detail. The detailed sampling allows understanding and comparison of textures, structures, geochemistry and possible flow dynamics between adjacent flows and flows at different stratigraphic depths.

The tumulus is a large scale feature, which has corresponding large scale minerals. The cumulates are an order of magnitude larger than the cumulates of the differentiated flows (0.5 mm). The tumulus has pyroxene spinifex (up to 15 cm), whilst the differentiated flows have olivine spinifex, which reaches 5 cm in length. The tumulus has a 20 m thick hyaloclastite layer, which represents the chill margin of the lava tube. The differentiated flows contain contact breccias that only reach 15 cm thick and make up a smaller proportion of the flows than the hyaloclastite does in the tumulus. The tumulus contains additional textural components: the harrisite and gabbro-pyroxenite layer that are absent in the thinner differentiated flows. The thickness of the hyaloclastite is attributed to continuous quench fragmentation during the inflation and doming of the tumulus feature.

The differentiated komatiite flows are directly comparable to one another as they consist of cumulates, spinifex and a chill margin. In some flows one or two of these textures are absent, but the overall rock-types are easily identifiable. The BARB 1 (89-118 m) package is spinifex dominated, whilst the BARB 1 (378-420 m) package is cumulate dominated. The BARB 2 (252-274 m) package has flows that are either cumulate-dominated or spinifex-dominated in different alternating flows. The olivine crystals in the cumulates have a similar, shape, size and relationship to the matrix. The spinifex in each flow consists exclusively of olivine plate spinifex that can be both randomly oriented or aligned. In the BARB 1 (89-118 m) package there is evidence of recrystallizing of olivine spinifex, as these crystals are much thicker than any other spinifex found in the core.

CHAPTER 7

MINERALOGY AND PETROGRAPHY OF THE DETAILED SECTIONS OF THE BARB 1 AND BARB 2 CORES

7.1 Introduction

Petrographic analysis of samples from the BARB 1 and BARB 2 cores allow a closer and more detailed observation of the mineralogy and textural features of the different rock types.

Thin sections were prepared from quarter core adjacent to that used for the geochemical sample. Four intervals were chosen for detailed chemical analysis and these have associated petrographic samples, which are described in this chapter. Approximately 40 thin sections were made of the tumulus zone, and nine thin sections from each of BARB 1 (89-118 m) and the BARB 1 (378-420 m) differentiated komatiite packages. The BARB 2 (252-274 m) differentiated komatiite package has a sample set of 20 thin sections. A further set of 10 slides were taken throughout the rest of the two cores with the specific goal of finding unaltered olivine or pyroxene. With this aim in mind, only massive komatiites and olivine cumulates were selected. A total of 94 thin sections were cut from the core samples.

A further six thin sections were cut from surface rocks at the drill site. The surface samples were taken as a means of comparing the lithologies on the surface maps, such as presented by Dann (2001), with those of the core. They complement the systematic sampling, petrography and geochemistry of the area undertaken by Robin-Popieul et al (2011). Due to the lack of surface weathering, the core is likely to illustrate better preserved contact relations and small scale features such as vesicle and spinifex development.

The samples were cut and ground to a thickness of 0.3 mm and covered with a glass cover slip. Observations were made using a petrographic binocular microscope and photomicrographs were taken with an ALTRA 20 Soft Imaging System, attached to an Olympus U-TV0.5XC-3 microscope. The full set of petrographic descriptions can be found in Appendix B and the full set of photomicrographs is compiled in Appendix C. Lengths of rock units given in this chapter relate to core thickness and are not the true thickness of the layer.

7.2 Metamorphism and Igneous Preservation of Rocks in the Komati Formation

Since the rocks from the Barberton Greenstone Belt are between 3.49 and 3.2 Ga old, (Chavagnac, 2004, Parman *et al.*, 2003, Robin-Popieul *et al.*, 2012) and have undergone a minimum of 5 regional deformation events (Dirks *et al.*, 2009), the original igneous mineralogy has largely been replaced. However, in some sections of the Barberton Greenstone Belt, and specifically in the Komati Formation, magmatic textures are well preserved even though the mineralogy is not. This preservation of texture indicates that the Komati Formation underwent chemical alteration via hydrothermal fluids, but experienced minimal mechanical deformation. Some zones of physical deformation are present but the mechanical weakening of the rocks appears to be confined to specific horizons of high strain.

The metamorphism of the Komati Formation has been studied and reported by many authors. Homogeneous mineral alteration to greenschist facies has occurred and is summarized by Chavagnac (2004), Cloete (1991), Dann and Grove (2007), Viljoen *et al.* (1983) as well as others. The common metamorphic minerals encountered in the lower Komati Formation are serpentine, chlorite, magnetite, actinolite and tremolite. Parman *et al.* (1997, p 306), indicate that olivine and pyroxene minerals are altered to serpentine and are surrounded by a glass groundmass, which is "altered to a serpentine, chlorite, tremolite and magnetite mixture". Robin-Popieul *et al.* (2012) state that serpentine replaces olivine; tremolite replaces clinopyroxene and the glass groundmass is converted to a combination of chlorite, tremolite and magnetite. This alteration is specific to the komatiites from the Komati Formation. Arndt *et al.* (2008), in their book on komatiites, note that the metamorphic minerals that form are related to bulk igneous composition, metamorphic fluid composition and to imposed P,T (Pressure, Temperature) conditions. They also note that carbonatisation is a common form of alteration.

Although these rocks have been completely metamorphosed, the igneous textures are well preserved allowing study of the original textures with inference to the igneous mineralogy (Robin-Popieul *et al.*, 2012). Komatiite flow textures are widely recognized and hence certain minerals have been associated with the different textures. For example: a cumulate zone (B2-4 zone) is defined by the presence of euhedral or subhedral olivine crystals. Optical properties, such as conchoidal fractures, relief and euhedral shape can be used to identify the olivines. Similarly the spinifex zones consist of olivine plates and interstitial pyroxene

needles, which can be texturally distinguished from one another. The olivine plates are larger in size (5 cm) whilst the pyroxene grew interstitially and formed smaller (1 -20 mm) and more fibrous acicular crystals (Arndt *et al.*, 2008). This is also consistent with fractionation processes, as it expected that the more magnesian olivine would have formed first, followed by the pyroxenes (Parman *et al.*, 2003, Robin-Popieul *et al.*, 2012).

Cloete (1991), Parman *et al.* (1997), Parman *et al.* (2003), Robin-Popieul *et al.* (2012), Viljoen *et al.* (1987) indicate the presence of unaltered olivine and augite pyroxenes in both the cumulate and spinifex zones of the differentiated komatiites in the lower Komati Formation. These unaltered minerals are found in centimetre-sized areas, which contain up to 80 % original igneous material (Parman *et al.*, 2003).

7.3 Igneous Textures and Mineralogy

Features used to determine original olivine are as follows:

Shape- The euhedral and subhedral shape of olivine grains is distinctive in thin section and in hand sample.

Fractures- Olivine has a unique conchoidal fracture system and no cleavage. The opaque minerals often exploit the fractures seen in olivines.

Size- Not a distinctive characteristic, but most olivines identified in other thin komatiite flow lobe facies are 0.5 – 1 mm in size (Arndt *et al.*, 2008).

Alteration- Robin-Popieul *et al.* (2012), Viljoen and Viljoen (1969) among other authors, indicate that olivine alters predominantly to serpentine. Hence, if serpentine is present it can indicate the possibility of original igneous olivine. The serpentine has a pale green pleochroism and a 1st order grey birefringence, which has a fibrous texture. In some olivines, the serpentine appears zoned (under cross polarized light) possibly reflecting compositional zoning in the original olivine crystals.

Colour and birefringence- Since the olivine is altered, the characteristic lack of colour and 3rd order birefringence is not evident.

In a single sample taken from the surface (GC–C-1), unaltered olivine is present as kernels within altered olivine grains. This is discussed in detail later in the chapter.

Features used to determine original pyroxene are as follows:

Shape- The pyroxenes have a euhedral to subhedral shape.

Relief- The pyroxenes have a high relief, but less than unaltered olivine.

Cleavage- A distinctive feature of the pyroxenes is their cleavage, which is still evident after alteration. The pyroxenes have fracture patterns similar to the olivines. This may be attributed to secondary fracturing during alteration and veining.

Extinction- The extinction angle is parallel to the elongate direction or to inherited cleavages for the orthopyroxene and it is inclined for the clinopyroxene.

Twinning- Often the clinopyroxene is twinned, especially when it occurs as spinifex.

Alteration- The pyroxenes alter to a combination of chlorite- actinolite- tremolite. In some cases it is possible to distinguish the individual minerals, but often the pyroxenes alter to a fine-grained mixture of these three minerals.

Colour- The chlorite or actinolite that replaces the pyroxene has a pale green to medium brown pleochroism. In crossed polarized light, they portray birefringence colours of chlorite- actinolite-tremolite. They commonly show small (<0.1mm) sized patches of all these minerals combined together. In the case of the brown pyroxenes, the brown colour is carried through to the crossed polarized light, which masks the actual birefringence colour.

It is important to note that some pyroxene grains contain relic cores or kernels of unaltered pyroxene. Typically clinopyroxene is more common, but instances of fresh orthopyroxene or pigeonite are observed. If the sample is completely altered, it is difficult to distinguish orthopyroxene from clinopyroxene unless the cleavage is evident.

Features used to determine the matrix are as follows:

Texture- the matrix is very fine grained and is interstitial to the major crystals.

Shape and boundaries- the matrix fills in the residual spaces between grains and has an irregular shape. The boundaries of the matrix are indistinct and often merge into the minerals due to recrystallization during alteration.

Alteration- The matrix alters to a variety of minerals, depending on the original composition of the matrix. In olivine-rich cumulate layers, the matrix is altered to serpentine with finely intergrown chlorite. In pyroxene-rich samples, the matrix can patches of each mineral will form. A final fibrous needle growth of actinolite commonly overprints all the formed minerals.

Features used to determine actinolite and tremolite:

Shape- The amphiboles, actinolite and tremolite do not have distinct crystal shapes, but often occur in patches that have irregular, needle-like ends.

Relief- the amphiboles have a low relief when compared to pyroxene and olivine.

Colour- Tremolite has a green pleochroism, whilst actinolite has a clear colour and no pleochroism. Both amphiboles, under crossed polarized light, show second order birefringence colours. Since they are end members of a solid solution, varying degrees of pleochroism is present in these amphiboles.

The fine-grained and inter-grown nature of the alteration minerals makes it difficult to distinguish chlorite, serpentine and actinolite. The fibrous blades have overgrown and cut across one another in some cases.

7.3.1 Tumulus Unit

The tumulus unit was sampled at near equal intervals so that changes in texture and chemistry could be detected. The tumulus is separated into five textural sections. Each section is described in detail using thin section observations.

7.3.1.1 Cumulate Unit

The cumulate zone of the tumulus is 15 m thick in the core. 10 thin section samples were taken through this interval to observe textural changes of the olivine with height. These samples consist of approximately more than 80 % olivine, which supports the given field name mesocumulate - adcumulate. The serpentine pseudomorphs of olivine are pale yellow-green under plane polarized light; they are commonly rimmed by magnetite and chromite and have a groundmass that is lighter green in colour. In cross polarized light the olivine grains are a first-order iron grey colour of serpentine, with an inward fibrous zonation. The matrix consists of the bright yellow-white colour of fibrous serpentine (Figure 7.1). Subhedral and

rounded olivines are between 0.5 and 5 mm in size, whilst in samples GC 2, GC 13, GC 15 and GC 18, elongated, ellipse shaped-grains (up to 10 mm) with rounded edges occur. These grains are often aligned (Figure 7.1). The rounded ends of these elongated olivines could indicate some type of resportion process, but no resorption reactions are evident on the rims of these elongated olivines. The grains are homogeneous in texture and show the typical conchoidal olivine fractures that are exploited by magnetite, chromite and serpentine veinlets. The large proportion of olivine crystals result in minimal matrix and close packing of the grains. The entire cumulate section is altered to serpentine, with serpentine veins crosscutting the cumulates. Magnesite is present as veins and as 1 mm sized circular patches of alteration within the olivines. Opaque minerals are irregular in shape, <0.5 mm in size and occur along the borders and within fractures of the olivine crystals.

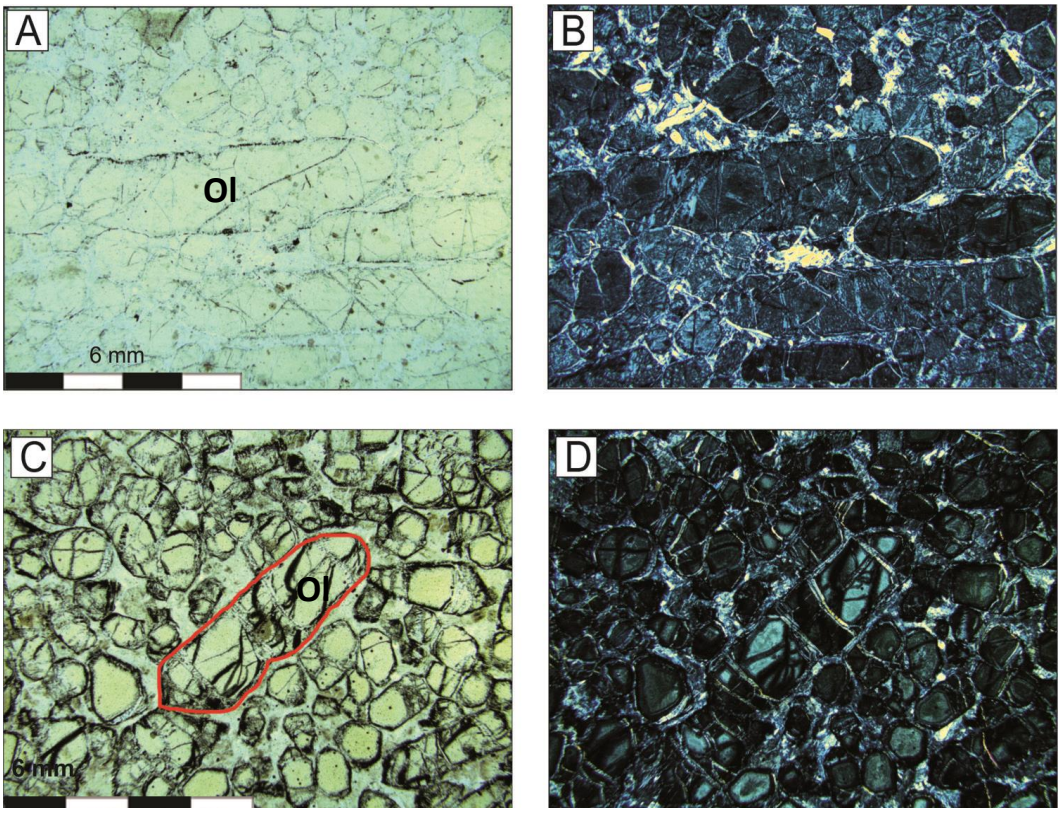

Figure 7.1
Olivine cumulate samples from the tumulus unit. Evident are the elongated aligned olivines that have rounded edges. Complete serpentine alteration is distinct. **(A,B)** are sample GC-2. (**C,D)** are sample GC-19.

7.3.1.2 Harrisite Unit

The harrisite layer is 15 m thick. It consists of 70 % skeletal olivine grains, which reach up to 5 cm in length. Nine thin sections were taken from the harrisite layer. All the samples consist of skeletal olivines that are surrounded by a melt residue. This residue contains smaller pyroxene blades, which reach only 0.5 mm in length and are slightly curved or crescent shaped and appear to consist of small, square to rectangular partitions of pyroxene within the blades (Figure 7.2). Also evident in the matrix of the harrisite are grains of unaltered clinopyroxene (Figure 7.3). The skeletal olivines have a light green colour, whereas the matrix is filled with crescent shaped pyroxene blades that are dark brown in plane polarized light. Under cross polarized light, the olivines show a 1st order steel grey, whilst the pyroxenes show the high 2nd order birefringence of actinolite. The matrix is a mixture of a dark, almost isotropic, glass and fibrous actinolite.

The general textures found in the harrisite is skeletal and dendritic olivines containing melt inclusions. Olivine has altered to serpentine whereas pyroxene has altered to chlorite-actinolite. Some of the clinopyroxenes have cores that are preserved with an alteration rim of actinolite. Magnetite and chromite rim the skeletal olivine blades and irregular <0.1 mm sized crystals are found within the pyroxene-rich matrix.

7.3.1.3 Gabbro and Pyroxenite Unit

The gabbro and pyroxenite layer is 3.8 m thick and has two alternating gabbro and pyroxenite layers. Four thin sections represent this layer and all have similar mineralogical components in different proportions. The pyroxenite samples have typical proportions of (50-60 %) pyroxenite, (10-20 %) plagioclase and (20-30 %) groundmass. The gabbro samples (GC 28 and GC 6) contain mineral proportions of 40 % pyroxene, (20-30 %) plagioclase and (20-40 %) groundmass.

The pyroxenite layer consist of pyroxene, plagioclase (<2 mm) and fine- grained groundmass (0.2 -0.5 mm), which could be more highly altered pyroxene or plagioclase. The “matrix” is medium-green with brown patches in plane polarized light and has a fibrous actinolite intergrowth. The pyroxenes are medium green in plane polarized light and have a high second order birefringence in cross polarized light. They are typically stubby subhedral shaped grains and have a green pleochroism. They appear to have alteration rims of chlorite, while the centre of the grain is often unaltered (Figure 7.4). The plagioclase is clear under

plane light and displays albite twinning under cross polarized light. The plagioclase grains show minimal alteration within the grains but have indistinct grain boundaries, which are overgrown by chlorite and tremolite (Figure 7.4). An orthocumulus texture is observed in these samples, but may have been produced via alteration.

The gabbro, by definition, contains more plagioclase crystals, which are seen by a 10% increase in plagioclase proportions in the thin sections. The pyroxenes, plagioclase and groundmass show the same optical properties as described above. However sample GC-29 contains small stubby grains of pyroxene randomly orientated in a chlorite-rich matrix and sample GC-8 has a sub-ophitic texture that contains 1-2 mm grains of altered plagioclase and highly altered grains of pyroxene (Figure 7.5).

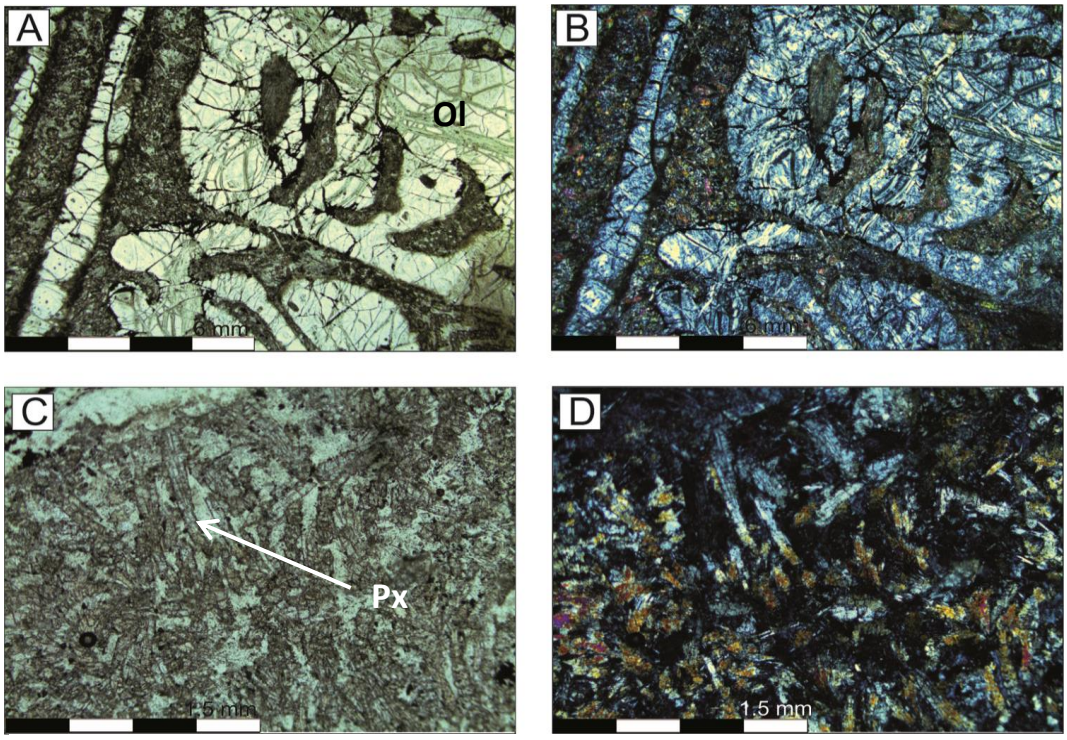

Figure 7.2
Harrisite texture formed by skeletal olivine blades surrounded by melt residue. The skeletal shape is evident in **(A,B)** from sample GC-20. Surrounding the olivines is melt containing crescent shaped pyroxene blades in sample GC-21 **(C,D)**. The olivine is altered to serpentine and the pyroxenes and melt residue are a combination of chlorite, tremolite and actinolite.

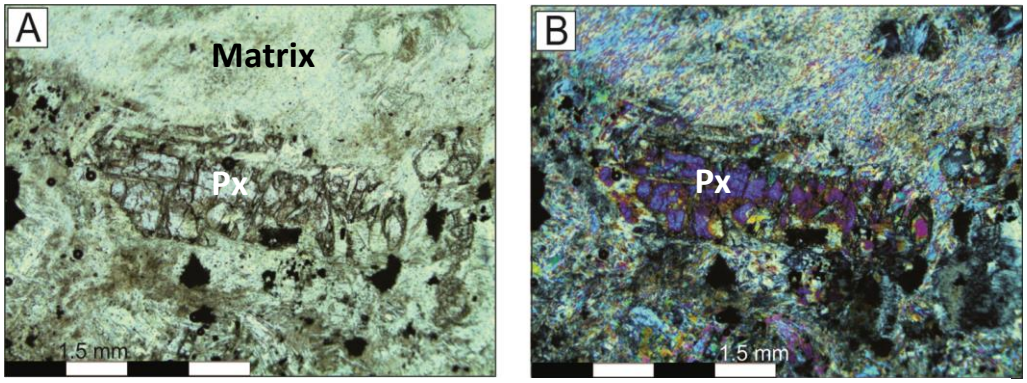

Figure 7.3
Unaltered pyroxene (Augite) present in the harrisite. Surrounding the pyroxene is matrix altered to fine grained actinolite and chlorite from sample GC-24.

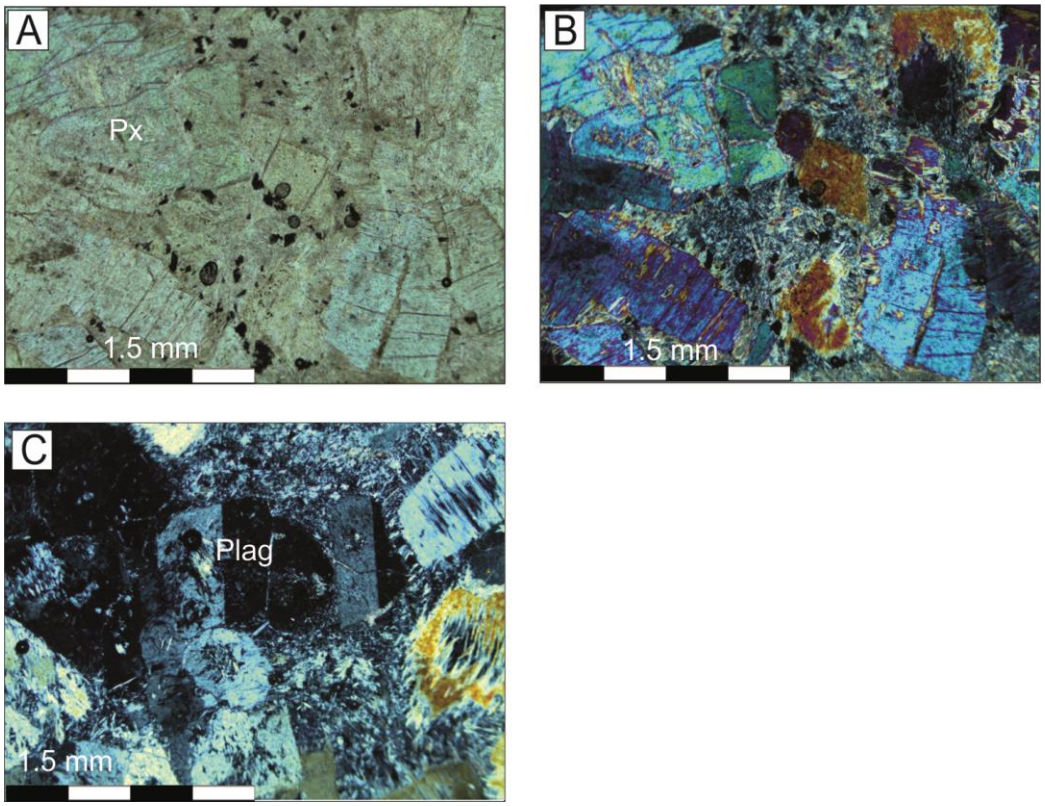

Figure 7.4
Pyroxenite layer consist of unaltered pyroxene grains, surrounded by a fine grained matrix in sample GC-27 **(A,B)**, altered to actinolite and chlorite. Present also is plagioclase grains, which are relatively unaltered in sample GC-27 **(C).**

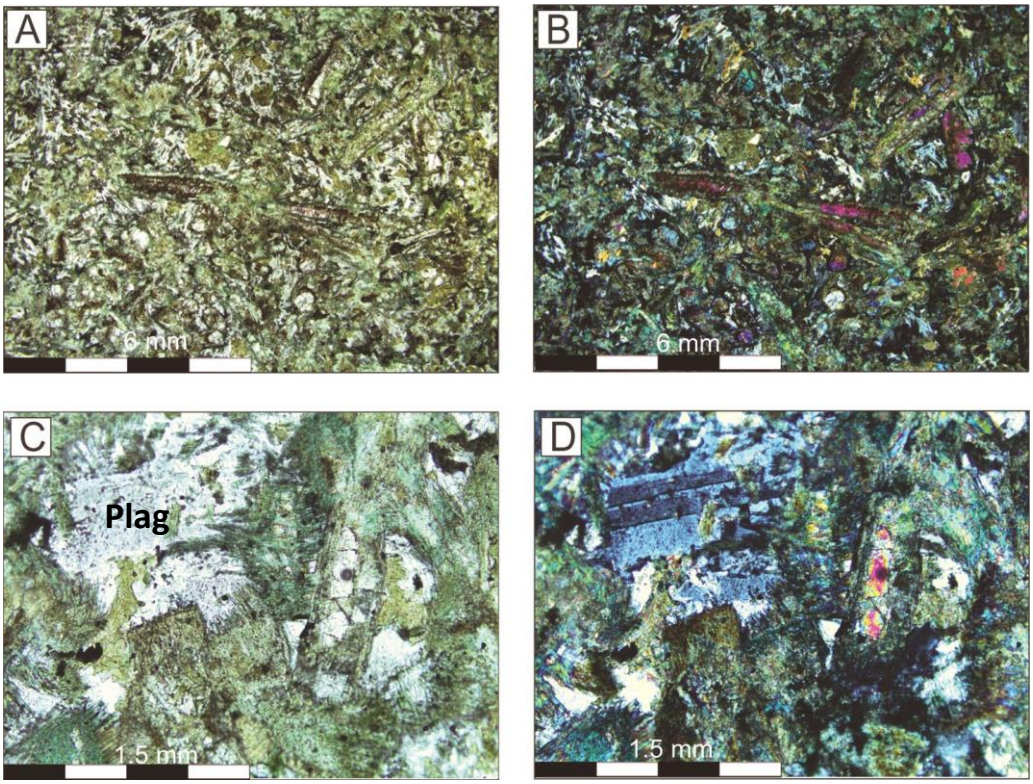

Figure 7.5
Gabbro samples from the tumulus unit. There is more chlorite alteration present in the gabbro layer with has blades of unaltered pyroxene in sample GC-29 **(A,B)**. Plagioclase and pyroxene are relatively unaltered, however they have become overgrown by chlorite, actinolite and tremolite in sample GC-8 **(C,D)**.

7.3.1.4 Pyroxene Spinifex Unit

The pyroxene spinifex is found in two layers separated by the 3.8 m thick pyroxenite- gabbro layer. Five samples were taken through these layers, three (GC 25, GC 4, GC 26) in the one below the gabbro- pyroxenite layer, and two (GC 7 and GC 29) above it. The two layers are similar in mineral composition. They consist of elongated, and commonly twinned, pyroxene grains that can reach up to 15 cm in length. The pyroxene spinifex blades are randomly orientated and define polygons of melt, which contain smaller 0.5 mm, euhedral pyroxene crystals and even smaller fibrous needle-like growths (Figures 7.6). These are surrounded by a glassy-melt residue. Four (GC 25, GC 4, GC 26 and GC 29) out of the five samples have a consistent feature of spinifex blades with green alteration rims, but sample GC 7 has the opposite, in that the rims of the pyroxenes are white, whilst the centres or cores are pale green brown. In all the samples the matrix is a pale green colour in plane light. In crossed polarized light, the pyroxenes range from a low first order grey on the rims, to a high second order blue in the centre of some pyroxenes (Figure 7.6). This high birefringence is found predominantly in the pyroxenes of sample GC 26. The centre of these pyroxene blades have a high relief and

green pleochroism. These aspects together with the high birefringence indicate fresh cores in some of the pyroxene grains. By contrast, in the remaining samples, most of the spinifex grains are highly altered in the centre of the grain and are rimmed by chlorite (Figure 7.6).

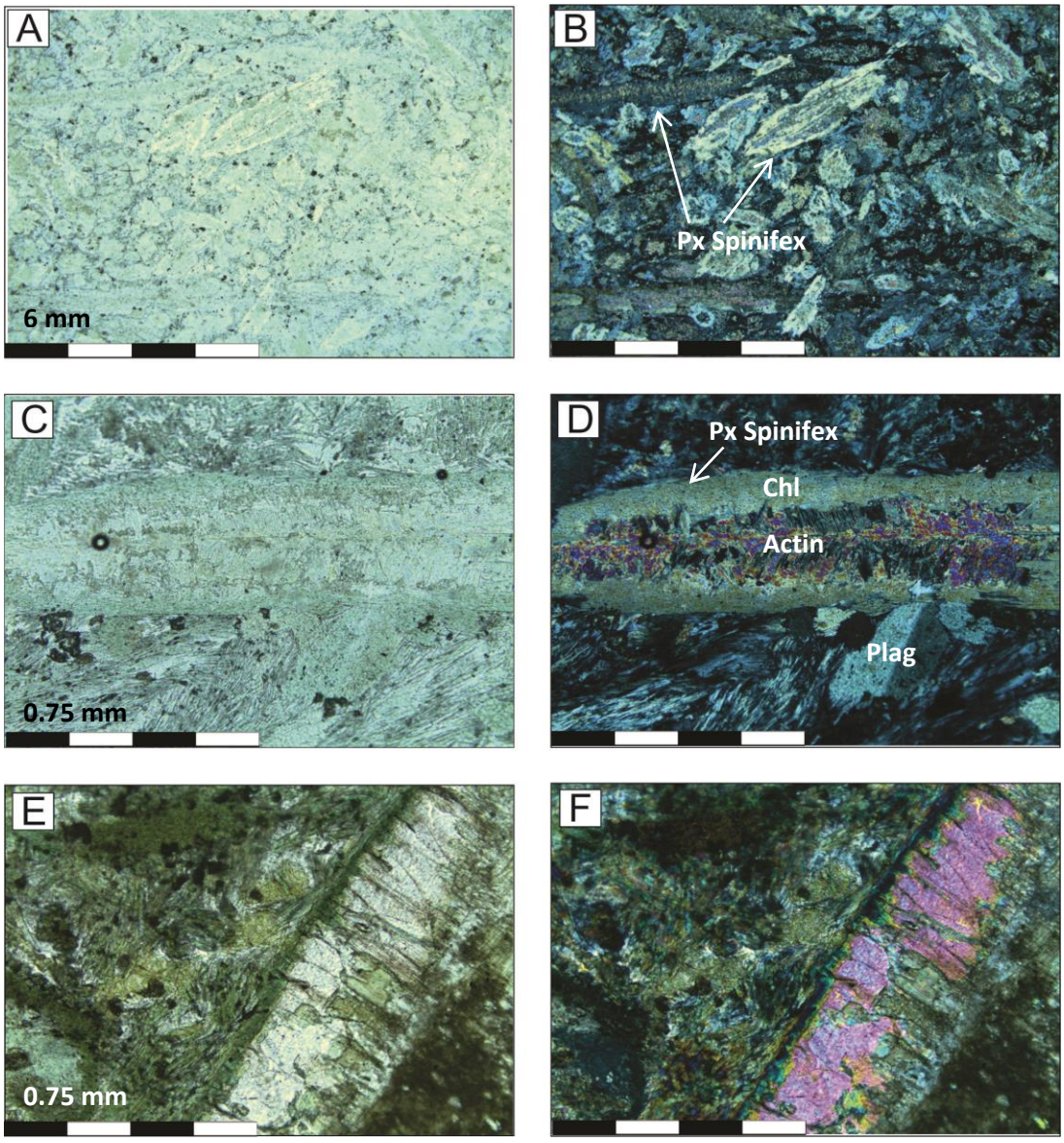

Figure 7.6
The pyroxene crystals found in the spinifex zone of the tumulus unit are randomly oriented and almost completely altered in sample GC-7 **(A,B)**. Chlorite alteration occurs on the rims of the blades and actinolite-tremolite alteration occurs in the centre of the blades, plagioclase is present and the matrix is altered to a fibrous serpentine chlorite combination in sample GC-4 **(C,D)**. In a single sample unaltered pyroxene (augite) is present within a fine grained altered matrix in sample GC-26 **(E,F)**.

The pyroxene grains are altered to a combination of chlorite and tremolite- actinolite, seen in the matrix and in the cores of zoned grains. Opaque minerals are <0.1 mm in size, are irregular shapes and are randomly dispersed throughout the matrix and within the pyroxene blades. Magnesite overgrowth is present and forms euhedral 0.5 mm-sized rhomboids, which occur predominantly in the matrix but can also overprint the pyroxene grains (Figure 7.7). It is noted that the sample containing the large proportion of unaltered clinopyroxene (sample GC 26) is within 3 m proximity of a known unaltered pyroxenite and gabbro layer.

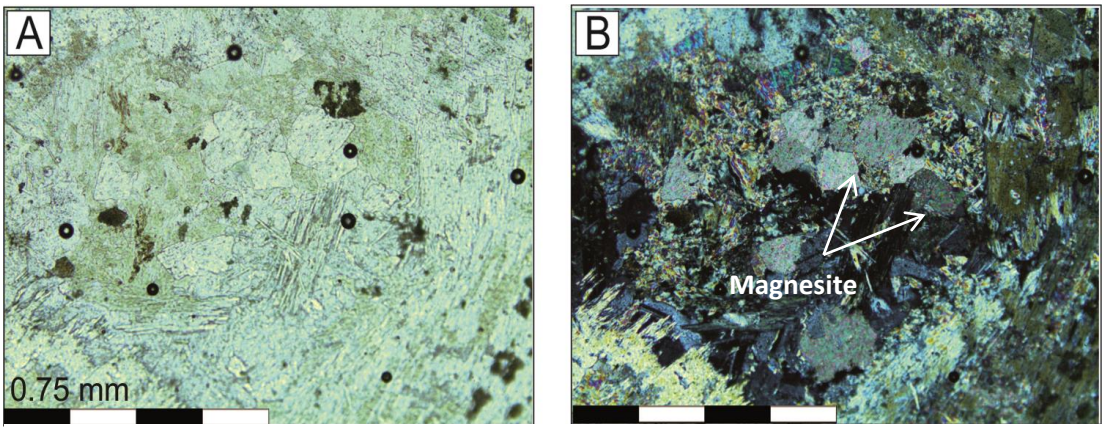

Figure 7.7
Magnesite overgrowth occurs in the pyroxene spinifex layer of the tumulus unit. They form euhedral grains which overprint the original igneous features and the serpentine alteration in sample GC-7.

7.3.1.5 Hyaloclastite Unit

The hyaloclastite section is 20 m thick and contains fragments of chilled lava surrounded by a glassy shard matrix. Nine thin sections were taken over the 20 m section, including sample GC 35, which is a chilled lava fragment in contact with the matrix (Figure 7.8).

Sections GC 8 and GC 30 are fine- grained and contain sparse (<5 %) small vesicles and mineral inclusions. These samples are considered to represent the fine- grained chill of a fractured lava block. These two sections have similar characteristics. They are fine- grained and dark green- brown in plane polarized light with patches of white constituents. In crossed polarized light they retain the same green- brown colour, but the white patches become dark, almost isotropic. These samples contain fragments or relics of grains such as olivine (up to 1 mm) and small (0.5 mm) sparse vesicle-like features that are filled with a glassy material (Figure 7.9). Sample GC 30 has evidence of spinifex blades and flow textures (Figure 7.9). The alteration minerals are difficult to determine due to the fine-grained nature of the

samples, but chlorite, serpentine, tremolite and actinolite are commonly present. Opaque minerals are disseminated throughout the fine grained samples, with some concentration around olivine grain boundaries.

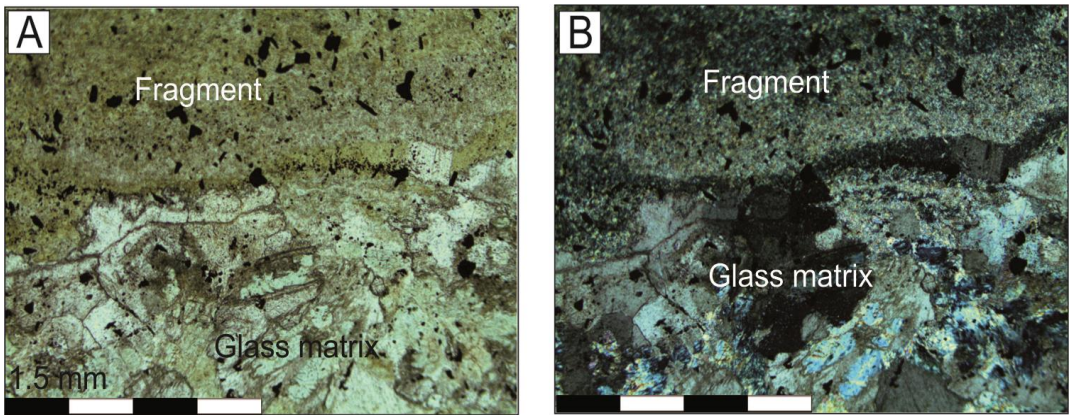

Figure 7.8
Subtype (1) the fragment in contact with subtype (2) the glass shard matrix. Both components create the hyaloclastite texture found in the tumulus unit. A clear sharp contact is evident, with magnesite overprinting the magmatic and metamorphic features from GC-25.

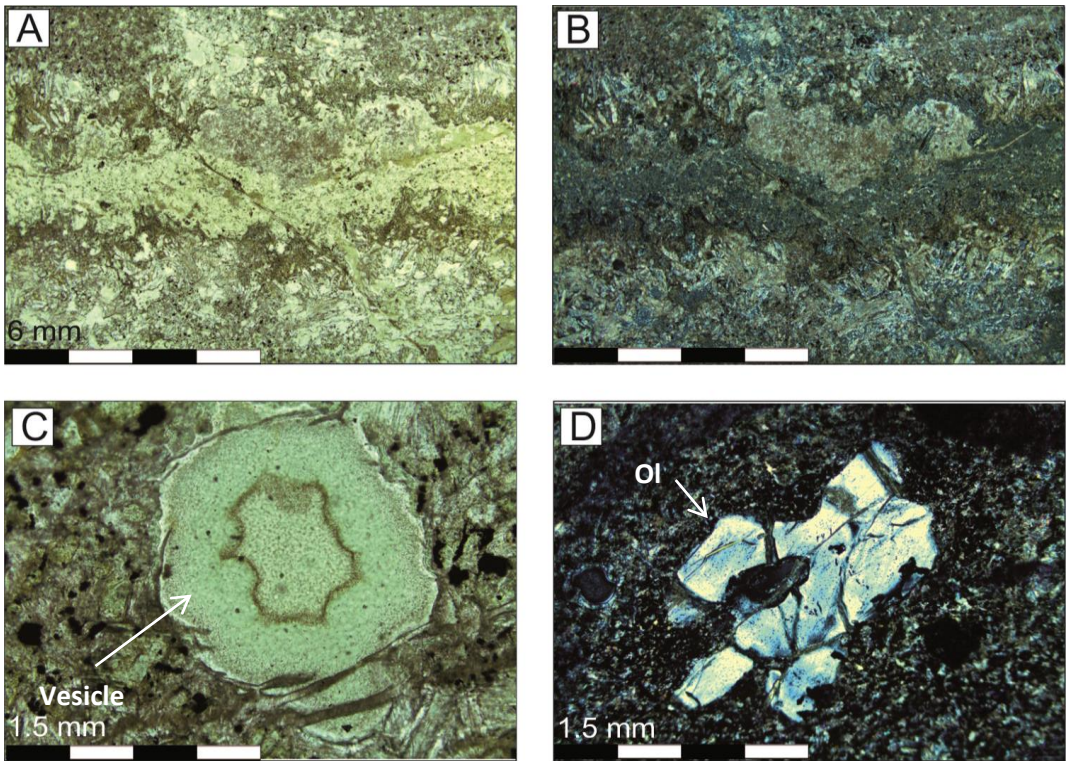

Figure 7.9
The chilled and fragmented blocks of the upper carapace of the tumulus unit, from sample GC-20, are fine grained and contain elements such as vesicles **(C)** and olivine grains **(D)** in the fine grained chill fragment **(A,B)**.

The remaining samples; GC 9, GC 10, GC 31, GC 32, GC 33 and GC 34, sample the glassy shard-like matrix that surrounds the chilled fragments. These are also fine-grained as evident in sample GC 32 and GC 33. Sample GC 31 contains larger fragments of spinifex but this is uncommon. A unique feature of these thin sections is the abundance of rounded to angular once-glassy fragments that make up most of the sample (Figure 7.10). Small vesicles are present in some samples – GC 31 for example– but contribute no more than 2% to the sample. They are medium-green in colour in plane polarized light and produce various colours in crossed polarized light, depending on the minerals present. The glassy fragments range in size (1 mm – 1 cm) and shape (spherical to irregular, rectangular or shard-like). They are closely packed and appear in some instances to mould around one another (Figure 7.10 C,D). Some of these shards, for example in sample GC 10, GC 33 and GC 34 – are highly zoned with alternating chlorite-tremolite and magnesite layers. This causes the colours in crossed polarized light to alternate between dark blue- black and high 6th order birefringence of magnesite, which has similar optical properties to calcite (Figure 7.10 C, D). Magnesite grains overprint the shard texture and microcrystalline magnesite forms alternating rings or layers around the shards or it occurs as veins. Some serpentine veins are also present. Moreover, the opaque minerals form stippled zones or rings around the shards.

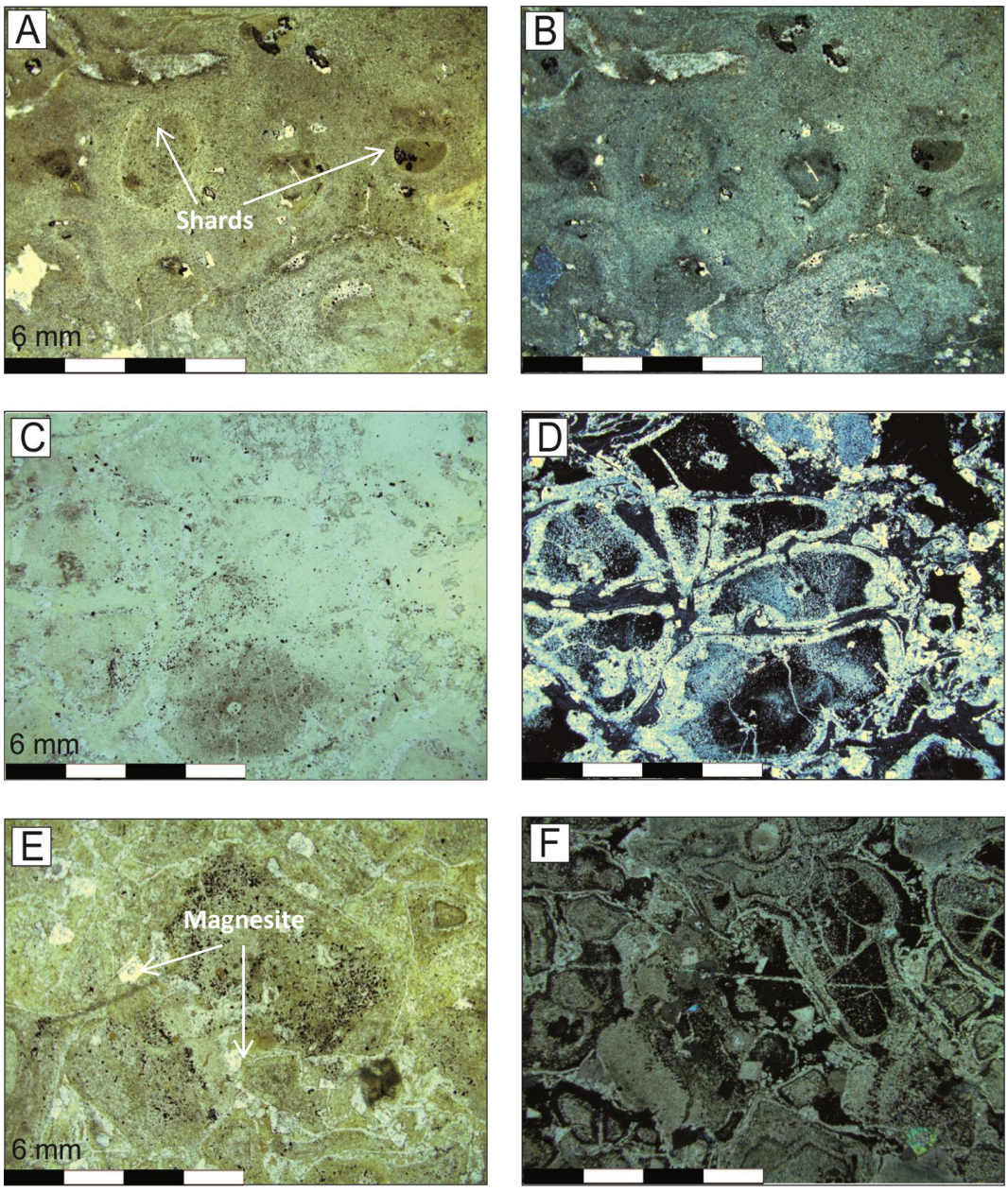

Figure 7.10
The glass shard matrix consists of zoned glass fragments that are rounded and irregular in shape in sample GC-32 **(A,B)**. These shards can amalgamate to form a single round shard made up of smaller irregular shards seen in sample GC-10 **(C,D)**. Microcrystalline magnesite occurs in zones around these shards causing the zoning of the shards evident in sample GC-34 **(E,F)**. Alteration to serpentine and chlorite is present, but the predominant alteration is to magnesite, as it forms as euhedral grains and as microcrystalline replacement.

7.3.2 Differentiated Komatiite Flows

The differentiated komatiite flows comprise three textural sections, the lower olivine cumulate (B2 unit), the spinifex layer (A2 unit) and commonly an upper chill margin (A1 unit). Each of these sections was sampled so that textural and mineralogical differences between equivalent textural sections could be identified and described. For example, the cumulate zone of numerous flows are sampled and then compared to determine any petrographic difference between flows. Changes in texture and mineral composition can indicate changes in lava flow processes and possibly different lava sources. As discussed in Chapter 5, the differentiated komatiite flows are found in packages between massive komatiites and komatiitic basalts.

7.3.2.1 Cumulates

The cumulate zones usually consist exclusively of cumulus olivine crystals and in one instance, a combination of cumulus olivine and pyroxene crystals.

The cumulate layers in the BARB 1 core contain 0.1- 2 mm sized, euhedral and subhedral olivine crystals. Each olivine grain is almost completely surrounded by melt residue, which comprises between 20 and 40 % of each sample. In general, the samples are pale green under plain polarized light, whilst under cross polarized light the olivines acquire the dark, 1st order grey of serpentine. The matrix is commonly serpentine, but in some samples the matrix can be microcrystalline and contain chlorite and tremolite-actinolite blades or fibres, which over-grow the cumulate texture. A common feature in the AHW/DM (BARB 1 (89-118m)) samples is that the olivines have chlorite rims (Figure 7.11). In the AHW/TM (BARB 1 (378-420 m)) samples the matrix is commonly dark, almost opaque, making identification of minerals between the olivine grains difficult (Figure 7.12). Closer inspection reveals the poikilitic nature of the cumulates, where the olivine cumulates are commonly embedded in large pyroxene oikocrysts. The olivine cumulates are homogeneous and there is no evidence of metamorphic recrystallization, other than serpentine and magnesite veining that does not obscure the original textures of the crystals, but rather crosscuts the cumulate grains. Opaque minerals (magnetite and chromite) are found around the edges of the olivines and along the fractures within the olivine grains. Commonly the opaque minerals are irregularly shaped and <0.1 mm in size. However a secondary phase of opaque formation allowed larger (0.1-0.5

mm) and very euhedral (commonly cubic shaped) minerals to form as an overprint of the textures in the rock.

In most samples the cumulus mineral is exclusively olivine. Sample AHW/DM 9 consists of euhedral cumulus olivine and pyroxene grains. The olivine crystals contain a large amount of magnetite, which distinguishes them from the opaque-free pyroxene cumulate grains (Figure 7.11).

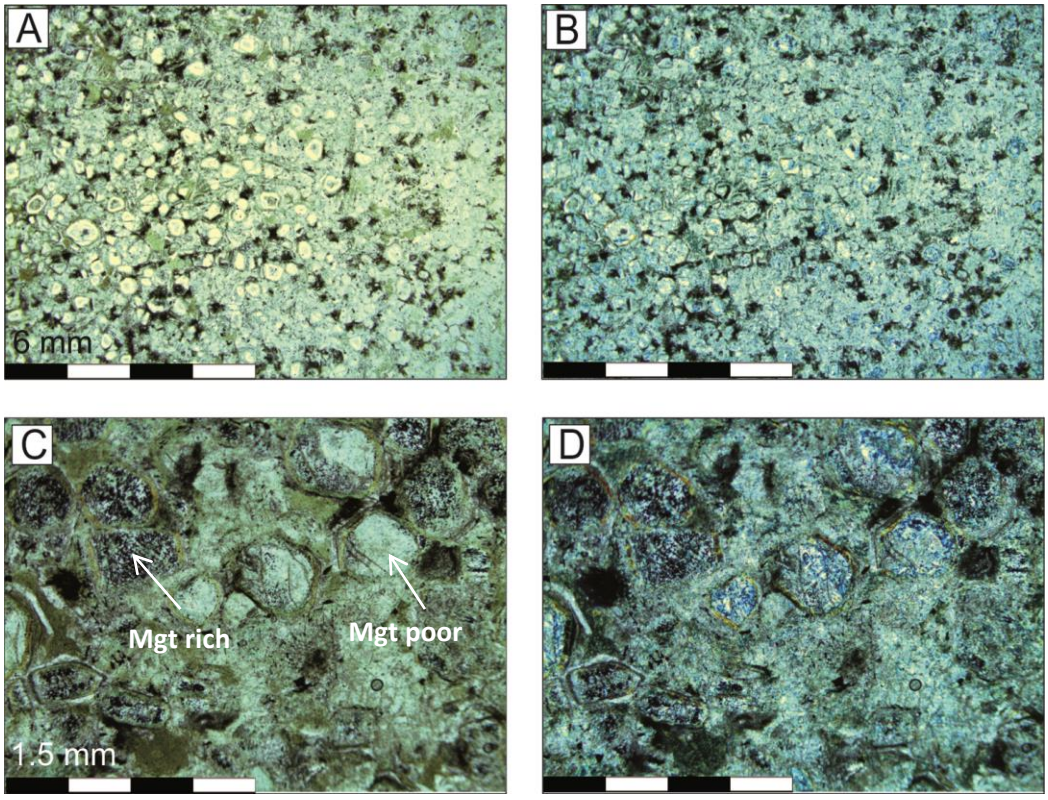

Figure 7.11
Olivines from the differentiated komatiite flows directly above the tumulus unit, between 89-118 m, are completely surrounded by melt residue as is evident in AHW/DM 9 **(A,B,C,D)**. Chlorite rims the olivines and magnetite (Mgt) is concentrated in specific grains (Mgt-rich vs. mgt-poor). The samples are altered to serpentine and chlorite.

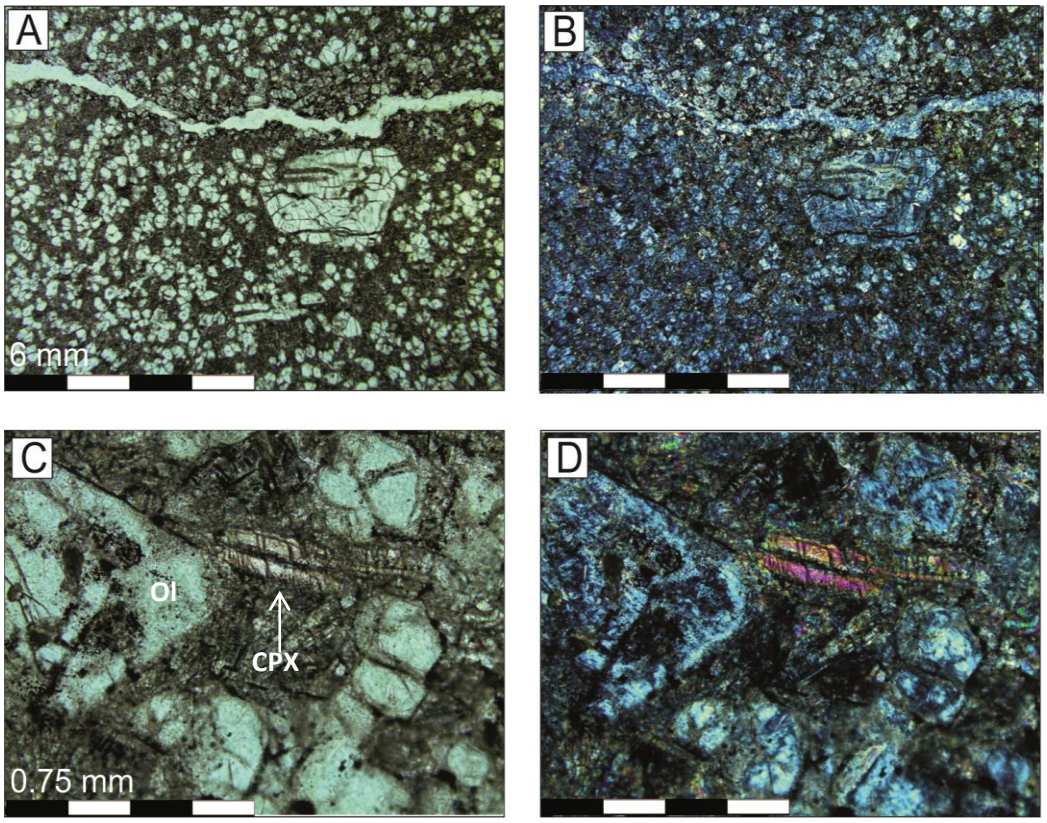

Figure 7.12
Olivine cumulates from the (378-420 m) differentiated komatiites have a dark matrix between the cumulates **(A,B)**. Unaltered pyroxene (CPX) grains are found in the matrix **(C,D)** and form oikocrysts around the olivine cumulates as evident in sample AHW/TM 42.

Olivine cumulate samples in BARB 2 core consist of clear to pale green olivine grains 0.5- 1 mm in size, which are replaced by serpentine, and surrounded by a pale to medium green matrix. Under crossed polarized light the olivines have the 1st order steel-grey colour of serpentine, whilst the matrix can vary in colour from the grey of serpentine to high second order birefringence colours of tremolite-actinolite or anomalous colours of chlorite. The matrix material comprises 40-60 % of each sample (Figure 7. 13). The alteration of these cumulates is the same as for the cumulates of BARB 1. In some samples (for example BARB 2-2) the cumulates are less distinct and the grain boundaries appear to be overgrown and obscured by metamorphic minerals such as chlorite. In this sample the melt residue appears to have collected in spherical pockets forming a pseudo-cumulate effect, with the actual olivine cumulate crystals occurring between these melt pockets (Figure 7.14).

In sample BARB 2-REF 5, the cumulus olivines have indistinct boundaries due to fibrous overgrowth of metamorphic minerals. Opaque minerals comprise less than 10 % of the cumulate samples. They are usually irregular in shape, <0.1 mm wide and are found associated with the olivines, either rimming the crystal boundary or lining fractures. Fine-

grained disseminates are present in the matrix, and minimal opaque minerals are related to the pyroxene crystals.

Only two of these BARB 2 cumulate samples, BARB 2-18 and BARB 2-19, contain both olivine and pyroxene. The samples contain between 10 and 15 % pyroxene, both orthopyroxene and clinopyroxene (augite), which are commonly fresh in the cores of the grains. The pyroxenes occur as oikocrysts that enclose cumulus grains of olivine (Figure 7.15). The boundaries are less distinct and alteration of the rims is present together with alteration of fractures that cut through the grains.

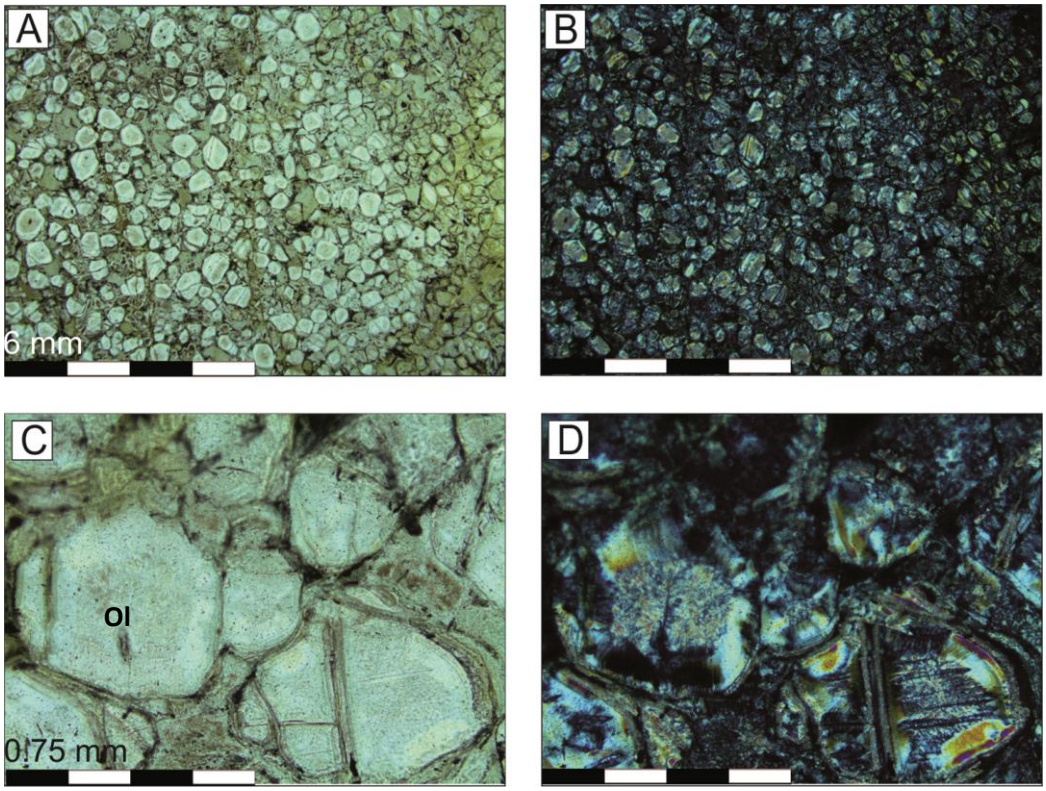

Figure 7.13
Olivine cumulates from sample BARB 2-22 in the BARB 2 (252-274 m) differentiated komatiite set. The olivines are surrounded by melt residue. The cumulates are altered to serpentine and the matrix to a tremolite-chlorite mixture.

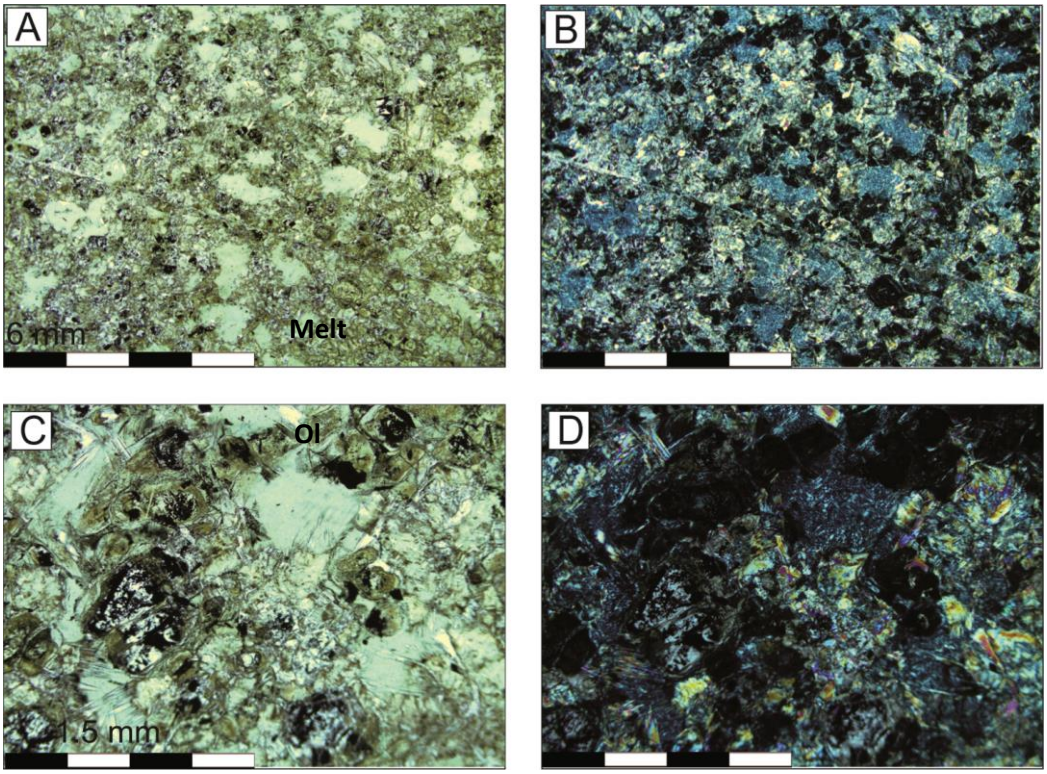

Figure 7.14
Sample BARB 2-2 showing pseudo cumulates, where the melt residue has formed pockets and is surrounded by olivine crystals. It appears that the cumulate and melt residue reversed textural roles in this sample. Alteration of the olivines to serpentine, while the matrix alters to a chlorite-actinolite combination.

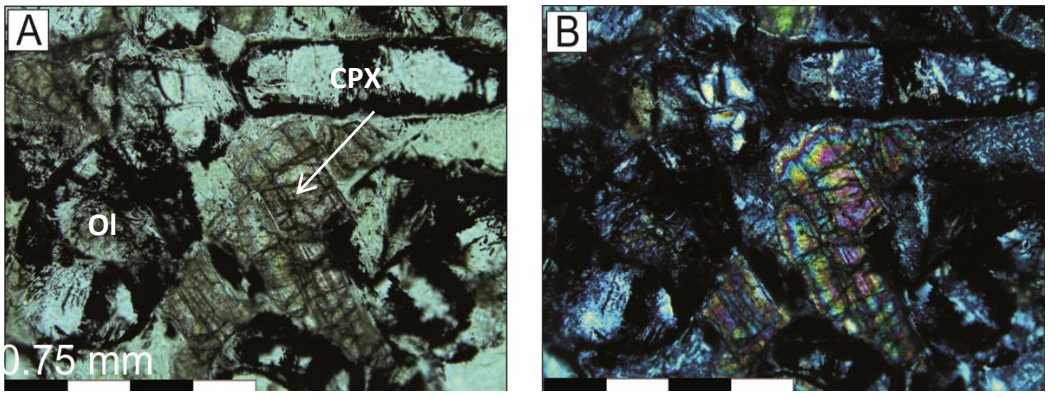

Figure 7.15
Evidence of unaltered pyroxene is present between the altered olivine crystals of the cumulate in sample BARB 2-19 from the differentiated komatiite package BARB 2 (252-274 m). The pyroxene is clearly formed after the olivine as it grows in the interstitial spaces and forms the beginning of an oikocryst.

7.3.2.2 Spinifex

The spinifex textured samples in the differentiated komatiite flows consist of olivine blades and pyroxene needles. As indicated by Arndt *et al.* (2008) , it is common to find large skeletal olivine blades or plates, with finer grained pyroxene fronds or needles, interstitial to the larger blades. This feature is present throughout the spinifex sections of the differentiated komatiite flows.

The suite of 12 samples from BARB 1 include olivine spinifex, a sample containing both spinifex and cumulate texture (GC 37) and a spinifex sample that also contains vesicles (AHW/TM 25). The spinifex samples are predominantly medium to dark green-brown colour in plane polarized light. Where large olivine laths are present, as in GC 41, AHW/DM 13, AHW/DM 23 and AHW/DM 25, the olivine blades are a white to pale green colour (Figure 7.16). Under crossed polarized light the samples have a darker green-brown colour and the olivine blades have the usual first-order grey of serpentine. The spinifex blades and needles range in size and morphology. The larger olivine blades, which define a dendritic or feather-like texture reach up to 5 cm in length, but are commonly between 5 mm and 2 cm and can be as wide as 3 mm. An exception to this case is found in the BARB 1 (89-118 m) differentiated komatiite package. In this section the spinifex texture has been recrystallized due to metamorphism and the spinifex blades are the typical length but exceptionally wide (up to 1 cm in width). The olivine laths create a framework for the pyroxene blades to infill. The melt became trapped between the large olivine blades then crystallized to form pyroxene spinifex. The pyroxene grains are typically a medium green brown in plane light; the needles reach a maximum of 5 mm in length and have a very obvious fibrous radiating texture between the olivine blades.

All spinifex samples are altered. Olivine typically is converted to serpentine with chlorite rims, whilst the pyroxene has altered to a combination of chlorite and tremolite. Often this combination is too fine grained to distinguish individual minerals. A single sample, AHW/TM 24, contains the usual olivine blades, but the interstitial pyroxene is completely chloritized and serpentinized, with no evidence for actinolite and tremolite. The spinifex sample, AHW/TM 25 contains vesicles (Figure 7.17) between needles of pyroxene, which preserve relics of fresh orthopyroxene and clinopyroxene (Figure 7.17). The opaque minerals are <0.2 mm in size, relatively euhedral, and are mostly associated with the larger olivine blades (Figure 7.16).

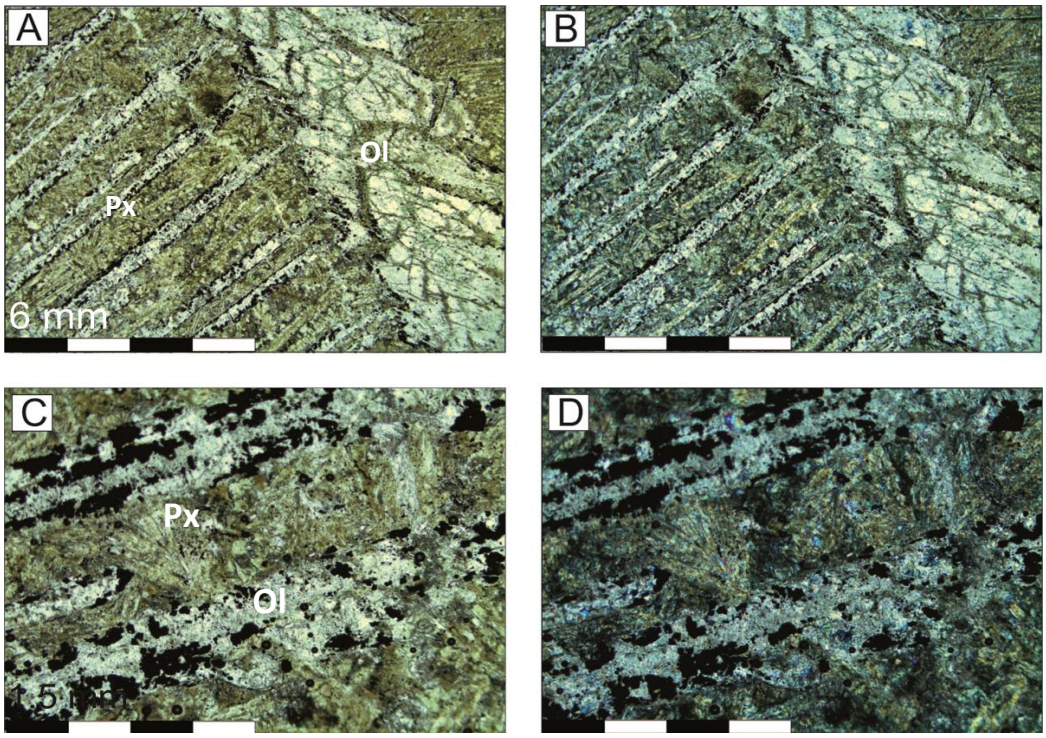

Figure 7.16
Olivine spinifex from sample GC-41 forms a dendritic or feather like structure **(A,B).** Between the olivine blades are smaller pyroxene blades and fibrous acicular pyroxene **(C,D)**. Opaque minerals are concentrated along the olivine blades.

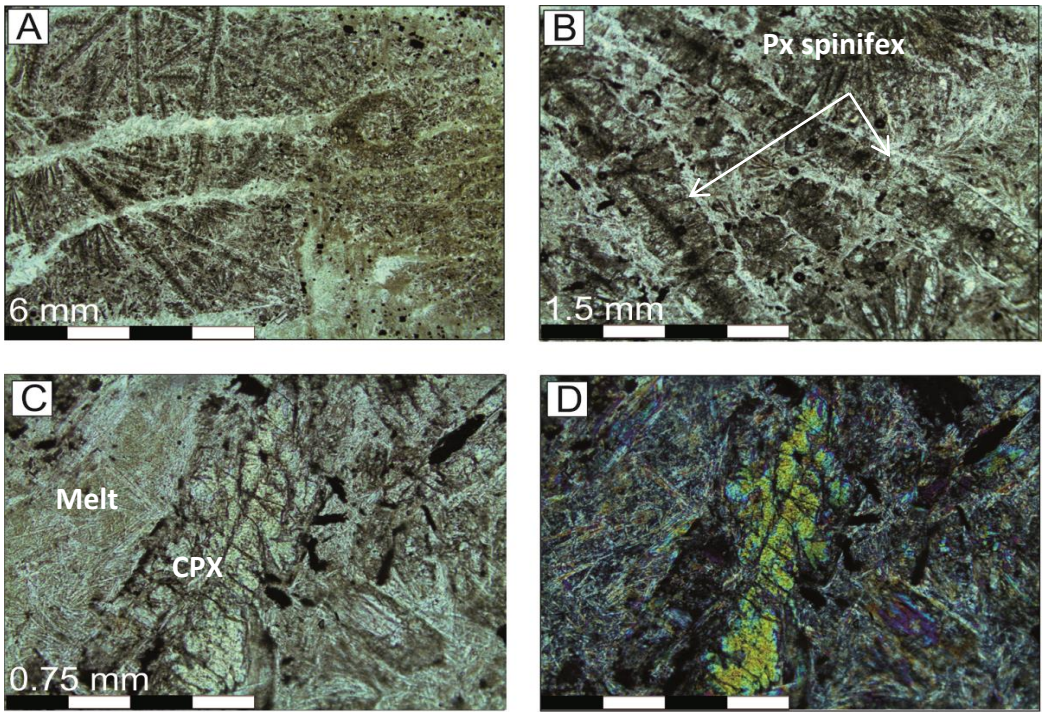

Figure 7.17
Pyroxene spinifex forms both large and small scale blades in sample AHW/TM 26 **(A,B)**. The blades are blocky and have sharp geometric shapes. Present in the pyroxene spinifex is kernels of fresh pyroxene **(C,D)** which is surrounded by needles of tremolite and chlorite.

11 olivine spinifex samples were taken from a differentiated komatiite flow package in BARB 2. Two samples (BARB 2-9 and BARB 2-20) contain both spinifex and olivine cumulate. The spinifex-textured samples are similar to those in BARB 1. The samples are grouped into two colour categories: (1) pale green with brown patches and (2) the dark green-brown samples. The paler samples have a larger quantity of olivine, whereas the darker samples contain a larger proportion of pyroxene. In cross polarized light the samples are typically 1st order grey, but most contain patches of high 2nd order birefringence associated with tremolite- actinolite, which is found predominantly in the matrix or replacing well-developed pyroxene crystals. At the thin section scale, textures are typically a radiating growth of pyroxene spinifex blades that formed between aligned olivine sheets. As in the case of the spinifex in BARB 1, different scales of spinifex are present in these samples. The large olivine plates create a framework, which is then filled in by thinner and shorter pyroxene spinifex that grows at various angles to the olivine blades. The spaces between the pyroxene spinifex are filled with acicular pyroxene growths.

Although these rocks are almost completely altered, some kernels or cores of pyroxene remain partially fresh and chemically intact (Figure 7.18). These unaltered pyroxene cores (up to 1 mm) are evident in 6 samples such as BARB 2-7, BARB 2-10 and BARB 2-20, where the unaltered grains have a higher relief than the surrounding matrix and are generally a pale green colour. Both orthopyroxene and clinopyroxene are present as unaltered minerals in these samples. These grains are always surrounded by an alteration rim and the remainder of the sample is altered to serpentine where olivine is present. The pyroxene crystals and the matrix are predominantly altered to actinolite and tremolite with patches of chlorite. The actinolite-tremolite grains mostly have blade- and needle-like shapes and commonly overprint the original igneous textures (Figure 7.18). The finer grained pyroxene spinifex is generally a dark brown, almost black colour, and alteration minerals are not readily identified. From the alteration in other parts of the core, it can be inferred that these pyroxenes are composed of similar metamorphic minerals namely; actinolite, tremolite and chlorite. Secondary magnesite and serpentine veins cross-cut all primary igneous features. The opaque minerals range from well-formed to irregular in shape and from <0.1 to 0.5 mm in size. They are generally associated with the olivine sheets and when those are not present, the opaque minerals are randomly dispersed through the sample. There is minimal association of opaque minerals and fresh pyroxene grains. In sample BARB 2-28, the opaque minerals in the olivine blades appear to be smeared out in a single direction, possibly indicating some

type of strain. However, the actual olivine grains remain undeformed. In some instances melt residue has accumulated into small spheres (much less than 0.1 mm) in between the fine-grained fibrous spinifex, causing a bubble-like feature to form, these are most likely vesicles. (Figure 7.19).

The spinifex texture occurs on multiple scales. One type consists of feather-like olivines with a central plate and smaller perpendicular plates branching off; or a radiating structure formed by the olivine plates (Figure 7.16 A and Figure 7.20 A). Pyroxene needles crystallized between the large olivine framework. These pyroxene grains may be large and well defined, often reaching up to 1 cm in length. They typically formed perpendicularly, or at an angle to the olivine plates and many have a notable block-like feature, as if the blades were composed of many aligned pyroxene cubes (Figure 7.20 C). Another texture, developed on a smaller scale, (less than 2 mm), is a fibrous growth of pyroxene, known as acicular pyroxene, which formed between the larger spinifex needles. These fibrous features typically radiate outwards from the point of origin (as illustrated in Figure 7.20 B,D). Figure 7.20 D shows a case where the olivine laths are not exceptionally thick and perpendicular growths of acicular pyroxene occur in between these laths.

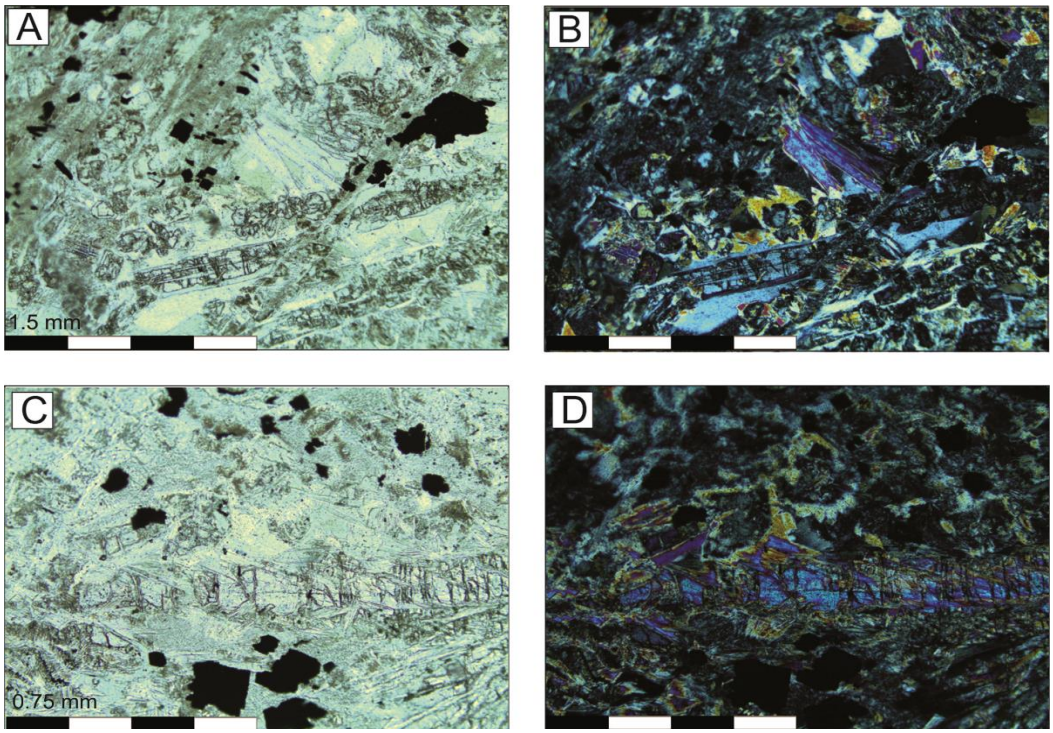

Figure 7.18
Sample BARB 2-10 shows evidence of partially unaltered pyroxene surrounded by a matrix of actinolite-tremolite blades and chlorite alteration in the BARB 2 (252-274 m) package **(A,B)**. Unaltered clinopyroxene is evident in **(C,D)** with a higher relief and minimal green colouring which is associated with alteration. The opaque minerals are irregular in shape and have no association to the pyroxenes.

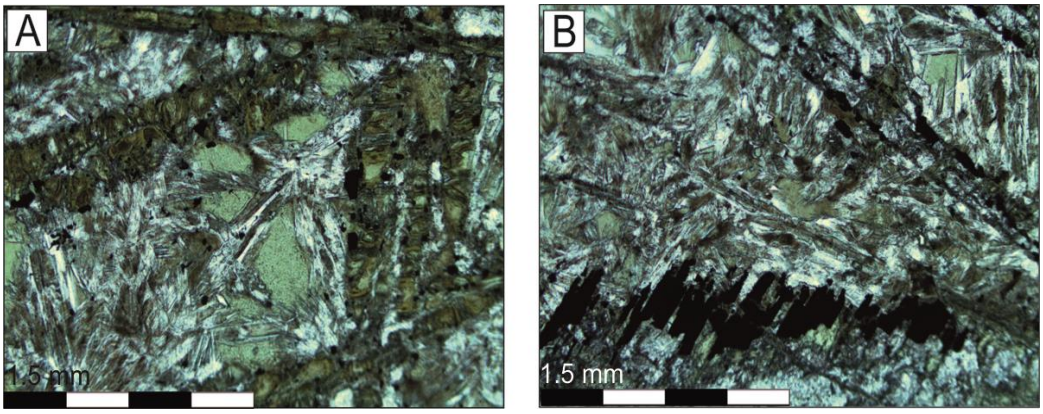

Figure 7.19
(A) Sample BARB 2-28 shows the small melt bubble inclusions that remain in the spinifex between the pyroxene blades and the elongated opaque minerals. The host minerals are unstrained (**B**).

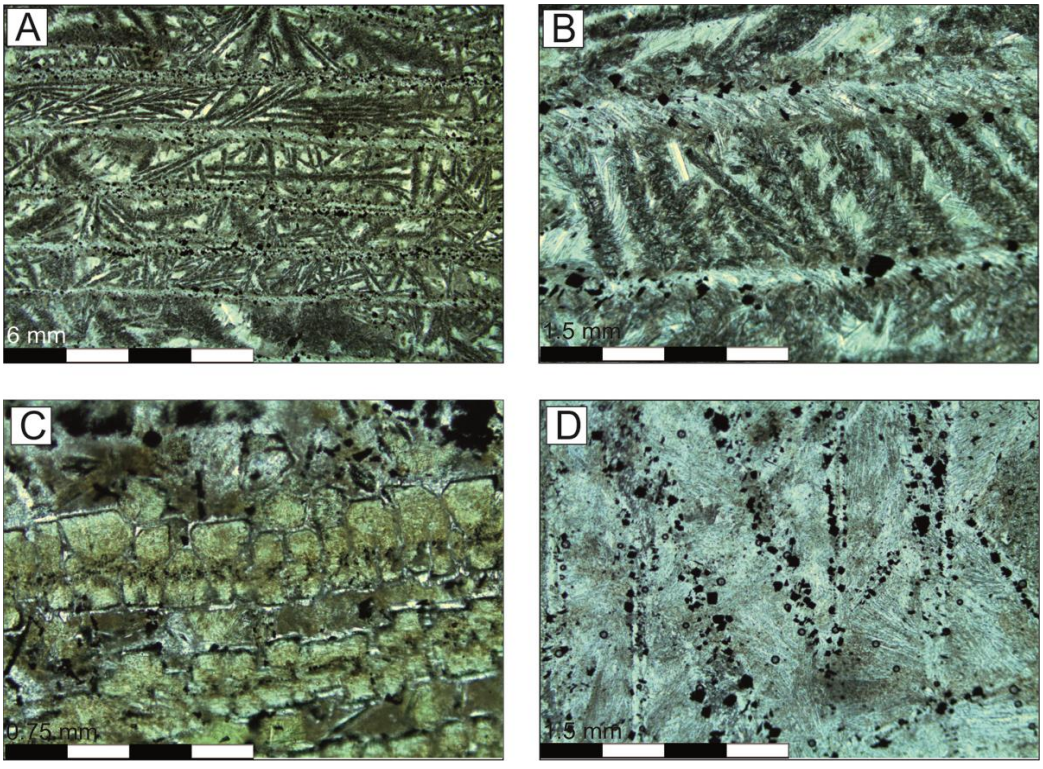

Figure 7.20
(A,B) Sample BARB 2-16 illustrate the large olivine blades which create a structure that is filled in by the smaller pyroxene blades. **(C)** Sample AHW/DM 24 shows the blocky nature of the pyroxene blades. Between the pyroxene blades are radiating fibrous pyroxene growths **(C,D)**. **(D)** Sample AHW/TM 18 shows the large olivine blades with only fibrous pyroxene between them, lacking the pyroxene spinifex.

7.3.2.3 Chill Margins and Contact Relationships

Three chill margins were sampled in the BARB 2 (252-274 m) differentiated komatiite package. These samples (BARB 2-1, BARB 2-8 and BARB 2-25) are fine-grained and illustrate that on a micro scale, the chill margins have similar features to the overlying or underlying textural forms. Thus the upper chill margin of a komatiite flow may contain micro-spinifex laths, whilst the lower chill of a komatiite flow contains micro olivine crystals transported in the melt (Renner *et al.*, 1993). For example, sample BARB 2-1, contains about 25% of small (0.1 mm) euhedral olivine grains in an altered glassy matrix which presumably is the transported olivine load . In sample BARB 2-25 micro-spinifex is evident, indicating that the chill represents the uppermost portion of a spinifex flow. Sample BARB 2-8 contains the actual sharp contact between the micro-spinifex-textured chill of the underlying flow and the porphyritic chill zone of the overlying flow (Figure 7.21). The grain-size of the olivine phenocrysts and skeletal crystals do not exceed 1 mm. The samples are dark green- brown in colour under plane polarized light and under crossed polarized light they have a dark grey-brown colour. The dark colours are attributed to the fine- grained nature of the rocks rather than to specific alteration. The alteration minerals present are serpentine, chlorite, tremolite and actinolite, which occur as inter-grown patches and are often present as an amalgamation of the metamorphic minerals. The opaque minerals are homogeneously distributed throughout the chill zones and are also fine grained in nature, being <0.1 mm in size and relatively regular in shape.

7.4.1 Massive Komatiites, Komatiitic Basalts, Basalts and Gabbros

The remaining sample-types from the BARB 1 and BARB 2 core consist of massive komatiites, komatiitic basalts, basalts and gabbros. These samples are taken for completeness of the core sampling and as a means of comparison between field identification and geochemical and petrographic rock-type identification.

Two massive komatiite samples were taken from the BARB 1 core. These samples contain about 50 % of 0.5 to 2 mm-sized euhedral to subhedral olivine grains in an altered glassy matrix. The alteration minerals are mainly serpentine with chlorite and actinolite present in small patches, forming a fibrous texture in the matrix surrounding the olivine grains (Figure 7.22).

Two komatiitic basalts were sampled. They are pale green under plane light with a 1st order grey in crossed polarized light and very small patches of low second-order birefringence that are microcrystalline. The samples consist of fine-grained, poorly-formed olivine crystals surrounded by melt residue that has been altered to a fibrous actinolite-tremolite-chlorite combination, which has most likely over-printed the original texture (Figure 7.23). The alteration minerals are a combination of serpentine, chlorite, tremolite and actinolite. These form small blades and patches, which overlap and interfere with one another. The opaque minerals are <0.1 mm and are scattered through the sample.

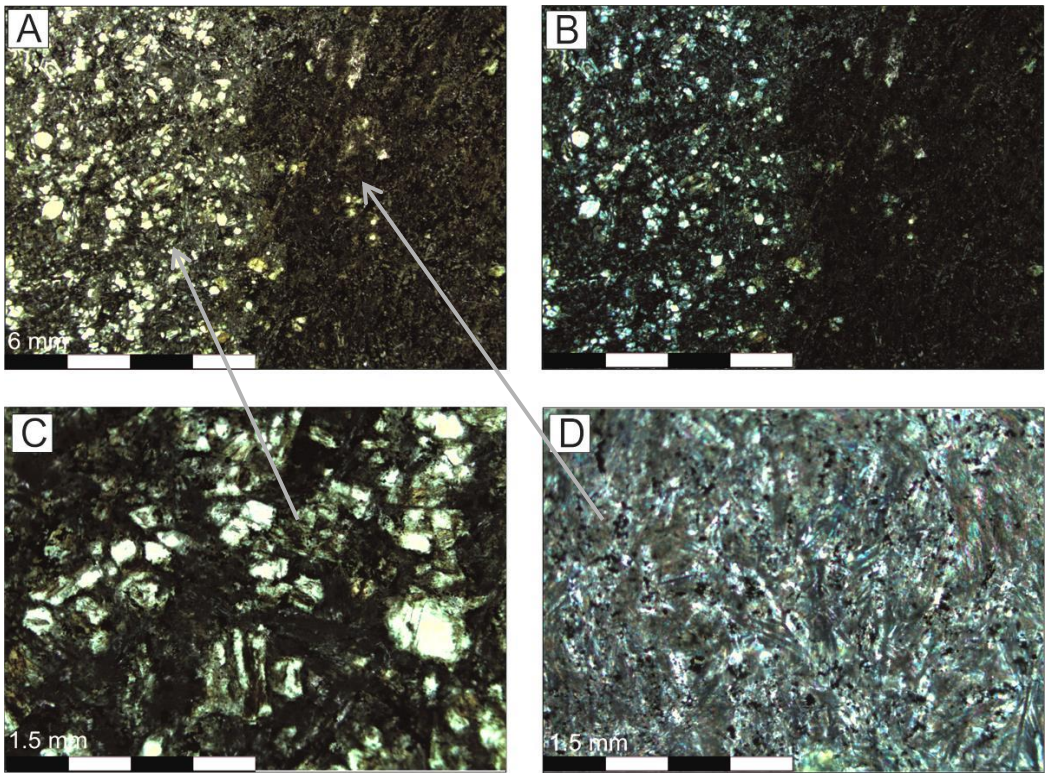

Figure 7.21
Chill zone with sharp contact from sample BARB 2-8 **(A,B)**. On the left hand side is the cumulate of the overlying flow **(C)** and on the right hand side is the spinifex from the underlying flow **(D).**

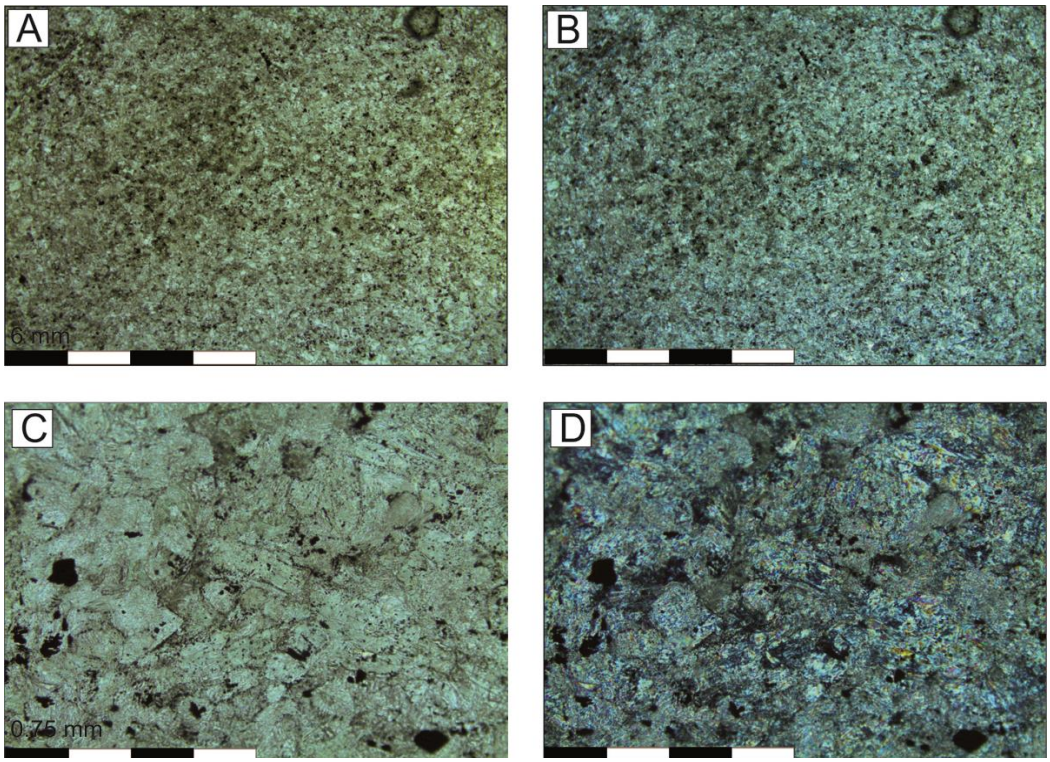

Figure 7.22
Sample BARB1 REF 21 shows a massive komatiite containing small (<0.5 mm) olivine grains which are altered to serpentine while the matrix is altered to chlorite and tremolite. The sample has a homogeneous texture.

Sample BARB 2 ref 29 has sharp contacts with the surrounding ultramafic rocks, indicating a later intrusion into a 4 m thick olivine cumulate layer. It contains no olivine or pyroxene but contains large (up to 4 mm- sized) plagioclase phenocrysts in a fine-grained groundmass. This makes it a plagioclase porphyry rather than a true basalt. The plagioclase grains are a medium-brown colour in a matrix of pale green, under plane polarized light. Under crossed polarized light, the plagioclase grains are a 1st order grey-brown whilst the matrix is a microcrystalline white-grey colour with patches of low 2nd order colours (Figure 7.24). Although the plagioclase is relatively unaltered, the matrix is altered to a chlorite, actinolite, tremolite combination, with very distinct needles of fibrous actinolite that grow radially from the nucleation site. The opaque minerals that are present are irregularly shaped and randomly dispersed through the sample.

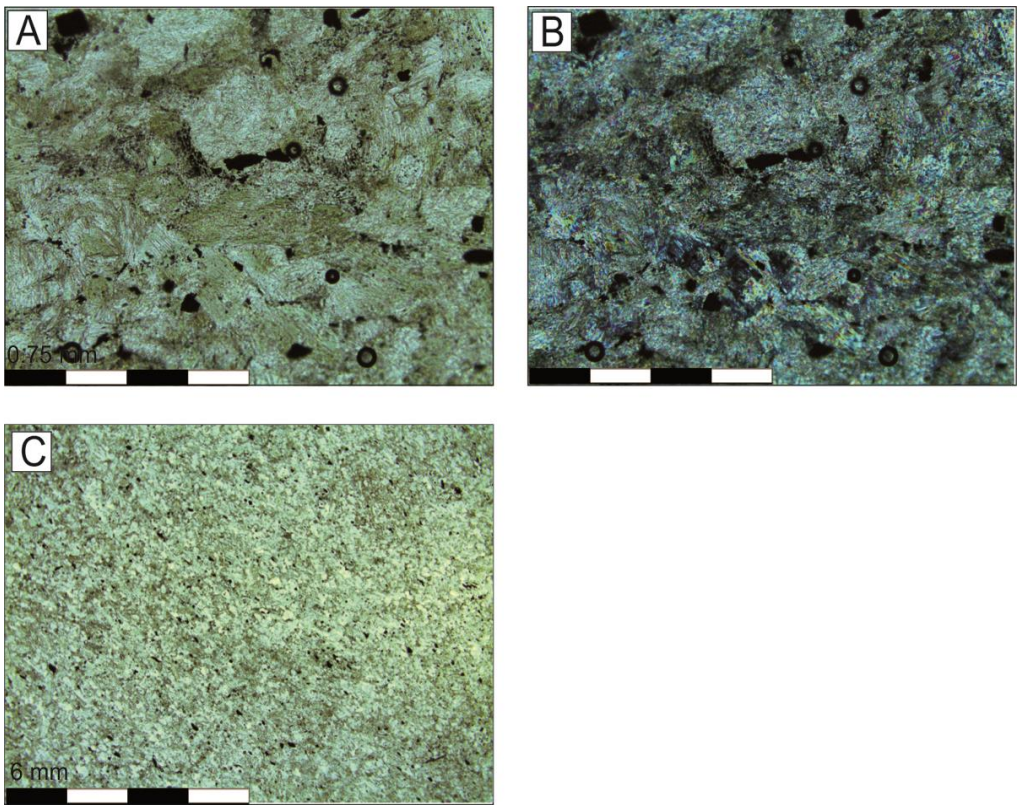

Figure 7.23
Sample BARB 1 REF 17 is a komatiitic basalt. Fine grained poorly formed olivines are altered to serpentine and the matrix is altered to chlorite, tremolite and actinolite. **(A,B)** show the mineralogy whilst **(C)** shows the large scale texture and structure of the homogeneous komatiitic basalt.

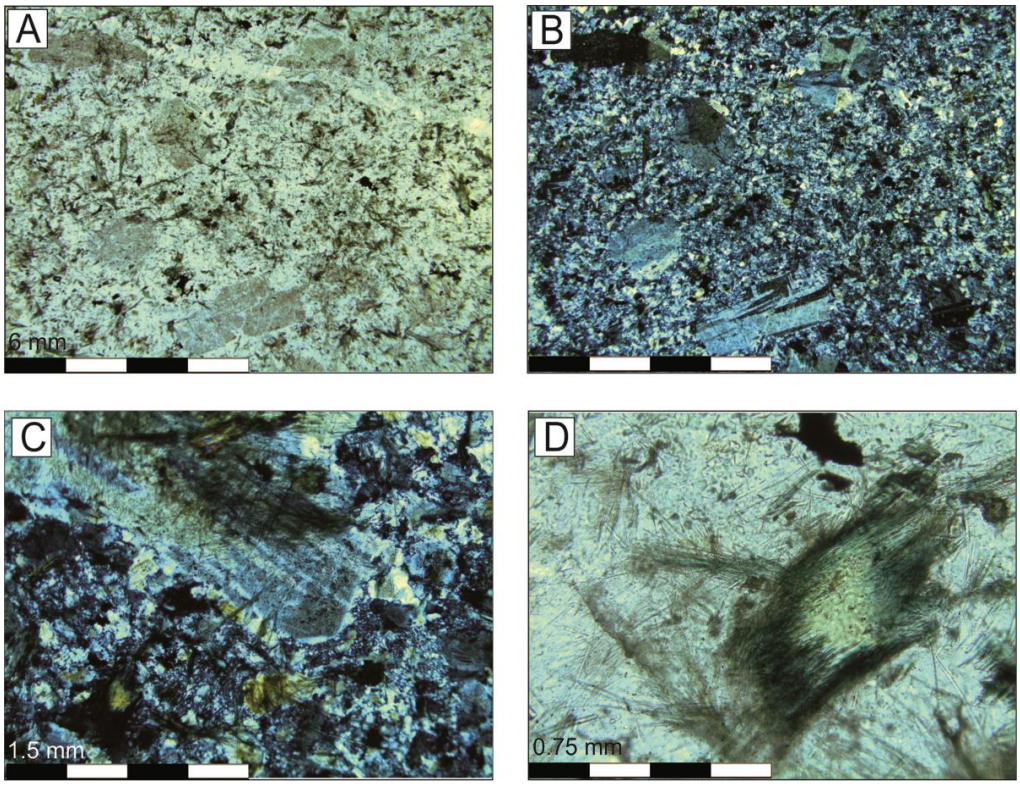

Figure 7.24
Sample BARB 2 REF 28 is an intrusive basalt sample. Fine grained matrix material containing plagioclase phenocrysts **(A,B,C)**. The matrix is altered to chlorite with tremolite fibres overgrowing the igneous features **(C,D)**.

Sample BARB 1 ref 30 is a gabbro and contains about 30 % pyroxene and 20 % well-formed plagioclase. The sample is pale green in plane polarized light. In cross polarized light the pyroxene crystals go a 2nd order colour of tremolite. The plagioclase turns the typical 1st order grey and is twinned and the matrix consists of fine-grained inter-grown needles of serpentine, chlorite and tremolite. Some unaltered pyroxene kernels occur as small fragments in close proximity to one another (Figure 7.25). Plagioclase appears to be relatively unaltered, and in conjunction with the fresh cores of pyroxene, this could indicate a later intrusion of gabbro as a sill. The opaque minerals are <0.5 mm in size and are randomly scattered through the sample.

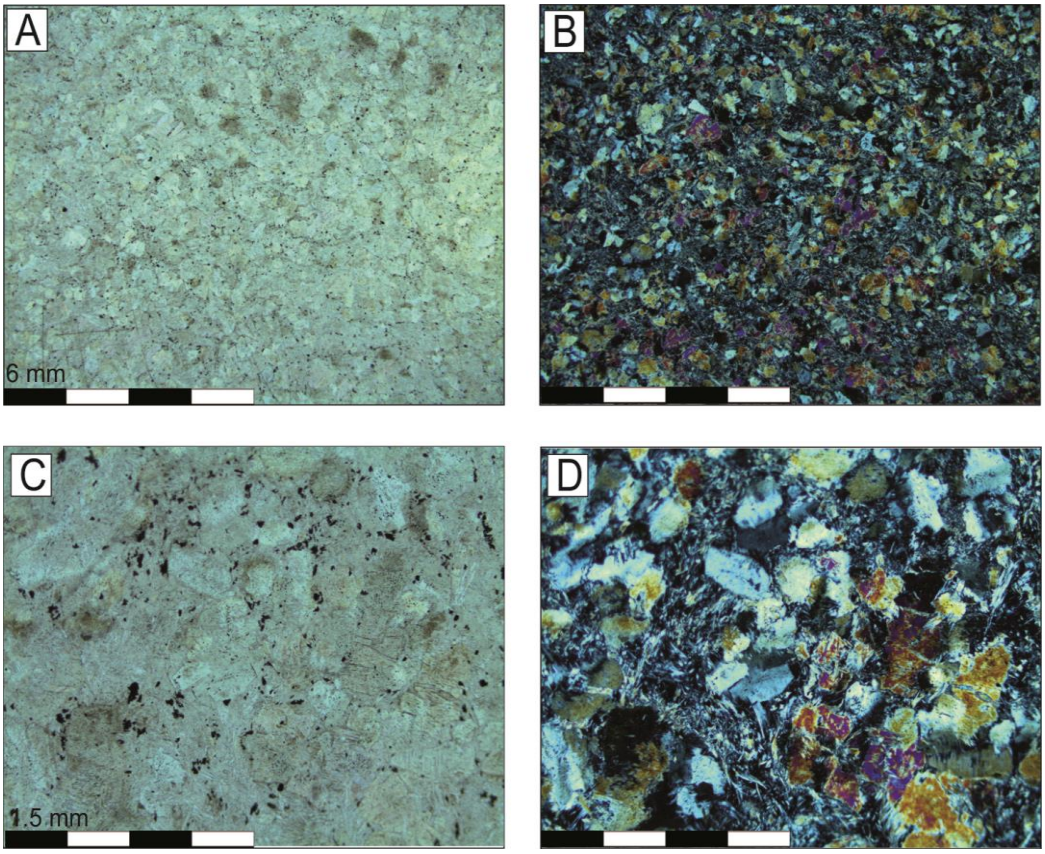

Figure 7.25
Sample BARB 1 REF 30 shows a gabbro containing plagioclase and fresh pyroxene. **(A,B)** illustrate the homogeneity of the texture. Plagioclase is evident in (**D).**

7.4.2 Surface Samples

Six surface samples were taken in order to compare the surface outcrop with the corresponding sections in the core. Three samples were taken from the surface outcrop above the BARB 2 hole (Figure 6.11). GC-C-1 and GC-C-2 are both medium green- brown in plane light, whilst GC-C-3 is a pale-green under plane polarized light. Under cross polarized light, GC-C-1 and GC-C-2 are generally a first order dark grey, and contain minerals of very high 2nd to 3rd order birefringence. GC-C-3 is generally a first order yellow under crossed polarized light. It is noted that all three of these surface samples contain between 20 and 35 % olivine, 20-40 % pyroxene and approximately 15 % groundmass; with opaque minerals comprising the remainder. The pyroxene crystals have a red-brown stain, which is pleochroic. This staining is most likely caused by surface weathering and oxidation. The pyroxene crystals present in these samples, constitute a poikilitic texture, surrounding the cumulus olivine crystals. This is evident in Figure 7.26 A,B. The settled olivine crystals are 0.5 mm in size, rounded to subhedral and are present within a single large (up to 6 mm) grain of pyroxene (both ortho and clino-pyroxene). In sample GC-C-1 and GC-C-2 the poikilitic pyroxenes are unaltered and large enough to be magnetically separated for Hf and Nd isotope studies. GC-C-2 is the only sample where kernels of unaltered olivine are evident (Figure 7.26 C,D). The olivines are enclosed by pyroxene and have alteration rims of serpentine. The cores of these grains have a relief higher than the surrounding serpentine and are high 3rd-order birefringence colours, indicating relic unaltered olivines. Veins of opaque minerals crosscut the olivines, creating a jigsaw effect. GC-C-1 has the same textures as GC-C-2 however, the olivines are completely altered. In sample GC-C-3 the texture is the same with poikilitic pyroxene containing olivine crystals, however the entire sample is completely altered to serpentine, chlorite and tremolite. It also contains 55 % groundmass, which is altered to serpentine. Opaque minerals make up a significant proportion of the samples GC-C-1 and GC-C-2 (15-20 %) but are a small portion of GC-C-3 (<5 %). They typically concentrate in the olivine fractures and around the rims, but are also present in the pyroxene crystals.

Three samples were taken from the tumulus outcrop (Figure 6.11) and were compared with the corresponding sections within the BARB 1 core. A single cumulate sample and two samples of the upper vesicular carapace were taken from the tumulus. Sample (GC-C-4) was taken from the cumulate zone at the surface close to the BARB 1 collar. It comprises of similar features to those observed in the cumulate zone of the BARB 1 core (Figure 7.1). The

only exception being that the surface sample has a slight red-brown tinge in some places, attributed to surface weathering and oxidation. The crystals are the typical pale-green in plane light and 1st order grey in crossed polarized light. They are between 0.5 and 1 mm in size and some have rounded ends and are altered to serpentine; similar to the olivines found in the core. The opaque minerals are not abundant, and are found as miniscule <0.1 mm sized grains contained within the fractures of the olivine crystals.

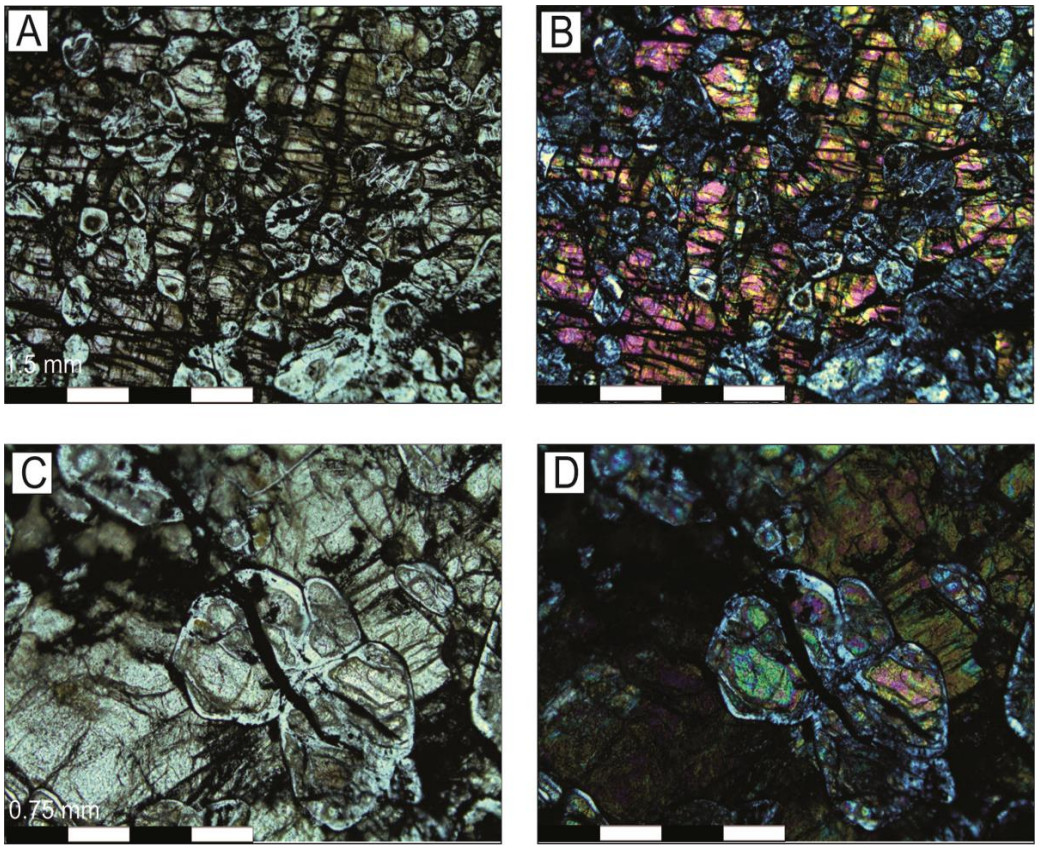

Figure 7.26
Surface cumulate sample GC-C-2. **(A,B)** indicate the presence of fresh pyroxene which creates a poikilitic texture with the olivine cumulates. **(C,D)** indicate the presence of kernels of fresh olivine which are <0.1 mm in size.

During surface mapping of the tumulus zone, Dann (2001) identified a 20 m-thick vesicular komatiite zone (Figure 7.27). Comparing the stratigraphy of the surface outcrop (mapped by Dann 2001) with the stratigraphy of the BARB 1 core (Figure 7.28), some discrepancies are evident. The most significant difference is that on the surface there is a vesicular komatiite, whereas the corresponding unit in the core is mainly hyaloclastite and vesicular lava is rare. A detailed comparison between the vesicular komatiite and the hyaloclastite is important to attempt to unify this discrepancy.

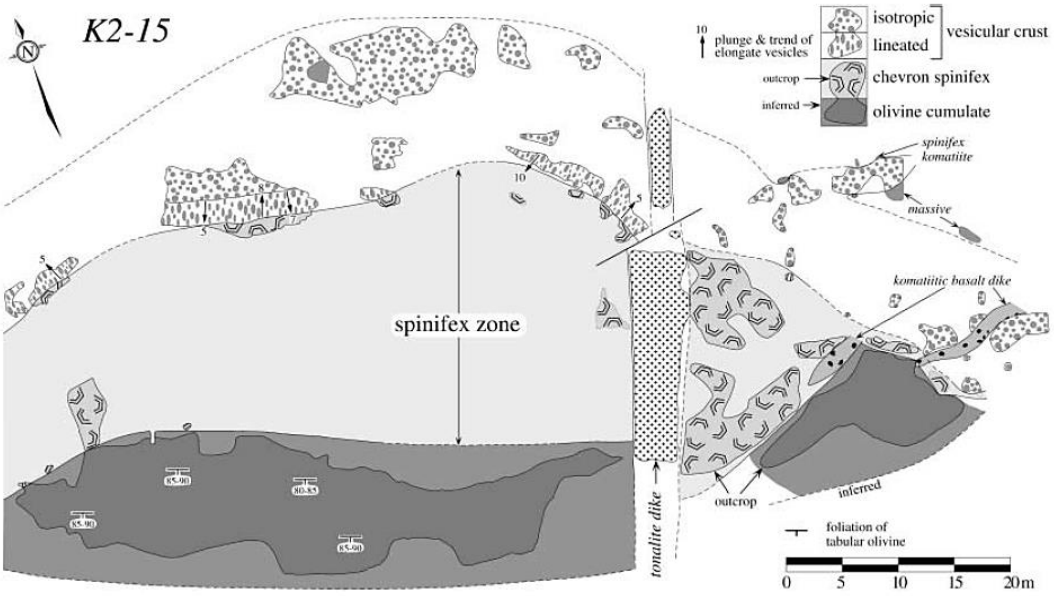

Figure 7.27
Surface map of tumulus zone, from Dann 2001.

The hyaloclastite samples have been described previously in this chapter. Surface samples GC-V1 and GC-V2 (Figure 6.11) are vesicle-rich olivine porphyries. The samples consist of vesicles (20-25 %), olivine phenocrysts (30-40 %) and the remainder is groundmass (35-50 %). The vesicles reach 4 mm in diameter and have distinct contacts with the surrounding olivine cumulates and groundmass. Some vesicles have slight interaction rims (up to 1 mm thick). The olivine crystals attain 1 mm in length. The samples are pale-green under plane polarized light and 1st order grey under crossed polarized light (Figure 7.29). The olivines are completely altered to serpentine, with small chlorite and tremolite patches that are present. The vesicles are filled with serpentine. The opaque minerals are associated with the olivine crystal boundaries and within fractures.

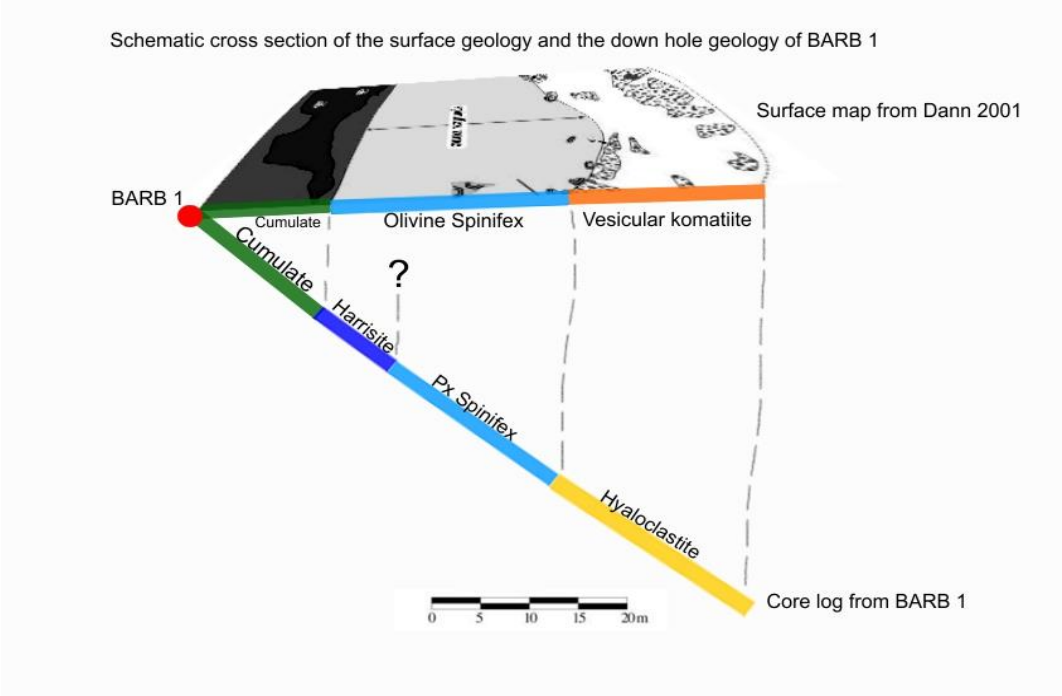

Figure 7.28
Schematic diagram comparing surface geology to geology found in the BARB 1 core, tumulus unit.

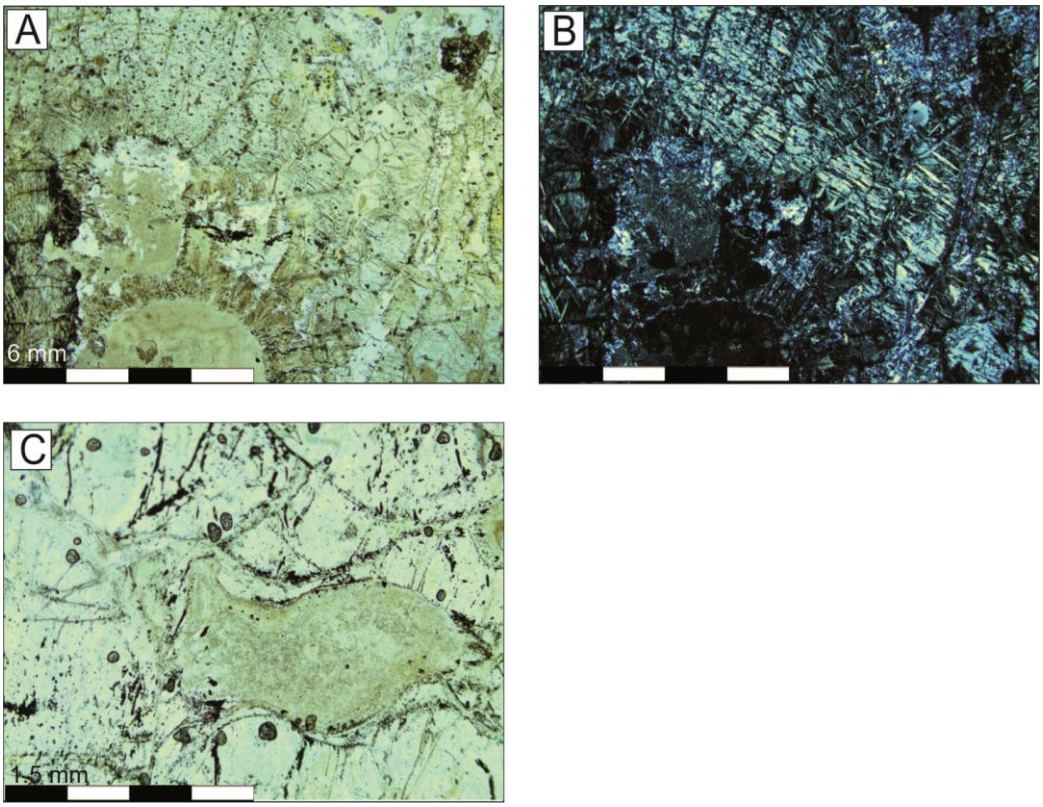

Figure 7.29
Vesicle rich olivine cumulate (sample GC-V2) taken from the surface outcrop above BARB 1, within the vesicular komatiite zone identified by Dann (2001). The distinct boundary between the vesicle and the cumulate is evident. Vesicles may have irregular shapes **(C)**.

7.4.3 Opaque Minerals

The opaque minerals (magnetite and chromite) occur in two textural forms. The primary phase is chromite that crystallized from the melt and resides in the melt residue. It is found in close association with olivine grain boundaries (Figures 4.1). Commonly, the chromite is present within, and defines the edges of olivine spinifex blades (Figure 7.16). The second opaque phase is magnetite that formed during alteration associated with hydrothermal activity (Arndt *et al.*, 2008, Parman *et al.*, 2003, Robin-Popieul *et al.*, 2012). It occurs as rims around the chromite grains. Euhedral and irregular shaped opaque crystals overprint the primary mineral textures particularly in serpentinized olivine grains. These secondary opaque minerals are usually distributed homogeneously throughout the sample, but in some instances they are concentrated along veins and in zones of obvious hydrothermal activity.

7.4.4 Magnesite and Serpentine Alteration and Veining

The rocks of the BARB 1 and BARB 2 cores are almost completely chemically altered, with the exception of a few unaltered pyroxene cores. The chemical alteration is predominantly serpentinization in the olivine rich samples. Tremolite- actinolite- chlorite alteration occurs in lower magnesium rocks, such as the spinifex and pyroxene-rich rocks.

Although there is minimal deformation, intense veining is present in some parts. The veins range in size between 0.5 and 5 mm and can become very concentrated. The veins cross cut almost all features and do not show offset within the samples. They are filled with either serpentine, as is common for the olivine rich rocks, or are filled with magnesite. The magnesite veining appears to be a secondary veining (post-serpentine) since it forms as distinct veins, as microcrystalline alteration patches and as euhedral grains in some places where it overgrows the serpentine alteration (Figure 7.30).

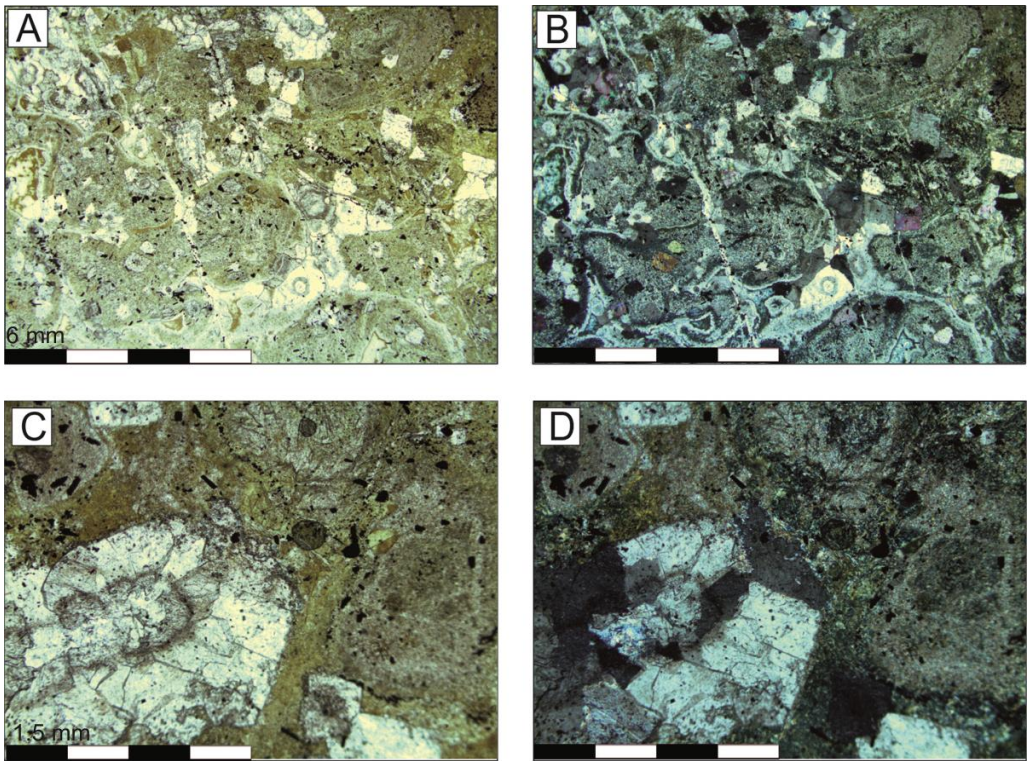

Figure 7.30
Illustrates the magnesite alteration present in the BARB 1 and BARB 2 cores. It forms as euhedral grains and as a microcrystalline infill observed in sample GC-35 **(C,D)** as well as forming veins. In the glass shard matrix of the tumulus unit in sample GC-34 **(A,B)** there is almost total magnesite alteration.

7.5 Discussion

Some important features have become evident as a result of the petrographic observation. This section highlights and discusses these features and their implications.

7.5.1 The Tumulus Cumulates

The rounded tips of the elongated olivines found in the tumulus (Figure 7.1) are an interesting feature that is not present anywhere else in the 800 m of BARB 1 and BARB 2 cores. Since no resorption reactions are evident, the rounded ends indicate possible melting of the sharp end points in a hot matrix liquid, rather than an equilibrium or resorption reaction. Not only are the olivines in the tumulus noticeably rounded, they are also very tightly packed, often with the cumulates being in contact with one another. This earns them the label ‘mesocumulate - adcumulate’ indicating a maximum of 20 % melt residue, which is evident in the samples. These tightly packed grains are associated with either (1) further crystallization of the melt or (2) with diagenetic compression or (3) a combination of both.

In case (1) the melt solidification causes growth of the olivine crystals. This process is commonly, but not exclusively, identified by magmatic zoning, which is not evident in these

samples. Furthermore, the growth of the olivines would have caused the crystals to grow into contact with one another, and hence some crystals would have inhibited the uniform growth of adjacent crystals. This expected irregular growth is not present in the olivines, which are typically well formed but can be rounded. Zonation is evident in crossed polarized light, which appears to be attributed to alteration zonation, as it is the serpentine that appears zoned. This zoning is not visible in plane polarized light; however it might be reflecting original igneous zoning.

The alternative explanation (2) with regards to the cumulates being diagenetically compressed after settling from the melt, is more appealing. As the cumulate crystals settled, the hot magma could have melted the sharp reactive edges causing a rounding of the tips. Alternative explanations are mechanical abrasion or imperfect textural preservation during serpentinization. Contemplating sedimentary environments, this settling could also account for the alignment of these elongated grains, since the grains would have settled in a position parallel to the base of the flow, as commonly seen in conglomerate beds. The depleted amount of melt residue can be explained by diagenetic compression of the cumulate bed. The pressure of the overlying cumulates could have caused further alignment of the elongated grains and also upward percolation of the melt residue. This concept of upward percolation of melt residue is consistent with the conditions required to form a harrisite pod or lens above a cumulate layer, as discussed in chapter 6. Explanation (3), a combination of process (1) and (2) is favoured.

7.5.2 Unaltered Pyroxenes Present in BARB 1 and BARB 2

It has been noted by various authors, including Arndt *et al.* (2008), Parman *et al.* (2003) and many others, that there are areas that contain cores of unaltered olivine and pyroxene. Observation of thin sections through the core reveals portions of the core, which contain relics of unaltered pyroxene. No fresh olivine is found in the core, however it has been found in a single sample taken from the surface.

Fresh pyroxene is found in (1) the harrisite layer, (2) within the gabbro and pyroxenite layer, (3) in the pyroxene spinifex unit in the tumulus, (4) in oikocryst form in the BARB 1 (378-420 m) package and, (5) in the cumulates and spinifex in the BARB 2 (252-274 m) package.

7.5.3 The Hyaloclastite vs. the Vesicular Komatiite

The hyaloclastite contains two components; (1) the fine grained, chilled lava fragments and (2) the surrounding glassy shard matrix. The fine grained chilled fragments (1) represent the upper lava carapace of the tumulus. This carapace became fractured due to pressure build up, and the fracturing formed (2) the glass shard matrix present between the large chilled fragments. This hyaloclastite breccia was thickened as the tumulus inflated. The inflation caused upward doming and fracturing of the outermost layer of the already fragmented crust (Anderson, 2012, Rossi & Gudmundsson, 1996). The outer-most part of the hyaloclastite consists of fewer, fine grained chill fragments and more glass shard matrix between the fragments. The stratigraphically lower portion of the hyaloclastite has a larger concentration of chilled fragments and less shard matrix to fill in the fractures. This stratigraphic change is noted in other tumuli structures (Hill, 2001, Walker, 1991).

The hyaloclastite layer has a depth in the core that corresponds to Dann's (2001) vesicle-rich komatiite layer on surface. It is tempting to re-label the vesicular komatiite zone as a hyaloclastite and attribute the vesicles to a weathering of the glassy shard matrix. However, after careful and detailed petrographic analysis, it is clear that the vesicular komatiites contain up to 25 % true vesicles, whereas the hyaloclastite has pseudo-vesicles made of these glassy shards and only 2 % true vesicles. Vesicles are present in layers of the hyaloclastite, notable at 75.5 - 76 m and at 78.4 - 78.5 m. These layers are not extensive or thick enough to correlate with the 30 m thick vesicle layer on surface. Furthermore, in terms of the mineralogy, the surface vesicle samples consist of serpentine vesicles within an olivine cumulate (Dann, 2001), which is altered to serpentine. In contrast, the glassy shards of the hyaloclastite consist of fine-grained, accreted shards that have been altered to magnesite.

7.5.4 Basalt and Gabbro Samples

A single basalt sample, together with the gabbro samples, (Figure 7.25) contain a higher proportion of unaltered minerals than the ultramafic rocks. In these samples, it is common to find partially unaltered pyroxenes and plagioclase.

The gabbro in the tumulus is not totally unaltered, since chlorite, tremolite and actinolite alteration is present, but they are better preserved than the other ultramafic samples. This implies some sort of resistance to alteration. Other gabbro samples present in the BARB 1 and BARB 2 core usually show intrusive contacts, indicating later stage intrusions. For

example, sample BARB 1 ref 30 contains about 30 % pyroxene and 20 % subhedral plagioclase grains. Some unaltered pyroxene kernels occur as small fragments in close proximity to one another, (Figure 7.22). Plagioclase appears to be relatively unaltered, which, in conjunction with the fresh cores of pyroxene, could indicate a later intrusion. The matrix is completely altered to serpentine and tremolite. The opaque minerals are <0.5 mm in size and are scattered through the sample. These intrusive gabbro layers have the same mineral composition and degree of alteration as the gabbro present in the tumulus.

The basalt has sharp contacts with the surrounding olivine cumulate, which it intruded. It contains plagioclase phenocrysts in a fine-grained matrix making it a plagioclase porphyry intrusion rather than a true basalt. Together with the lack of olivine and pyroxene crystals, it indicates a more evolved, plagioclase rich, source for the late stage sill.

The gabbros and plagioclase porphyry (basalt) show less alteration than the surrounding ultramafic rocks. These mafic rocks are, in most cases, later intrusions into the ultramafic pile and the freshness of the minerals indicates the intrusions occurred after the main metamorphic event that altered the ultramafics. In the case of the tumulus gabbros, it is suggested that the thickness of the tumulus insulated the gabbro at the centre.

7.6 Summary and Conclusions

7.6.1 On the Tumulus

The tumulus is identified as a single unit consisting of basal cumulates, harrisite, pyroxene spinifex, pyroxenite and gabbros and capped by a hyaloclastite. The olivine grains in the cumulates are larger in size than expected (up to 15 mm) than in the differentiated komatiite flows and the crystals are elongated and in some places aligned. These features point towards magmatic flow settling, as is common within the cumulate zone of a differentiated komatiite. Furthermore, the rounded nature of the crystals indicates either chemical or mechanical erosion. The cumulates are tightly packed, most likely as a result of melt-escape during compression from the overlying layers. They are completely serpentinized and contain small amounts of melt residue. Secondary magnetite is found predominantly surrounding the olivine boundaries and within the fractures in the olivine grains.

The harrisite was identified on the surface as a crescumulate, which is similar in texture and nature to the olivine spinifex found on the surface. On closer inspection from the BARB 1 core, it is evident that the harrisite is a skeletal olivine unit, found adjacent to the pyroxene

spinifex unit. Kernels of unaltered pyroxene are present in the matrix of the harrisite. The opaque minerals surround the olivine blades and are present as 0.1 mm sized, well-formed secondary growth.

Contained within the pyroxene spinifex layer is a gabbro-pyroxenite layer (3.8 m thick), which contains a rare occurrence of unaltered pyroxene and plagioclase. This gabbro-pyroxenite layer is not evident on the surface and in the core it has gradational boundaries and no chill zones (fine- grained areas) with the surrounding pyroxene spinifex. The gabbro and pyroxenite layers are distinguishable only by the plagioclase content. The gabbro grades into the pyroxenite and no direct contact is evident. The opaque minerals are 0.1 mm in size and are randomly dispersed through the sample.

The pyroxene spinifex layer consists of twinned pyroxene blades with actinolite-tremolite cores surrounded by chlorite rims. The larger spinifex blades define polygon-shaped pockets of melt residue. These are filled with either fibrous pyroxene laths or melt residue. The opaque minerals present are fine -grained, irregular in shape and are randomly dispersed. Euhedral magnesite grains (1 mm) overprint the igneous features.

7.6.2 On the Differentiated Komatiite Flows

The differentiated komatiite flows are found in both BARB 1 and BARB 2. Thin section samples were taken of each textural section of the differentiated flow, namely the cumulates, spinifex and chill zones.

The olivine cumulates are consistent in their grain size (0.1–2 mm), euhedral in shape, entirely surrounded by melt residue (between 20-40 % of the sample) and are completely serpentinized. Two intervals, namely the BARB 1 (378-420 m) and BARB 2 (252-274 m) packages contain unaltered pyroxene as an in-situ growth mineral, where the pyroxene occurs as partially formed to well-formed oikocrysts between the settled cumulus olivine crystals. The opaque minerals are predominantly associated with the olivine grain boundaries and fractures, but are also found in the matrix. The BARB 1 (89-118 m) package contains two cumulate phases. The olivine cumulates contain opaque minerals within the grain, whilst the pyroxene cumulates are devoid of opaque minerals, making them distinguishable from each other.

The spinifex zones of the differentiated komatiite flows are similar in all occurrences studied. They consist of large olivine plates or sheets, forming a dendritic or feather-like structure. Pyroxene needles fill in the spaces between the olivine blades and acicular pyroxene fills the remaining space. Notably thick olivine spinifex (1 cm wide) occurs in the BARB 1 (89-118 m) package, this is attributed to metamorphic regrowth. Opaque minerals are commonly associated with the olivine sheets, and are found as 0.1-0.5 mm euhedral grains within the olivine crystals.

7.6.3 On the Fresh Pyroxenes and Olivines

Unaltered pyroxene crystals occur at various intervals in the core as well as in the two cumulates (GC-C-1 and GC-C-2) taken from the surface. In the core the fresh pyroxene is found in the harrisite layer, in the pyroxenite layer, the pyroxene spinifex layer, in some differentiated komatiites and in the surface cumulates. The pyroxene grains in the latter samples are large oikocrysts that enclose smaller rounded olivine grains. The surface samples are the only samples with large enough pyroxenes for mineral separation.

Unaltered olivine is exceptionally rare and is found as partially altered cores in only a single surface sample of oikocrystic olivine cumulate (GC-C-2). The olivine cumulates are surrounded by large unaltered pyroxene crystals, creating a poikilitic texture. The fresh kernels are less than 0.5 mm in size, rounded, with serpentinized rims.

CHAPTER 8

WHOLE-ROCK GEOCHEMISTRY

8.1 Introduction

The BARB 1 and BARB 2 cores were sampled for geochemical analysis. In total 225 major and trace element analyses were carried out (152 from BARB 1 and 73 from BARB 2) along with 75 ICP-MS analyses (55 on BARB 1 and 20 on BARB 2). The major and certain trace element abundances were determined using XRF analyses, whilst another group of trace elements were analysed using ICP-MS methods to give lower detection limits and improve precision and accuracy and include elements that were not detected using XRF. The details of the processes are explained in Appendix D (In-house publication).

The purpose of the geochemical study is to determine the basic rock-type and range in chemistry associated with the rock types present in the BARB 1 and BARB 2 core. Detailed chemical plots can indicate the relationship between crystal fractionation and magma evolution as well as giving insight into the origin of the magma and the possible tectonic environment. Element vs. depth plots indicate the change in chemistry with stratigraphic position and can show overall trends of enrichment or depletion in a specific element, which has implications for the magma origin. The detailed sections, as defined and discussed in Chapter 6 and Chapter 7, have been analysed geochemically.

Major elements (weight %) analysed: SiO_2, Al_2O_3, Fe_2O_3, FeO, MnO, MgO, CaO, Na_2O, K_2O, TiO_2, P_2O_5, Cr_2O_3, NiO and LOI (Loss On Ignition).

Trace elements (ppm) analysed: Sc, V, Cr, Co, Ni, Cu, Zn, Ga, Rb, Sr, Y, Zr, Nb, Mo, Ba, Pb, Th, U, Li, P, Ti, As, Sn, Cs, Hf, Ta, W; Also the REE's (Rare Earth Elements): La, Ce, Pr, Nd, Sm, Eu, Gd, Tb, Dy, Ho, Er, Tm, Yb and Lu.

All thicknesses give in this chapter are related to core intersection depth and therefore do not represent true thicknesses of the strata. True strata thickness will be clearly noted.

With respect to Fe value, Fe^{2+} and Fe^{3+} were not determined directly due to the altered nature of the rocks. Rather a constant proportion of 10% of the total Fe was allocated as Fe^{3+} and 90% as Fe^{2+}. The FeO graphs are based on FeO_{total} value and are not corrected for Fe^{3+}.

8.2 Geochemistry of the Komati Formation

The compositions of the Onverwacht suite have been previously studied, with a strong focus on the Komati Formation, renamed as the Komati Complex by de Wit *et al.* (2011) and Furnes *et al.* (2013). Major and trace element chemistry of the komatiite and komatiitic basalt rocks have been analysed by Chavagnac (2004), Furnes *et al.* (2013), Jahn *et al.* (1982), Parman *et al.* (2003), Smith and Erlank (1982), Viljoen and Viljoen (1969) as well as other authors.

Several elements have been shown to be less affected by metamorphic processes than other elements. The elements considered immobile are: Ti, Al, Cr, V, Nb, Ta, Zr, Hf, Y, Th and REE, except for Eu and possibly Ce as identified by Arndt et al. (2008), Furnes et al. (2013), Nesbitt and Sun (1976). Robin-Popieul et al. (2012) indicate the immobility of MgO, TiO2, Al2O3, Zr, La, REE and HFSE (High Field Strength Elements: Nb, Th, Hf and Y). Parman et al. (2003), Nesbitt and Sun (1976) and Stiegler et al. (2010) support the immobility of REE, HFSE, Y, Ti and Zr, but according to Parman et al.(2003) crystallization of chromite may have affected the perceived immobility of Ti and Zr and they advise caution with the interpretation of those two elements. Chavagnac (2004), Barnes *et al.* (2004) states that the REE, with the exception of Eu, are relatively unaffected by secondary fluid processes unless the fluids present are fluoride or carbonate rich. The elements affected by mobilizing metamorphic processes are: SiO_2, FeO, CaO, MnO, Na_2O and LILE (Large Ion Lithophile Elements: Cs, Rb, Ba and Sr) (Robin-Popieul *et al.*, 2012). Parman *et al.* (2003) highlight the mobility of Sr and Eu trace elements, while (Smith *et al.*, 1980) add K, Cu, Zn and S to the list.

Various methods can be employed to determine the mobility of elements. One of the best-known and widely used is the method of plotting elements of unknown mobility against elements of known immobility, particularly where these are also incompatible with the mineral suite, such as K, Cs and Rb. If there is a good correlation between the immobile and the unknown element, it is likely that the unknown element also is immobile (Arndt *et al.*, 2008). However, caution is necessary since some elements may have been homogeneously mobilized, creating a false correlation. Elements that are immobile and unaffected by alteration are therefore deduced to have attained their specific values via original igneous processes (Parman *et al.*, 2003). Another method is known as the "olivine control line

criterion" (Arndt *et al.* 2008 p 131). In this method two elements, typically MgO and another immobile element, are plotted on a binary diagram, together with the olivine control line. If the binary plot creates a trend at an angle to the olivine fractionation trends, then the rock suite has presumably been altered. Alternatively the olivine control line has been modified by contamination at some point during the magmatic evolution.

Arndt *et al.* (2008), Chavagnac (2004), Jahn *et al.* (1982), Nesbitt and Sun (1976), Parman *et al.* (1997), Puchtel *et al.* (2013), Robin-Popieul *et al.* (2012), Smith *et al.* (1980), Stiegler *et al.* (2010), Viljoen and Viljoen (1969), Viljoen *et al.* (1983) along with many others, analysed the compositions of the komatiites from the Komati Formation and certain patterns and correlations were evident in the results. The degree of Al depletion (represented by Al_2O_3/TiO_2) ranged between 10 (depleted) and 20 (undepleted), illustrating the two major types of komatiite present in the Barberton Greenstone Belt. It is noted that the lower Komati Formation consists predominantly of the Al-depleted type of komatiites (Chavagnac, 2004, Nesbitt & Sun, 1976, Robin-Popieul *et al.*, 2012, Viljoen & Viljoen, 1969). On binary diagrams, this type is associated with Al_2O_3/TiO_2 ratios between 8 and 12; high CaO/Al_2O_3 ratios between 1.15 and 2.81; slight depletion in HREE, and good correlations between HSFE, REE and Y. Furnes *et al.* (2013), Grove *et al.* (1999), Parman *et al.* (1997), Parman *et al.* (2001) indicate the flat REE patterns in the komatiites are similar to modern subduction zone REE patterns. But often a slight LREE enrichment is observed in the komatiites.

8.3 Classification Diagrams

Ternary or rock type classification diagrams using three predominant minerals or elements are commonly employed to establish the type of rock and its tectonic setting. Drawbacks of these diagrams are that some rock types are not accurately represented by only three minerals or three elements. Elements and ratios such as MgO, SiO_2, Al_2O_3/TiO_2 and Al_2O_3/CaO, together with various trace element ratios, are used to identify and classify komatiites.

The Jensen cation plot is used to distinguish komatiite and komatiitic basalt from typical tholeiite basalts (Rollinson, 1993). This ternary plot uses Al, Mg and ($Fe^{2+}Fe^{3+}Ti$), elements, which are relatively immobile at low grade metamorphism. The samples from BARB 1 and BARB 2 are located within the komatiite and komatiitic basalt fields (Figure 8.1 A and B). A single point representing a basalt intrusion in the differentiated komatiite package in BARB 1 (89-118 m) at 113 m depth plots in the high Fe-tholeiite basalt zone. The BARB 1 samples

plot as a curve, indicating changing olivine composition during fractional crystallization. Likewise the BARB 2 samples plot as a slight curve. Figures 8.2 A, B and C reveal that the cumulate zones of the differentiated komatiite flows plot in the komatiite part of the graph, as a result of increased Mg content caused by the accumulation of olivine. The corresponding spinifex samples from the same flows plot in the komatiitic basalt part of the graph due to the lower Mg content, since the Mg is concentrated in the olivine in the cumulate layers. Hence much of the observed trend is created by the distribution of Mg within a differentiated flow.

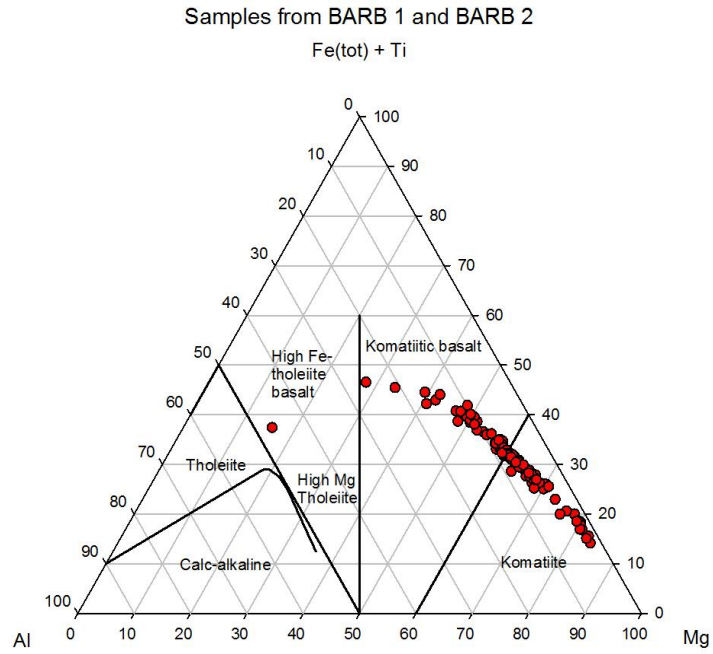

Figure 8.1 (A)
Jensen cation plot showing the sample positions of the BARB 1 samples. The majority plot near the komatiite-komatiitic basalt boundary. The samples plot in a curve, indicating a systematically changing olivine composition during fractional crystallization. A single tholeiite basalt is present and identified as an intrusion in chapter 4.

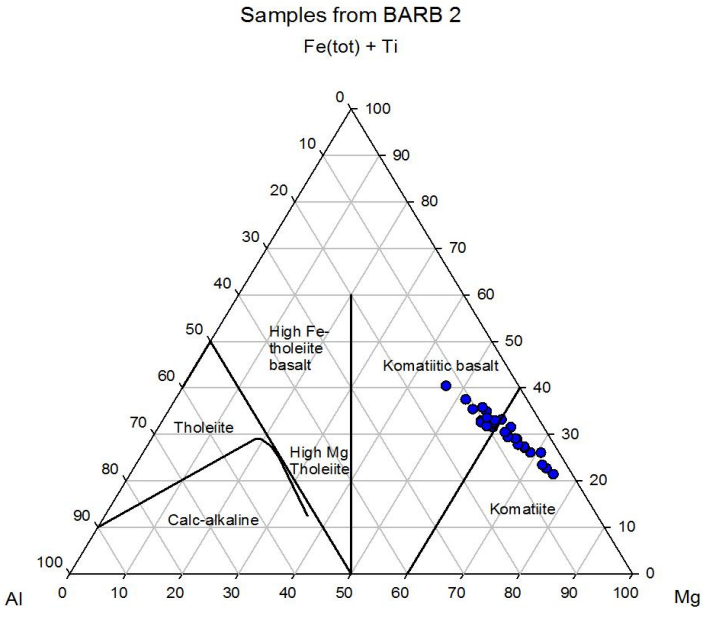

Figure 8.1 (B)
Jensen cation plot showing the chemistry of all the BARB 2 samples. The majority plot near the komatiite-komatiitic basalt boundary. The samples plot in a line, indicating a chemical relationship.

The CIPW norm calculations are based on whole-rock geochemistry and are used to determine normative mineral abundances. A summary of the CIPW norm mineral proportions is presented in Appendix E and a comparison is made with the mineral proportions from the thin sections in Appendix B.

As has been previously described, two types of komatiite lava are found in the Komati Formation. These are Al-depleted and Al-undepleted. The komatiites of the BARB 1 and BARB 2 cores are Al-depleted (Figure 8.3), as shown by the Al_2O_3/TiO_2 ratio having a minimum value of 7, a maximum of 14 with an average value of 10. One sample has a value of 21, but this is an intrusive basalt and therefore is not included in the graph.

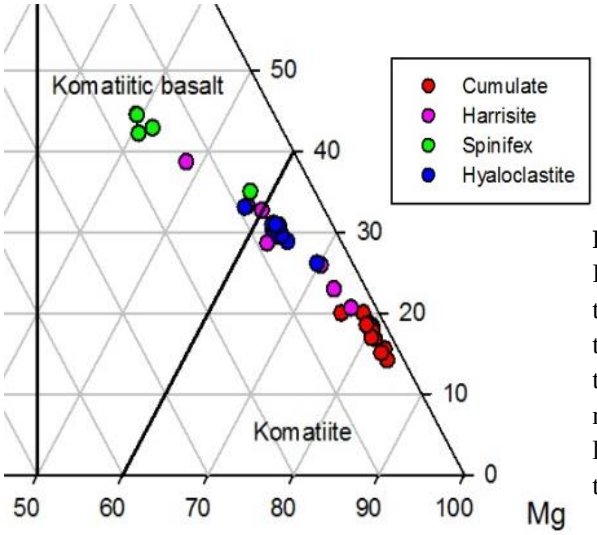

Figure 8.2 (A)
Portion of a Jensen cation plot for the samples taken from the tumlus section. A chemical trend is evident between the cumulates and the spinifex, with the hyaloclastite (which represents the chill zone and hence original liquid composition) plotting midway between them.

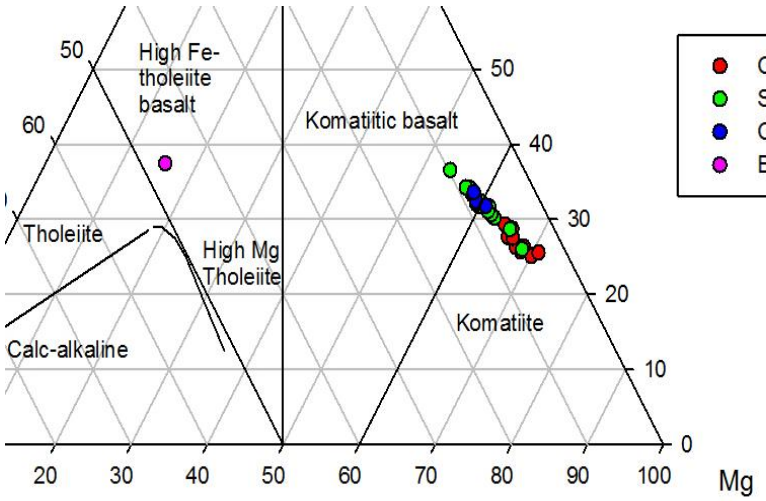

Figure 8.2 (B)
Portion of a Jensen cation plot for the samples taken from the BARB 1 section between 89-118 m. A chemical trend is evident between the cumulates and the spinifex, with the chill plotting midway between them. A single basalt sample from an intrusive layer plots in the high Fe-tholeiite basalt field, however, it is unrelated to the chemical process of the komatiites.

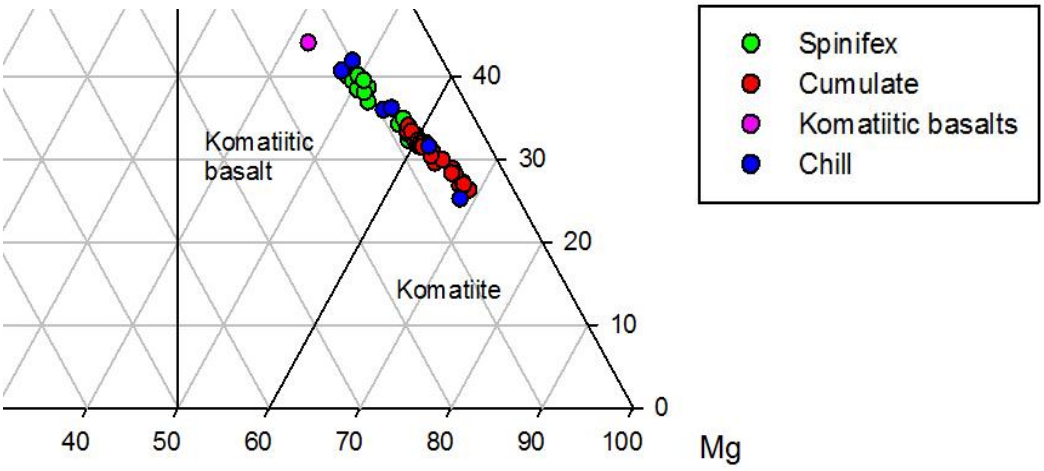

Figure 8.2 (C)
Portion of a Jensen cation plot for the samples taken from the BARB 1 (378-420 m) section. A chemical trend is evident between the cumulates and the spinifex, with the chill plotting throughout the cumulate and spinifex composition. A single komatiitic basalt sample is present and indicates a chemical relationship between the differentiated komatiite flows and the more evolved komatiitic basalt.

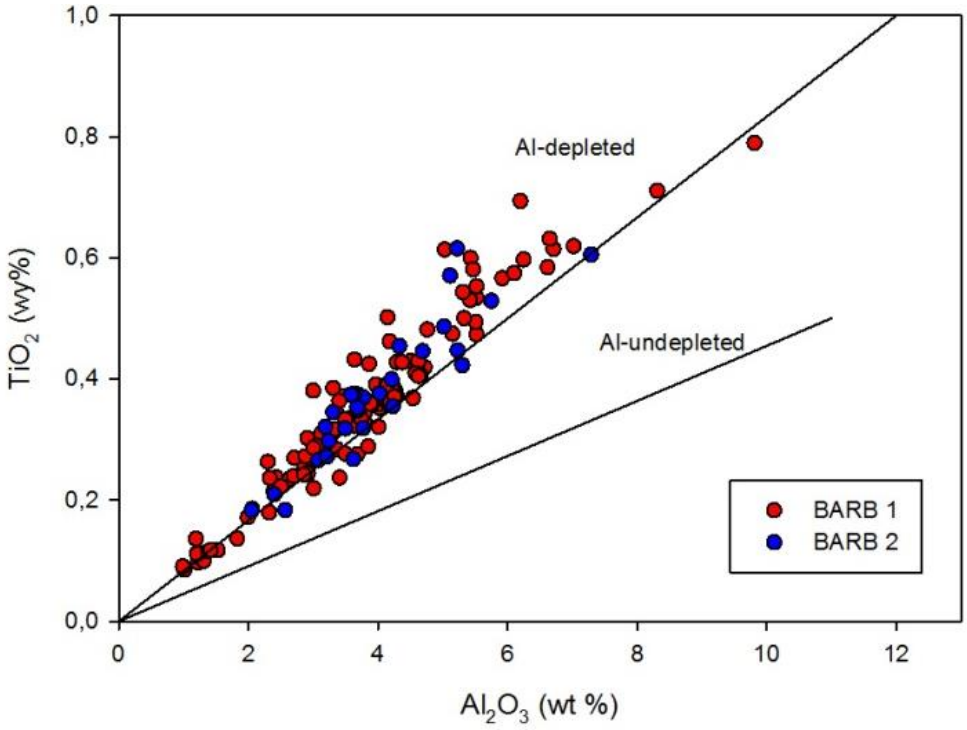

Figure 8.3
Al_2O_3 vs. TiO_2 graph shows the samples from BARB 1 and BARB 2 plot within the Al-depleted ratio line of the graph. Some samples plot in the Al-undepleted area, but they plot close to the boundary line, indicating that they most likely belong to the depleted population.

8.4 Element vs. Depth Plots of BARB 1 and BARB 2

The BARB 1 and BARB 2 cores were sampled at approximately equally spaced intervals. Samples were taken within 10 m from the previous sample position, unless fracturing and rubble prohibited sample collection. The close spacing of the samples gives a realistic portrayal of the general geochemical trends of the core. For the detailed sample sets (Tumulus, BARB 1 (89-118 m), BARB 1 (378-420 m) and BARB 2 (252-274 m)), the closer spaced and more detailed sampling allows a better representation of the change in composition over the sections and within individual flows. In some cases the plots display a 'zigzag' pattern due to the chemistry of the different rock-types being sampled.

The strata are overturned, and hence the top of the core correlates to the lowest point in stratigraphy. In the element vs. depth plots, the top of the hole, which is the lowest point in the stratigraphy, is placed at the base of the graph. As the depth increases, so does the stratigraphic height.

Major elements plotted in (Figures 8.10 to 8.18) are MgO, FeO, SiO_2, Al_2O_3, TiO_2 and trace element plots of Ni, Cr, Zr, Y, Zn, V and Sc. Elements such at Na_2O, K_2O, Rb, Sr, Mo, Ba and Pb are known to be mobile and therefore do not portray changes in igneous composition with stratigraphic height. Similarly Cu shows no trend and 40% of the values are at detection limit for XRF. Further, the only measurements of Pb, Th and U are very close to the detection levels and cannot be assumed to be accurate in the XRF analyses. These elements, and likewise the mobile elements Na_2O, K_2O, Rb, Sr, Mo and Ba are excluded from the graphical representations as they do not contain any information regarding igneous mineralogy and processes.

8.4.1 Entire BARB 1 Core

The BARB 1 core sample set consists of 150 samples, some of which are closely spaced and represent the detailed sections of the tumulus, BARB 1 (89-118 m) and BARB 1 (378-420 m). The rock types between these detailed sections consist predominantly of komatiitic basalt, massive komatiite, basalt and gabbro.

The major and trace element vs. depth diagrams display trends on both large and small scales. MgO and SiO_2 have mirror image trends, where the highest MgO content in the cumulate rocks corresponds to the lowest SiO_2 content in the cumulate rocks (Figure 8.4 A, B). MgO

and Ni vs. depth have similar patterns. The start and the end of the core contains higher concentrations of MgO and Ni than the middle section of the core (150-350 m), creating a crescent or bow shape trend. SiO_2, TiO_2, Al_2O_3, CaO, Zr and Y show the opposite trend to MgO: the middle section of the core (150-350 m) contains a higher concentration in these elements than the beginning and end of the core (Figure 8.4 B, E, F, G). Plots of FeO, Zn, V and Sc, with depth, give an overall increasing trend rather than the bow or crescent shaped trend of the above mentioned elements (Figure 8.4 C, H).

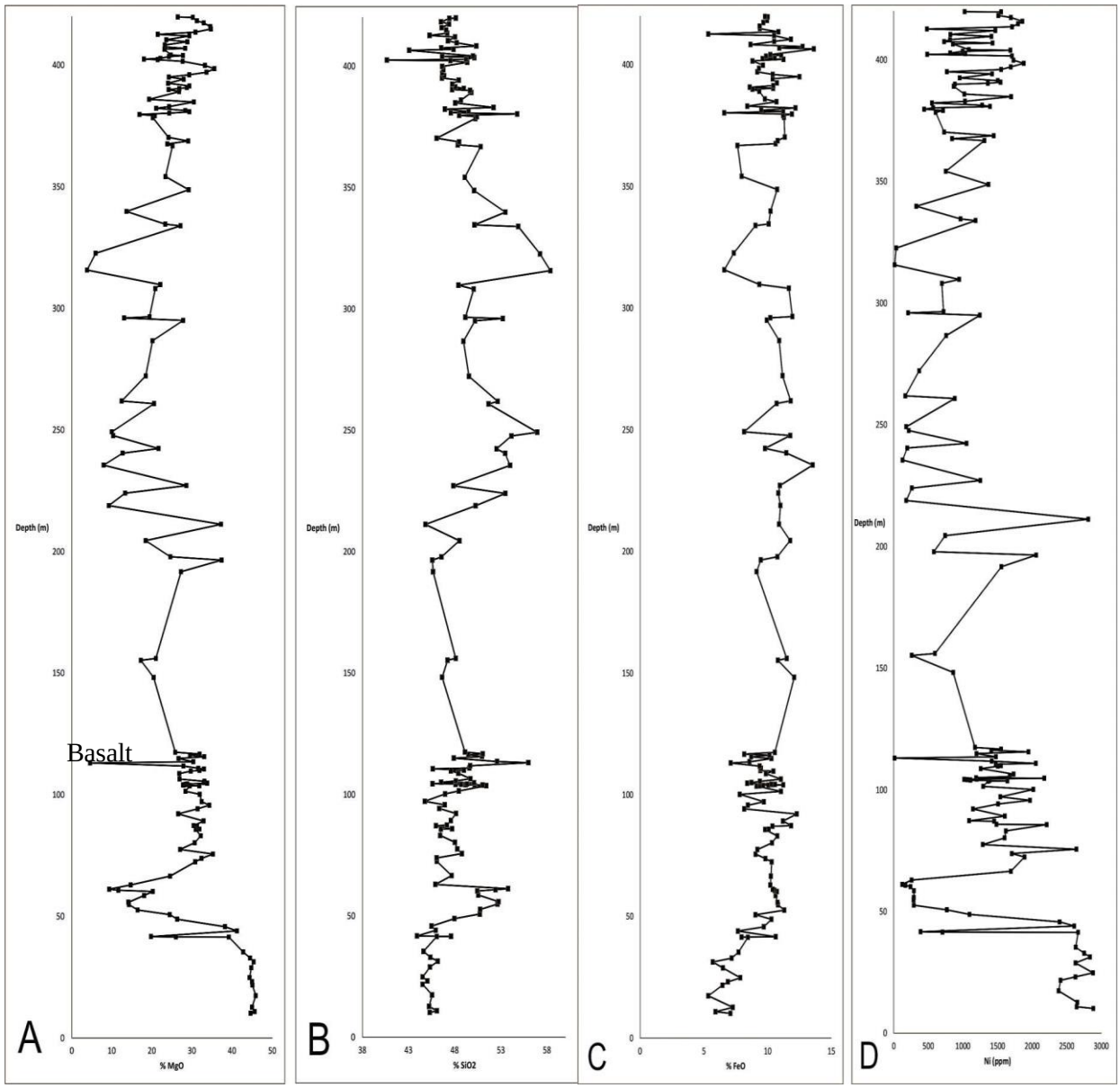

Figure 8.4
Depth vs. major element oxide plot of the entire BARB 1 core showing detailed and overall variations. The top of the core represents the lowest stratigraphic point, thus the graphs show changes in element abundance with stratigraphic height. Base section and top section are sampled in more detail and represent differentiated komatiites, whilst the middle section (150-350 m) is a combination of komatiitic basalt, basalt/gabbro and massive komatiites. A) is MgO, B)SiO_2, C)FeO, D)Ni

There is a clear correlation between rock-type and element concentration as illustrated by a comparison of the core log with the depth graphs. Also evident are distinctly different compositions of certain rock-types, such as the basalt intrusion in the section of differentiated komatiites (Figure 8.4 A).

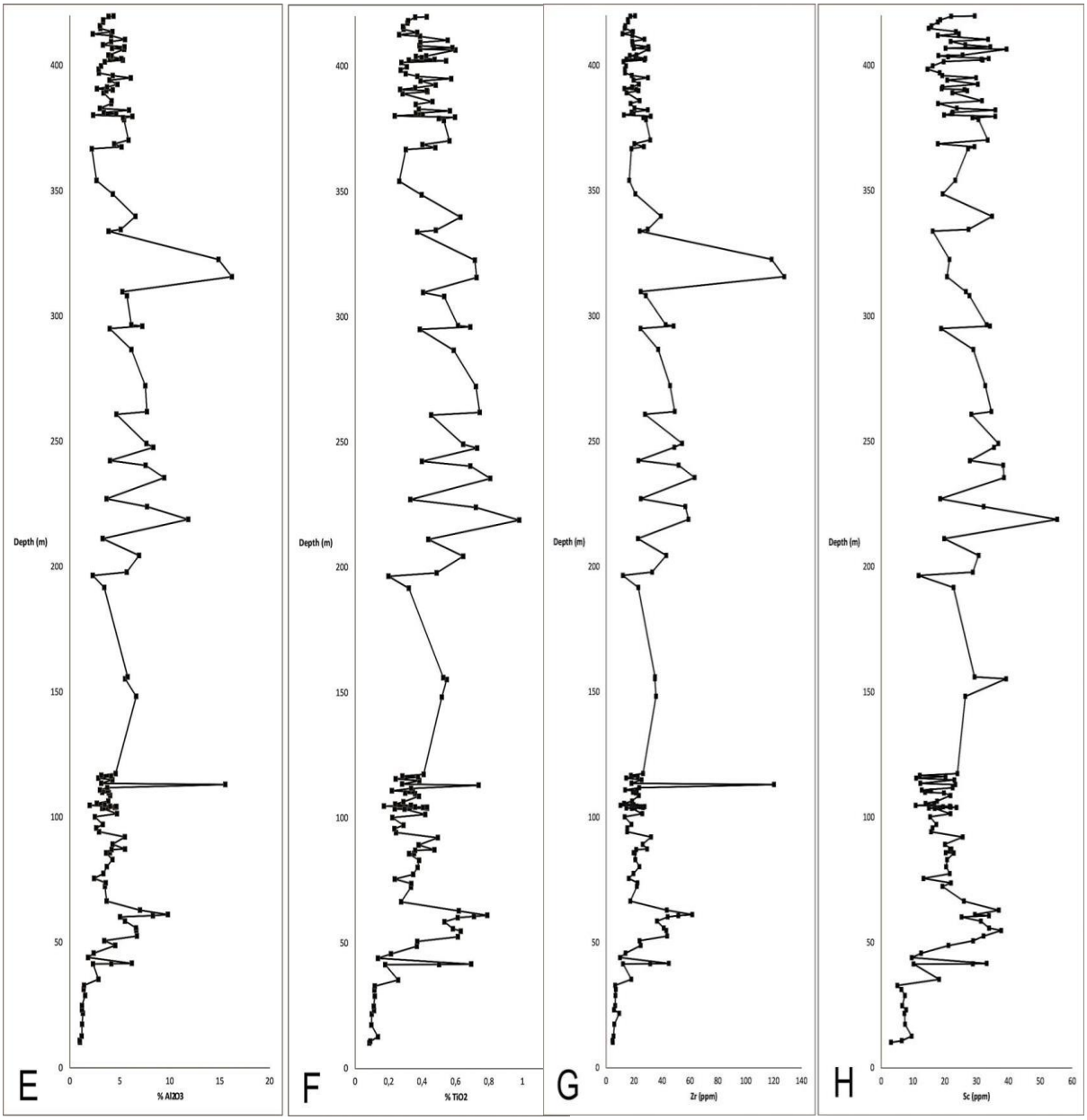

Figure 8.4 cont.
Depth vs. major element oxide plot of the entire BARB 1 core showing detailed and overall variations. E) plots Al_2O_3, F) plots TiO_2, G) plots Zr, H) plots Sc

8.4.2 Entire BARB 2 Core

70 samples were taken throughout the entire section of BARB 2 core. Sample spacing is less than 10 m and the sample set contains each rock-type present in the core. A single package of differentiated komatiites between 236 and 297 m was sampled in detail (BARB 2 252-274 m). On either side of the differentiated komatiite package is massive komatiite, komatiitic basalt, with tholeiitic basalt and gabbro intrusions.

There are no overall patterns of increasing or decreasing element concentration through the section. The different rock types create a zigzag pattern in the element abundance with depth. BARB 2 has only one differentiated komatiite package and contains a variety of alternating mafic to ultramafic rock-types. A detailed analysis of the differentiated komatiite package (252-274 m) is presented later in this chapter. The zigzag patterns illustrate the rock type, as the mafic basalts/gabbros have low percentage MgO (<15%) and thus are easily distinguishable from the ultramafic komatiites (MgO>18%). As observed previously for BARB 1, the MgO and SiO_2 have mirrored and opposing trends. MgO, FeO and Zn have similar shaped graphs, with the same anomalies as the MgO graph (Figure 8.5 A, B, C). SiO_2, Al_2O_3 and Zr have similar patterns, with a high concentration in mafic rocks (basalt and gabbro) (Figure 8. 5 D, E, F).

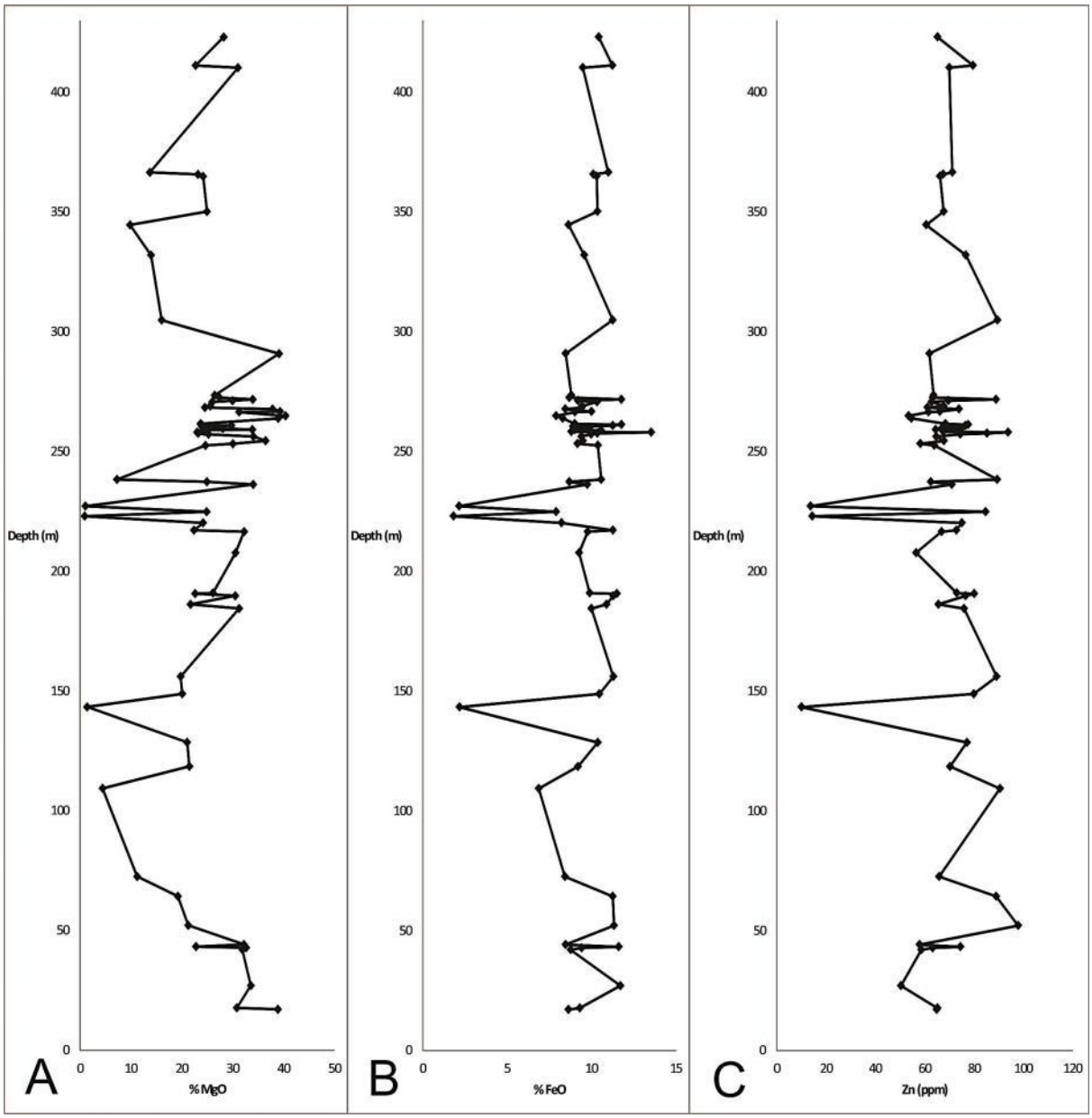

Figure 8.5
Depth vs. element plot of the entire BARB 2 core. The mafic rock types are distinguishable by low or high element anomalies. A detailed sample section is present in the middle of the core (252-274 m). Alternating rock types are responsible for the zig-zag pattern present in the depth graphs.

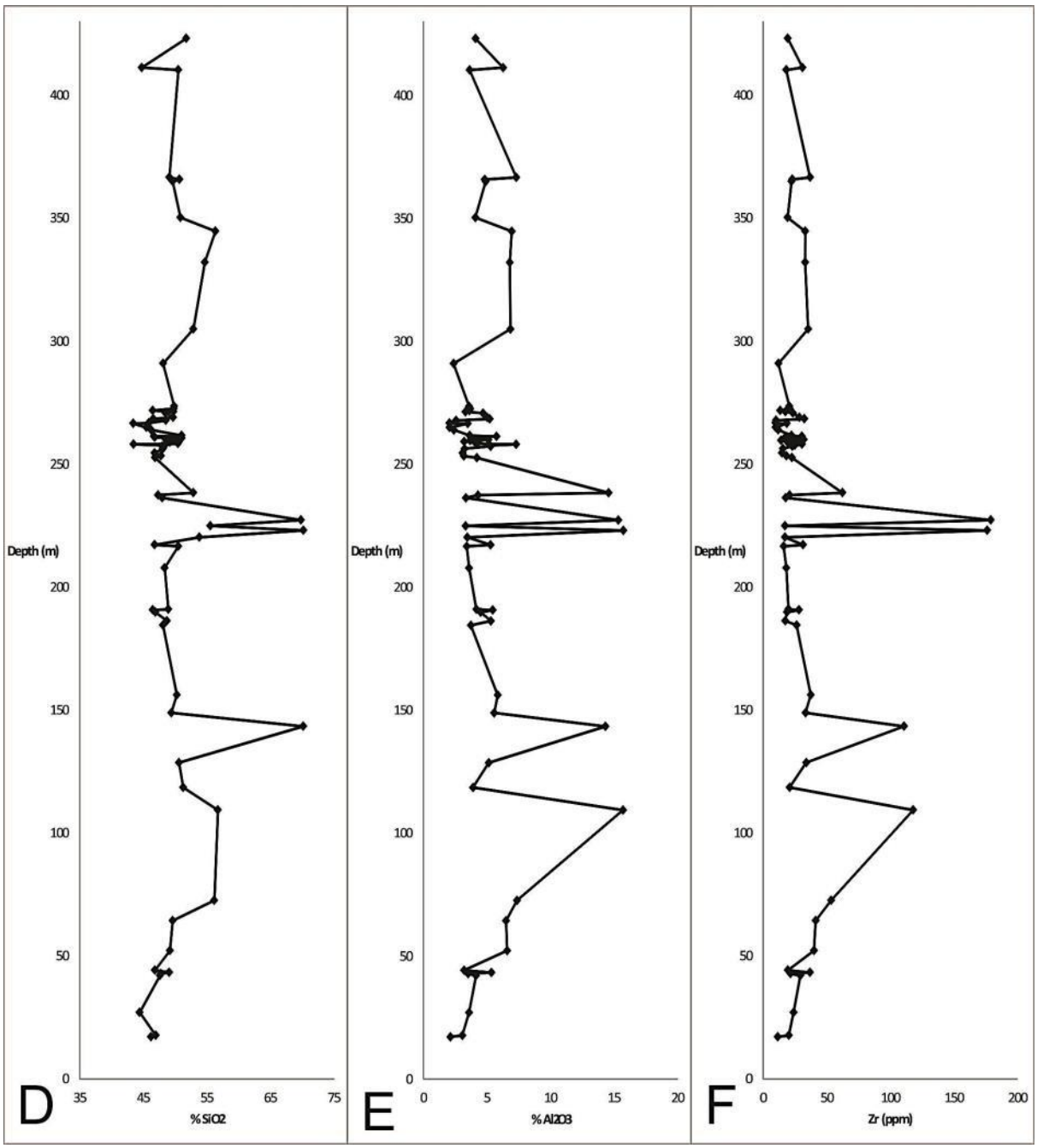

Figure 8.5 cont.
Depth vs. major element oxide plot of the entire BARB 2 core.

8.4.3 Detailed Stratigraphic Plot of the Tumulus

The tumulus unit is the lowest and oldest unit in the BARB 1 core. It is 90 m thick in the core, corresponding to 50 m true thickness, and contains five different rock types with a variety of textures. Forty geochemical samples define the trends in the tumulus unit.

The pattern of MgO and Ni vs. depth begins with a high concentration (40-44 % MgO) within the cumulate layers (base), decreasing markedly to 14 % MgO in the pyroxene spinifex and pyroxenite/gabbro layers (centre) then increasing to 27-33 % MgO in the upper hyaloclastite layer. The SiO_2 trend shows the inverse variation, with the cumulates having the lowest SiO_2 content and the pyroxene spinifex and pyroxenite/gabbro the highest concentrations (Figure 8.6 A, B). Al_2O_3, TiO_2, Cr, Zr, Y, V and Sc have similar trends to SiO_2 (Figure 8.6 B, E). FeO, Zn and Cr are the only elements that show a consistently increasing trend with increasing stratigraphic height (Figure 8.6 C, F).

8.4.4 Detailed Plots of the Differentiated Komatiite Flows in BARB 1 (89-118 m)

The differentiated komatiite package in BARB 1 (89-118 m) is represented by 30 geochemical samples. This package consists of nine discernible komatiite flows, and a single intrusive basalt. The basalt is highly vesiculated and has a significantly different composition from the komatiites above and below. The occurrence of the basalt is evident in most of the element vs. depth plots except for FeO and Zn (Figure 8.7 C).

The general variations are observed as a slight zigzag between the cumulate and spinifex samples but overall the element abundance does not drastically change with depth. CaO, Ni and Sc show quite pronounced changes between the cumulate and spinifex samples. This zigzag pattern is highlighted by plotting the olivine cumulates as red points. For example, MgO vs. depth (Figure 8.7 A) indicates that the cumulates have the highest MgO values. The basalt sample is easily identifiable since it occurs as a distinct anomaly in the trend of the komatiite magma compositions. As expected, MgO and SiO_2 have inverse proportions in the basalt sample and create a mirror image of one another (Figure 8.7 A, B). MgO and Ni have similar trends, whereas Al_2O_3, TiO_2, Cr, Zr, Y, V and Sc have similar trends to SiO_2 which are the inverse of the MgO patterns.

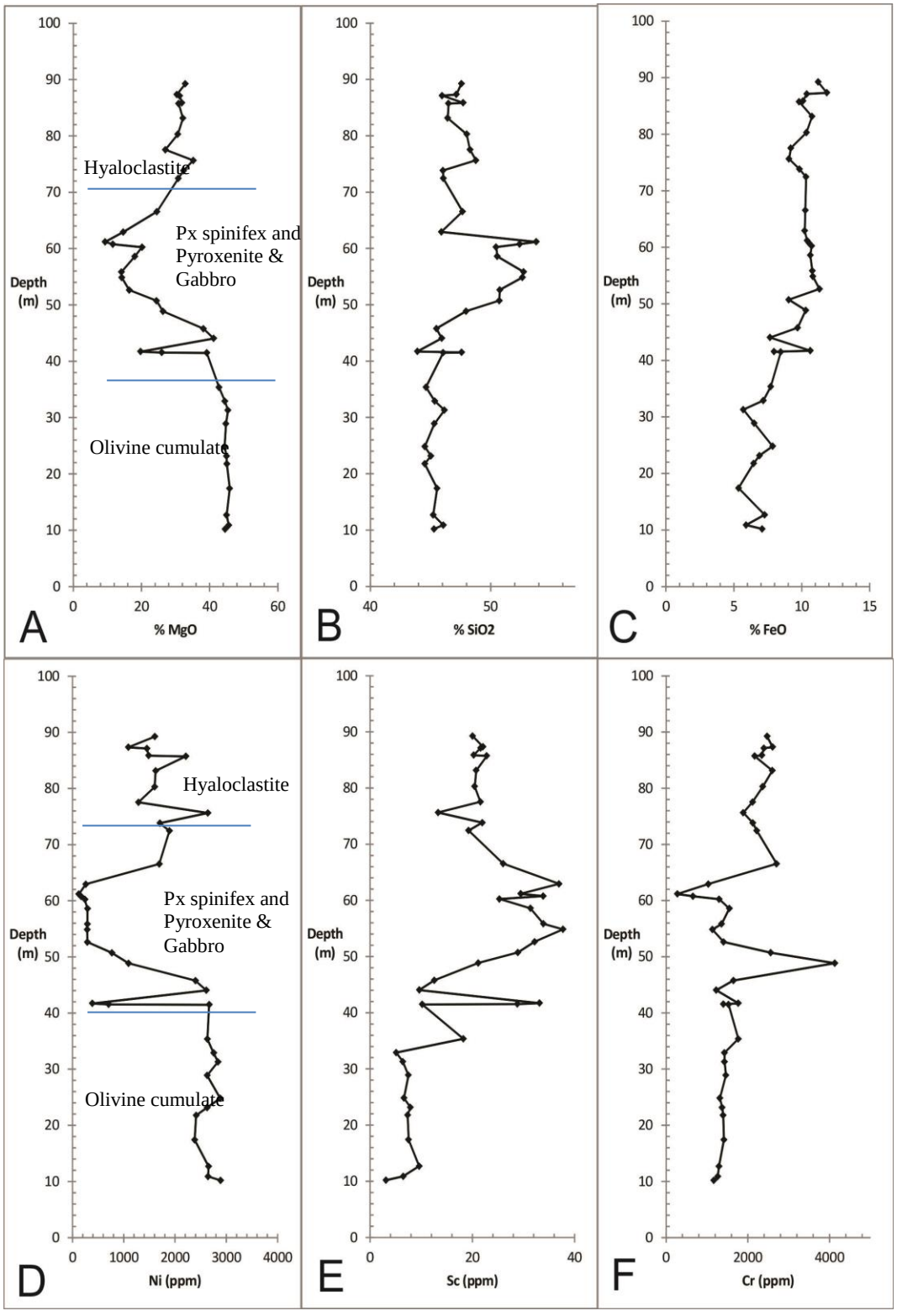

Figure 8.6
Stratigraphic change in element concentrations through the 90 m thick tumulus unit. **A,D** illustrate the high concentration of MgO and Ni in the cumulates, decrease in the pyroxene rich layers and slight increase in the hyaloclastite. **B,E** show the mirror image of the MgO and Ni plots. **C,F** show a consistent increase with stratigraphy in FeO and Cr.

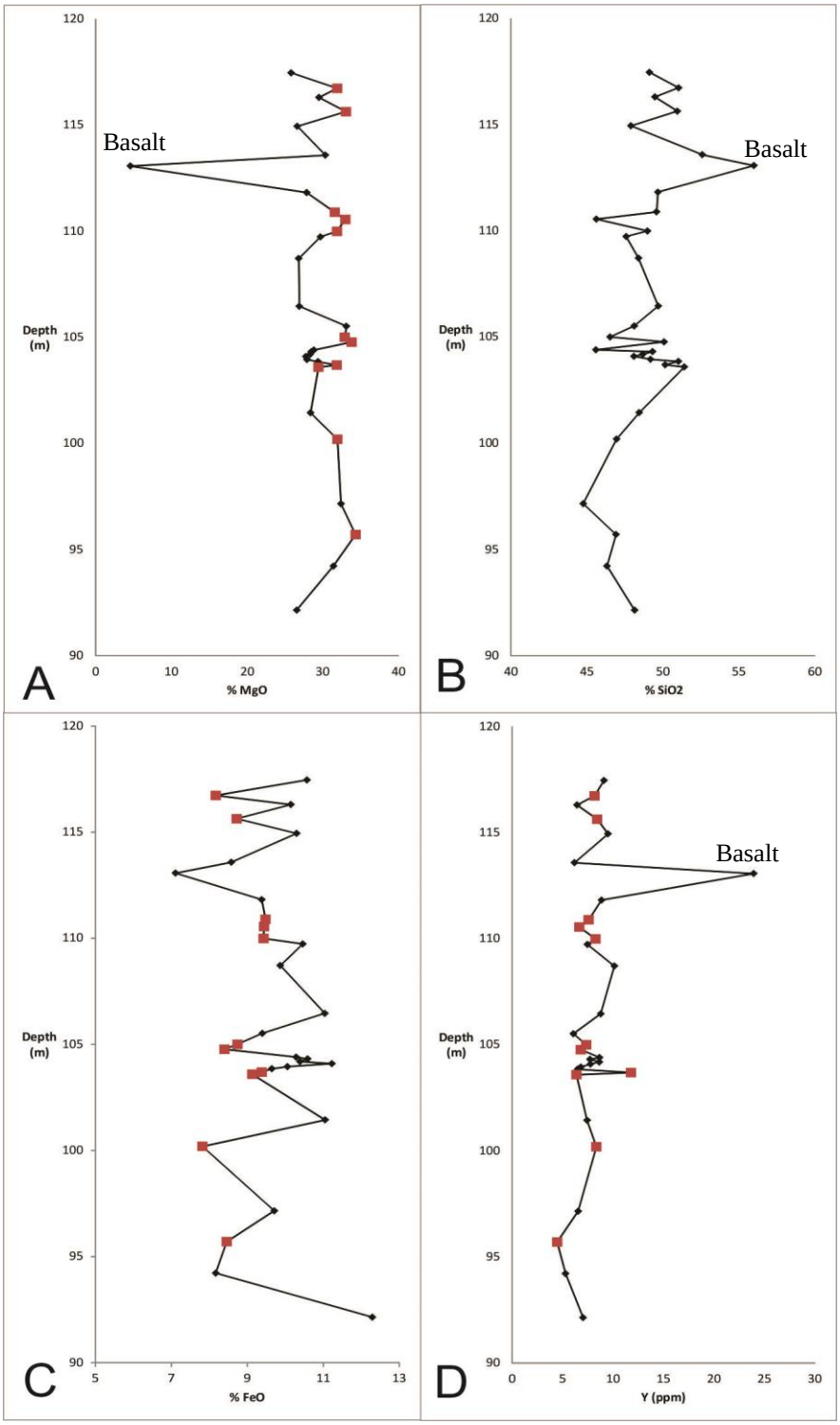

Figure 8.7
Stratigraphic changes in element concentrations through the differentiated komatiite package BARB 1 (89-118 m). All the figures illustrate the element variation with stratigraphic height. **A,B,D** illustrate the basalt layer (113.03 m) via an extremely low or high value with respect to the surrounding komatiites. **C** illustrates the irregular change in FeO concentration throughout the different rock-types. The red plots indicate samples of olivine cumulates.

8.4.5 Detailed Plots of the Differentiated Komatiite Flows in BARB 1 (378-420 m)

The second section of differentiated komatiites, from 378-420 m consists of 45 geochemical samples and ten distinct komatiite flows, together with a komatiitic basalt unit. The komatiitic basalt is not clearly distinguishable from the spinifex and chill plots in the element vs. depth graphs. A vesicle-rich sample at 402.48 m shows as an abnormal point in the SiO_2, CaO and Ni graphs (Figure 8.8 A, B).

The MgO vs. depth plot illustrates the high concentration of MgO in the cumulates, and lower MgO in spinifex and chill samples. As is expected, MgO and Ni show similar patterns, with a slight increase in concentration with depth (up stratigraphy) from 25 to 30 % MgO. In SiO_2, Al_2O_3, TiO_2, Zr, Cr, Y, V and Sc vs. depth plots, the trend is opposite and shows a slight decrease with depth (Figure 8.8 B, C, D). In general, the cumulates have lower concentrations of these elements than their spinifex and chill margin counterparts, with a few exceptions. FeO and Zn show no change in concentration with depth, but vary with rock type (cumulate or spinifex).

8.4.6 Detailed Plots of the Differentiated Komatiite Flows in BARB 2 (252-274 m)

The differentiated komatiite package in BARB 2 is represented by 29 samples from seven differentiated flows. This package contains only cumulates, spinifex and chill zones, but some samples contain mixed spinifex and cumulate lithologies.

The MgO and Ni plots are similar, with the cumulates containing the largest concentration of those two elements. There is no overall pattern, and the element concentrations remain quite consistent with change in stratigraphic height. However, between the intervals 253-255 m and 260-268 m there is a notable increase in the MgO content, which creates a slight sinusoidal trend (Figure 8.9 A, C). This sinusoidal pattern is present as a mirror image in Al_2O_3, TiO_2, Cr, Zr, Y, V and Sc graphs. The SiO_2 vs. depth plot does not show a consistent trend and has a large range of values and an erratic pattern (Figure 8.9 B). FeO and Zn have similar shaped plots but do not show a change in concentration with depth and only vaguely show the sinusoidal pattern evident in the other plots.

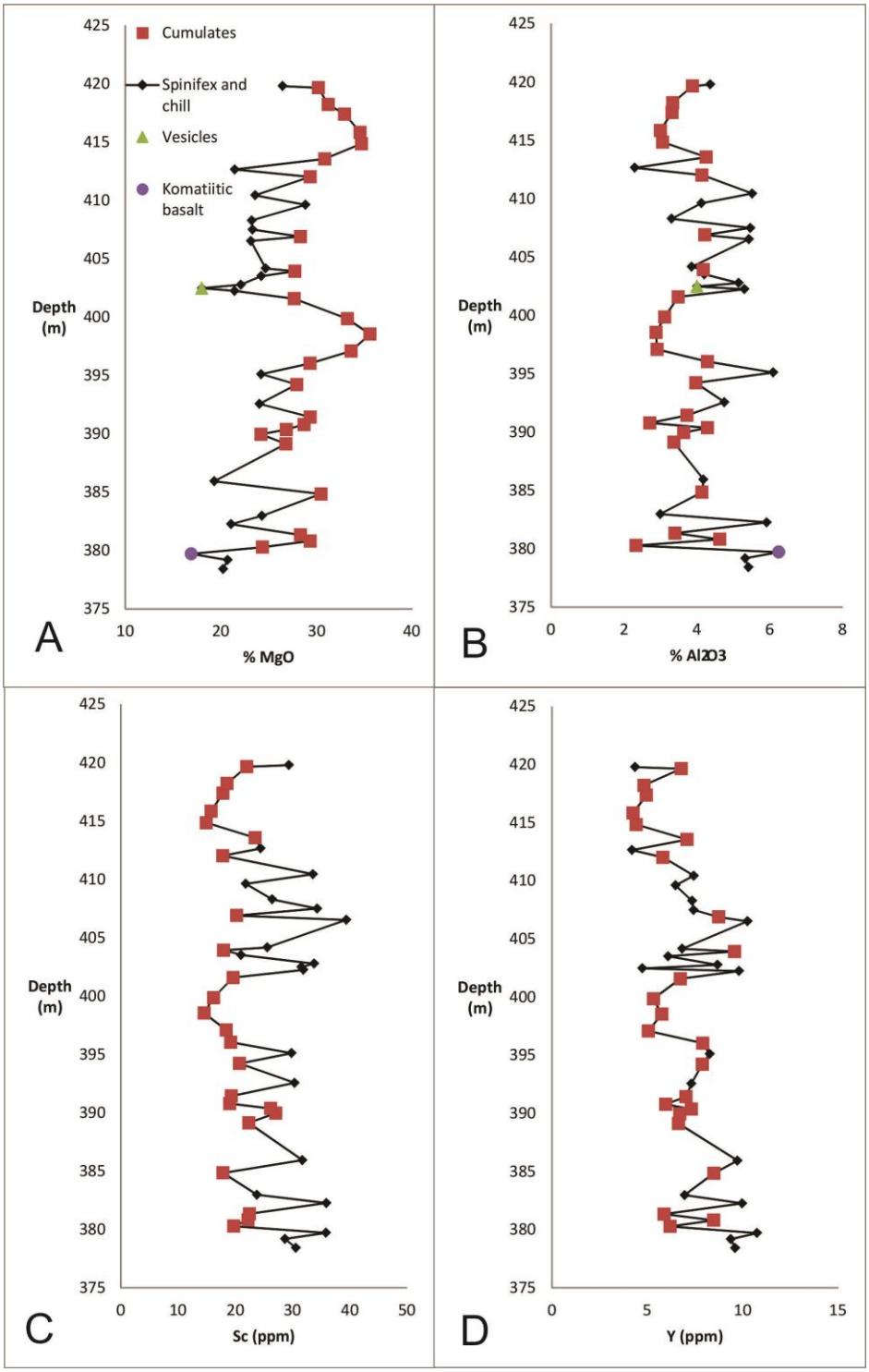

Figure 8.8
Stratigraphic change in element concentrations through the differentiated komatiite package in BARB 1 (378-420 m). The figures illustrate the slight concentration change with depth. **A** illustrates the increase in MgO with stratigraphic height. **B,C,D** illustrate the predominant decreasing trend (opposite to MgO and Ni) with stratigraphic height. The vesicle rich sample and komatiitic basalt sample are plotted in **A,B** to illustrate the effect they possess over the trend. Clearly they do not alter the trends greatly.

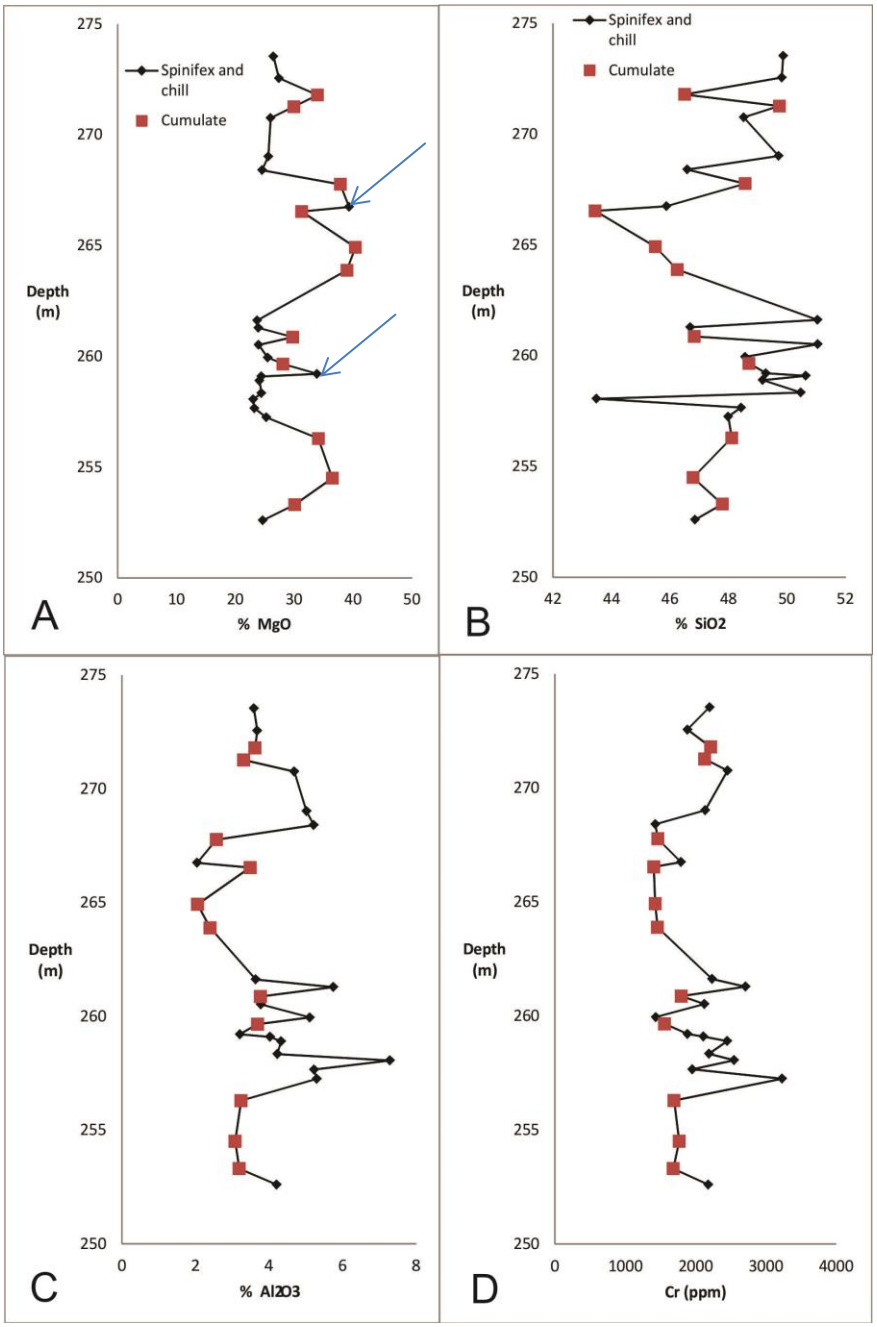

Figure 8.9
Stratigraphic change in element concentrations through the differentiated komatiite package in BARB 2 at (252-274 m). The graphs illustrate a slight sinusoidal trend on a small scale, while no overall pattern is present. **A,C,D** illustrate the sinusoidal trend. **A,C** are mirror images of one another. **B** indicates that SiO_2 has no trend with depth or association between cumulate and SiO_2 content. The two MgO rich samples marked with arrows are chill zones which contain phemnocrysts which increase the MgO content.

8.5 Variation Diagrams of Whole Rock Geochemistry (Major and Trace Elements) of BARB 1 and BARB 2

The major elements analysed using XRF are listed in the introduction. As discussed earlier, some of these elements are immobile and others are mobile. Immobile elements include MgO, TiO_2 and Al_2O_3. To determine the mobility of the other elements, they are plotted against the immobile elements and the trends that occur are analysed to determine mobility. The trends also give insight into the crystallization processes and other processes occurring in the lava flows.

Given the different mineralogies of komatiites and komatiitic basalts, certain chemical compositions are expected and discrepancies can usually be attributed to alteration. To minimize this problem, samples were selected with minimal veining and were screened geochemically. Samples with high LOI levels (above 10%) in conjunction with CaO: Al_2O_3 ratios above 2.5 were eliminated from the sample set as they were identified as being excessively altered.

Each differentiated komatiite package and the tumulus will be considered in separate sections to simplify presentation of the results. A full list of geochemical results is given in Appendix E.

MgO is plotted against FeO, SiO_2, TiO_2, Al_2O_3, LOI, V, Zr, Cr and Ni in Figures 8.10 to 8.18 and Al_2O_3 is plotted against TiO_2, CaO, Zr and Ni in Figure 8.10. Olivine composition lines (Figure 8.11 A) are plotted on the diagrams to determine the role olivine plays in the crystallization of the magma. Table 8.1 shows the MgO values associated with Fo content (Kd value of 0.33). The equation relating Forsterite content to MgO (wt. %) is:

$$Fo_x = \frac{2MgO * (x)}{2(MgO * (x) + FeO * (1 - x)) + SiO_2}$$

Where *x* is the forsertite content/100
Molar mass MgO=40.32 g/mol
Molar mass FeO= 60.09 g/mol
Molar mass SiO_2=71.85 g/mol

Forsterite content	% MgO
Fo_{89}	48.6
Fo_{90}	49.36
Fo_{91}	50.12
Fo_{92}	50.89
Fo_{93}	51.67
Fo_{94}	52.45
Fo_{95}	53.24
Fo_{96}	54.08

Table 8.1: Forsterite content and associated MgO %.

8.5.1 Tumulus

Table 8.2 summarizes the chemical range in select elements from the tumulus.

Element	**MgO**	**SiO_2**	**FeO**	**Al_2O_3**	**CaO**	**TiO_2**	**LOI**	**Cr**	**Ni**	**V**	**Zr**
Min	9.38	43.92	5.35	0.99	0.02	0.08	1.72	281	124	28	4.6
Max	45.9	53.79	11.85	9.81	16.62	0.79	14	4131	2886	254	61.72
Average	31.05	47.39	9.11	3.74	5.06	0.34	9.38	1746	1637	112	22
St. Dev.	11.37	2.60	1.80	2.22	4.78	0.21	4.18	695	978	65	15

Table 8.2: Summary of select major and trace element ranges from the tumulus unit.

MgO and SiO_2 range widely in the tumulus unit. The low MgO and high SiO_2 values are associated with the gabbro and pyroxenite layer and high MgO and low SiO_2 values are associated with the olivine cumulate layer.

Variation diagrams are plotted with different colours representing different rock types (Figure 8.10 and 8.11). Good linear trends are seen for MgO vs. TiO_2, Al_2O_3, Zr and Ni and Al_2O_3 vs. TiO_2, Zr and less so with Ni and V (Figure 8.10). MgO vs. LOI creates a reasonable trend, with the hyaloclastite plotting at higher values than expected and the gabbro-pyroxenite plotting lower than expected. MgO vs.SiO_2 shows a good trend with the exception of two points. The MgO vs. TiO_2, Al_2O_3 and Zr variation diagrams have strong negative correlations with MgO intercepts between 50 and 52%. These are the values associated with olivine and this indicates that the data broadly correspond to olivine control lines. In the case of MgO vs.

Ni a positive kinked correlation is present which flattens out at 20 % MgO, since both MgO and Ni partition strongly into olivine. Hence, as olivine crystalized, both MgO and Ni were concentrated in the olivine cumulates, at the same time resulting in an increase in the concentration of the incompatible elements in the melt. The flattening out at 20 % MgO may reflect accumulation of pyroxene, which has high MgO but low Ni, in these rocks. Graphs of Al_2O_3 vs. TiO_2, CaO, Ni and Zr are plotted to observe the trends of immobile elements other than MgO. Al_2O_3 vs. TiO_2 and Zr forms very distinct positive linear trends, whilst Al_2O_3 vs. Ni forms a negative exponential trend. CaO forms no trend, which indicates mobility of CaO. MgO vs. CaO reveals complete loss of CaO in the cumulates (Figure 8.10 cont.).

The MgO vs. Cr diagram shows a maximum at about 30 % MgO, with a negative correlation in the more magnesian samples and a positive trend in the less magnesian samples (<30 % MgO). This behaviour can be explained by the presence of olivine in the cumulates and the onset of chromite crystallization in the more evolved liquids that produced the spinifex samples and gabbros (Barnes, 1998).

The trends of these graphs reflect the rock-types in the tumulus. In MgO vs. FeO, and similarly for Al_2O_3 and TiO_2 (Figure 8.11), a trend scatters around a Forsterite 92-93 (Fo_{92-93}) control line. The cumulates are the most magnesian and least FeO, Al_2O_3, TiO_2 rich samples. The harrisites plot at an intermediate position, with less magnesium and slightly more FeO, Al_2O_3, and TiO_2. This trend is continued by the pyroxene spinifex, which is less magnesian and correspondingly more FeO, Al_2O_3 and TiO_2 rich. The final stage of crystallization, from liquid with the lowest magnesium and highest FeO, Al_2O_3 and TiO_2 contents, produced the gabbros and pyroxenites in the centre of the unit (60-66 m).

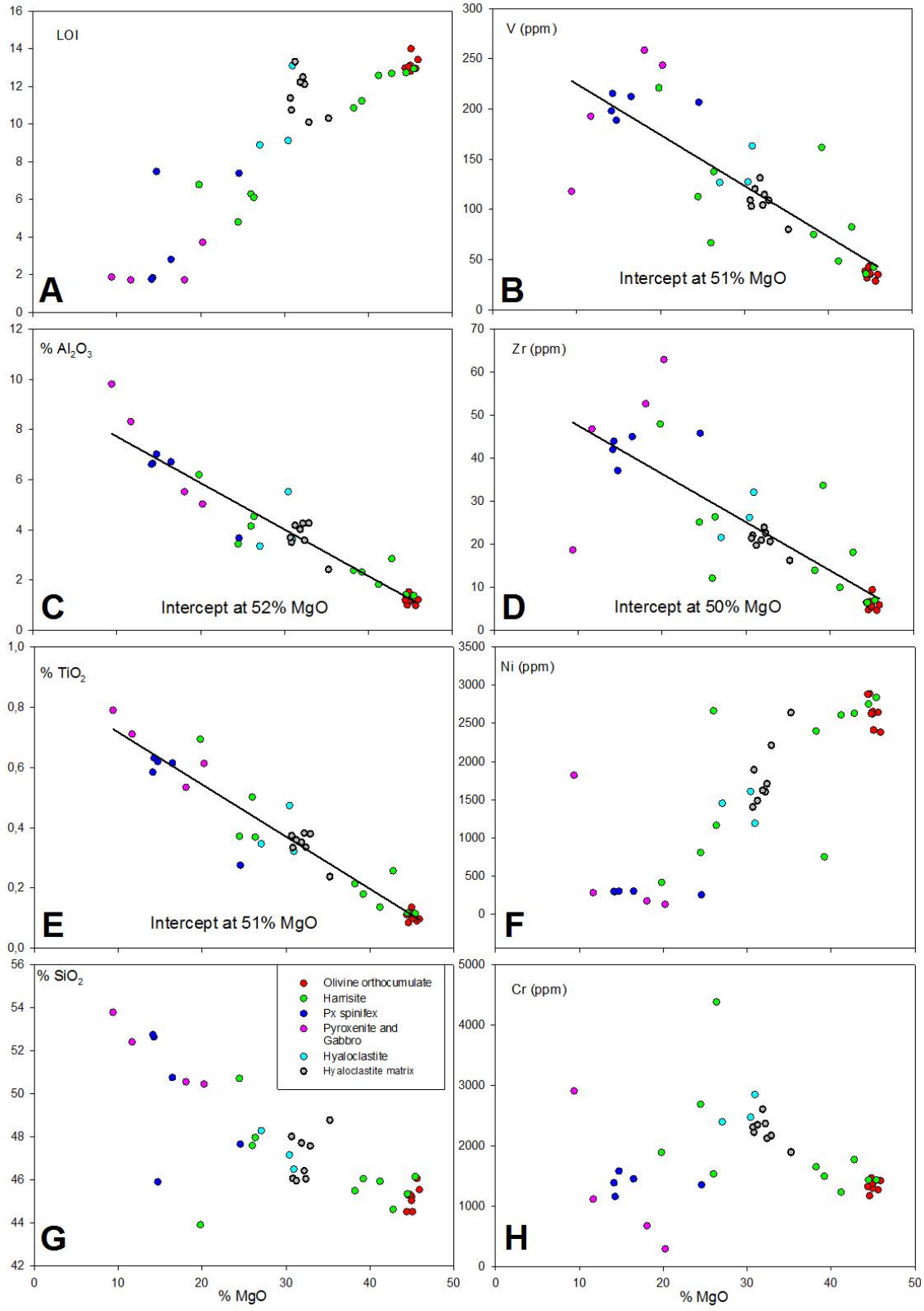

Figure 8.10
Variation diagrams of MgO and various elements for the tumulus section in BARB 1. **A,F** show positive linear/kinked correlations of LOI and Ni with MgO respectively. In **F** the trend flattens out at 20% MgO. **C,D,E,G** illustrate a negative correlation with MgO and indicate a MgO intercept of 50-52%. **B** shows no trend with MgO. **H** illustrates the typical chromite parabola trend associated with komatiites, where Cr is concentrated in the melt until a critical level (occurring at MgO < 25%) is reached and chromite is able to crystalize.

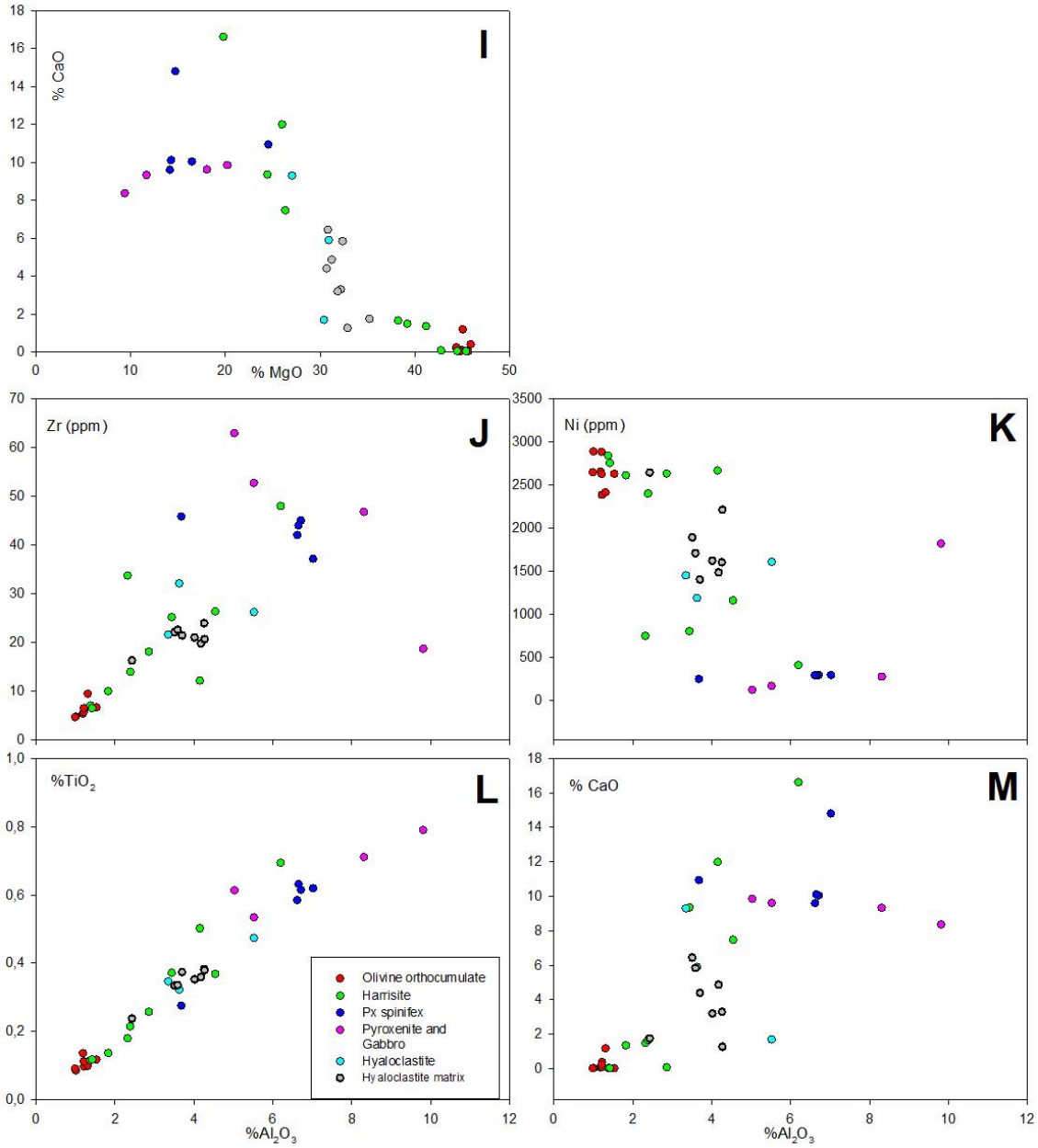

Figure 8.10 cont.
Harker diagrams of Al_2O_3 vs. various elements. **J,L** show good positive linear correlations with Al_2O_3. **I** shows an inverse exponential trend whilst **K,M** show no correlation between Al_2O_3 and Ni, CaO, respectively which is most likely due to mobilization of CaO.

The hyaloclastite unit is the equivalent of a chill zone and therefore should best represent the original magma composition. These samples plot between the olivine cumulate and the pyroxene spinifex, as is predicted for most chill margin compositions. The matrix of the hyaloclastite has a higher MgO value than the chilled fragments (noted as hyaloclastite in the graph). The composition of the chilled fragments and the hyaloclastite matrix is discussed later in the chapter. The most magnesian olivine cumulates create a second trend within the general array. This trend runs parallel to the olivine control line (Figure 8.11 B) and indicates that another process, in addition to magma differentiation, occurred in the tumulus flow unit. Trends that run parallel to olivine composition lines often indicate orthopyroxene fractionation (Wilson, 2012). However this is not supported by thin sections of the cumulate zone of the tumulus, which show only olivine and no pyroxene. Therefore the trend in the cumulates is attributed to alteration and Fe loss. An alternative explanation centres around olivine cumulates with the same trapped liquid composition but different forsterite contents.

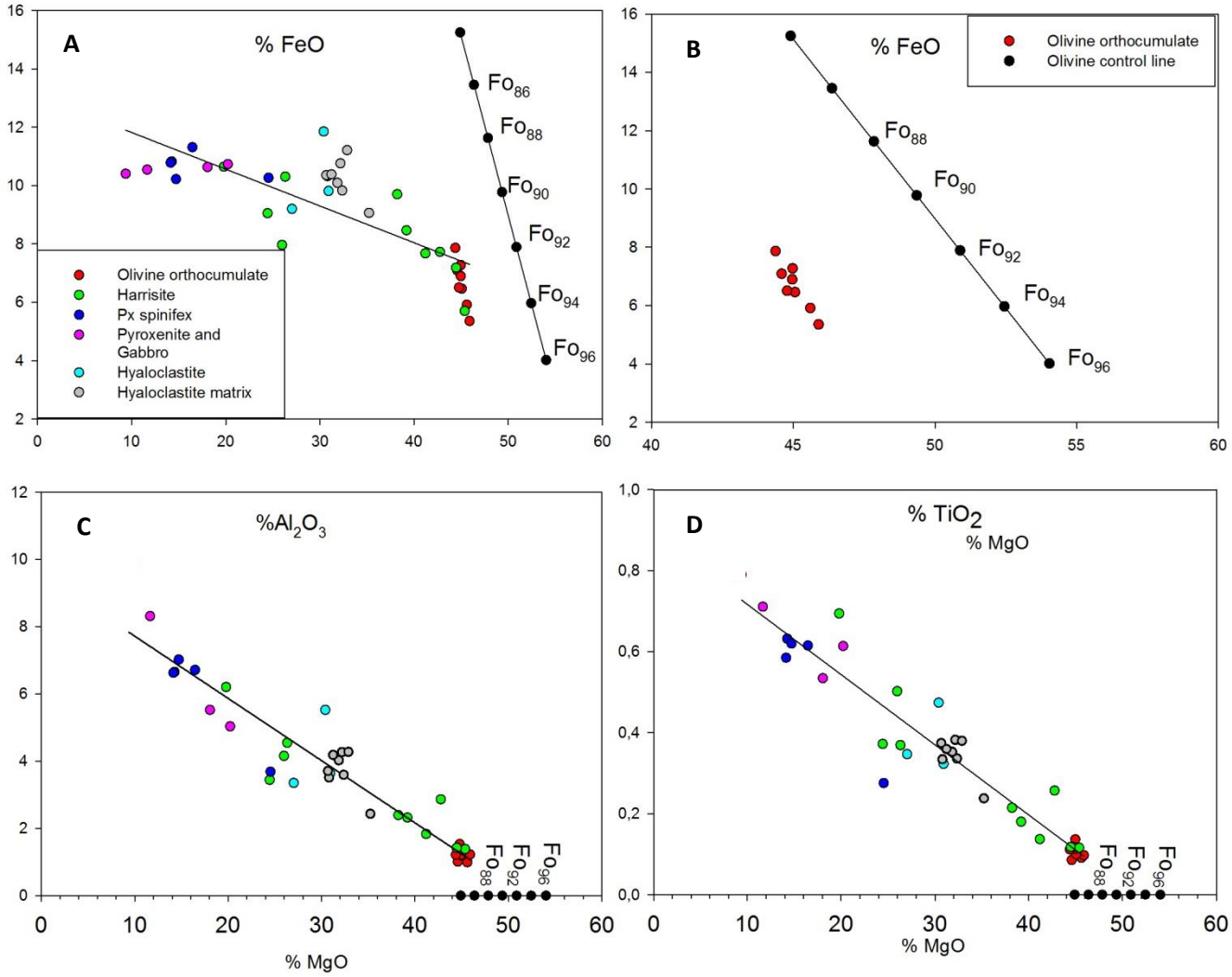

Figure 8.11
Plot of MgO vs. FeO, TiO_2, Al_2O_3 (**A,C,D**) of the tumulus unit in BARB 1 shows a $Fo_{92\text{-}93}$ control. A trend is evident, beginning with the olivine cumulates moving to the harrisite and then into the pyroxene spinifex and lastly into the pyroxenite and gabbro layer, found at the centre of the tumulus unit. The hyaloclastite represents the chill, since it plots between the MgO enriched cumulates and the MgO depleted spinifex. The hyaloclastite (blue) is the closest composition to the original liquid composition. The olivine cumulates create their own individual trend (**B**) that is parallel to the olivine control line and has an MgO intercept of 48 %.

8.5.2 BARB 1 Differentiated Komatiites (89-118 m)

The BARB 1 (89-118 m) differentiated komatiite package directly overlies the tumulus unit and consists of nine komatiite flows and an intrusive basalt layer. Since the basalt is not genetically related to the komatiite package, its composition has not been included in the maximum, minimum and average values and is not plotted in the variation diagrams. Table 8.3 summarizes the range in composition for chosen elements.

Element	MgO	SiO_2	FeO	Al_2O_3	CaO	TiO_2	LOI	Cr	Ni	V	Zr
Min	25.83	44.77	7.82	1.99	2.31	0.172	7.33	1337	1019	62	10
Max	34.33	52.6	12.29	5.51	8.32	0.494	15.08	2514	2177	189	32
Average	29.13	48.67	9.57	4.09	5.57	0.34	12.72	1762	1445	107	24
St. Dev.	5.55	2.32	1.17	2.43	1.81	0.11	3.57	504	435	29	20

Table 8.3: Summary of select major and trace element ranges from the BARB 1 differentiated komatiite flows from 89-118m.

In major and trace element binary diagrams, various trends emerge. Plots of MgO vs. TiO_2, Al_2O_3, Zr and V reveal linear negative trends with MgO intercepts of 40-42 % (Figure 8.12). This is a much lower intercept than would be expected if the compositions were controlled by olivine accumulation or fractionation and therefore indicates the presence of another phase in the mineral assemblage. MgO vs. SiO_2 and CaO show a large scatter, most likely explained by Ca mobility. MgO vs. Ni shows a positive trend. Al_2O_3 vs. TiO_2 and Zr show well constrained positive linear trends, whilst Al_2O_3 vs. Ni shows a negative linear trend with an Al_2O_3 intercept of 8 % (Figure 8.12 cont.).

MgO vs. FeO is plotted to determine whether olivine has a crystallization control within the flows in the BARB 1 (89-118 m) package (Figure 8.13 a). As for the MgO vs. TiO_2, Al_2O_3, Zr and V diagrams, the trend line through the data does not intersect the olivine control line, implying that olivine is not the sole mineral controlling crystallization. When plotting the orthopyroxene control line (Figure 8.13 b) and adding tie lines between the olivine and orthopyroxene control lines (En_x ties to Fo_{x-1}), it is clear that the data trend intersects the En-Fo tie lines. Using the MgO intercept at 40-42 %, allows the calculation of the proportion of olivine (Fo_{91}, ca. 33%) and orthopyroxene (En_{92}, ca. 67%) in the crystallizing assemblage. The petrography supports this interpretation, since both olivine and pyroxene are present in the cumulates. The MgO vs. Cr graph has a steep negative linear correlation with an MgO intercept at 35 %. This trend is formed due to the presence of orthopyroxene which takes in Cr, and hinders chromite crystallization.

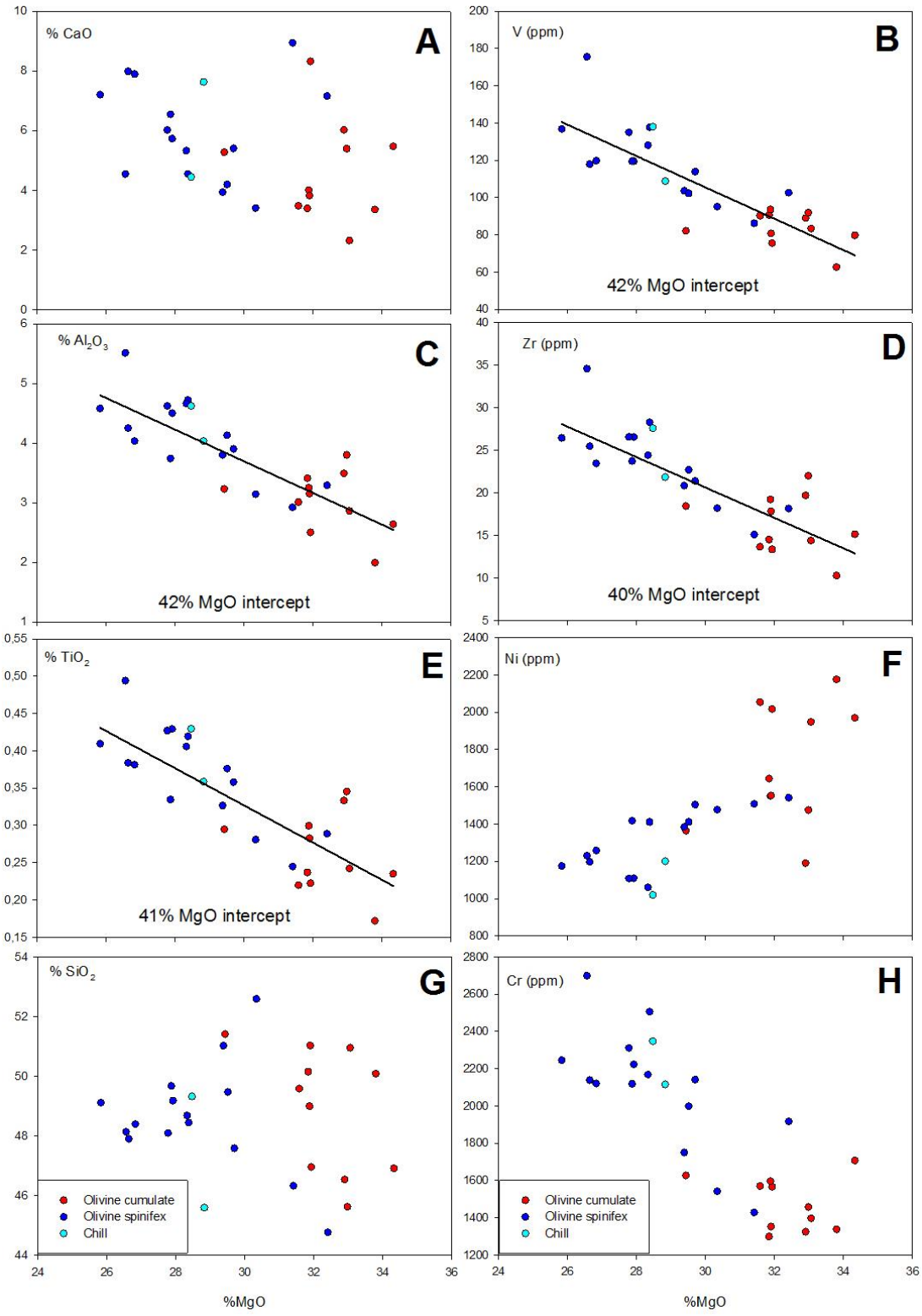

Figure 8.12
Variation diagrams of MgO and various elements in the BARB 1 (89-118 m) differentiated package. **F** shows a positive linear correlations with MgO. **C,D,E,H** illustrate a negative correlation with MgO and indicate a MgO intercept of 40-42 % **A,G** show no trend with MgO indicting mobilization of SiO_2 and CaO. Regression lines calculated in SigmaPlot.

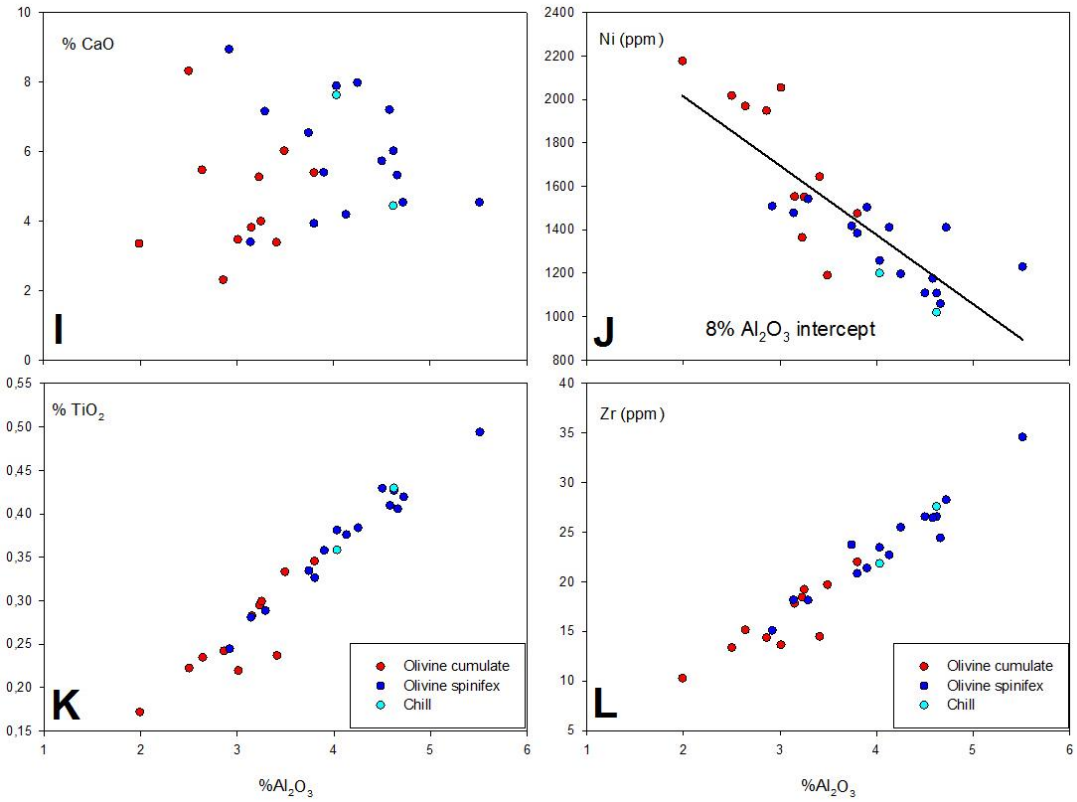

Figure 8.12 cont.
Variation diagrams of Al_2O_3 and various elements. **K,L** show good positive linear correlations with Al_2O_3. **J** shows a negative linear trend with an 8 % intercept whilst **L** shows no correlation between Al_2O_3 and CaO, which is most likely due to mobilization of CaO.

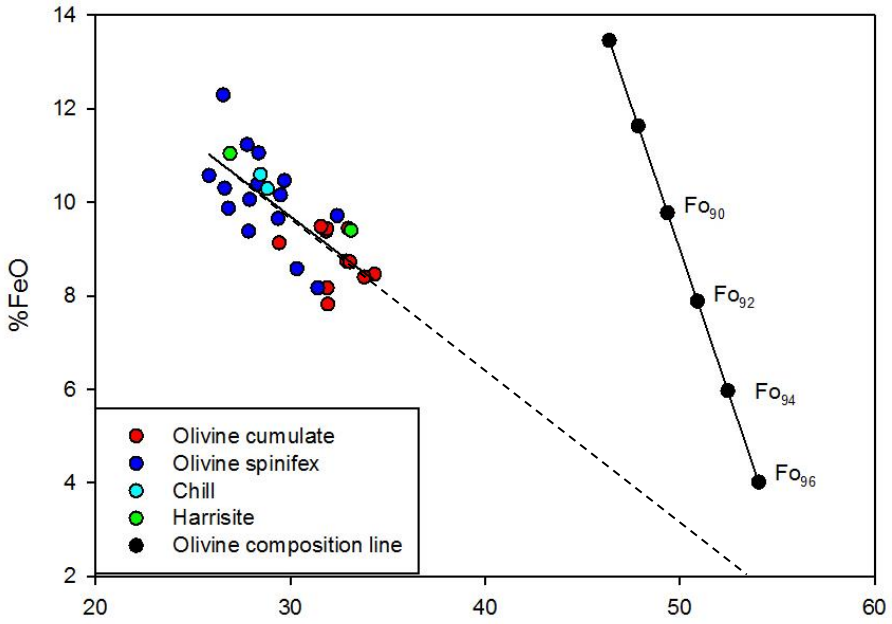

Figure 8.13 a
Diagram of MgO vs. FeO in the BARB 1 (89-118 m) differentiated package. The olivine (Forsterite) composition line is plotted to determine whether olivine controls the crystallization processes in these flows. Clearly the trend line does not intercept the olivine control line, which indicates that olivine does not solely control the crystal processes of these flows.

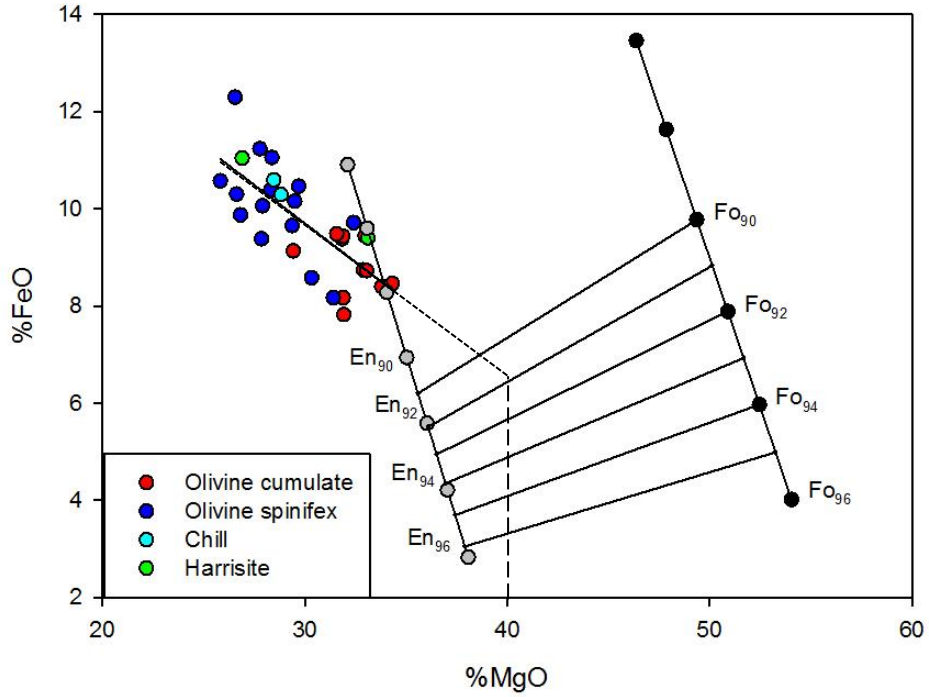

Figure 8.13 b
Diagram of MgO vs. FeO in the BARB 1 (89-118 m) differentiated package. The olivine (Forsterite) and orthopyroxene (Enstatite) contrl lines are plotted, with tie lines. Extrapolating the MgO intercept of 40-42 % from Figure 8.12 , it intersects the data trend line, along the Fo_{91}-En_{92} tie line. Indicating an olivine pyroxene dual control on the crystallization processes in a proportion of 1(ol):2(px).

8.5.3 BARB 1 (378-420 m) Differentiated Komatiites

The BARB 1 (378-420 m) differentiated komatiite package consists of ten flows. This package contains a single conformable komatiitic basalt, which is interpreted to have been emplaced during the eruption of the komatiites. This komatiitic basalt is not removed from the data set because it may have been co-magmatic with the komatiites. The range of element values is shown in Table 8.4 where maximum, minimum and average values are given.

Element	MgO	SiO_2	FeO	Al_2O_3	CaO	TiO_2	LOI	Cr	Ni	V	Zr
Min	16.92	40.66	5.35	2.3	3.38	0.2263	2.57	1186	441	57	12
Max	35.59	54.78	13.63	6.25	24.65	0.5999	14.06	3050	1880	203	32
Average	26.47	48.01	10.17	4.10	8.49	0.40	7.36	2212	1188	129	20
St. Dev.	4.64	2.18	1.47	1.00	4.25	0.10	2.40	433	434	35	6

Table 8.4: Summary of select major and trace element ranges from the BARB 1 differentiated komatiite flows between 378 and 420 m.

The binary diagrams plotted for this komatiite package have a high degree of scatter, with no trends being evident in even the most immobile elements such as MgO, TiO_2, Al_2O_3 and several trace elements. MgO vs. FeO epitomizes the scatter in the data (Figure 8.14 A). Clearly there is no discernible trend in this plot. Two distinct explanations can account for and reduce this scatter. Firstly, the scatter could be caused by different parental compositions, which would indicate a variety of sources for the komatiite flows. The presence of the komatiitic basalt lends strength to this idea, since the komatiitic basalt is part of the package but has a different chemistry, which indicates a different source. To determine whether this is the case, each flow must be identified and the samples from each flow plotted in the same colours. Hence, each flow and its components (cumulate, spinifex and chill) are represented by one colour in the variation diagrams. If individual flows create separate trends, seen by colour groupings, then the concept of multiple populations is a possible explanation for the scatter in the data. A plot of MgO vs. FeO and Al_2O_3 (TiO2 and Zr show the same features but are not plotted) for individual flows (Figure 8.14 B), do not show these clear populations and therefore option 2 must be considered. In option 2, the data are filtered and samples that do not fit the criteria are removed. The criteria used to filter the data are as follows:

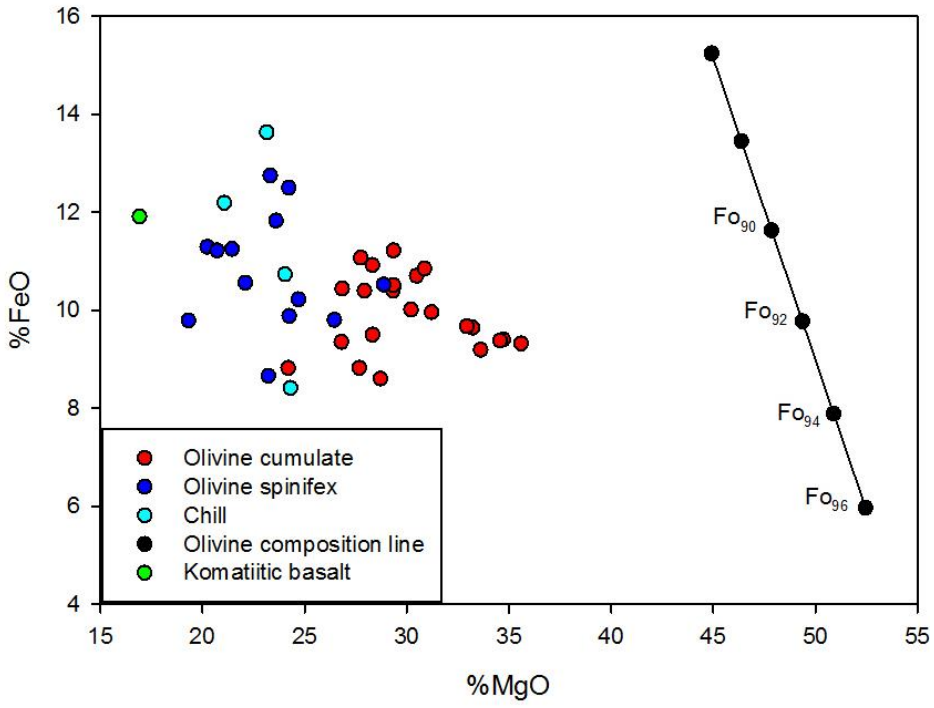

Figure 8.14 a
BARB 1 (378-420 m) differentiated package shows a large scatter in values with no trends emerging from any binary diagrams.

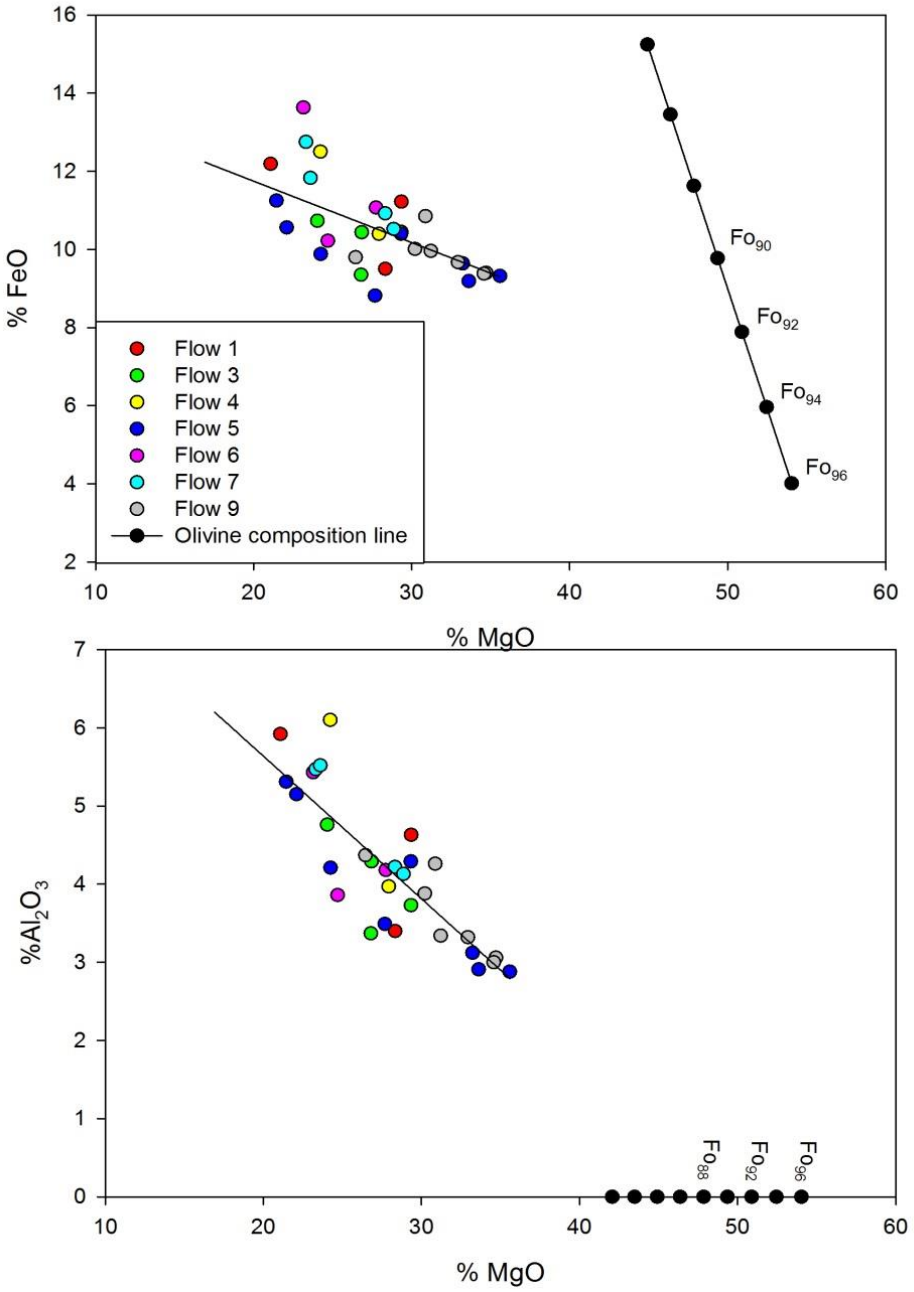

Figure 8.14 b
BARB 1 (378-420 m) data set of samples separated into individual flow units within the package. This sample set does not show individual flows creating distinct trends which would indicate different sources.

1. CaO/Al_2O_3 <2.5- samples with a higher ratio are removed if they show clear evidence of CaO mobility.
2. LOI> 10- these samples are analysed and often found to consist of criteria 1 and therefore are removed.

Using these two major criteria, the data were filtered and eight samples out of 45 were removed (Figure 8.14 C). The resultant MgO vs. FeO data defines a reasonable trend line. The filtered data was used then to draw the subsequent variation diagrams.

The MgO vs. FeO binary diagram illustrates the control of the crystallization of relatively forsterite-rich olivine. The data regression intercepts the olivine control line at Fo_{93}. The MgO vs. TiO_2, Al_2O_3, V and Zr have negative linear trends and indicate an MgO intercept of 50 to 52 %, which coincides olivine with Fo contents of 92 to 93 (Figure 8.15). The V and Zr intercepts are lower at 48 % but these trends are influenced by a set of low-MgO samples, with high contents of these element. MgO vs. Ni shows a positive trend. The MgO vs. Cr data define a scattered negative trend without the typical decrease in Cr content in the less magnesian samples, which typically results from chromite fractionation. The range in MgO intercepts may be due to slight MgO mobility in the differentiated package. Al_2O_3 vs. TiO_2 and Zr have positive linear trends. Al_2O_3 vs. CaO has no trend and indicates the mobility of CaO.

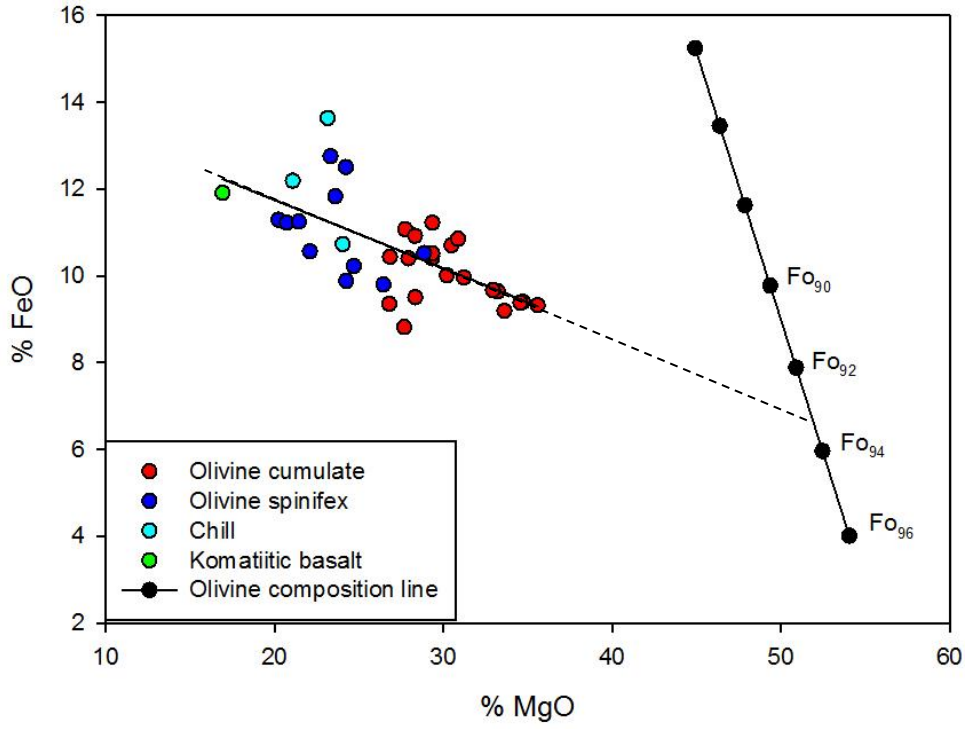

Figure 8.14 c
BARB 1 (378-420 m) data set of samples classified by texture. This sample set has been filtered using certain realistic criteria, to remove samples that are unrepresentative of typical komatiites. The data now shows a Fo_{93} control on crystallization.

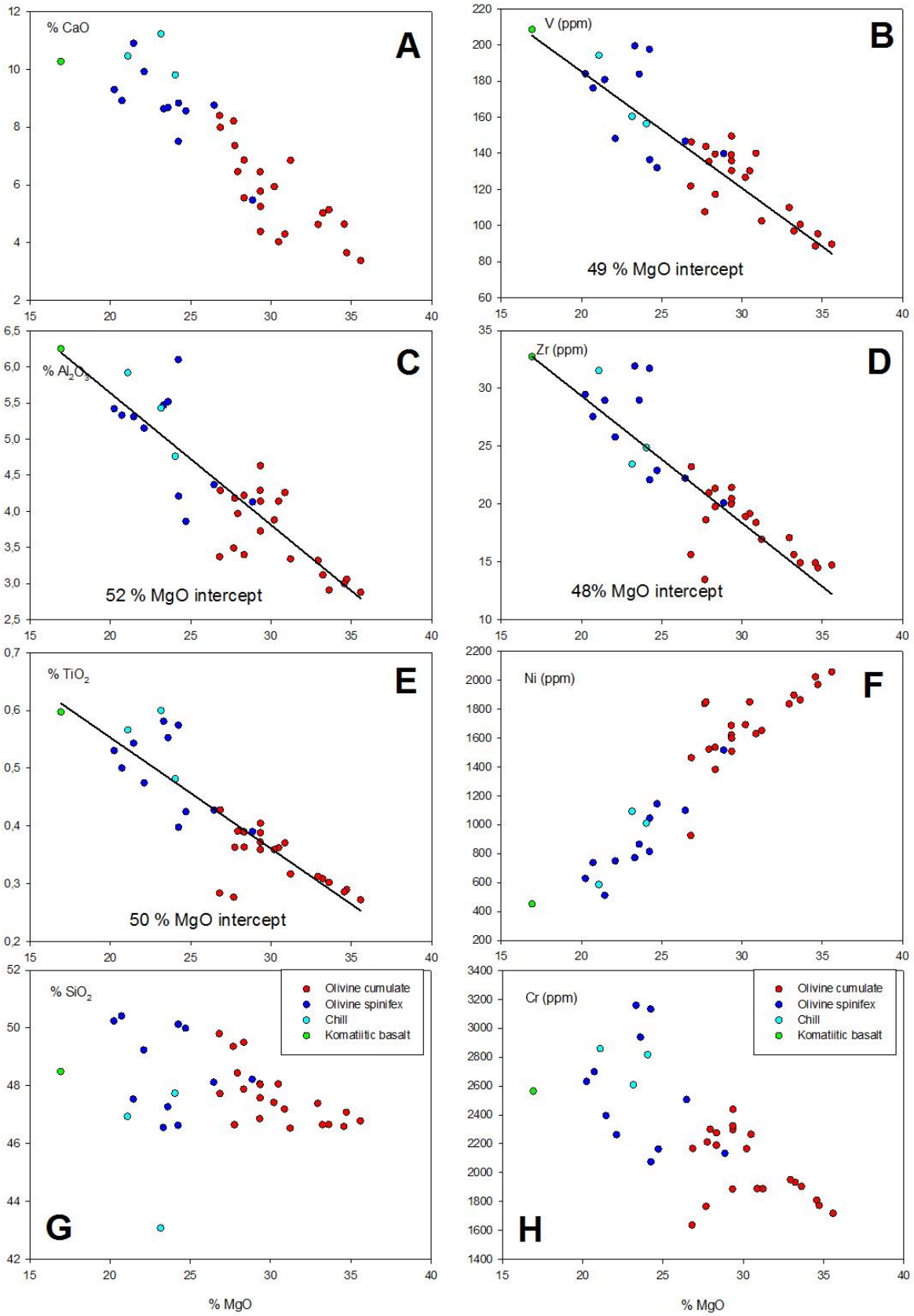

Figure 8.15
BARB 1 (378-420 m) filtered data set. **B,C,D,E** show negative linear trends with an MgO intercept at 48-52 %. **F** shows a positive linear trend with the most magnesian rocks containing the highest Ni content. **G** shows no trend. **H** shows two trends, the negative linear trend, and within the cumulates a dome shaped trend. Regression lines calculated in SigmaPlot.

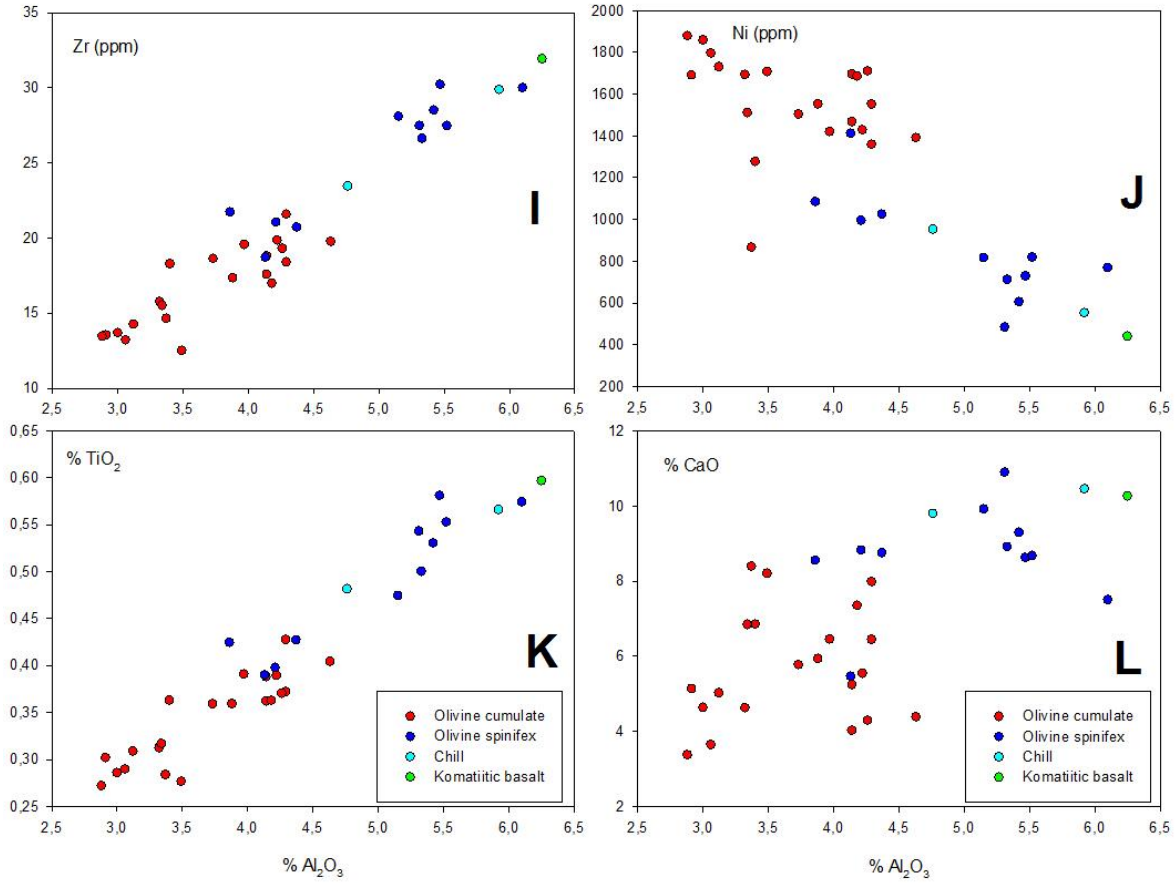

Figure 8.15 cont.
BARB 1 (378-420 m) filtered data set. **I,K** show positive linear trends and the process of fractionation. **J** shows a rather scattered negative trend and **L** shows no trend in CaO, again indicating the likelihood of CaO mobility.

8.5.4 BARB 2 (252-274 m) Differentiated Komatiites

The BARB 2 (252-274 m) differentiated komatiite package consists of seven differentiated flows. There are no intrusive layers or mafic layers in this package. Table 8.5 summarizes the range in selected elements.

Element	MgO	SiO_2	FeO	Al_2O_3	CaO	TiO_2	LOI	Cr	Ni	V	Zr
Min	23.05	43.44	7.9	2.05	0.45	0.1831	4.94	1251	408	56	9
Max	40.4	51.05	13.53	7.29	11.81	0.6153	12.52	3234	2298	205	32
Average	28.99	48.01	9.69	3.96	6.70	0.37	8.35	1956	1342	121	20
St. Dev.	5.55	2.02	1.21	1.16	3.51	0.12	2.41	476	544	36	7

Table 8.5: Summary of select major and trace element ranges from the BARB 2 differentiated komatiite flows between 252 and 274 m.

The BARB 2 (252-274 m) package is similar to the BARB 1 (378-420 m) package in that it displays a large scatter in the data. The same criteria were applied to this package and six samples of 29 were removed. Again samples with only one criterion were scrutinized before being removed, and many were not removed.

In the MgO vs. FeO binary diagram the filtered data intersect the olivine control line at Fo_{93} (Figure 8.16). This corresponds to an MgO intercept of 51.6 % (Table 8.1), which is within the range of the intercepts in the MgO vs. TiO_2, Al_2O_3, Zr, V diagrams (52-55 %, Figure 8.17). MgO vs. Ni shows a positive trend, whilst MgO vs. SiO_2 has no trend. Similarly Al_2O_3 vs. TiO_2 and Zr show positive linear trends while Ni illustrates a slightly scattered negative trend. The chill zone compositions plot between the cumulate and spinifex compositions with the exception of two points which have higher MgO. This implies that they are not true chill margins and under closer inspection, they are fine grained chill margins containing up to 35 % micro olivine cumulates, which has caused an increase in the MgO content.

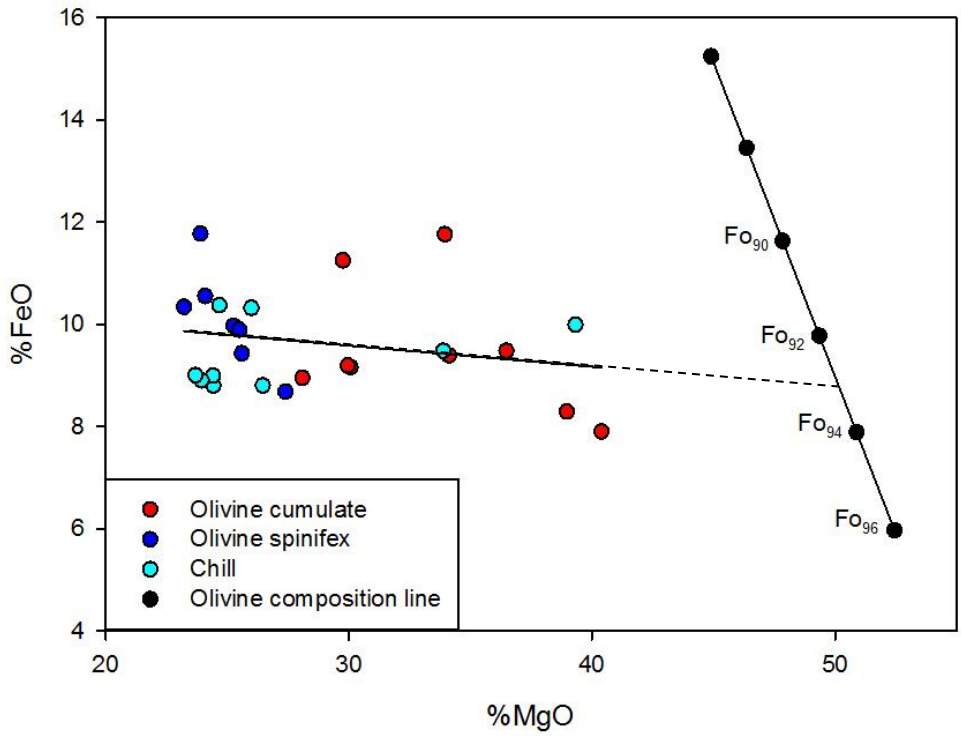

Figure 8.16
BARB 2 (252-274 m) differentiated komatiite package. The data were filtered using the given criteria and 6 out of 29 samples were removed. They yield a trend line with an intercept of Fo_{93} on the olivine control line.

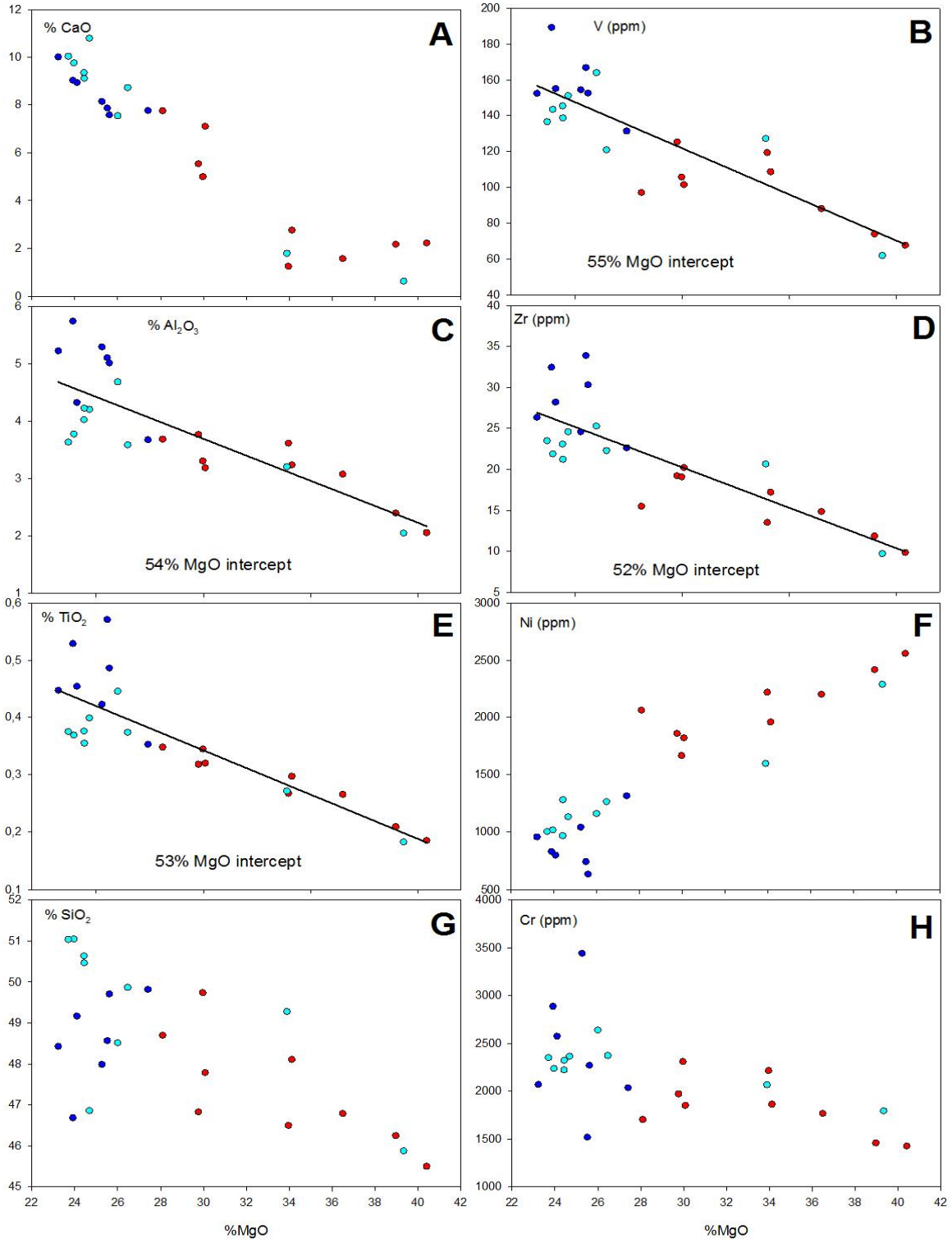

Figure 8.17
BARB 2 (252-274 m) filtered data set. **A,C,D,E** show negative linear trends with an MgO intercept between 52-55 %. **F** shows a positive linear trend with the most magnesian rocks containing the highest Ni content. **G** shows no trend. **H** shows two trends, the negative linear trend, and within the cumulates a dome shaped chromite trend. The lines drawn are regression lines.

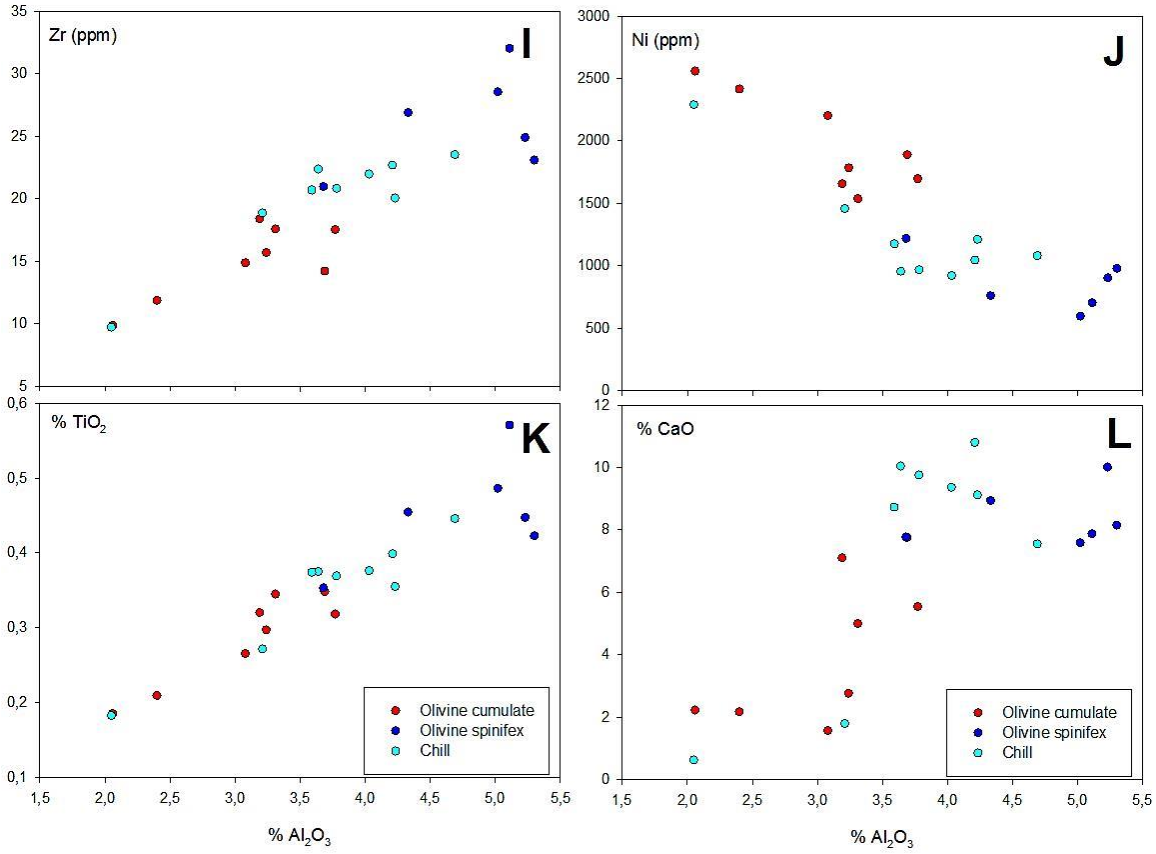

Figure 8.17 cont.
BARB 2 (252-274 m) filtered data set. **I,K** show positive linear trends whilst **J** shows a negative scattered trend and **L** shows no trend.

8.5.5 Comparison of Hyaloclastite and Chill Margins

The hyaloclastite zone of the tumulus represents the chilled magma of the upper crust of the unit. As noted previously the hyaloclastite is composed of chilled magma that is fractured and forms blocks, which became rotated due to the flow pressure. These blocks are surrounded by a glass shard matrix that supports the fractured blocks of chilled magma. These magmas are thought to represent the original liquid composition of the komatiite source magma.

The chemistry of this glass shard matrix can instructively be compared with the chilled fragments of magma from the tumulus. This comparison determines whether there is a difference in composition and if there is; which constituent is better to use as a liquid composition.

Variation diagrams are plotted with the hyaloclastite (chilled fragments and glass shard matrix) and chill margin compositions from each differentiated package (Figure 8.18). The

MgO vs. FeO diagram shows the distribution of chill zone compositions. The hyaloclastite blocks have an MgO range from 27-30 % and a large FeO range from 9-12 %. The hyaloclastite glass shard matrix has MgO compositions mainly between 30 and 32 % with one sample at 35 % and FeO compositions from 9 to 11.5 %. The two BARB 1 (89-118 m) chill margins have good precision with MgO values at 28 % and FeO of 10.5 %. The four BARB 1 (378-420 m) chill samples have low MgO values of 22-25 % and a wide FeO composition range from 8.5 to 13.5 %. The BARB 2 (252-274 m) chill samples have a cluster of points around MgO 24-27 % and FeO 9-10 %.

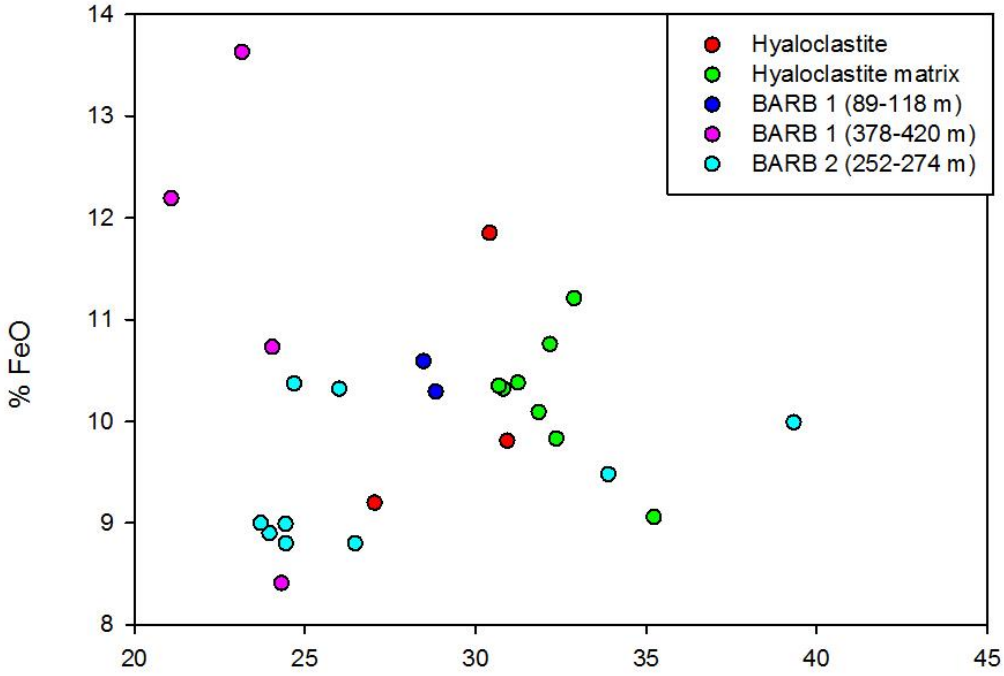

Figure 8.18
MgO vs. FeO binary diagram illustrating the range in compositions for the chill margins of each differentiated komatiite package together with the chilled hyaloclastite block and the hyaloclastite matrix.

The high MgO content of the glass shard matrix is attributed to alteration, where the shards are completely altered to magnesite, which imparts excess MgO to the rock. This is acknowledged in modern altered submarine glasses and demonstrated in the Alexo komatiites (Arndt *et al.*, 2008). The high MgO content places the glass shards above the acceptable komatiite liquid composition of 30 % MgO, and therefore the chilled fragments of the hyaloclastite better represent the liquid composition.

8.6 Trace Elements

The trace elements were analysed using the ICP-MS methods (see Appendix D for method). The REE are plotted with the element values normalized to chondrite values from McDonough & Sun (1995) after (Anders & Grevesse, 1989). The multi-element diagrams are normalized to primitive mantle values from McDonough and Sun (1995). These diagrams give information about the tectonic setting and source of the magmas. Certain mantle processes caused the enrichment or depletion of the HREE and the removal or concentration of the LREE in varying proportions. These effects are indicative of certain tectonic environments.

Chavagnac (2004) noted that the REE patterns in the Barberton komatiites are unaffected by alteration, because the REEs are relatively immobile unless in the presence of fluoride or carbonate rich fluids. Since no evidence of carbonates or fluoride had been found on surface, it was assumed that the Barberton REE chemistry represented the original igneous REE chemistry. In the outcrop no carbonates are visible, but the drill core gives a better and more detailed window into the rock-types present and reveals a vast network of thin (5 mm wide) magnesite (magnesium carbonate) veins, which are pervasive throughout the BARB 1 and BARB 2 core. The presence of carbonate veins in these rocks indicates that the REE diagrams must be treated with care and possibly that they do not illustrate original magmatic conditions. Lahaye *et al.* (1995) indicate that the HFSE and REE are mobile in the rocks of the Komati Formation due to carbonate fluids. Furnes *et al.* (2013) demonstrate the trends of the REE in the Komati Formation (Figure 8.19), which show a slight LREE enrichment. The concentrations range between 1 and 10 times chondrite values with a small (+ and -) anomaly at Eu.

In the graph from Robin-Popieul *et al.* (2012) (Figure 8.20) the Komati Formation shows well constrained trace element distributions, which are between 1 and 10 times primitive mantle (PM) values. Variations of Ti and Nb may be due to minor crustal contamination. To gain more insight into the multi-element diagrams, plots of MgO vs. $(Gd/Yb)_N$ and $(La/Sm)_N$ show depletion or enrichment of HREE $(Gd/Yb)_N$ and LREE $(La/Sm)_N$ in the different komatiite packages (Figure 8.21).

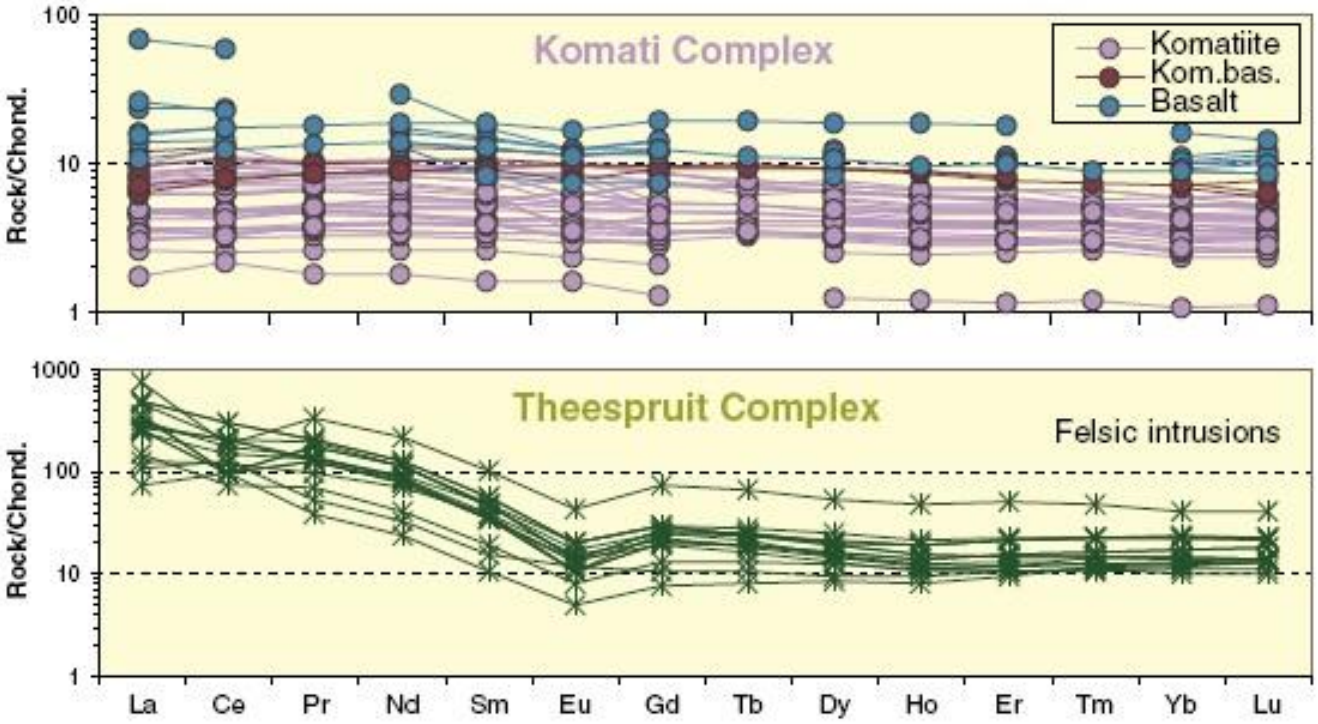

Figure 8.19
REE diagram from Furnes et al. (2013) illustrates the flat pattern found in the Komati Formation. Values for komatiites are 1-10 times chondrite values, while komatiitic basalts are between 8 and 11 times chondrite. Basalts are up to 100 times chondrite value.

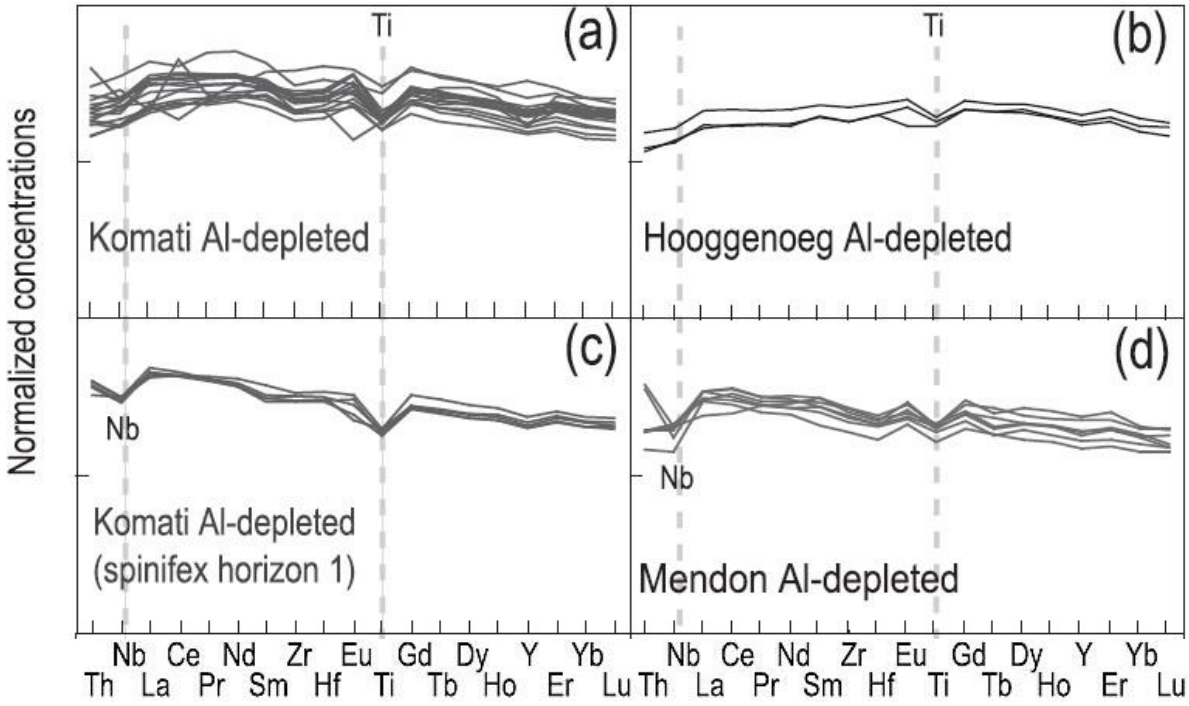

Figure 8.20
Multi element diagram from (Robin-Popieul *et al.*, 2012) for Al-depleted komatiites from the Komati Formation. The pattern is relatively flat and only the slightest LREE concentration is present. Nb and Ti anomalies are identified. The plots are >10 times primitive mantle values and plot in a well constrained shape.

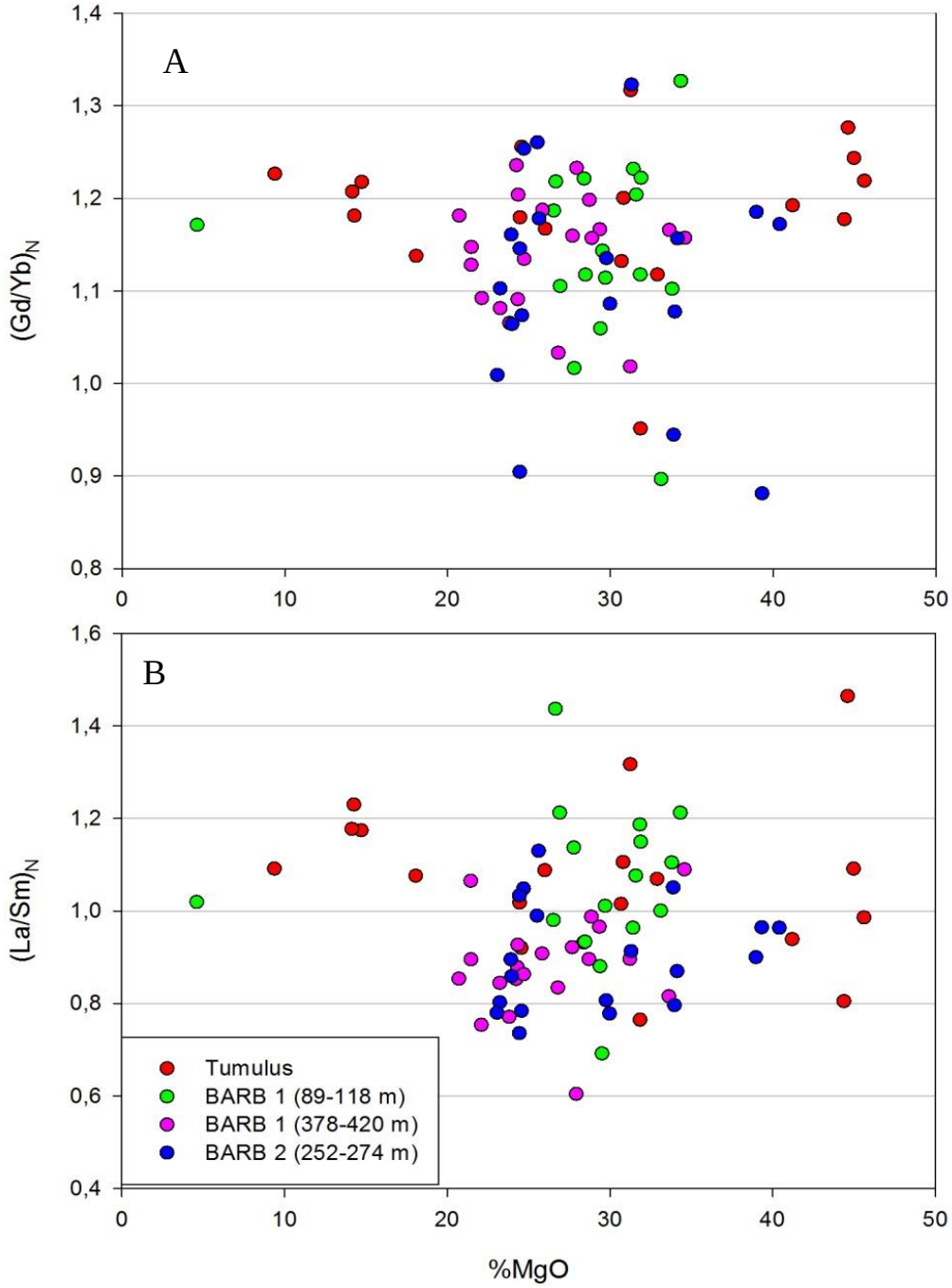

Figure 8.21
MgO vs. $(Gd/Yb)_N$ and $(La/Sm)_N$ give details about slopes and trends in the immobile multi-element diagrams.

Since the BARB 1 and BARB 2 komatiites are of the Al-depleted-type, similar trends with similar anomalies would be expected. These plots are useful in terms of comparing surface-sample data from other areas of the Komati Formation, to the core data from BARB 1 and BARB 2.

8.6.1 Tumulus

The tumulus consists of five major textural sections: basal olivine cumulates, harrisite, pyroxene spinifex, pyroxenite - gabbro and hyaloclastite. 20 representative samples from the five textural sections are plotted in REE and multi-element diagrams to illustrate the trends present in the tumulus unit.

The REE diagram plots the elements La through to Lu, which are shown chondrite normalized. The emerging trend from the tumulus contains a slight LREE enriched pattern, supported by the $(La/Sm)_N$ ratio of 0.76 to 1.46 with an average of 1.07 (Figure 8.22). There is a sloping HREE as defined by $(Gd/Lu)_N$ ratio of 1.07 to 1.63 with an average of 1.35. The maximum point occurs at Pr and both La and Ce are slightly depleted. A small negative Eu anomaly is present for most samples, with some showing no anomaly and others a small positive anomaly (Figure 8.22). The plots are in the 1 to 11 times chondrite range and are essentially parallel to one another.

The multi-element diagram (Figure 8.23) from the tumulus unit has a dome shape from Th to Hf. A small anomaly is present at Eu and a notable negative Ti anomaly is present in some samples. The graph shows a gentle decreasing slope from Gd to Lu as illustrated in Figure 8.21 (values between 1 and 1.3). A block (fragment) from the hyaloclastite has a more irregular pattern with excess Nb, Zr, Hf and Ti and flatter HREE. It is most likely that the relatively large range in Gd/Yb results from analytical uncertainty in the data from these very poor samples. This figure shows concentrations from 0.3 times primitive mantle (PM) in the cumulates, to 9 times PM in the pyroxenite – gabbro layer. The cumulates have the lowest concentrations and the progressively more fractionated rocks have a higher concentration. The patterns are all parallel but plot over a range of values.

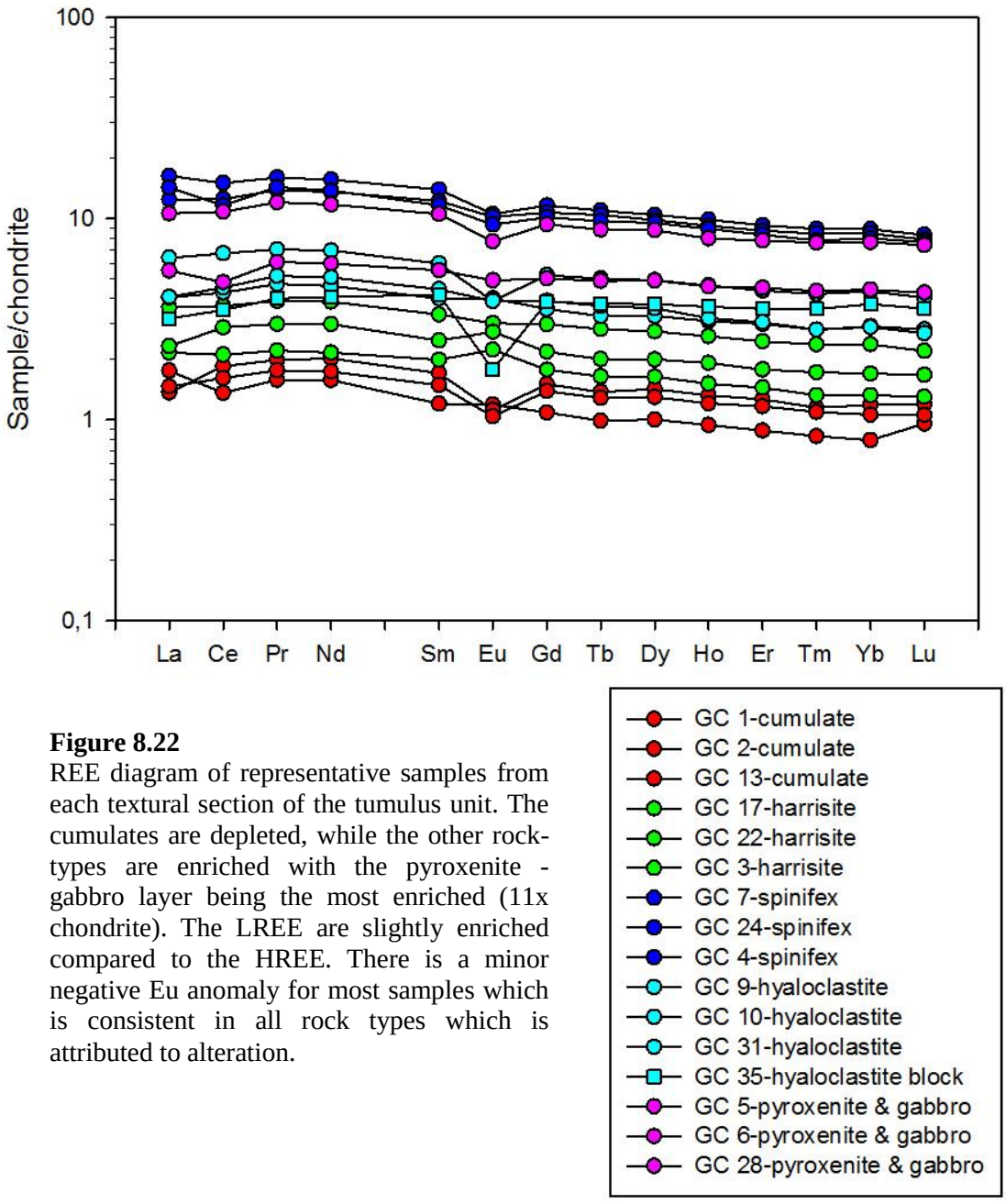

Figure 8.22
REE diagram of representative samples from each textural section of the tumulus unit. The cumulates are depleted, while the other rock-types are enriched with the pyroxenite - gabbro layer being the most enriched (11x chondrite). The LREE are slightly enriched compared to the HREE. There is a minor negative Eu anomaly for most samples which is consistent in all rock types which is attributed to alteration.

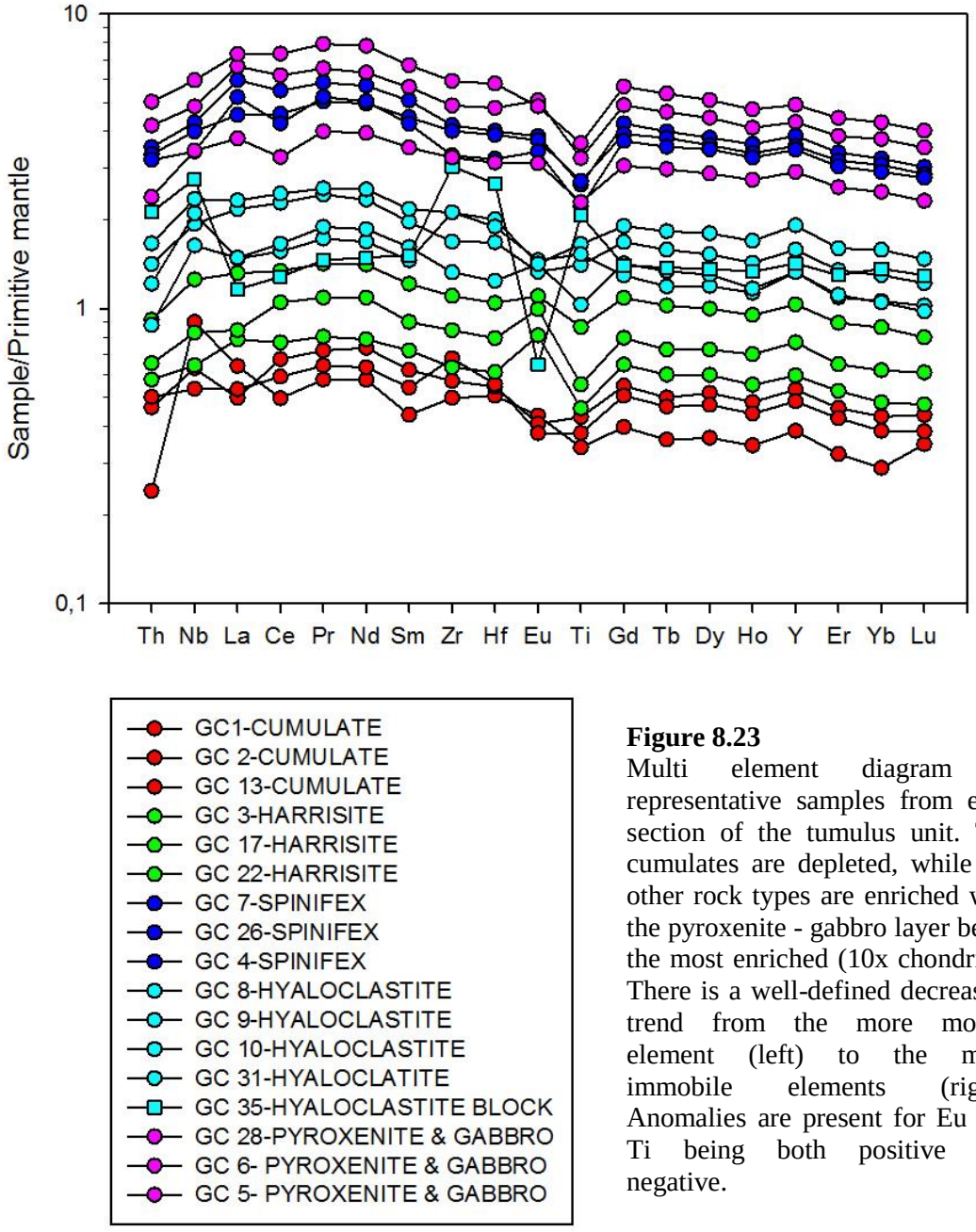

Figure 8.23
Multi element diagram of representative samples from each section of the tumulus unit. The cumulates are depleted, while the other rock types are enriched with the pyroxenite - gabbro layer being the most enriched (10x chondrite). There is a well-defined decreasing trend from the more mobile element (left) to the more immobile elements (right). Anomalies are present for Eu and Ti being both positive and negative.

8.6.2 BARB 1 (89-118 m) Differentiated Komatiites

The BARB 1 (89-118 m) differentiated komatiite package has 15 ICP-MS samples from the cumulate, spinifex and chill zones of the komatiite flows. A single harrisite sample was also analysed. The REE plot shows an increase in LREE as observed by the $(La/Sm)_N$ ratio from 0.69 to 1.43 with an average of 1.04. There is a dome shaped pattern from La to Sm with a maximum at Pr, and a slight depletion in La and Ce to form the dome shape (Figure 8.24). The HREE have a gently decreasing slope from Gd to Lu as seen by $(Gd/Lu)_N$ 0.97 to 1.45 with an average of 1.28. The samples range between 5 and 9 times chondrite values except for Eu, which ranges between 2.5 and 8 times chondrite and has both positive and negative anomalies. The Eu anomaly in this sample suite (Figure 8.24) is positive in the cumulates (1.07 to 1.38) and negative in the spinifex (0.48 to 0.92) and chill zones (0.74 to 0.84). A small negative Ce anomaly is present in some samples. The samples plot in a parallel and well confined pattern. The cumulates, in general, have lower values, but two spinifex samples plot at the same normalized concentrations as the cumulates. The chill samples have higher concentrations than the cumulates and similar concentrations to the spinifex.

The multi-element plot for BARB 1 (89-118 m) has a dome shape from Th to Hf (Figure 8.25), with a maximum value at Pr. A positive and negative anomaly occurs at Eu, a negative anomaly at Ti and a slight positive one at Y. The trend from Gd to Lu has a gentle decreasing slope (Figure 8.21). Element concentration values range from 1 to 3 times PM and are very well constrained. The spinifex and cumulate samples concentrations overlap, indicating later stage alteration that possibly mobilized the elements.

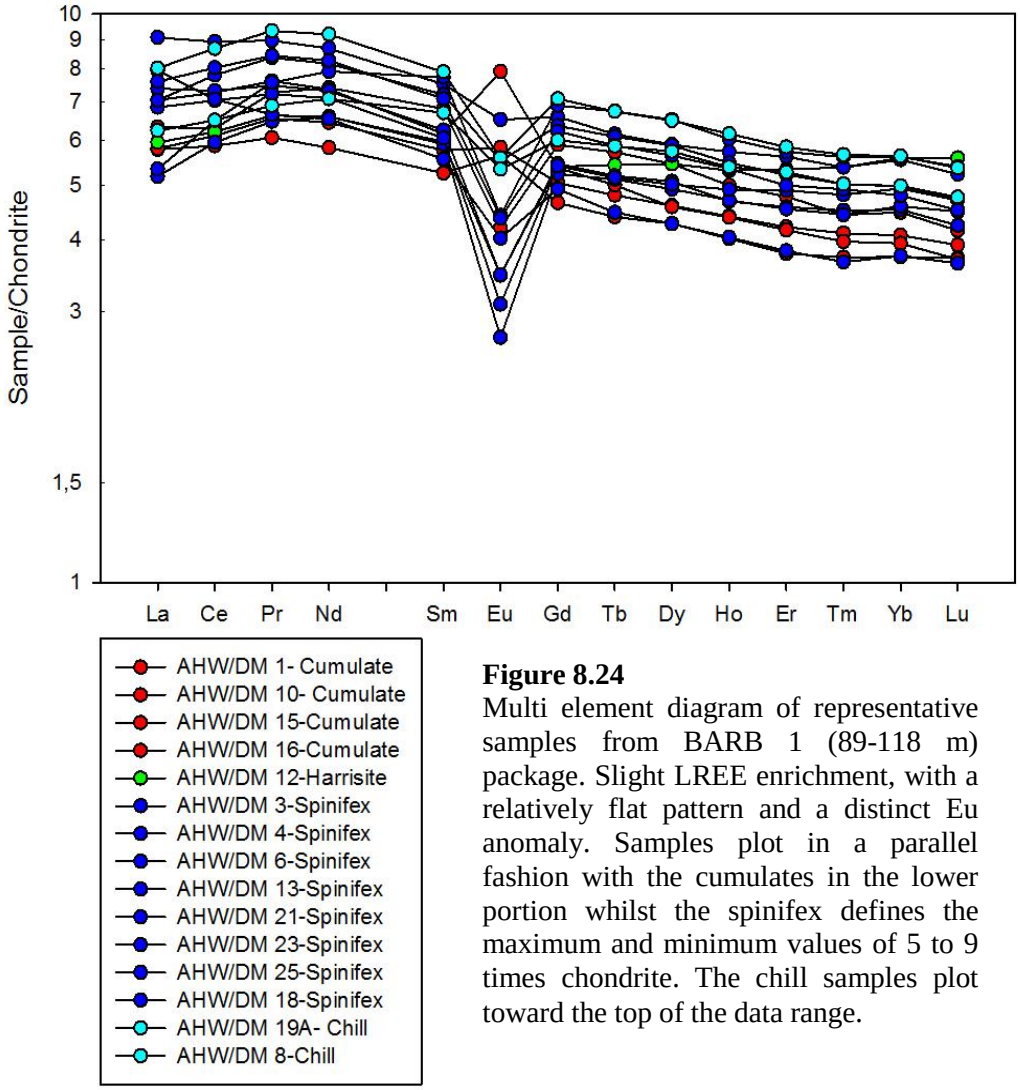

Figure 8.24
Multi element diagram of representative samples from BARB 1 (89-118 m) package. Slight LREE enrichment, with a relatively flat pattern and a distinct Eu anomaly. Samples plot in a parallel fashion with the cumulates in the lower portion whilst the spinifex defines the maximum and minimum values of 5 to 9 times chondrite. The chill samples plot toward the top of the data range.

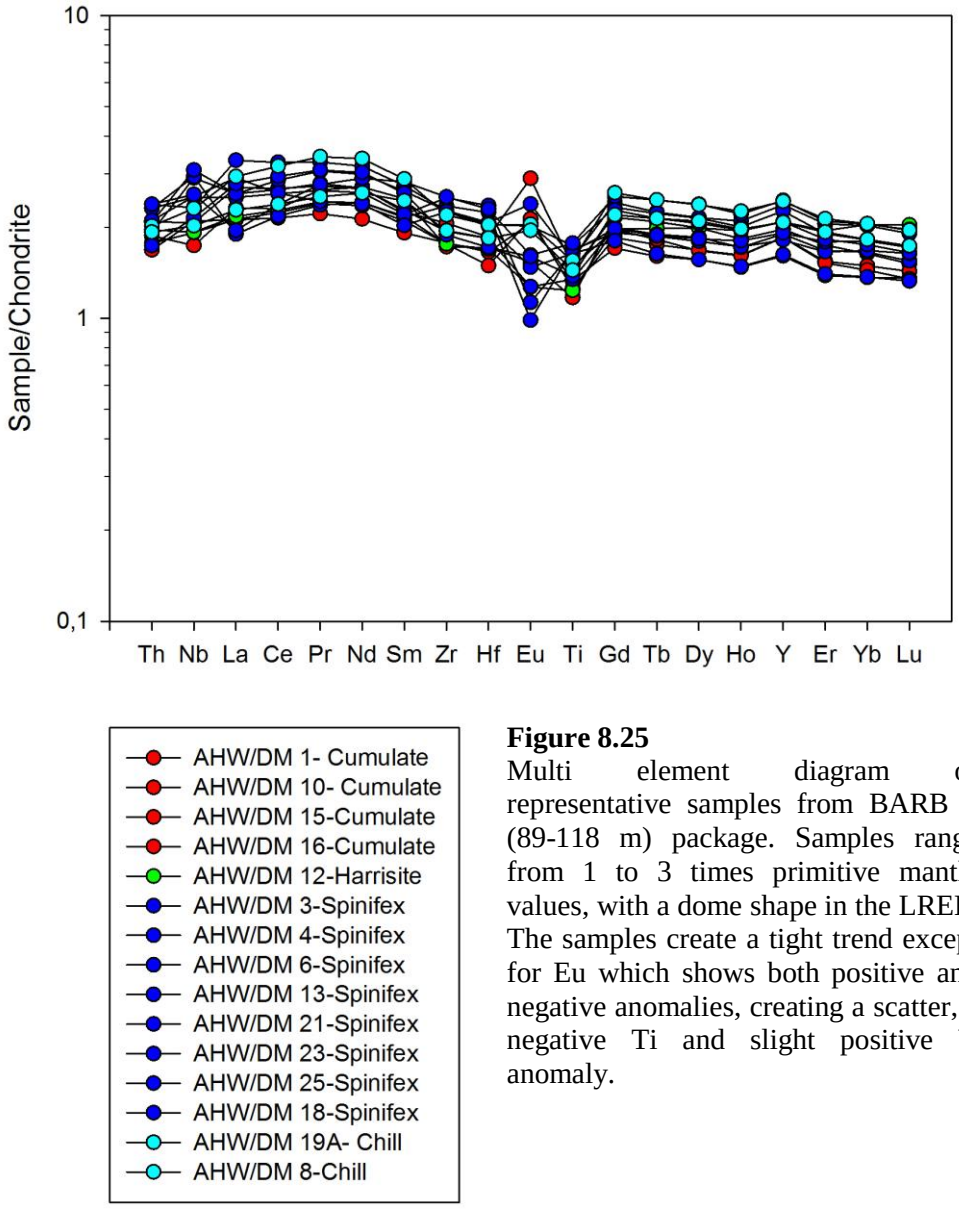

Figure 8.25
Multi element diagram of representative samples from BARB 1 (89-118 m) package. Samples range from 1 to 3 times primitive mantle values, with a dome shape in the LREE. The samples create a tight trend except for Eu which shows both positive and negative anomalies, creating a scatter, a negative Ti and slight positive Y anomaly.

8.6.3 BARB 1 (378-420 m) Differentiated Komatiites

The BARB 1 (378-420 m) differentiated komatiite package has 20 ICP-MS samples. 18 of the samples are cumulates and spinifex. There is also a single chill and a single vesicle rich sample, which were analysed. This package contains small unaltered pyroxene crystals, interstitial to the olivine cumulate, and unaltered pyroxene spinifex.

The REE plots of the BARB 1 (378-420 m) komatiite flows show a slight dome shape between La and Sm, which is supported by $(La/Sm)_N$ of 0.60 to 1.09 with an average of 0.88. The dome shape reaches its peak at Nd. The HREE show a gently sloping pattern from Gd to Lu, with $(Gd/Lu)_N$ values ranging from 1.09 to 1.39 with an average of 1.25. The samples are 2 to 9 times chondrite values and plot in a parallel fashion creating a tight trend. The cumulates are found in the lower portion of the graph, while the spinifex samples define the top boundary of the data range. The chill is found mid-way between the spinifex and cumulates, as expected from the variation diagrams and the vesicle rich sample is situated at lower concentrations with the cumulates. The data has minimal scatter apart from Eu. The Eu anomaly is both negative and positive. The negative anomaly is associated with Eu/Eu* values of 0.46 to 0.90 and is found mostly in the spinifex samples. The positive Eu anomalies (1.04 to 2.22) are mostly associated with the cumulate zones and the vesicle rich layer, but the largest positive Eu anomaly belongs to a spinifex sample (Figure 8.26). These anomalies are associated with alteration.

The BARB 1 (378-420 m) package has the similar dome shape present from Th to Hf (Figure 8.27). An anomaly occurs at Eu, and from Gd to Lu there is an almost flat trend as revealed by slightly lower $(Gd/Yb)_N$ values in Figure 8.21. These samples have flatter patterns than the other komatiites, as revealed by slightly lower La/Sm and Gd/Yb ratios (Figure 8.21) The data ranges from 0.4 to 4 times primitive mantle values and are well constrained, with the exception of two samples which produce scatter. The first is a cumulate, which contains a large amount of Nb and the second is a spinifex sample, which contains the large Eu anomaly.

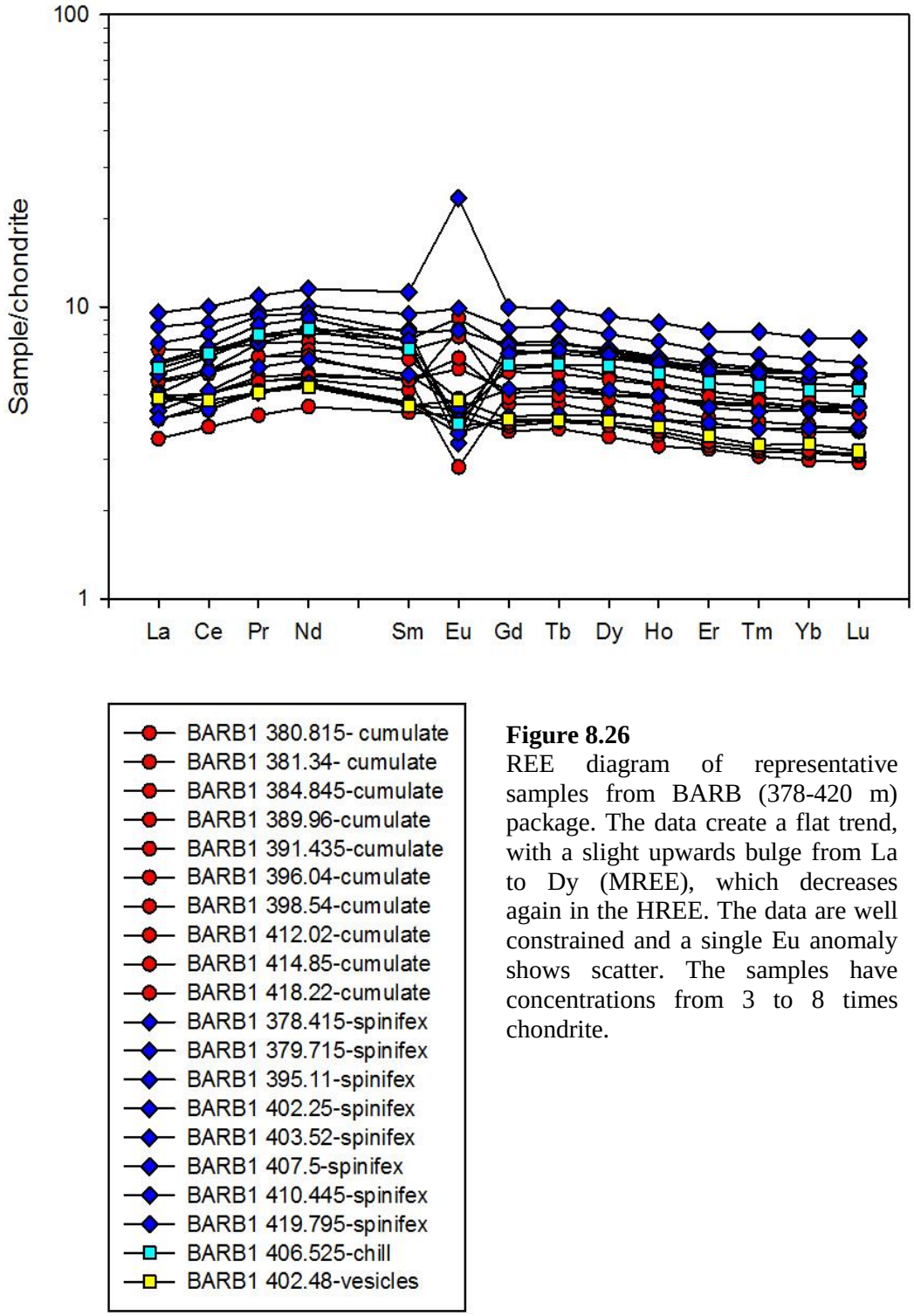

Figure 8.26
REE diagram of representative samples from BARB (378-420 m) package. The data create a flat trend, with a slight upwards bulge from La to Dy (MREE), which decreases again in the HREE. The data are well constrained and a single Eu anomaly shows scatter. The samples have concentrations from 3 to 8 times chondrite.

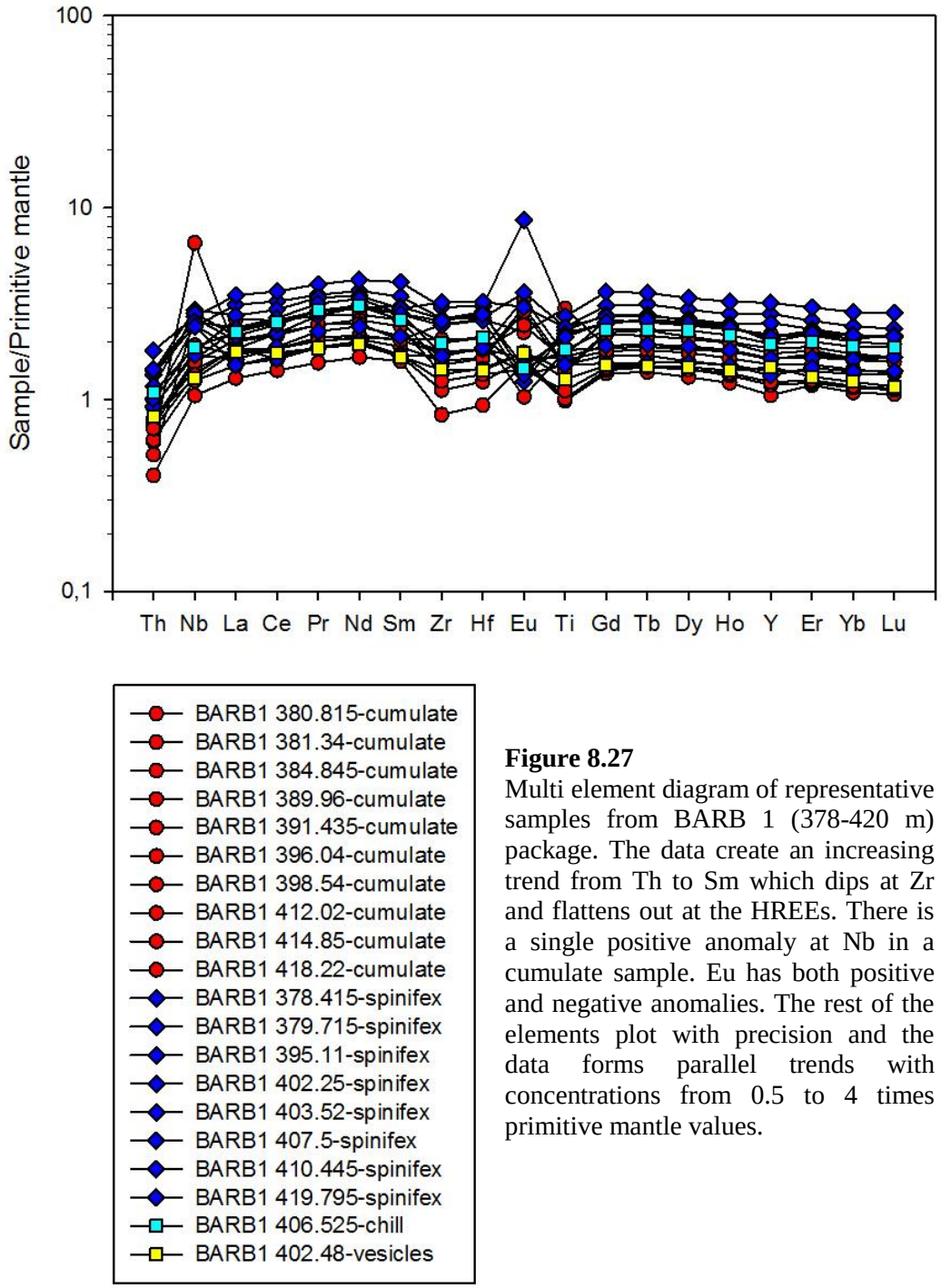

Figure 8.27
Multi element diagram of representative samples from BARB 1 (378-420 m) package. The data create an increasing trend from Th to Sm which dips at Zr and flattens out at the HREEs. There is a single positive anomaly at Nb in a cumulate sample. Eu has both positive and negative anomalies. The rest of the elements plot with precision and the data forms parallel trends with concentrations from 0.5 to 4 times primitive mantle values.

8.6.4 BARB 2 (252-274 m) Differentiated Komatiites

The BARB 2 (252-274 m) differentiated komatiite package has 20 ICP-MS samples taken from cumulate, spinifex and chill zones. This package contains small unaltered pyroxene crystals between the altered olivine cumulate and fresh pyroxene spinifex blades between the altered olivine spinifex blades.

The REE pattern from the BARB 2 (252-274 m) (Figure 8.28) package has an increasing slope from La to Sm, seen by the $(La/Sm)_N$ ratio of 0.73 to 1.23, with an average value of 0.89. The maximum point is at Nd. The HREE show a gentle decreasing slope from Gd to Lu, as seen in $(Gd/Lu)_N$ values from 0.92 to 1.49, with an average of 1.23. The samples plot in a well constrained pattern with concentrations ranging from 1.5 to 8 times chondrite values and there is a slight increase in the LREE. A positive and negative anomaly occurs at Eu, where the cumulates are associated with a positive anomaly (Eu/Eu*) = 1.71 to 2.43 and the spinifex and chill zone samples have (Eu/Eu*) values ranging from 0.37 to 0.98, with two chill zone samples reaching 1.1. There is minimal scatter in the other elements and they create well constrained plots.

In the multi-element plot of the BARB2 (252-274 m) package the shape of the graph increases from Th to Sm (Figure 8.29), it dips slightly at Zr and starts gradually decreasing from Hf to Lu (Figure 8.21). The samples range from 0.4 to 3 times primitive mantle values. A small spike in concentration occurs at Nb in half the samples. A minor negative anomaly occurs at Zr and a small positive anomaly at Ti, which is almost unnoticeable. The cumulates are grouped in the lower portion of the plot, the spinifex samples are grouped in the upper portion of the graph and the chill zone samples have a range of values. The two chill zone samples that plot within the cumulates are the same two that have high MgO content and are shown to be micro cumulates rather than true chill margins.

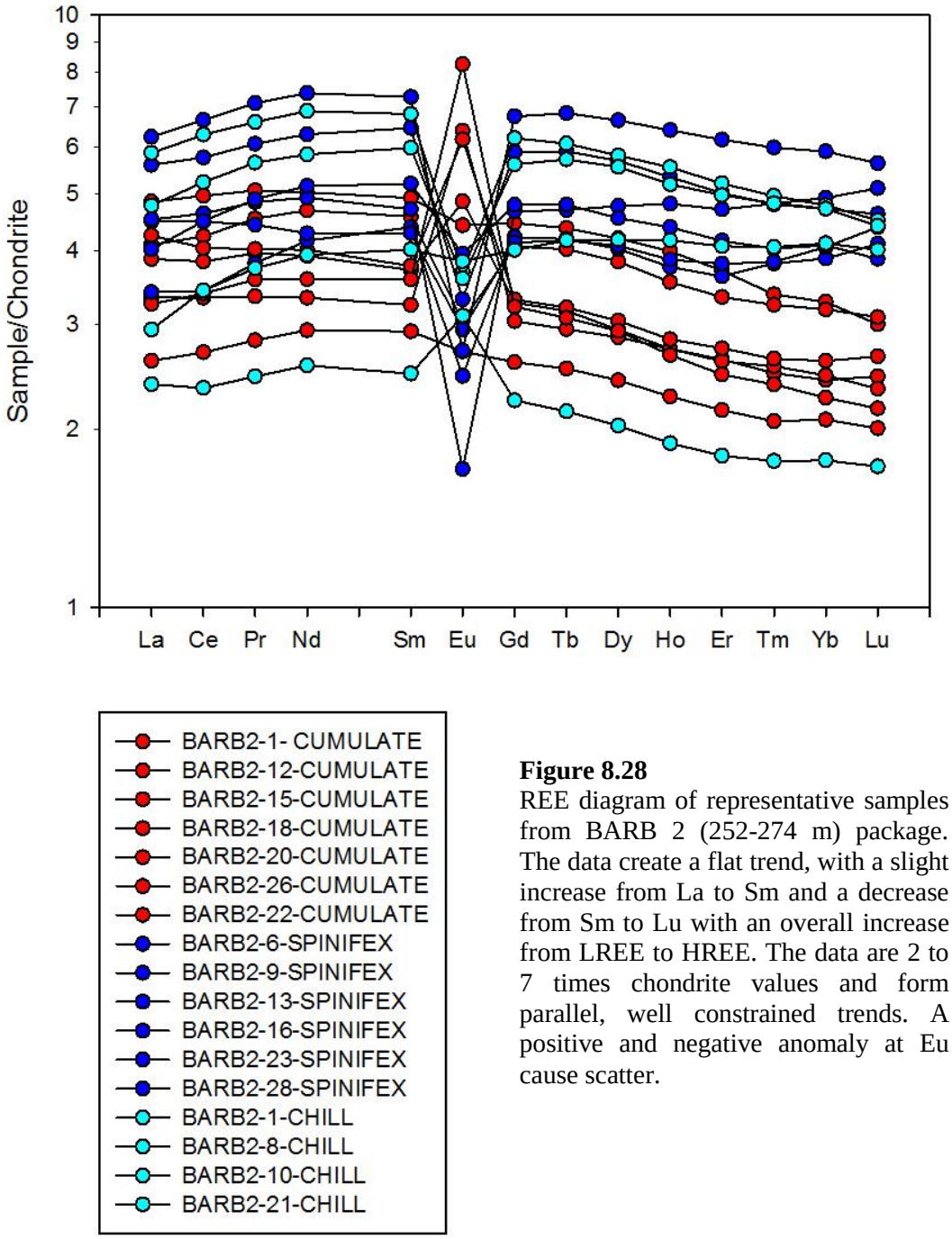

Figure 8.28
REE diagram of representative samples from BARB 2 (252-274 m) package. The data create a flat trend, with a slight increase from La to Sm and a decrease from Sm to Lu with an overall increase from LREE to HREE. The data are 2 to 7 times chondrite values and form parallel, well constrained trends. A positive and negative anomaly at Eu cause scatter.

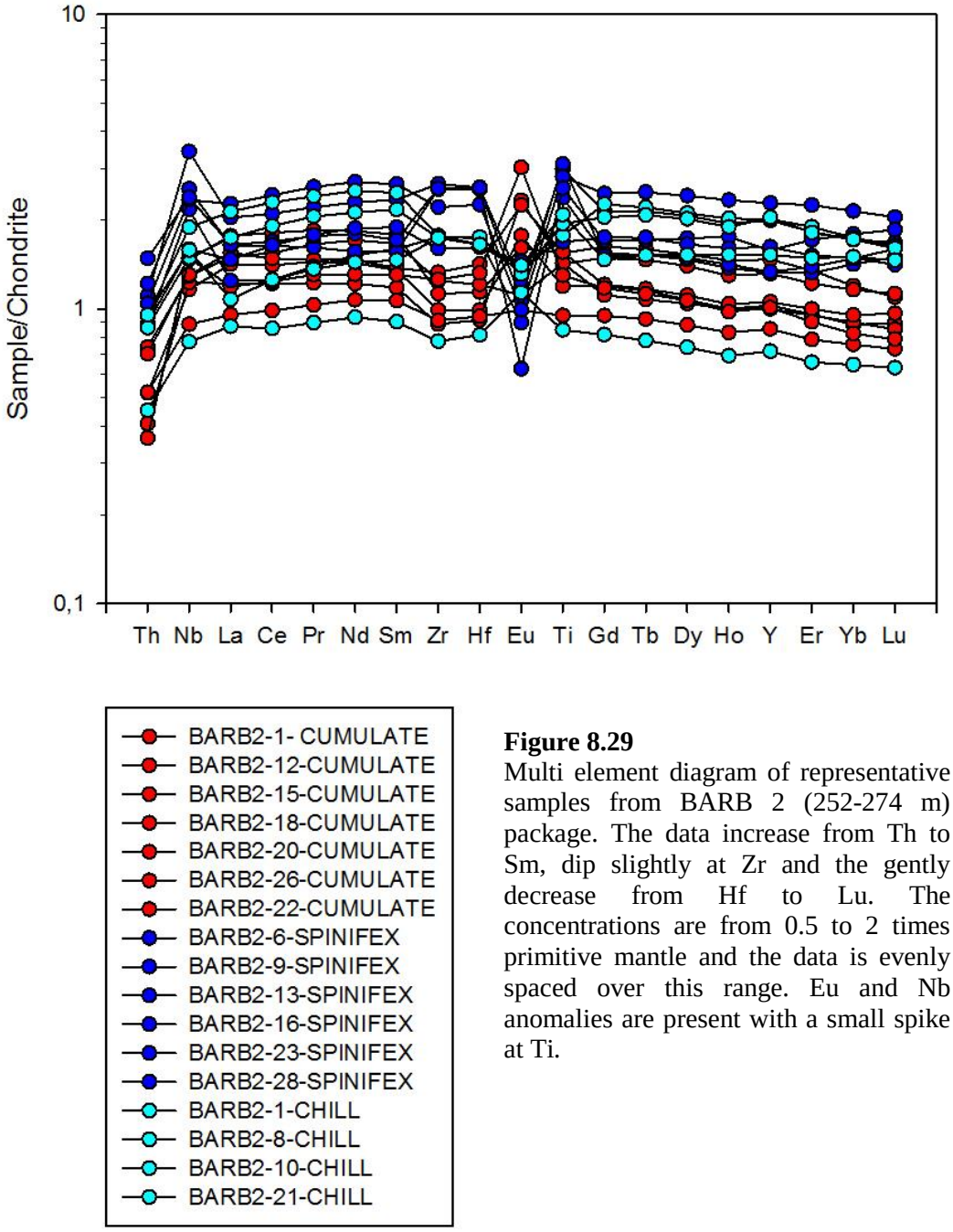

Figure 8.29
Multi element diagram of representative samples from BARB 2 (252-274 m) package. The data increase from Th to Sm, dip slightly at Zr and the gently decrease from Hf to Lu. The concentrations are from 0.5 to 2 times primitive mantle and the data is evenly spaced over this range. Eu and Nb anomalies are present with a small spike at Ti.

8.7 Summary and Discussion

8.7.1 Element vs. Depth Plots

It is evident from the large scale trends seen in the depth vs. element graphs of BARB 1 and BARB 2 that certain elements behave in a similar manner. For example MgO and FeO commonly have similar patterns, whilst SiO_2 has the mirror image trend to MgO. The tumulus unit and the differentiated komatiite packages at (89-118 m) and at (378-420 m) in BARB 1 have generally higher MgO contents than the rest of the core. The rocks between the differentiated packages are predominantly komatiitic basalt, basalt and gabbro with minor massive komatiites and no visible cumulate or spinifex textures. These are associated with a lower MgO content than the tumulus and the differentiated komatiite flows. Due to the alternating nature of rock-types and large sampling intervals in BARB 2, no large scale trends are evident.

Since the base of the tumulus is composed of olivine cumulate, it is expected to be the most magnesian. The hyaloclastite represents the chill margin of the tumulus unit and therefore should correspond to the original liquid composition. The pyroxenite/gabbro layers are the last to crystallize from the most evolved magma. The trends clearly indicate the partitioning of some elements into the cumulates and others into the later crystallized pyroxene spinifex and pyroxenite/gabbro.

The BARB 1 (89-118 m) differentiated komatiite package shows no evolutionary trend in chemistry. As in the tumulus, the changes are created by element partitioning into olivine crystals of the cumulate, or the melt, which later formed the spinifex. The basalt sample has a very different chemistry, which is clearly visible in the plots. This basalt sample is a later intrusion into the rocks and should not be incorporated or accounted for in terms of magma source composition.

The BARB 1 (378-420 m) set shows a slight trend with depth. The MgO and Ni content increases, whilst SiO_2, Al_2O_3, TiO_2, Zr, Cr, Y, V and Sc decrease with stratigraphic height. Thus this increasing trend in MgO indicates that the rocks lower in stratigraphy have lower MgO content and rocks higher in stratigraphy have a higher MgO content. This is opposite to what is found in a conventional magma package, where the lower flows are expected to have the highest MgO content, and as the source differentiated, the MgO content decreases in the overlying flows. This inversion of the MgO fractionation trend could be explained by

continuous renewal of magma source by magma, which is consistently more MgO rich than the previous source.

BARB 2 (252-274 m) differentiated komatiites show no general trend. However, on the smaller scale there appears to be a sinusoidal trend. The MgO and Ni have a mirror image pattern of Al_2O_3, TiO_2, Cr, Zr, Y, V and Sc. SiO_2 has a completely irregular pattern, which most likely indicates mobility of SiO_2 within this suite of samples. The sinusoidal trend indicates a replenishment of MgO in the source of the magma half way up the package. Alternatively it could indicate magmas originating from a different source.

8.7.2 Major and Trace Element Chemistry

The tumulus has a Fo_{92-93} control on crystallization, which is observed in the MgO vs. FeO, Al_2O_3 and TiO_2 variation diagrams and corresponds to MgO intercepts of 50-52 %. The variation diagrams of MgO vs. incompatible elements have good negative, linear correlations where there is an evident trend from the cumulates, through the harrisite to the spinifex and ending with the gabbro and pyroxenite layer, which is the most evolved. The hyaloclastite lies midway between the cumulates and the gabbro and pyroxenite layer, as expected for the liquid composition. The cumulates themselves create a different trend, which runs parallel to the forsterite line and has an MgO 48 % intercept. Multiple injections of magma would have replenished the melt within the tumulus. This would have caused the olivine cumulate pile to have a very constant primitive olivine composition and consistent ratios of MgO and FeO. Moreover, the mobility of FeO, which is seen in the FeO vs. depth plot and the reduced FeO content in the cumulates, can be explained by means of alteration. The pyroxenite layer is not enriched in Sc, indicating that it is chemically related to the tumulus unit and not a pyroxene cumulate from a later intrusion. Immobile trace elements in the tumulus show the fractionation process from olivine cumulates, (1-2 sample/chondrite), through the harrisite and pyroxene spinifex (2-9 sample/ chondrite), to the gabbro and pyroxenite layer, which has the highest values (9-11 sample/chondrite). The hyaloclastite has concentrations in the middle of the range (3-7). The chilled fragments of the hyaloclastite are the best representative for the original liquid composition. The surrounding glass shard matrix has MgO >30 %, which it has acquired during alteration.

The BARB 1 (89-118 m) differentiated package shows good correlation between MgO and the immobile elements, all of which have a lower than expected MgO intercept of 40 %. This

indicates a dual, olivine and orthopyroxene, control on crystallization (Fo_{91}, ca. 33 % and En_{92}, ca. 67 %). The two cumulate phases are evident in thin sections taken from two flows within this package. The presence of orthopyroxene typically creates a distinct geochemical signature in Cr and Ni, which is evident in the MgO vs. Cr graph. A possible explanation of the reduced MgO arises from the tumulus, which directly underlies this package and may have depleted the magma source of MgO, which subsequently fed the overlying flows. REE plots show LREE enrichment and anomalies occur at Eu (+ and -), Ti (small -) and Y (+).

BARB 1 (378-420 m) and BARB 2 (252-274 m) packages have very similar chemical trends. The immobile elements have good correlations with MgO intercepts 50-52 % associated with Fo_{92-93} control lines (Table 8.1). These packages have similar multi-element diagrams with slight LREE enrichment that creates a dome shape and a decreasing HREE pattern. In both of these packages the elements form tight trends with the cumulates plotting at lower concentrations and the more evolved spinifex samples plotting at the higher concentrations. Anomalies occur at Eu (+ and -), Zr (small neg), Ti (small + and -).

Comparing the REE diagrams to previous studies, the trends are similar, with slight LREE enrichment and concentrations ranging between 1 and 10 times chondrite values. In previous studies there was no Eu anomaly, but in the BARB 1 and BARB 2 differentiated komatiite packages, there are distinct Eu anomalies. In some layers, the type of anomaly is linked with the rock type and in other packages the anomaly is random. This Eu anomaly is attributed to alteration since there is no plagioclase present within komatiite rocks.

8.8 Conclusions

The four detailed sections analysed geochemically have different physical features, the tumulus being 90 m thick and the komatiite flows only 5 m thick. However, apart from the physical differences, the chemistry of each section proves to be very similar. The process of crystal fractionation and the concentration of incompatible elements in the melt is evident in the tumulus, BARB 1 (378-420 m), BARB 2 (252-274 m), and slightly less so in BARB 1 (89-118 m). These effects are seen in the element vs. depth graphs, the variation diagrams and in the multi element diagrams. The major element chemistry is similar in three sections, with Fo_{93} control over the tumulus, BARB 1 (378-420 m) and BARB 2 (252-274 m) packages. The BARB 1 (89-118 m) package, however, shows evidence of co-crystallization of orthopyroxene with olivine as observed by two cumulate phases seen in thin section. The

REE and multi element trends are characterized by a shallow dome shape in the LREE, with a maximum around Nd and depleted HREE. The BARB 1 (89-118 m) package is an exception as it contains a slightly larger LREE enrichment than the others. This together with the dual olivine-pyroxene control, could indicate a slight different liquid magma composition for the BARB 1 (89-118 m) package.

CHAPTER 9

A COMPARISON BETWEEN THE TUMULUS UNIT AND THE DIFFERENTIATED FLOWS

9.1 Introduction

The tumulus unit of the Komati Formation was identified by Dann (2000) as an inflation feature in the upper crust of a lava tube. The tumulus has been described in terms of physical appearance, texture and basic mineralogy by Dann (2000) and Dan (2001) but few geochemical studies have been carried out on the unit. de Wit *et al.* (1987) are noted to have analysed samples from the tumulus unit.

Due to the continuity of the core, and relative freshness of the samples, the ICDP BARB `1 core produced the best opportunity to sample the tumulus geochemically. A further benefit of the BARB 1 drill core is that it introduces a third dimension to the tumulus, allowing a better understanding of the shape and internal features. Finally, the core sampled the parts of the unit that do not crop out at the surface. A detailed comparison between the tumulus and the flows will give insight into the processes that formed the tumulus and possibly give information on the origin of the tumulus lava.

9.2 The Tumulus Unit

9.2.1 Comparison of the Tumulus in the Core to Surface Geology from Previous Mapping

The BARB 1 core allows a comparison to be made between the surface features mapped by Dann (2001) and features in the core taken through the tumulus unit. Figure 7.28 illustrates the major similarities and differences between the surface map and the BARB 1 core.

Using the 48° inclination of the borehole and the surface map of Dann (2001) it is possible to predict the thicknesses of the corresponding textural units found in the core. The predicted core length can be compared to the actual length of the unit in the core and any discrepancies can give information on the shape of the tumulus feature and the continuity of the textural zones. Table 9.1 summarizes the surface length, the predicted length in the core and the actual length of the textural zone in the core. The BARB 1 drill core is situated on the side of the tumulus and did not intersect the thickest portion of the tumulus (the surface section). This most likely indicates that the plunge of the tumulus axis is not vertical.

Textural zone on surface	Surface map (m)	Predicted length in core (m)	Actual length in core (m)	Textural zone in the core
Olivine cumulates	15	22	15	Olivine cumulate
Olivine spinifex	25	37	31	Harrisite, Pyroxene spinifex and Gabbro-Pyroxenite layer
Vesicular Komatiite	17	25	20	Hyaloclastite

Table 9.1: Summary of the length of textural zones on the surface with predicted length for the core and actual length measured in the core.

There is reasonably good agreement between the predicted lengths of the textural zones and the true lengths as measured in the core. Discrepancies are less than 6 m thick and these can be attributed to variably in the lens shape of the tumulus, contact surface irregularities and undulations.

The olivine cumulate layer described by Dann (2000) corresponds to the core both in thickness and in mineralogical description. The core gives further insight into the ellipsoidal crystals, which are aligned in certain horizons and represent the base of upward-fining sequences. The zone of olivine spinifex in the surface section corresponds to the harrisite, pyroxene spinifex and gabbro-pyroxenite layers observed in the core. Since the surface outcrop is poor it is probable that the 3.8 m thick gabbro-pyroxenite layer is not exposed. The surface and core sections both contain skeletal and bladed textures indicating that they are texturally the same. The core provides less altered material and a more detailed section and thereby separates the olivine spinifex unit into a lower skeletal olivine harrisite,which is described by Dann (2001) as a crescumulate; and an upper pyroxene spinifex. The "vesicular komatiite" in surface outcrops corresponds to the hyaloclastite unit in thickness but does not correspond in terms of texture and mineralogy. The vesicular komatiite commonly contains abundant vesicles (20 %) in an olivine-rich host rock. The hyaloclastite consists mainly of fine grained material containing few vesicles (< 2 %) in the chill margin fragments and a glass shard matrix that has no vesicles. A single exception in the hyaloclastite is sample GC 31, which has the same characteristics as the vesicular komatiite described by Dann (2001) and is seen in surface samples taken during this project. The presence of 'curved bubble walls and angular fragments" is noted by Dann (2001, p 427). This is a similar description to the glass shard matrix and chill fragments of the hyaloclastite unit as observed in the core. It is possible that the non-vesicular hyaloclastite outcrops poorly, or that the section of the unit sampled by the core was less vesicular than the central part (surface section).

The relatively minor discrepancies in thickness and unit types between the surface and the core observations can be explained by considering the possible shape of the tumulus and the processes that occurred. The surface section represents the thickest part of the tumulus (as identified by Dann 2000), while the core section represents the flank of the tumulus bulge. It is expected that the vesicles will gather in the thickest section of the tumulus, since it has the highest relative relief. Therefore it would have been the ideal zone for migrating vesicles to accumulate. Conversely the flanks of the tumulus would not have had as thick a layer of vesicles because the vesicles that formed on the flanks would have migrated upwards to create a thicker vesicular zone at the highest part of the tumulus (Figure 9.1).

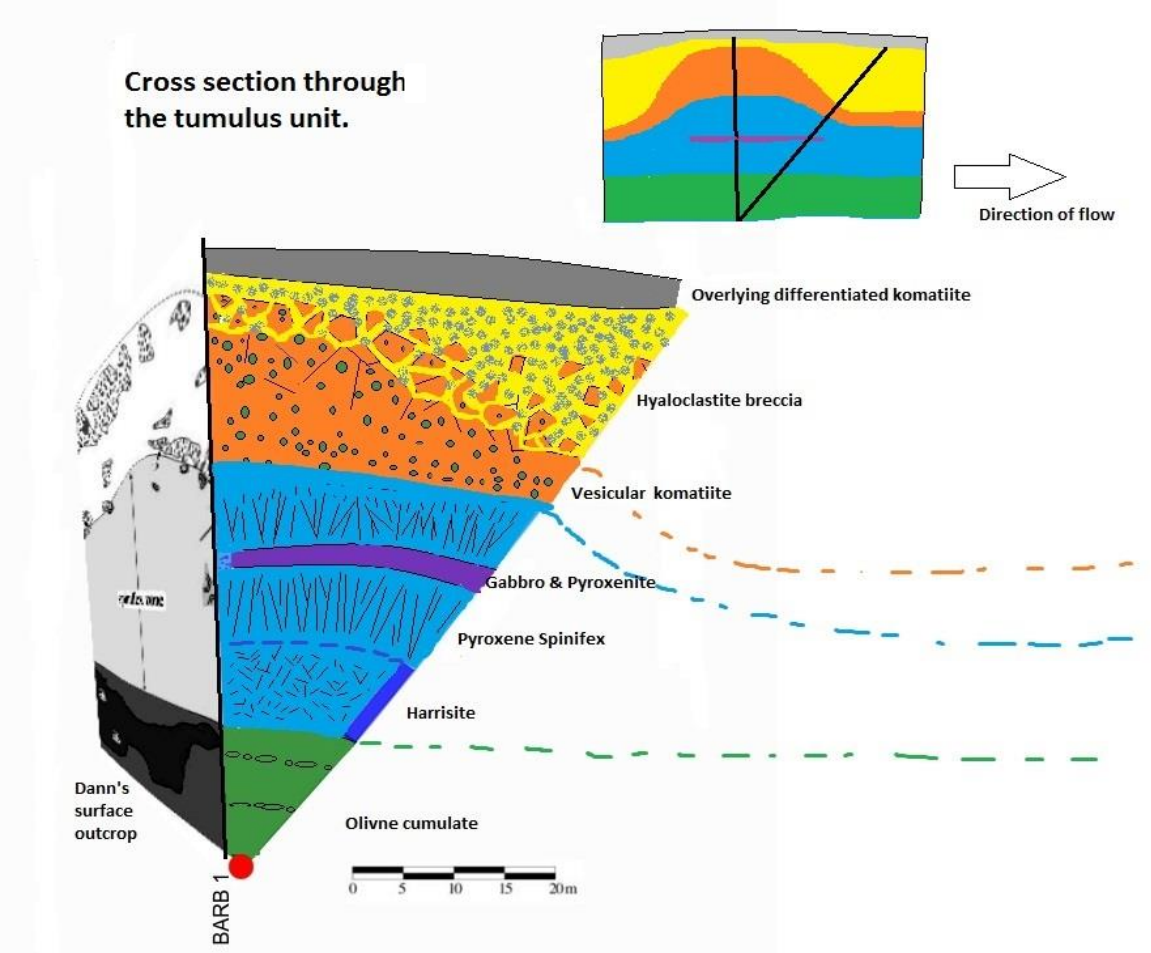

Figure 9.1
Schematic cross section of the tumulus unit perpendicular to flow direction. The textural sections of the surface map correspond to the textural zones of the core.

9.2.2 Formation of the Tumulus Unit

Anderson *et al.* (2012), in their study on tumuli formation, indicate that the cooling rate and the effusion rate are the major controlling factors in tumuli formations and need to be ideal in order to create a tumulus structure. Too-rapid cooling would have solidified the rocks and prevented the upper crust from bulging and bending outwards. Similarly, an effusion rate that was too high, the crust would not have contained the volume of magma and breakout structures would have occurred. These two processes, operating in the correct proportions, could have created localised stress, which caused the upward bulging of the roof of the lava tube. The formation of a tumulus requires the inner crust to have visco-plastic rheology in order to accommodate the pressure of the underlying magma. Once solidified the crust is tilted, rotated and cracked to form blocks (Kauahikaua *et al.*, 1998). In current-day situations this localized stress often occurs where the lava channel changes flow direction (Anderson, 2012).

inflation of the crust to form the tumulus requires that the inner part of it was still in the zone of viscoplastic rheology - i.e it behaves like a rubber skin and stretches to accommodate the hydrostatic pressure of the magma underneath it. Solidified crust above the viscoplastic layer gets tilted and cracked to form the characteristic "breadcrust" tumulus cleft. Check out the Kauahikaua et al paper on Kilauea flows.

Arndt *et al.* (2008) identified tumuli on Gilmour Island and indicated that the channels containing tumuli also contained evidence of repeated magma injections. Dann (2001) indicated that thickening of the tumulus in the Komati Formation was caused by repeated magma inflation. The tumulus began as a lava tube that contained suspended cumulus crystals, which settled out as the vesicles accumulated beneath the upper crust. Further magma influx caused the upwards and outwards bending of the upper crust to create the dome shape and additional fracturing and fragmenting of the hyaloclastite. The interior of the tumulus crystalized to form skeletal olivines and spinifex textures and finally coarse-grained gabbro.

The most likely conditions for tumulus formation are temperature and effusion rates suitable to create a viscoelastic crust that would bend but not allow breakouts during multiple injections. The upper crust would eventually bulge outwards to form the dome shape of the tumulus. This resulted in solidification of the tumulus as a closed environment allowing differentiation of the magma and the crystallization of the observed late-stage gabbro layer.

9.2.3 Why is the Cumulus Olivine Crystals Larger than in Other Komatiites?

The olivine cumulate crystals in the tumulus are much larger (up to 15 mm) than the commonly encountered 0.5 mm cumulus grains in the differentiated flows. The large size of the grains could imply further growth after settling, which is consistent with the noted lack of matrix and the formation process of adcumulates. Alternatively, the crystals may have grown to the full size in a sub-chamber and then became melted or slightly corroded along the edges as they settled out through the magma after eruption. The lack of matrix can be attributed to the accumulation of these enlarged olivine grains. The greater the number of crystals that settled, the higher the mass would have been in the overlying layers and the greater the compaction that would have occurred at the lower levels, which caused the residual melt to be squeezed out.

9.2.4 What Does the Presence of Harrisite Indicate?

Harrisite is a skeletal form of olivine that was identified in the Rum intrusion by Donaldson (1974). In the Rum intrusion the occurrence of harrisite is attributed to the growth of olivine in a supersaturated magma with the presence of water, commonly at the cumulate-magma boundary. Donaldson (1982) noted the formation of harrisite lenses within a cumulate mush, due to upward percolation and collection of melt residue in the cumulate layer.

Features similar to the Rum intrusion are present in the tumulus but on a smaller scale. The main harrisite layer occurs between the cumulate and spinifex layers, but an 80 cm thick harrisite lens is present within the upper section of the cumulate layer. In both instances the harrisite grew in an upward direction from the pre-existing olivine cumulates into a supersaturated magma. The formation of harrisite requires a tranquil cooling environment, indicating that the lava channel became dormant to form the harrisite, which would eventually solidify completely without re-inflation or reinjection of any new magma. The 80 cm-thick lens also supports the theory of compaction in the cumulates, which causes upward percolation of the melt and thus closer packing of the cumulate crystals to form an adcumulate. The presence of the lens or pod indicates upward movement of melt and also the trapping of this melt at an impermeable boundary within the cumulate zone. Therefore the escape of melt via compression from overlying crystals is confirmed by the presence of a harrisite lens, which requires this melt migration to have been operative. Alternative explanation of the skeletal texture is an intrusive spinifex dyke as described by Houle *et al.* (2009).

9.2.5 Hyaloclastite: Depositional Environment, Textures and Chemistry

Hyaloclastite breccias form when lava is intruded into water. They can form a variety of different fracture patterns, from jigsaw blocks that are separated by small amount of matrix, to large boulders that have been reworked into a volcaniclastic breccia (McPhie, 1993). Further information can be gleaned about the environment of deposition by observing the material that fills in the space between the brecciated magma.

The tumulus in BARB 1 has a 20 m thick hyaloclastite carapace, which is formed from quench fragmentation as the lava erupted into an aqueous environment. Further fracturing and brecciation occurred during the inflation phases of the tumulus. Various authors note the deposition of the Komati Formation in a marine environment (Arndt *et al.*, 2008, Chavagnac, 2004, Dann, 2001, de Wit *et al.*, 1987, Viljoen & Viljoen, 1969) and the hyaloclastite further confirms the aqueous eruptive setting. The material between the brecciated fragments is a glass shard matrix. This consists of irregular to rounded, fine-grained, zoned, 1-5 mm sized fragments, which illustrate the lack of sedimentation and minimal reworking of the hyaloclastite.

Using textures and chemistry, it is possible to compare the chilled lava fragments to the glass shard matrix surrounding and supporting the fragments. As discussed previously, the chill fragments are fine- grained and contain a small proportion of vesicles, except for two distinct horizons that are vesicle-rich. The chill fragments contain 27-30 % MgO, which is close to the maximum value inferred for komatiite liquids. In contrast the matrix supporting the fragments is fine grained and consists of irregular to rounded glass shards, which have no vesicles and are altered to magnesite. The MgO contents of the glass shard matrix range from 30-35 %. This is significantly higher than that of the chill fragments. From a comparison of the chilled fragments and the glass shard matrix to the chill margins of differentiated komatiite flows (Figure 8.18), it is evident that the composition of the chilled fragments is similar to that of the chill margins of thinner komatiite flows. Therefore the chilled fragments are a better estimate of liquid composition. The high MgO content of the glass shard matrix is attributed to an increase in MgO during alteration, which preferentially affected the glassy material. This has been noted previously by de Wit *et al.* (1987).

9.3 Comparison of the Tumulus to Differentiated Komatiite Flows

9.3.1 Physical and Textural Features of the Tumulus and Differentiated Flows

The tumulus unit (90 m thick) consists of five major sections: basal cumulates, harrisite, pyroxene spinifex, pyroxenite-gabbro layer (within the pyroxene spinifex) and a hyaloclastite layer at the top. The differentiated komatiite flows (0.5 to 4 m thick) consist of three major sections: basal cumulate and a spinifex zone, which is capped by a chill margin.

The cumulate zone of the tumulus consists of tightly packed olivine cumulate grains. At certain stratigraphic horizons, these cumulus grains reach 2 cm in length. They are ellipse-shaped and aligned in layers with progressively smaller and more rounded cumulate crystals overlying them. This creates repeated cycles of upward-fining sequences. Overlying the cumulate is a harrisite layer, which is similar in structure to an olivine spinifex but consists of less elongated and more complex crystals than typical bladed spinifex. The skeletal olivine crystals are white in colour, possibly due to alteration. They are surrounded by pockets of black melt residue. The harrisite layer grades into a pyroxene spinifex layer. These pyroxene blades are randomly oriented, aligned and reach lengths of up to 20 cm. A gabbro and pyroxenite layer is present within the pyroxene spinifex layer. This is associated with final stage crystallization of the tumulus. The tumulus is capped by a 20 m thick hyaloclastite. This layer consists of brecciated chilled magma surrounded by a matrix of small glassy shards.

The cumulate part of the differentiated flows consists of fine grained (0.5 mm) euhedral olivine crystals that create a homogeneous texture to the cumulate zone. The olivine spinifex can be randomly oriented or aligned and reach a maximum length of 5 cm. The olivine spinifex is a light grey colour surrounded by a black melt residue. Chill margins are present as fine grained zones and occasionally contain contact breccia. These contacts are between 3 and 10 cm wide and the breccia is filled in by magnesite.

When comparing the tumulus to the differentiated komatiite flows, certain patterns are evident. The tumulus is thicker (90 m) than the differentiated flows (0.5 to 4 m) and therefore has correspondingly larger crystals and textural features. The olivine cumulate and the spinifex zones of the tumulus are larger than the corresponding zones in the differentiated komatiites. The chill zones of the differentiated flows are a much smaller proportion of the flows (0-40 cm), while the hyaloclastite is a large component of the tumulus (20 m thick). Finally and most significantly, the tumulus contains two additional textural zones: the

harrisite and the pyroxenite-gabbro layer. The harrisite can be likened to the olivine spinifex zones, because both have skeletal forms of olivine. However, the harrisite grew upwards from a cumulate layer into a super cooled magma, while the spinifex grew downwards from the chill margin due to a temperature gradient, indicating slightly different growth processes. The pyroxenite and gabbro layer is attributed to the thickness of the flow, which allowed the magma enough time to differentiate and evolve to more silica-rich compositions. The komatiite flows are too thin to have been formed in the same manner, and reached the solidus during spinifex crystallization. Therefore, the sheer size of the tumulus allowed the larger textures to form, whilst the differentiated flows of limited size have smaller sized crystals and textures.

9.3.2 Mineralogical Features of the Tumulus and Differentiate Flows

A detailed presentation of the mineralogy has been given in chapter 7- Petrography and Appendix B. The major primary minerals present are olivine, pyroxene and chromite, and plagioclase in the gabbro, with the contained melt having crystalized in interstitial pockets within the rock. These minerals are altered to greenschist mineral assemblages including tremolite, epidote, serpentine and chlorite.

The olivine adcumulates of the tumulus reach up to 15 mm in length, are rounded to ellipsoidal shape in certain zones and are tightly packed with minimal matrix surrounding them (Figure 7.1). Opaque minerals (mainly magnetite) are associated with the olivine crystal boundaries and fractures within the olivine grains. Crystals in the cumulates from the differentiated komatiite flows are 0.5 – 1 mm in size, euhedral and well surrounded by melt residue. The differentiated komatiite flows contain orthocumulates, in some cases with pyroxene oikocrysts instead of melt residue. In the BARB 2 (252-274 m) package the pyroxenes constitute a poikilitic texture but the magma solidified before the complete formation of pyroxene oikocrysts. In the BARB 1 (89-118 m) flow at 104.77 m (sample AHW/DM/9), there is the unusual occurrence of two cumulate phases, in which both olivine and pyroxene cumulus minerals are present and are surrounded by melt residue.

The tumulus spinifex is composed of pyroxene needles that form in discrete bundles. They are twinned and have chlorite reaction rims surrounding tremolite, and sometimes augite cores. The pyroxene spinifex is supported by a fine grained matrix, which contains fibres of inter-grown chlorite and tremolite (Figure 7.6). The spinifex of the differentiated komatiite

flows consist of olivine blades that form parallel or radiating growth patterns (Figure 7.16). These in turn are filled-in by smaller (up to 1 cm), well-formed pyroxene needles that grew perpendicular to the olivine blades. Between the pyroxene blades are radiating growths of acicular pyroxene (up to 3 mm). The spinifex zones of the tumulus and differentiated komatiite flows are different in that the tumulus contains pyroxene spinifex, whereas the differentiated flows contain olivine spinifex.

The chill margins of the differentiated komatiite flows are fine grained and contain micro-textures representing the part of the flow they grade into. Therefore micro-spinifex is associated with the spinifex zones and the chill represents the upper contact of the flows. The opposite case is observed with the micro-olivine cumulates in the chill zone (Figure 7.21). The hyaloclastite zone of the tumulus contains chilled magma, which is fragmented into blocks surrounded by a glass shard matrix. The chilled magma blocks are fine-grained and contain small, sparse vesicles and micro-olivine cumulates. These can be compared to the chill zones of the differentiated komatiite flows. However the glass shard matrix is unique and has no equivalent in the differentiated komatiites (Figure 7.10). As noted previously, the tumulus has extra textural zones: the harrisite and the gabbro-pyroxenite layers.

The harrisite under the microscope shows portions of skeletal olivine crystals, surrounded by a melt residue containing small (<1 mm) crescent shaped pyroxene laths, within a fine grained matrix that is altered to chlorite and tremolite (Figure 7.2). The gabbro and pyroxenite do not have an equivalent texture in the differentiated komatiite flows. They consist of regular shaped pyroxene crystals surrounded by a fine- grained chlorite-tremolite matrix. A single pyroxenite sample contains some partially unaltered plagioclase crystals (Figure 7.4). The gabbro samples are slightly more chloritized, but generally this layer is less altered than the other layers in the tumulus (Figure 7.5). The reduced alteration together with the well-formed grains, indicates a late stage crystallization and possible insulation from alteration.

9.3.3 Geochemistry of the Tumulus and Differentiated Flows

Binary diagrams of the tumulus unit illustrate a Fo_{93} control for olivine in the fractionation process (Figure 8.11). Furthermore the fractionation process is evident in the rock types: the cumulates having the highest MgO contents. The rock types evolved in a linear manner to the harrisite, pyroxene spinifex and finally the gabbro-pyroxenite, which has the lowest MgO

content. The incompatible elements show an inverse trend. As is expected, the hyaloclastite, being the chill equivalent, plots at a mid-point between the cumulates and gabbro. The differentiated komatiite flow packages BARB 1 (378-420 m) and BARB 2 (252-274 m) show a Fo_{93} and a Fo_{94} control over fractionation respectively. The BARB 1 (89-118 m) package shows a combined olivine: pyroxene control in ratio 1:2. These proportions are supported by thin section observations.

The REE patterns of the tumulus are flat and consistent between 1 and 11 times chondrite values. The differentiated komatiite flows have slight LREE enrichment and are well constrained between 2 and 9 times chondrite values. The samples plot in parallel, tight trends with larger positive and negative Eu anomalies than in the tumulus.

The multi-element diagrams give insight into mobilization and the concentration or the depletion of elements. All plots have tight trends. The tumulus unit shows concentrations between 0.3 and 9 times primitive mantle (PM) values, with a flat pattern except for a negative Ti anomaly (Figure 8.23). The differentiated komatiite packages all have similar trends and anomalies (Figure 8.25/27/29). The majority of the element concentrations are between 0.3 and 3 times PM values. BARB 1 (378-420 m) and BARB 2 (252-274 m) packages have almost flat (slight LREE enriched) trends with no distinct anomalies besides the positive and negative Eu anomalies. BARB 1 (89-118 m) has anomalies at positive and negative Eu negative Ti and positive Y.

Geochemically the tumulus has similar features and processes to the BARB 1 (378-420 m) and BARB 2 (252-274 m) packages. The BARB 1 (89-118 m) package shows atypical crystallization processes (dual olivine, pyroxene controls) and high levels of alteration, which is supported by thin section and core log observations.

9.4 Conclusion

The tumulus is a distinct unit found in the base of the Komati Formation. Close inspection of the surface maps together with the ICDP drill core reveals that some aspects of the tumulus are unique, whilst other processes can be compared with the more common and better understood differentiated komatiite flows.

The surface map by Dann (2000) and the ICDP core log of the tumulus correspond well, with the exception of a vesicle- rich horizon present on the surface that is absent in the core. The

tumulus formed through channel inflation, during which the crust remained sufficiently elastic to stretch and bulge rather than freeze and crack. Evidence for inflation is the bulge or dome shape of the tumulus, together with upward fining sequences in the cumulate zone, which are considered to have formed during repeated injection of new magma that brought in larger olivine crystals. Once the channel became inactive, the remaining magma crystalized skeletal structures such as harrisite and pyroxene spinifex and eventually gabbro from a continuously fractionating liquid.

A comparison between the tumulus and the differentiated komatiite flows, may, on the superficial level appear to be inappropriate. The tumulus is thicker (90 m) and the flows only reach 10 m thick. The tumulus contains cumulate, spinifex, harrisite, pyroxenite-gabbro and hyaloclastite layers, while the komatiite flows only have cumulates, spinifex and chill zones. Upon closer textural and mineralogical inspection it is clear that the cumulate, spinifex and chill zones of the flows are similar to the cumulates, harrisite and spinifex and hyaloclastite zones in the tumulus. They contain the same minerals that create similar textures and alter to the same greenschist assemblages. Slight differences are noted in specific flows, such as pyroxene cumulates and pyroxene oikocrysts present in the cumulate zones of the differentiated flows. The harrisite and pyroxene spinifex are not directly comparable to the olivine spinifex of the differentiated flows. Moreover the hyaloclastite is a much larger scale chill feature than the chill zones of the differentiated flows. Finally, the composition of the tumulus is comparable to that of the differentiated komatiite flows and apart from the BARB 1 (89-118m) package, which appears to be extensively altered; the detailed sections correspond well chemically. The tumulus, BARB 1 (378-420 m) and BARB 2 (252-274 m) packages all have an olivine Fo_{93-94} control on crystallization with MgO, Al_2O_3, TiO_2, Ni and Zr appearing to be essentially immobile. The REEs all show slight LREE enrichment in consistent patterns that are 1 to 11 times chondrite values in the tumulus and 2 to 9 times chondrite values for the differentiated komatiite packages.

Therefore the tumulus and the differentiated komatiites have a number of corresponding aspects, such as the composition and mineralogy of different textural zones. The differences between the tumulus and differentiated flows are based on the scale of the features. The tumulus being a larger and thicker flow fractionated until gabbro formed, while the differentiated flows being thinner, solidified during the spinifex crystallization phase. This difference in thickness allowed the extra textures to form in the tumulus that are absent in the flows.

CHAPTER 10

SUMMARY AND INTERPRETATION

10.1 Overview of the Rock-Types Sampled by the BARB 1 and BARB 2 Cores

The BARB 1 and BARB 2 cores, drilled into the Komati Formation, sample over 367 m of continuous strata (700 m core length). Between them they intersect the majority, if not all, of the rock types present in the Komati Formation. The most abundant rock types are massive and differentiated komatiite flows, closely followed by komatiitic basalts and then basalts. The beginning of the BARB 1 core represents the lowest point in stratigraphy, whilst the end of the BARB 2 hole corresponds to the highest point in stratigraphy, because of the overturned strata.

The komatiites present in the BARB 1 and BARB 2 drill cores occur in two distinct textural forms; massive komatiite and differentiated komatiite. The massive komatiites are homogeneous, fine grained, dark green to black in colour and have olivine crystals that are typically < 0.5 mm in size and are often not visible on a hand sample scale. In BARB 1 there are 37 massive flows ranging in thickness from 0.5 to 10 m, whereas in BARB 2 there are no distinct massive komatiite flows. The differentiated komatiites are composed of three textural types (cumulate, spinifex and fine grained chill margin) and are found in packages of five or more differentiated flows. The cumulates are made up of olivine crystals <1 mm in size, which are visible on the hand-sample scale as the olivine crystals are often a darker green than the surrounding melt residue. The olivine spinifex present in the differentiated komatiites range in size and shape depending on the position within the flow. The spinifex close to the chill margin is small <2 mm and randomly oriented. However, toward the centre of the flow the spinifex blades become longer (up to 5 cm) and blades align parallel to each other and perpendicular to the flow boundary. The olivine spinifex blades are medium to light grey in colour and are surrounded by a dark grey to black melt residue. The contacts between the cumulates and the spinifex occasionally contain 1 mm sized spinifex blades aligned parallel to the contact (B1 layer). The chill margins are fine-grained medium-grey in colour and are typically 1-5 cm thick. Occasionally the contact is present as a hyaloclastite breccia created by extrusion of hot lava into a hydrous environment. There are 25 differentiated

komatiite flow units present in BARB 1 and range between 1 and 3 m thick, and in BARB 2 there are 41 differentiated flows that range from 1 to 10 m thick.

The komatiitic basalts, by definition, have slightly higher silica than the komatiites and are spatially associated with komatiites. In the BARB 1 and BARB 2 cores the komatiitic basalts are a medium grey-green colour, fine-grained with minimal olivine crystals visible. The komatiitic basalts have a "felty" or fine-grained speckled texture used to identify them in the field. These flows are homogeneous and show no grain textures, other than veining and white tricuspate features, which are considered to be possible pillow selvages (the material interstitial to pillow lavas). These flows range in thickness from 1 to 23 m thick and are more prominent in the BARB 2 core, where they intersect at a higher stratigraphic level.

The basalt layers are fine-grained, dark-grey with a blue tinge and commonly contain varioles in the middle of the layer. Thin chill margins are associated with the basalts. There are no minerals visible on the hand sample scale and the basalt was not sampled for thin section analysis.

Gabbros are present within the drill core as either the final stage of crystallization of thick flows or as intrusive layers. The intrusive gabbros appear to be post-volcanic, as the gabbro layers have distinct chill margins but a coarse grain-size indicating that the intrusion must have occurred within the pile of volcanic flows, which insulated the gabbro sill. Similarly an 18 m thick dolerite dyke is present in BARB 1 between 118 and 136 m. Evidence points towards intrusion of this dyke post strata rotation of the komatiite section because it is an exceptionally coherent unit (not fragmented in the core tray), with much less veining in comparison to the ultramafic lavas and the latter intruded gabbro sills. It also has a distinctly different composition. This implies two distinct intrusive episodes, the first being the gabbro sills, which intrude the still warm volcanic flow pile of the Komati Formation, and the second being the intrusion of the dolerite dyke after deformation of the volcanic flows field. .

10.2 Overview of the Selected Detailed Sections

Four sections were selected for detailed analysis. These sections focussed on the differentiated komatiite packages and the unique tumulus feature found in the lowest part of the stratigraphy. The tumulus is unique but shows similar textures and mineralogy to the smaller-scale differentiated komatiite flows. Three differentiated komatiite packages were sampled; (1) BARB 1 (89-118 m), (2) BARB 1 (378-420 m) and (3) BARB 2 (252-274 m).

The tumulus unit consists of five textural zones; basal cumulus crystals, harrisite, pyroxene spinifex containing a gabbro layer and upper most hyaloclastite. The tumulus is 90 m thick in the core, which translates to 50 m true thickness. The cumulates are notably large, reaching 15 mm and are ellipsoid in shape and aligned in certain horizons. These layers of large olivine crystals are evidence of flow inflation, since each injection of magma would have brought with it a new batch of large olivine phenocrysts. The cumulates are well packed with a maximum of 20 % melt between the crystals. The harrisite overlies the cumulate zone, with the exception of a single 80 cm- thick lens that lies towards the top of the cumulate pile. This lens is evidence of the upward percolation of melt residue from the underlying cumulates. Above the harrisite is pyroxene spinifex, which has blades reaching 20 cm in length. Spinifex and harrisite formed in a tranquil environment, which indicates that the lava tube ceased flowing and solidified in a temperature gradient. The harrisite grew upwards from the cumulate, while the spinifex crystalized from the roof towards the centre of the flow. Contained within the pyroxene spinifex layer is a gabbro and pyroxenite layer, interpreted to be the final stage of crystallization of the tumulus unit. The hyaloclastite represents the chilled upper margin of the tumulus. This upper margin is brecciated and between the fragments is a glass shard matrix.

The differentiated komatiite flow packages of BARB 1 (89-118 m), BARB 1 (378-420 m) and BARB 2 (252-274 m) all consist of differentiated komatiite flows, which are texturally divided into three sections: basal cumulates, olivine spinifex and chill margins. The olivine cumulates are typically <0.5 mm in size and are surrounded by between 30 to 60 % melt residue. The olivine spinifex ranges from 0.5 to 50 mm depending on the position within the flow. Typically the 0.5 mm blades occur near the chill margin at the top of the flow and are randomly oriented. The larger spinifex blades are found toward the centre of the flow and are aligned. Evidence of metamorphic re-crystallization of the spinifex blades is present in the BARB 1 (89-118 m) package, where the spinifex blades are not only long but over 10 mm wide, which is not a characteristic feature of igneous spinifex. Between the olivine spinifex blades are smaller- scale pyroxene blades, however this is only evident in the thin sections and not visible in the hand sample.

10.3 Whole Rock Chemistry and Petrography of Detailed Sections

The petrological observations and chemical analyses of the selected sections reveal details of flow processes within individual flows and larger scale processes of the flow package.

Petrographically the textures and mineral assemblages seen in the tumulus are visible on hand sample scale and therefore the thin sections reveal only small scale features such as mineral grain boundaries, alteration minerals and opaque mineral distribution. The cumulus minerals are elliptical in shape and subhedral with opaque minerals associated with the olivine grain boundaries and fractures within the crystals. The olivine cumulate is completely altered to serpentine. The harrisite is a large- scale (2-3 cm) feature and thin sections do not adequately reflect the skeletal features of the olivines. The matrix surrounding the harrisite contains small (2 mm) crescent-shaped pyroxene blades and fine grained melt residue. Opaque minerals are found exclusively along the boundaries of the skeletal olivines. The olivines are altered to serpentine; the pyroxenes and the melt residue are altered to a fine- grained combination of chlorite, tremolite and serpentine. A minor proportion of the pyroxene crystals are unaltered. The pyroxene spinifex consists of large-scale pyroxene blades surrounded by a fine-grained melt residue. The pyroxenes are altered to chlorite on the rims and tremolite in the centre, while the matrix is an indistinguishable combination of inter-grown tremolite and chlorite. The gabbro and pyroxenite layer consists of equant to slightly elongated pyroxene grains, which are mostly unaltered. The gabbro contains unaltered plagioclase grains. The pyroxenes are typically altered to chlorite on the rim and are fresh in the core. The fragmented chill of the hyaloclastite is fine grained and is altered to a combination of serpentine, chlorite and tremolite. The glass-shard matrix, which supports the fragments in the chill margins, is fine grained and the glass shards are irregular to rounded in shape. The shards are zoned and altered to magnesite. The contact margin between the fragments and the glass shards is sharp, and there is no evidence of interaction.

Chemically the tumulus shows clear evidence of fractionation processes from the cumulates to the final stage of crystallization (the gabbro and pyroxenite layer). The chill fragments of the hyaloclastite represent the liquid composition and the harrisite and pyroxene spinifex are intermediate chemical phases. Variation diagrams confirm the immobility of MgO, TiO_2, Al_2O_3, Zr and Ni. The tumulus has a Fo_{93} control on the crystallization process. Rare Earth Element (REE) patterns are between 1 and 11 times chondrite values, the trend is almost flat, with the slightest LREE enrichment and with both positive and negative Eu anomalies.

The differentiated komatiite packages BARB 1 (89-118 m), BARB 1 (378-420 m) and BARB 2 (252-274 m) have similar petrographic characteristics. The cumulate layers are composed of euhedral, 0.5 mm- sized olivine crystals, surrounded by melt residue. The opaque minerals are associated with the olivine crystal boundaries and the fractures within the grains. Olivine

is altered to serpentine and the matrix is commonly serpentinized and also contains a combination of chlorite and tremolite. The BARB 1 (89-118 m) package is the first flow unit immediately overlying the tumulus, in which there are two phases of cumulates. The olivine cumulates have indistinct grain boundaries and are filled with opaque minerals, while the pyroxene cumulates have definite grain boundaries and no opaque minerals associated with them. In the BARB 1 (378-420 m) and BARB 2 (252-274 m) packages some (20 %) of the cumulates have poikilitic pyroxenes surrounding the olivines instead of fine grained melt residue. This may be caused by slower cooling in more insulated flow units. The pyroxene oikocrysts are mostly altered to chlorite and tremolite, but in some cases, portions of the crystal are unaltered. The olivines are, however, completely altered to serpentine. The olivine spinifex in the flows is evident on a hand-sample scale. In thin section, the presence of smaller (1 mm- 5 mm) sized pyroxene blades are present interstitially to the large olivine blade framework. The pyroxene spinifex usually grew perpendicular to the olivine blades. Between the pyroxene spinifex blades are radiating fibrous growths of finely grained acicular pyroxene and small pockets (<0.5 mm) of melt residue. The olivine blades are altered to serpentine and have concentrations of opaque minerals along their length. The thicker and larger olivine blades have distinct grain boundaries, while the thinner, smaller olivine blades do not show clear grain boundaries. The pyroxene spinifex between the olivine blades has distinct grain boundaries and is usually altered to chlorite and tremolite. Some instances of fresh pyroxene spinifex are present in BARB 1 (378-420 m) and BARB 2 (252-274 m). The chill margins of the differentiated flows are fine grained. However in some cases they may either contain micro textures, such as micro-spinifex, if the chill is the top of the spinifex layer, or they may contain micro-cumulates if it is a basal chill. The chill margins are altered to a fine-grained combination of serpentine, chlorite and tremolite.

The composition of the differentiated package BARB 1 (89-118 m) is unique in that the MgO intercept is at 40 % rather than the typical 50 % found in the other differentiated packages and in the tumulus. This lower MgO intercept is caused by both olivine and pyroxene controlling the crystallization trends. The combined olivine: pyroxene control in a ratio of 1:2 is confirmed by the petrographic evidence of both minerals occurring in the cumulate zones. Furthermore, it is confirmed by CIPW norm calculations. The BARB 1 (378-420 m) and BARB 2 (252-274 m) packages have Fo_{93} and Fo_{94} olivine crystallization controls, respectively. Trends of element vs. depth show that the element patterns in BARB 1 (89-118 m) package are consistent. BARB 1 (378-420 m) shows an increase of MgO with height,

indicating replenishment of MgO in the chamber supplying the flows, and the BARB 2 (252-274 m) package has an s- shaped pattern of MgO indicating that an influx of MgO rich magma took place halfway through the eruption sequence. The REE patterns of the differentiated packages are similar. They are between 2 and 9 times chondrite values, with the cumulates having lower, and the spinifex having higher ratio values. This shows the fractionation process within each flow, where the REE did not partition into olivine, but rather concentrated in the remaining liquid that later formed the spinifex. There is a slight LREE enrichment in the trends, but the ratio values do not reach those of typical MORB. Eu anomalies are present and are attributed to mobility during alteration rather than being controlled by plagioclase.

Opaque minerals are found in association with olivine crystals and are notably not present in the pyroxene crystals or melt residue. There are two forms of opaque minerals: the first is chromite, which crystalized during solidification of the magma and is irregularly shaped and very fine grained (<0.1 mm). The second opaque mineral phase is magnetite, which mostly overgrew the chromite and formed euhedral grains (<0.5 mm in size) during the alteration stage.

The alteration mineral assemblage is: serpentine, chlorite, tremolite and magnesite. Typically the olivine alters to serpentine, while the pyroxenes and melt residue alter to a fine-grained combination of chlorite and tremolite. Serpentine and magnesite veins are present. Cross cutting relationships clearly indicate that the serpentine veins formed first and a later stage alteration event caused the magnesite veins.

10.4 Comparison of the Tumulus to Differentiated Flows

The tumulus is an order of magnitude thicker than the differentiated komatiite flows. It is far more differentiated, with compositions ranging from olivine adcumulates to gabbro. The upper hyaloclastite unit represents the composition of the emplaced liquid which, with about 30% MgO, is among the most magnesian of komatiite melts. In comparison the differentiated flows are separated into three distinct textures: basal cumulate, olivine spinifex and chill margin. The cumulus olivines of the tumulus are larger than in the cumulates of the differentiated flows. The pyroxene spinifex of the tumulus is surrounded by fine grained melt residue. In the differentiated flows, both olivine and pyroxene spinifex is present. The hyaloclastite is the fine grained chill breccia of the top margin of a flow or lava tube, which is

similar to the contacts present in the differentiated flows, but on a larger scale. Equivalents of the harrisite, gabbro and pyroxenite layers are absent from the differentiated flows. .

Compositionally the tumulus, the BARB 1 (378-420 m) and the BARB 2 (252-274 m) sequences are similar. They all have a Fo_{93}-Fo_{94} control over crystallization. As noted previously the BARB 1 (89-118 m) package has combined olivine - pyroxene control and therefore is not comparable. The tumulus has similar MgO intercepts (48-50%) to the BABB 1 (378-420 m) and BARB 2 (252-274 m) packages. REE diagrams have similar concentrations (1-11 times chondrite) but the differentiated komatiite flows have a slightly larger LREE enrichment than the tumulus does. Evident in the tumulus and the flows is the process of fractionation via variation diagrams, REE and multi element plots, where the cumulate zone has low incompatible element values and the spinifex layers have increased concentrations of incompatible elements.

To summarize, the tumulus contains some texturally similar layers to the differentiated flows, but the harrisite and gabbro-pyroxenite layers are unique to the tumulus. Chemically the tumulus and the differentiated flows (except the BARB 1 (89-118 m)) are the same, indicating the magmas crystallization process is the same. The tumulus, being thicker, fractionated to a greater extent, which resulted in the final-stage crystallization of gabbro and pyroxenite.

10.5 Conclusions

One of the main IDCP Barberton drilling project objectives was to drill through a section of the komatiite stratigraphy of the Komati Formation in order to study the contact relationships and internal structures of ultramafic lava flows. Drilling was justified because outcrops of individual flows are poor and no continuous sections are preserved at the surface. Therefore the core has created the opportunity for a detailed investigation of contacts and flow structure over 367 m of stratigraphy (700 m of core length).

The BARB 1 and BARB 2 cores provided the basis for the study. The major findings are:

- BARB 1 consists of 85 distinct flows, while BARB 2 intersects 65 distinct flows. These consist of massive and differentiated komatiites, komatiitic basalts, basalts and intrusive gabbro sills.

- BARB 1 contains two packages of differentiated komatiite flows, (1) BARB 1 (89-118 m), which is composed of 12 differentiated flows, (2) BARB 1 (378-420 m), which is composed of 8 differentiated flows. BARB 2 has one differentiated package (252-274 m) and contains 7 differentiated flows. As discussed previously it is possible that these flows represent multiple lobes of a compound flow, rather than individual flows.
- The unique tumulus unit is thicker (90 m) than the differentiated flows (1-5 m thick). It has three textural sections that correspond with the differentiated flows (cumulate, spinifex, chill), but also has two extra textural zones, which are not present in the flows (harrisite and gabbro-pyroxenite layers).
- Petrographically, the cumulus olivines in the tumulus are larger (15 mm) than those in the differentiated flows (0.5-1 mm). The spinifex in the tumulus contains only pyroxene needles (20 cm), while in the flows the large scale (5 cm) spinifex is composed of olivine blades and the smaller scale (<1 cm) spinifex consists of pyroxene blades. The hyaloclastite of the tumulus is thicker (20 m) than the typical flow top breccia (5-15 cm).
- Geochemically the tumulus is a coherent unit, the cumulates being the most MgO rich and the gabbro- pyroxenite layer being the most chemically evolved. The samples create a trend controlled by Fo_{93}. The chilled fragments of the hyaloclastite best represent the liquid composition of the magma. REE patterns are between 1 and 11 times chondrite and have only a slight LREE enrichment.
- The differentiated flow packages BARB 1 (378-420 m) and BARB 2 (252-274 m) have similar geochemistry to the tumulus. They have a Fo_{93} and Fo_{94} control respectively. The REE patterns range between 2 and 9 times chondrite and are well constrained with a small LREE enrichment.
- BARB 1 (89-118 m) package does not contain the same textural, mineralogical or chemical features as the tumulus or BARB 1 (378-420 m) and BARB 2 (252-274 m). This package has a 40 % MgO intercept and the samples are controlled by both olivine and pyroxene crystallization. Two cumulus phases (olivine and pyroxene) support this chemical interpretation, as does the CIPW norm calculation.
- The core log of the tumulus corresponds well with the surface map by Dann (2000), but the vesicular komatiite of the study by Dann (2000) had a different mineralogical composition to the corresponding hyaloclastite zone.

CHAPTER 11

REFERENCE LIST

Anders, E. & Grevesse, N. (1989). Abundances of the elements: Meteoritic and solar. *Geochemica et Cosmochimica Acta* **53**, 197-214.

Anderson, S. W., Smrekar, S. E. & Stofan, E. R. (2012). Tumulus development on lava flows: insights from observations of active tumuli and analysis of formation models. *Bulletin of Volcanology* **74**, 931-946.

Armstrong, R. A., Compston, W., de Wit, M. J. & Williams, I. J. (1990). The stratigraphy of the 3.5-3.2 Ga Barberton Greenstone Belt revisited: A single zircon ion microprobe study. *Earth and Planetary Science Letters* **101**, 90–106.

Arndt, N. T. & Nisbet, E. G. (1982). *Komatiites*. London: Allen and Unwin.

Arndt, N. T., Lesher, C. M. & Barnes, S. J. (2008). *Komatiites*. United Kingdom: University Press, Cambridge.

Barnes, S.J., (1985). The petrography and geochemistry of komatiite flows from the Abitibi Greenstone Belt and a model for their formation, *Lithos*, **18.4**, 241-270.

Barnes, S. J. (1998). Chromite in komatiites, 1. Magmatic controls on crystallisation and composition. *J. Petrol.* **39**, 1689-1720.

Barnes, S.J., (2000). Chromites in komatiites II: Modification during greenschist to mid-amphibolite facies metamorphism, *J. Pertrol.*,**41**, 387-409.

Barnes, S.J., Hill, R.E.T., Perring, C.S., Dowling, S.E., (2004). Lithogeochemical exploration for Komatiite- associated Ni-sulfide deposits: strategies and limitations, *Mineralogy and Petrology*, **82**, 259-293.

Brandl, G., Cloete, M. & Anhaeusser, C. R. (2006). Archean greenstone belts. In: Johnson, M. R., Anhaeusser, C. R. & Thomas, R. J. (eds.) *In: The Geology of South Africa*. Pretoria: Geological Society of South Africa/ Council for Geoscience, 9-56.

Byerly, G. R. (1999). Komatiites of the Mendon Formation: Late-stage ultramafic volcanism in the Barberton Greenstone Belt. In: Lowe, D. R. & Byerly, G. R. (eds.) *Geologic Evolution of the Barberton Greenstone Belt, South Africa*. Boulder, Colorado: The Geological Society of America. Special Paper 329, 189-211.

Cameron, W. E. & Nisbet, E. G. (1982). *Komatiities: Chapter 3: Phanerozoic analogues of komatiitic basalt*. London: George Allen & Unwin (Publishers) Ltd.

Chavagnac, V. (2004). A geochemical and Nd isotopic study of the Barberton komatiites (South Africa): Implications for the Archean mantle. *Lithos* **75**, 253-281.

Cloete, M. (1991). The structure and metamorphism of the Komati Formation at Spinifex Stream and the Hooggenoeg Formation in the Songimvelo Game Reserve. In: Ashwal, L. D. (ed.) *Two Cratons and an Orogeny. Excursion guidebk. and review articles for afield workshop through*

selectedArchaean terranes of Swaziland, South Africa, and Zimbabwe. Univ. Witwatersrand, Johannesburg, S. Afr. , 123—133.

Dann, J. C. & Grove, T. L. (2007). Earth's oldest rocks: Chapter 5.4 : Volcanology of the Barberton Greenstone Belt, South Africa: Inflation and evolution of flow fields. *Developments in precambrian geology* **15**, 527-570.

Dann, J. C. (2000). The 3.5 Ga Komati Formation, Barberton Greenstone Belt, South Africa, Part I: New maps and magmatic architecture. *S.Afr.J.Geol* **103**, 47-68.

Dann, J. C. (2001). Vesicular komatiites, 3.5- Ga Komati formation, Barberton Greenstone Belt, South Africa: inflation of submarine lavas and origin of spinifex zones. *Bull Volcanol* **63**, 462-481.

de Ronde, C. E. J., de Wit, M. J. & Spooner, E. T. C. (1994). Early Archean (>3.2 Ga) Fe-oxide-rich, hydrothermal discharge vents in the Barberton greenstone belt, South Africa. *Geological Society of America Bulletin* **106**, 86-104.

de Wit, M. J., Hart, R. A. & Hart, R. J. (1987). The Jamestown ophiolite complex, Barberton mountain belt: a section through 3.5 Ga oceanic crust. *J. Afr. Earth Sci.* **6**, 681– 730.

de Wit, M. J., Roering, C., Hart, R. J., Armstrong, R. A., de Ronde, C. E. J., Green, R. W. E., Tredoux, M., Peberdy, E. & Hart, R. A. (1992). Formation of an Archaean continent. *Nature* **357**, 553-562.

de Wit, M., Furnes, H. & Robins, B. (2011). Geology and tectonostratigraphy of the Onverwacht Suite, Barberton Greenstone Belt, South Africa. *Precambrian Research* **186**, 1-27.

Dirks, P. H. G. M., Charlesworth, E. G. & Munyai, M. R. (2009). Cratonic extension and Archaean gold mineralisation in the Sheba-Fairview mine, Barberton greenstone belt, South Africa. *South African Journal of Geology* **112**, 291-316.

Donaldson, C. H. (1974). Olivine crystal types in harrisitic rocks of the Rhum pluton and Archean spinifex. *Bulletin of the Geological Society of America* **85**, 1721-1726.

Donaldson, C. H. (1982). Origin of some of the Rhum harrisite by segregation of intercumulus liquid. *Mineralogical magazine* **45**, 201-209.

Donaldson, C. H. (1982). Spinifex - textured komatiites: a review of textures, compositions and layering. In: Arndt, N. T. & Nisbet, E. G. (eds.) *Komatiites*. London: George Allen and Unwin Publishers, 213-244.

Dowling, S.E., Barnes, S.J., Hill, R.E.T., Hicks, J.D., (2004). Komatiites and nickel sulfide ores of the Black Swan area, Yilgarn Craton, Western Australia. 2: Geology and genesis of the orebodies, *Mineralium Deposita*, **39**, 707-728.

Faure, F., Arndt, N. & Libourel, G. (2006). Formation of Spinifex Texture in Komatiites: an Experimental Study. *Journal of Petrology* **47**, 1591–1610.

Furnes, H., de Wit, M. & B., R. (2013). A review of new interpretations of the tectonostratigraphy, geochemistry and evolution of the Onverwacht Suite, Barberton Greenstone Belt, South Africa. *Gondwana Research*, 403–428.

Gole, M., Barnes, S.J., Hill, R.E.T. (1987). The role of fluids in the metamorphism of komatiites, Agnew nickel deposit, western Australia, *Contrib. Mineral. Pertol*, **96**, 151-162.

Godel, B., Barnes, S.J., Gurer, D., Austin, P., Fiorentini, M.L., (2013), Chromite in komatiites: 3D morphologies with implications for crystallization mechanisms, *Contrib. Mineral. Pertol.*,**165**, 173-189.

Grove, T. L. & Parman, S. W. (2004). Thermal evolution of the Earth as recorded by komatiites. *Earth and Planetary Science Letters* **219**, 173-187.

Grove, T., Parman, S. W. & Dann, J. C. (1999). Conditions of magma generation for Archean komatiites from the Barberton Mountainland, South Africa. In: Fei, Y., Bertka, C. M. & Mysen, B. (eds.) *Mantle Petrology: Field Observations and High Pressure Experimentation*. Houston: The Geochemical Society, 155-167.

Hill, R. E. T. (2001). Komatiite volcanology, volcanological setting and primary geochemical properties of komatiite-associated nickel deposits. *Geochemistry: Exploration, Environment, Analysis* **1**, 365-381.

Hill, R. E. T., Barnes, S. J., Gole, M. J. & Dowling, S. E. (1995). The volcanology of komatiites as deduced from field relationships in the Norman-Wiluna greenstone belt, Western Australia. *Lithos* **34**, 159-188.

Hon, K., Kauahikaua, J., Delinger, R. & MacKay, K. (1994). Emplacement and inflation of pahoehoe sheet flows: Observations and measurements of active lava flows on Kilauea Volcano, Hawaii. *Geological Society of America Bulletin* **106**, 351-370.

Houle, M.G., Prefontaine, S., Fowler, A.D., Gibson, H.L., (2009) Endogenous growth in channelized - komatiite lava flows: evidence from spinifex textured sills at Pyke Hill and Serpentine Mountain, Western Abitibi Greenstone Belt, Northeastern Ontario, Canada, *Bull. Volcanol.* **71**, 881-901.

Huppert, H. E., Sparks, R. S. J., Turner, J. S. & Arndt, N. T. (1984). Emplacement and cooling of komatiite lavas. *Nature* **309**, 19-22.

Jahn, B.-M., Gruau, G. & Glikson, A. Y. (1982). Komatiites of the Onverwacht Group, South Africa: REE geochemistry, Sm/Nd age and mantle evolution. *Contributions to Mineralogy and Petrology* **80**, 25-40.

Kauahikaua, J., Cashman, K.V., Mattox, T.N., Heliker, C.C., Hon, K.A., Mangan, M.T., Thornber, C.R. (1998) Observations on basaltic lava steams in tubes from Kilauea Volcano, island of Hawai'i, *Journal of Geophysical Research*, **103,** 303-323.

Kröner, A., Hegner, E., Wendt, J. I. & Byerly, G. R. (1996). The oldest part of the Barberton granitoid-greenstone terrain, South Africa: evidence for crust formation between 3.5 and 3.7 Ga. *Precambrian Research* **78**, 105–124.

Lahaye, Y., Arndt, N. T., Byerly, B., Chauvel, C., Fourcade, S. & Gruau, G. (1995). The influence of alteration on the trace-element and Nd isotopic compositions of komatiites. *Chemical Geology* **126**, 43-64.

Lopez-Martinez, M., York, D. & Hanes J.A. (1992). A 40Ar/39Ar geochronological study of komatiites and komatiitic basalts from the Lower Onverwacht Volcanics: Barberton Mountain Land, South Africa. *Precambrian Research* **57**, 91-119.

Lowe, D. R. & Byerly, G. R. (2007). Earths oldest rocks: Chapter 5.3: An overview of the geology of the Barberton greenstone belt and vicinity: Implications for crustal development. *Developments in precambrian geology* **15**, 481-526.

Lowe, D. R. (1994). Accretionary history of the Archean Barberton greenstone belt (3.55 - 3.22 Ga), southern Africa. *Geology* **22**, 1099-1102.

McDonough, W. F. & Sun, S. S. (1995). The composition of the Earth. *Chemical Geology* **120**, 223-253.

McPhie, J., Doyle, M., Allen, R., . (1993). Volcanic textures- a guide to the interpretation of textures in volcanic rocks. Tasmania: PAT, Hobart, 191.

Nesbitt, R. W. & Sun, S. S. (1976). Geochemistry of Archaean spinifex-textured peridotites and magnesian and low-magnesian tholeiites. *Earth and Planetary Science Letters* **31**, 433-453.

Nesbitt, R. W., Jahn, B. M. & Purvis, A. C. (1982). Komatiites: An early precambrian phenomenon. *Journal of Volcanology and Geothermal Research* **14,** 31-45.

Nisbet, E. G. (1982). The tectonic setting and petrogenesis of komatiites. In: Arndt, N. T. & Nisbet, E. G. (eds.) *Komatiites* London: George Allen and Unwin, 501-520.

Nisbet, E. G., Arndt, N. T., Bickle, M. J., Cameron, W. E., Chauvel, C., Cheadle, M., Hegner, E., Kyser, T. K., Martin, A., Renner, R. & Roedder, E. (1987). Uniquely fresh 2.7 Ga komatiites from the Belingwe greenstone belt, Zimbabwe. *Geology* **15**, 1147-1150.

Nisbet, E. G., Cheadle, M. J., Arndt, N. T. & Bickle, M. J. (1993). Constraining the potential temperature of the Archaean mantle: A review of the evidence from komatiites. *Lithos* **30**, 291–307.

Papunen, H., Halkoaho, T., Liimatainen, J. & Tulenheimo, T. (1998). Komatiite geology of the Siivikkovaara and Kellojärvi areas of the Kuhmo greenstone belt. *Integrated technologies for mineral exploration pilot project for nickel ore deposits*. Geological Survey of Finland, GeoNickel Technical Reports: Turku University Department of Geology.

Parman, S. W., Dann, J. C., Grove, T. L. & de Wit, M. J. (1997). Emplacement conditions of komatiite magmas from the 3.49 Ga Komati Formation, Barberton greenstone belt, South Africa. *Earth and Planetary Science Letters* **150**, 303-323.

Parman, S. W., Grove, T. L. & Dann, J. C. (2001). The production of Barberton komatiites in an Archean subduction zone. *Geophysical Research Letters* **28**, 2513-2516.

Parman, S. W., Grove, T. L., Dann, J. C. & de Wit, M. J. (2004). Subduction origin for komatiites and cratonic lithosphere mantle. *South African Journal of Geology* **107**, 107-118.

Parman, S. W., Shimizu, N., Grove, T. L. & Dann, J. C. (2003). Constraints on the pre-metamorphic trace element composition of Barberton komatiites from ion probe analyses of preserved clinopyroxene. *Contributions to Mineralogy and Petrology* **144**, 383-396.

Puchtel, I. S., Blichert-Toft, J., Touboul, M., Walker, R. J., Byerly, G. R., Nisbet, E. G. & Anhaeusser, C. R. (2013). Insights into early Earth from Barberton komatiites: Evidence from lithophile isotope and trace element systematics. *Geochimica et Cosmochimica Acta* **108**, 63–90.

Pyke, D. R., Naldrett, A. J. & Eckstrand, O. R. (1973). Archean ultramafic flows in Munro Township. *Geological Society of American Bulletin of Volcanology* **4**, 955–978.

Renner, R., Nisbet, E. G., Cheadle, M. J., Arndt, N. T., Bickle, M. J. & Cameron, W. E. (1993). Komatiite Flows from the Reliance Formation, Belingwe Belt, Zimbabwe: 1. Petrography and Mineralogy. *Journal of Petrology* **35**, 361-400.

Robin-Popieul, C. M., Arndt, N. T., Chauvel, C., Byerly, G. R., Sobolev, A. V. & Wilson, A. (2012). A New Model for Barberton Komatiites: Deep Critical Melting with High Melt Retention. *Journal of Petrology*, 1-39.

Rollinson, H. (1993). *Using Geochemical Data*. New York: John Wiley and Sons.

Rossi, M. J. & Gudmundsson, A. (1996). The morphology and formation of flow-lobe tumuli on Icelandic shield volcanoes. *Journal of Volcanology and Geothermal Research* **72**, 291-308.

Smith, H. S. & Erlank, A. J. (1982). Geochemistry and petrogenesis of komatiites from the Barberton greenstone belt, South Africa. In: Arndt, N. T. & Nisbet, E. G. (eds.) *Komatiites*. London, England: George Allen and Unwin, 347-398.

Smith, H. S., Erlank, A. J. & Duncan, A. R. (1980). Geochemistry of some ultramafic komatiite lava flows from the Barberton Mountain Land, South Africa. *Precambrian Research* **11**, 399-415.

Stiegler, M. T., Lowe, D. R. & Byerly, G. R. (2010). The Petrogenesis of Volcaniclastic Komatiites in the Barberton Greenstone Belt, South Africa: a Textural and Geochemical Study. *Journal of Petrology* **51**, 947-972.

Tait, S. R., Huppert, H. E. & Sparks, R. S. J. (1984). The role of compositional convection in the formation of adcumulate rocks. *Lithos*, 139-146.

Viljoen, M. J. & Viljoen, R. P. (1969). The geology and geochemistry of the lower ultramafic unit of the Onverwacht group and a proposed new class of igneous rocks. *Special Publication of the Geological Society of South Africa* **2**, 55-85.

Viljoen, M. J., Viljoen, R. P. & Pearton, T. N. (1982). *Komatiites : Chapter 4: The nature of distribution of Archaean komatiite volcanic in South Africa*. London: George Allen & Unwin (Publishers) Ltd.

Viljoen, M. J., Viljoen, R. P., Smith, H. S. & Erlank, A. J. (1983). Geological, textural and geochemical features of komatiite flows from the Komati Formation. In: Anhaeusser, C. R. (ed.) *Contributions to the Geology of the Barberton Mountain Land*. Johannesburg: The Geological Society of South Africa. Special publication **9**, 1-20

Viljoen, M. J., Viljoen, R. P., Smith, H. S. & Erlank, A. J. (1987). Geological, textural and geochemical features of komatiitic flows from the Komati Formation. In: Anhaeuser, C. R. (ed.) *Contributions to the Geology of the Barberton Mountain Land*. Johannesburg: The Geological Society of South Africa.

Wager, L. R., Brown, G. M. & Wadsworth, W. J. (1960). Types of Igneous Cumulates. *Journal of Petrology* **1**, 73-85.

Walker, G. P. L. (1991). Structure, and origin by injection under surface crust, of tumuli, 'lava rises', 'lava-rise pits', and 'lava inflation clefts' in Hawaii. *Bulletin of Volcanology* **53**, 546-558.

Williams, D. A., Kerr, R. C. & Lesher, C. M. (1999). Thermal and Fluid Dynamics of Komatiitic Lavas Associated with Magmatic Fe-Ni-Cu-(PGE) Sulphide Deposits. In: Keays, R. R., Lesher, C. M., Lightfoot, P. C. & Farrow, C. E. G. (eds.) *Dynamic Processes in Magmatic Ore Deposits and their Application to Mineral Exploration. Geological Association of Canada Short Course*, 477.

Wilson, A. H., Shirey, S. B. & Carlson, R. W. (2003). Archaean ultra-depleted komatiites formed by hydrous melting of cratonic mantle. *Nature* **423**, 858-861.

Wilson, A., H.,. (2012). Chill Sequence to the Bushveld Complex: Insight into the First Stage of Emplacement and Implications for the Parental Magmas. *Journal of Petrology* **53**, 1123-1168.